AN ABSTRACT OF THE DISSERTATION OF

Maureen Helen Davies for the degree of Doctor of Philosophy in Oceanography presented on June 3, 2011.

Title: Paleoclimate, Paleoventilation, and Paleomagnetism as Recorded in a 17kyr Marine Sediment Record from the SE Alaska margin

Abstract approved:____

Alan C. Mix   Joseph S. Stoner

The deglacial behavior of the sub-Arctic North Pacific is poorly constrained, with many published records suffering from limited age control due to extensive post-depositional biogenic carbonate dissolution. Potential alternative dating methods could include the correlation of stable-isotopic and/or paleomagnetic secular variation records to an independently-dated regional template, however no such template currently exists. Cores EW0408-85JC (59°33.32'N, 144°9.21'W, 682 m water depth) and EW0408-79JC (59°33.32'N, 144°9.21'W, 682 m water depth) are located above the carbonate compensation depth on the Gulf of Alaska margin, affording an opportunity to inter-compare stable-isotopic and paleomagnetic variability from a single location, as well as to place observations of Northeast Pacific paleoclimate and paleomagnetic secular variation in a global context via an independent radiocarbon-based chronology.

We evaluate three possible age models for core EW0408-85JC and their implications for North Pacific stable isotopic and paleoventilation behavior. These include calibrated planktonic and benthic foraminiferal radiocarbon dates, assuming constant reservoir ages, as well as a correlation of planktonic $\delta^{18}O$ in foraminifera to $\delta^{18}O$ in a layer-counted Greenland ice core (NGRIP). We conclude that the calibrated

planktonic dates provide the most accurate chronology. Benthic foraminiferal radiocarbon dates evaluated on this age model indicate that intermediate-depth ventilation ages at the site increased to >2,670 ± 180 during Termination 1, implying reduced ventilation relative to the Holocene average of 1,740 ± 210 yr. The shift to lower ventilation ages occurs at ~10,500 cal ybp, coeval with the flooding of Beringia and the opening of the Bering Strait, suggesting that flooded shelves and net export of low-salinity surface waters enhanced ventilation of the North Pacific.

Oxygen isotope data from planktonic and benthic foraminifera, interpreted on this age model, document surface freshening by 16,650 ± 170 cal ybp, likely due to freshwater input from retreating regional glaciers. A sharp transition to laminated hemipelagic sedimentation at 14,790 ± 380 cal ybp is coincident with abrupt warming and/or freshening of the surface ocean (i.e. additional $\delta^{18}O$ reduction of 0.9 ‰), essentially coincident with the Bolling Interstade of Northern Europe and Greenland. Cooling and/or higher salinities returned during the Allerod interval, coeval with the Antarctic Cold Reversal and continuing until 11,740 ± 200 cal ybp, when the onset of warming coincides with the end of the Younger Dryas. This may indicate convolved Northern and Southern drivers of climate variability in the North Pacific. Two laminated opal-rich intervals record episodes of high productivity are observed from 14,790 ± 380 to 12,990 ± 190 cal ybp, and from 11,160 ± 130 to 10,750 ± 220 cal ybp. These events likely correlate to similar observations elsewhere on the margins of the North Pacific, and may be driven my remobilization of iron from newly inundated continental shelves during episodes of rapid sea-level rise.

High-resolution paleomagnetic secular variation (PSV) records from the Gulf of

Alaska constrain regional field behavior and provide information on larger scale geomagnetic dynamics. Both cores studied (EW0408-79JC and 85JC) preserve a generally strong and relatively stable (MAD <5°) magnetization for the period of overlap, though the quality of the magnetization at 85JC deteriorates beyond 8,000 cal ybp, in association with deglacial and early Holocene shifts in magnetic mineralogy. Component inclinations from both sites are consistent with historical reconstructions and consistent with a geocentric axial dipole (GAD), supporting spherical-harmonic attempts to model the Holocene field. Comparison with regional reconstructions suggest that even the earlier component of 85JC captures PSV fairly accurately, providing new information on this part of the record. Normalized remanence is reconstructed using NRM/ARM, though variability in the magnetic remanence carrier precludes us from interpreting these records as robust reflections of North Pacific relative paleointensity. The independently-dated directional records, however, are consistent with other regional reconstructions as well as those derived further afield in North America, suggesting that the concept of coherent North American flux lobe behavior through the majority of the Holocene can now be extended to the Gulf of Alaska.

Paleoclimate, Paleoventilation, and Paleomagnetism as Recorded in a 17kyr Marine Sediment Record from the SE Alaska Margin

by

Maureen Helen Davies

A DISSERTATION

submitted to

Oregon State University

in partial fulfillment of
the requirements for the
degree of

Doctor of Philosophy

Presented June 3, 2011
Commencement June 2012

Doctor of Philosophy dissertation of Maureen Helen Davies presented on June 3, 2011.

APPROVED:

Co-major Professor, representing Oceanography

Co-major Professor, representing Oceanography

Dean of the College of Oceanic and Atmospheric Sciences

Dean of the Graduate School

I understand that my dissertation will become part of the permanent collection of Oregon State University libraries. My signature below authorizes release of my dissertation to any reader upon request.

Maureen Helen Davies, Author

ACKNOWLEDGEMENTS

I would like to express a tremendous amount of gratitude to my advisors at COAS, Dr. Joseph Stoner and Dr. Alan Mix, whom have graced me with an excellent education, a lot of support, and a humbling amount of patience. I'm also grateful for the thoughtful input and oversight of my committee members: Andreas Schmittner, Nick Pisias, Ed Brook, and Stephen Lancaster. I've never faced a closed door.

Many thanks to the members of the stable isotope laboratory and core repository facilities at COAS, including Andy Ross, June Padman, Nancy Kyle, Bobbi Conard, Mysti Weber, and my dear friend Maziet Cheseby. Thanks to John Southon, Guaciara dos Santos Winston, Kiyo Beverly, and members of the UC Irvine Keck AMS lab at large for their education and assistance with our radiocarbon work. Thanks to John Jaeger, Joe Ortiz, Cris Lopes, Ingrid Hendy, Jason Addison, and Amelia Shevenell for allowing me to assault them with questions.

Thanks to Matthew Wolhowe, Jeremy Shakun, Sean Marcott, Lica and Carmen Ersek, Faron Anslow, Aaron Hartz, Summer Praetorious, Sarah Strano, Rob Hatfield, Jesse Muratli, Rebecca Poulson, Alex Jonko, Maria Winterfield, Diego Figueroa, Nikki Scott, Greg Wilson, Ann Morey-Ross, Jay Patton, Carole Abourachad, Patrick Monagle, and Tommaso Tesi; these friends and comrades in arms all kept me going through some portion of this path. Thanks to Chuan Xuan and Morgan Erhardt for their assistance with Matlab, ARC GIS, CT-scan processing, and the occasional motorcycle ride. Thanks to Karina Nordhousen, Jennifer McKay, and Karin and Peter Walczak for taking care of me and helping me look like the grown-up I need to convince people I am.

Thanks to Amy Simmons, Paul Walczak, Chelsea Stephen, and David Langner; I love you and am more grateful for your friendship through this experience than I could say. Thanks to my wonderfully miscreant dog, Kumo. Finally, thanks to my extended family: Connie, Maxine, and Miles Davies, Chris, Alan, and Andrew Worsley, Cecilia and Phillip Hughes, Nina, Hugh, and the Gales, Lynn, Adrian, Nick, and Ian Anderson, Jim and Mona Elsey, Doug and Jan McLemore, Denia, Bill, and Chris Acord, Francis and Dick Ohmes, Jessica Tam, Peter Lee, Ellen Range, Chris Carrico, Cait Rippey, Jay Thompson, Raz Barnea, Liz Nixon, Sarah Ortner, Wabi, Helen Davies, and Roger and Blanch Horne. I love you all and I owe you everything.

CONTRIBUTION OF AUTHORS

My co-advisors, Alan Mix and Joseph Stoner, oversaw every step of the work presented herein and contributed substantially to all scientific and literary efforts. John Southon contributed to the generation and interpretation of radiocarbon data, and Maziet Cheseby assisted in radiocarbon sample preparation used in generating the age models discussed in Chapter 2. Chaun Xuan generated Matlab code used to evaluate errors in projection age calculations in Chapter 2, as well as for optimizing paleomagnetic component directional data in Chapter 4. Jason Addison generated the opal and trace metal data integral for interpretations of EW0408-85JC, and assisted substantially with the writing of Chapter 3. John Jaeger assisted with the sedimentological interpretations of Chapters 3 and 4, and also contributed to the generation of the paleomagnetic data set in Chapter 4. Bruce Finney assisted with interpretations of the paleo-productivity data presented in Chapter 3. Jason Wiest generated the computerized tomographic scan data for the cores, presented in Chapters 3 and 4. Gillian P. Rosen and Jim Channell contributed to the collection of the natural and laboratory remanent magnetization data.

TABLE OF CONTENTS

TABLE OF CONTENTS (continued)

TABLE OF CONTENTS (continued)

Page

LIST OF FIGURES

LIST OF TABLES

For my close friend, role model, and grandfather, RADM Roger B. Horne.

Paleoclimate, paleoventilation, and paleomagnetism as recorded in a 17kyr marine sediment record from the Southeastern Alaska margin

Chapter 1

Introduction

1.1 Research Context

This thesis comprises an attempt to understand late glacial and Holocene paleoceanography, paleoclimate and paleomagnetic variability as recorded in sediments from the Gulf of Alaska continental margin. The North Pacific is a relatively understudied region in every branch of paleo-science. This is partially driven by a relatively shallow carbonate compensation depth, which complicates the development and/or radiocarbon dating of paleo-proxies. Alternative dating strategies could include correlation of millennial-scale features in stable isotope and/or paleomagnetic secular variation records to a well-dated regional template. However, to date there has been no published record of sufficient temporal resolution and with enough age control to serve this function. Core EW0408-85JC, collected from the Southeast Alaskan continental margin on cruise R/V Ewing cruise EW0408 offers a rare opportunity. This record captures the last retreat of Pleistocene glaciers in the Northeast Pacific, as well as a complete Holocene sedimentary sequence at average accumulation rates of ~60 cm/kyr. Laminated sequences are captured during deglaciation, offering insight into drivers of Northeast Pacific productivity and benthic hypoxia. Natural remanent magnetizations in the Holocene section of the core are strong and relatively stable, offering the potential to extend high-resolution observations of paleomagnetic secular variation to a previously unconstrained marine margin. Carbonate preservation is complete enough to develop benthic and planktonic stable-isotope records documenting sub-millennial scale climate variability through regional deglaciation and the Holocene, and most remarkably we have been able to generate a foraminiferal radiocarbon-based chronology with 39 benthic-planktonic pairs constraining sedimentation and paleoceanographic ventilation behavior over the last ~17,000 ybp. Via these multiple proxies, we endeavor to resolve a poorly-studied region of the world ocean, placing Northeast Pacific oceanographic, climatic, and geomagnetic variability in a global context on a detailed independent chronology, and furthering our understanding of the drivers of environmental change.

1.2 Research Motivation and Approach

1.2.1 Chapter 2: The flooding of Beringia and the onset of North Pacific Intermediate Water formation.

During the most recent deglaciation (Termination 1), atmospheric CO_2 content increased by ~50%, accompanied by a depletion in atmospheric $\Delta^{14}C$ apparently unsupported by changes in rates of cosmogenic production (Hughen et al., 2006; Broecker and Barker, 2007). This observation has been hypothesized to reflect the exchange of carbon between the deep sea and the atmosphere, in which case there should be a notable increase in the ventilation, and concomitant decrease in the radiocarbon age, of some portion of the interior ocean associated with deglaciation (Broecker, 1982; Sigman and Boyle, 2000). Support for an anomalously aged late-glacial watermass remains equivocal, however the strongest evidence to date has come from the intermediate-depth Northeast Pacific off the coast of California (Marchitto et al., 2007). The lateral extent of an aged intermediate watermass would need to be substantial to drive the observed variability in atmospheric CO_2, and the deglacial carbon inventory of the high-latitude Northeast Pacific remains poorly resolved.

Using paired radiocarbon measurements of benthic and planktonic foraminifera, in conjunction with stable-isotope records capturing regional deglacial surface ocean variability, we attempt to reconstruct paleoventilation behavior for our site. To accomplish this, we inter-compare results from three commonly-employed chronological methods, including calibrated benthic and planktonic foraminifera, as well as a tuning to stable-isotopic variability in a layer-counted Greenland ice-core.

1.2.2 Chapter 3: The deglacial transition on the Southeastern Alaska margin: meltwater input, sea-level rise, marine productivity, and sedimentary anoxia.

The high-latitudes are thought to be sensitive to (and potential drivers of) rapid environmental change (Manabe and Stouffer, 1980). However, there is little agreement on the mechanisms responsible for the generation and transmission of millennial-scale climate and productivity variability observed in these environments. Establishing the timing of Northeast Pacific climate and productivity perturbations relative to regional, North Atlantic, Antarctic, and global changes in temperature, ice-volume, and sea-level would contribute substantially to our understanding of the drivers of this variability. To this end, we have developed stable-isotopic records of sub-millennial resolution, which we interpret in the context of variability in sediment lithology, opal content, and trace metal geochemistry on an independent (non-tuned) radiocarbon-based age model. This multi-proxy approach allows us establish the timing of Cordilleran retreat on the Southeastern Alaskan margin, and places observed excursions in surface ocean temperature/salinity and productivity in a global context, shedding light on potential drivers of Northeast Pacific environmental change.

1.2.3 Chapter 4: Holocene paleomagnetic secular variation from the Gulf of Alaska

The structure of the geomagnetic field of the earth can be coarsely described as a dipole centered on the axis of rotation (Merrill, et al., 1996). This may be true averaged over tens of thousands of years, however historical observations indicate a substantially more complex morphology. The axis of the best-fitting dipole is offset from the axis of rotation, and the North magnetic dip-pole is presently moving at a rate of ~50 km/year (Olsen and Mandea, 2007). This sub-reversal scale geomagnetic change, termed paleomagnetic secular variation (PSV), may be driven by fluctuations in the size and strength of non-dipolar geomagnetic flux patches, the most prominent of which are located over North America, Europe, and Siberia in the Northern Hemisphere. The temporal persistence of these features, as well as the spatial extent over which geomagnetic behavior can be considered coherent, is important for understanding processes ranging from cosmogenic isotope production (St-Onge et al. 2003; Snowball and Muscheler, 2007) to the convective behavior of the outer core (Gubbins, 1988). Coherence of Holocene PSV behavior across the contiguous United States was first proposed by Lund et al., (1996), and has since been extended to Eastern Canada. Building off the well-resolved radiocarbon-based chronologies outlined in Chapter 2 and 3, we evaluate whether the Northeast Pacific shows this North American-type geomagnetic variability. Our findings contribute to efforts to model the geomagnetic field and understand the drivers of geomagnetic change, and may in the future contribute to a paleomagnetic template useful for climate-independent stratigraphy.

1.3 Current publication status

As of this writing, Chapter 2 is in preparation for submission to *Science*, Chapter 3 has been published in *Paleoceanography*, and Chapter 4 is in preparation for submission to *Geochemistry, Geophysics, Geosystems* (G3).

1.4 References

Broecker, W.S. (1982), Glacial to interglacial changes in ocean chemistry. *Progress in Oceanography,* 11, 151–197.

Broecker, W., E. Clark, and S. Barker (2008), Near constancy of the Pacific Ocean surface to mid-depth radiocarbon age difference over the last 20 kyr, *Earth and Planetary Science Letters,* 274, 322-326.

Gubbins, D. (1988), Thermal core-mantle interactions and time-averaged paleomagnetic field., *J. Geophys. Res.,* 93, 3413-3420.

Hughen, K., J. Southon, S. Lehman, C. Bertrand, and J. Turnbull (2006), Marine-derived ^{14}C calibration and activity record for the past 50,000 years updated from the Cariaco Basin, *Quaternary Science Reviews,* 25, 3216–3227.

Lund, S.P. (1996), A comparison of Holocene paleomagnetic secular variation records from North America, *Journal of Geophysical Research,* 101, 8007-8024.

Manabe, S. and R.J. Stouffer (1980), Sensitivity of a global climate model to an increase of CO2 concentration in the atmosphere. J Geophys Res 85: 5529–5554

Olsen, N. and M. Mandea (2007), Will the magnetic north Pole move to Siberia?, *Eos*, 88, 293-300.

Sigman, D.M., and E.A. Boyle (2000), Glacial/interglacial variations in atmospheric carbon dioxide, *Nature,* 407, 859-869.

Snowball, I., and R. Muscheler (2007), Palaeomagnetic intensity data: an Achilles heel of solar activity reconstructions, *Holocene,* 17(6), 851-859, doi:10.1177/0959683607080531.

Stoner, J.S. And G. St-Onge (2007), Magnetic stratigraphy: Reversals, excursions, paleointensity and secular variation, in *Development in Marine Geology: Volume 1, Proxies in Late-Cenezoic Paleoceanography,* Edited by Hillaire-Marcel, C., and A. de Vernal, pp. 99-138.

Chapter 2

The flooding of Beringia and North Pacific Intermediate Water formation

M.H. Davies, A.C. Mix, J.S. Stoner, J.R. Southon, M. Cheseby, C. Xuan

Science

In Preparation

2.1 Abstract

Here we reconstruct Northeast Pacific paleoventilation over the last 17,000 ybp from radiocarbon in a sediment core 682 m deep on the Southeast Alaska margin. Alternate age models are based on 1) calibrated planktonic foraminiferal radiocarbon dates with fixed surface-ocean reservoir ages of 880 ± 80 yr, 2) fixed benthic reservoir ages at their modern value of 1390 ± 100 yr and 3) correlation of $\delta^{18}O$ in planktonic foraminifera (*N. pachyderma sinistral*) to $\delta^{18}O$ in a layer-counted Greenland ice core (NGRIP). Age model 2 yields implausible negative reservoir ages for planktonic foraminifera, and is rejected. Age model 3 reproduces the extremely old intermediate waters previously inferred off Baja California (*Marchitto et al*., 2007), but also yields covarying reservoir ages for planktonic foraminifera of >2,500 years, implying that subsurface ventilation anomalies are an artifact of age model tuning. Under age model 1, intermediate water reservoir ages increased to 2,670 ± 180 during Termination 1, implying low ventilation prior to the Holocene. A shift to lower ventilation ages at ~10,500 ybp is coeval with flooding of Beringia and opening of the Bering Strait, suggesting that flooded shelves and net export of low-salinity surface waters enhanced ventilation of the North Pacific.

2.2 Introduction

Increases in atmospheric CO_2 content during the last deglaciation (Termination 1, ~19,000-11,000 ybp) were accompanied by a decrease in atmospheric $\Delta^{14}C$, apparently unsupported by abrupt changes in ^{14}C production rate (*Hughen et al*., 2006; *Broecker and Barker*, 2007). An increase in the ventilation (the rate of gas exchange between the interior ocean and the deep sea) of abyssal waters, releasing CO_2 stored in the deep sea, is frequently invoked to explain the apparent introduction of aged carbon to the atmosphere (*Toggweiler*, 1999; *Sigman and Boyle*, 2000; *Stephens and Keeling*, 2000; *Monnin et al.*, 2001; *Skinner and Shackelton*, 2004; *de Boer et al*., 2007; *Marchitto et al.*, 2007; *Keeling*, 2007; *Pena et al*., 2008; *Stott et al*., 2009; *Bryan et al*., 2010; *Basak et al*., 2010; *Skinner et al*., 2010). Evidence of two discrete events of ^{14}C-depletion some parts of the intermediate depth Indo-Pacific concomitant with abrupt rises in atmospheric CO_2 (*Marchitto et al.*, 2007; *Stott et al*., 2009; *Bryan et al*., 2010; *Basak et al*., 2010) is consistent with a release of aged CO_2 from the deep sea, presumably around Antarctica, followed by redistribution in the upper ocean via Antarctic Intermediate Water (AAIW). However, attempts to find the old source waters in the deepest ocean have been equivocal (*Broecker and Clark*, 2010), and no evidence is found for these events in AAIW near its southern source (*De Pol-Holz* et al., 2010; *Rose et al.*, 2010).

The two most common approaches to reconstructing paleoventilation are: 1) paired benthic-planktic foraminiferal dates placed on a planktic chronology, assuming constant surface reservoir age (e.g. *Broecker et al., 1990; Kennet and Ingram*, 1995; *Van Geen*, 1996; *Mix et al*., 1999; *Keigwin*, 2002; *McKay et al*., 2005; *Broecker et al.*, 2008) and 2) benthic foraminiferal ^{14}C anomalies, placed on a chronology derived by correlation of some measure of local climate change to the layer-counted $\delta^{18}O$ record of the Greenland ice cores (e.g. *Marchitto et al.*, 2007; *Bryan et al.*, 2010), projected to the atmospheric $\Delta^{14}C$ history. Here we employ the projection method, but evaluate three different age model assumptions based on correlation, planktonic ^{14}C, and benthic ^{14}C, to assess the range of possible interpretations.

2.3 Methods

We analyzed 39 pairs of benthic and planktonic foraminiferal radiocarbon measurements (Table 2.1), and 177 analyses of $\delta^{18}O$ and $\delta^{13}C$ (*Davies et al.*, 2011), measured at an average sample interval of 5 cm in jumbo piston core EW0408-85JC (59°33.32′ N, 144°9.21′ W, 682 m water depth), from the Gulf of Alaska continental slope (Figure 2.1). This core includes clear lithologic evidence of the glacial/interglacial transition, with a basal unit composed of glacial-marine diamict overlain by laminated hemipelagic muds. Average post-glacial sedimentation rates are ~56 cm/kyr (*Davies et al.*, 2011).

Benthic and planktonic foraminifera were picked from the >150 μm sediment fraction. The two predominant planktonic species for the site, *N. pachyderma* (sinistral) and *G. bulloides*, were analyzed separetely at 555 centimeters below sea-floor (cmbsf), with the resultant *N. pachyderma* age being 65 ± 50 years greater than that for the *G. bulloides* (*Davies et al.*, 2011). As this difference approximates the measurement uncertainty for the individual samples, for all other depths the species were combined to increase sample size and reduce analytical error. Benthic foraminiferal ^{14}C analyses were run on mixed species, although care was taken to avoid agglutinated and deep-infaunal species. Radiocarbon analyses were performed at the UC Irvine Keck AMS facility (Figure 2.2).

Age Model 1 was derived by calibrating radiocarbon dates from planktic foraminiferal samples using the Marine04 $\Delta^{14}C$ reconstruction (*Hughen et al*., 2004) in CALIB 5.0.1 (*Stuiver et al.*, 2005) (Table 2.1, Figures 2.3 and 2.4). Assuming constant surface-ocean reservoir ages of 880 ± 80 (*McNeely et al*., 2006), a ΔR of 470 ± 80 yr was applied to all raw planktic radiocarbon dates. In the high-sedimentation rate interval of the late Pleistocene, we used a linear best fit through the dates that increased with depth (Figure 2.3). This compromise falls within the 1σ uncertainties of all but one of the calibrated dates in this sedimentary unit, as outlined in *Davies et* *al.*, (2011). Age Model 2 employed a similar strategy to benthic foraminiferal dates, with a constant ΔR of 980 ± 100 yr (Table 2.1, Figures 2.3 and 2.4). Age Model 3 was derived by assigning ages to the core top and bottom with calibrated planktic foraminiferal radiocarbon dates, then correlating $\delta^{18}O$ in *N. pachyderma sinistral* to the NGRIP Greenland ice core $\delta^{18}O$ record on the GICC05 chronology (Figure 2.4) (*Rasmussen et al.,* 2006). We defined six correlation tie points, equivalent to those used to date Baja California core MV99 GC31/PC08 (*Marchitto et al.,* 2007) (Table 2.2 and Figure 2.4). Errors for the tie points in Age Model 3 reflect the resolution of the EW0408-85JC stable isotope record, as well as the errors on the layer-counted GICC05 chronology. A Monte Carlo approach (1000 simulations) was then applied to generate a 1-σ error envelope for the entire age-depth model (Table 2.1; Figure 2.3).

We calculated $\Delta^{14}C$ values from raw benthic radiocarbon dates for the Age Model 1 and 3 scenarios (*Stuiver and Polach,* 1977; Figure 2.5), as well as from the raw planktic radiocarbon dates as a test of calibrated-benthic Age Model 2 (Figure 2.6). Apparent ventilation ages are calculated by projecting decay curves back to the INTCAL04 atmospheric $\Delta^{14}C$ reconstruction *(Reimer et al.,* 2004*),* following common practice (Adkins and Boyle, 1997*)* (Figure 2.7). We perform the same analysis on data from site MV99-GC31/PC08 (*Marchitto et al.,* 2007), to allow for direct comparison.

2.4 Results and Discussion

Age Model 2 implies negative reservoir ages for planktonic foraminifera during the deglaciation, and is rejected on that basis (Figure 2.6). Compared to modern ventilation ages of 1390 ± 100 yr, Age Model 1 yields mean benthic ventilation ages for Holocene time (<10,000 cal ybp) of 1,740 ± 210 yr, and of 2,070 ±

200 yr for the interval prior to 10,000 cal ybp (Figure 2.8). Within the older interval, relatively high apparent benthic ventilation ages (i.e., >2000 yr) occur during the intervals >16,000 cal ybp (a time of local glaciation), ~14,000 cal ybp (after retreat of local marine glaciers onto land), ~12,000 cal ybp (within the Younger Dryas interval) and near 10,300 cal ybp (within the earliest Holocene). The greatest apparent benthic ventilation age, 2,670 ± 180 yr, occurs at 12,210 ± 170 cal ybp and coincides with anomalously high benthic-planktonic ^{14}C age differences. The youngest radiocarbon-dated benthic sample, at 190 ± 190 cal ybp, yields the lowest apparent benthic ventilation age of the record: 1,190 ± 260 cal ybp, consistent with modern watercolumn values nearby, on a similar density horizon (1,390 ± 100 yr) (*Sabine et al.,* 2005).

In Age Model 3, correlation to Greenland Ice Core $\delta^{18}O$ produces two distinct intervals of high apparent benthic ventilation age (Figure 2.8). The older and larger event indicates an increase in intermediate-water ventilation age to ≥ 3000 yr between 15,920 ± 140 and 14,810 ± 70 cal ybp, and peaking at 3,630 ± 80 years at 15,090 ± 70 ybp. In the younger event, apparent benthic ventilation ages were >2,500 yr between 13,480 ± 270 and 12, 370 ± 190 cal ybp, with a peak of 2,900 ± 250 yr at 12,840 ± 240 cal ybp. These inferred ventilation age anomalies are similar in both timing and amplitude to those inferred off Baja California from an age model tuned to $\delta^{18}O$ in the Greenland GISP2 ice core (*Marchitto et al.,* 2007; Figures 2.7 and 2.8).

Based on Age Model 3, the plantkonic foraminifera ^{14}C data also produce anomalously high near-surface water ventilation ages, approaching 3000 years during the older of the two events. It is tempting to infer that these episodes of apparently high ventilation age in both planktonic and benthic foraminifera at our Gulf of Alaska site reflect the transfer of aged deep ocean water to the upper ocean, as inferred in benthic foraminifera off Baja California and Oman. (*Marchitto et al.*, 2007*, Bryan et al.,* 2010). If correct, this inference would imply that the aged watermass spread in essentially unaltered form as far as the high North Pacific, and vented to the atmosphere here, contributing to the abrupt drop in atmospheric $\Delta^{14}C$ observed during Termination 1 (*Broecker and Barker*, 2007*).* However these deglacial ventilation ages for planktonic foraminifera are higher than any ever reported, and the planktonic events have roughly the sample amplitude as the benthic events. The alternate scenario, that planktic reservoir ages were relatively constant, implies that the apparent ventilation age anomalies during deglaciation for both planktonic and benthic foraminifera are an artifact of tuning the age model by correlation to Greenland at just a few discrete points. To evaluate these two options, we consider the implications of the Age Models 1 and 3 for local sedimentation rates as well as the timing of deglacial events in Alaska.

Age model 1 produces accumulation rates in the glacial-marine diamict unit of >500 cm/kyr, an order of magnitude greater than average Holocene sedimentation, with a fall-off in accumulation rates to ~50 cm/kyr by 16,390 ± 215 cal ybp, prior to the end of glacial-marine sedimentation, but coincident with a change in texture, magnetic susceptibility, and $\delta^{18}O$ (Figure 2.9). This gradual decease in sedimentation rate suggests a sequential retreat of the Bering Glacier between ~17,000 and ~15,000 cal ybp, and pull back of the marine glacier onto land by 14,790 ± 380 cal ybp.

In contrast, Age model 3 assumes constant sedimentation rates within the glacial-marine unit (older than ~15,000 cal ybp) and an abrupt reduction in rates from ~180 cm/kyr in the late glacial to ~40 cm/kyr in the Bølling (Figure 2.9). As marine sedimentation rates in the modern marine environment are known to fall off exponentially with distance from ice terminus (*Cowan and Powell,* 1991), Age Model

3 would require an unrealistic geologically-instantaneous glacial retreat, much younger than the dated retreat of Cordilleran ice elsewhere in the region (*Porter and Swanson,* 1998; *Briner et al.,* 2005; *Cosma and Hendy,* 2008).

In both Age Model 1 and 3, the abrupt peak in oxygen-isotope evidence of surface warming and/or freshening and the transition to laminated sedimentation in the core is essentially synchronous with the Bølling warming in the North Atlantic (*Rasmussen et al.,* 2006; Figure 2.4). Significant differences between the age models occur during the Allerød warm interval; Age Model 1 implies surface-ocean cooling (and/or increased salinity) prior to the onset of the Younger-Dryas cool event in the Greenland ice-cores (*Rasmussen et al.,* 2006; Figure 2.4). A similar leading cool event observed in other independently-dated North Pacific isotope records (*Mix et al.,* 1999; *Davies et al.,* 2011; *Ortiz et al.,* 2004; *Cook et al.,* 2005; *Dean et al.,* 2006), and has been inferred as a North Pacific climate oscillation that mimics the Antarctic Cold Reversal (*Mix et al.*, 1999; *Davies et al.*, 2011). Local land-based records are not sufficiently well dated to resolve these events (*Kaufmann et al.*, 2010). If the North Pacific climate does respond to a combination of Northern and Southern Hemisphere drivers, correlation of local deglacial events to Greenland would impose systematic age errors. Assumptions of constant sedimentation rates between age model tie points exacerbate the problem.

Age Model 1 implies an increase in North Pacific intermediate water ventilation age to >2000 years during deglaciation, followed by an abrupt decrease at 10,310 ± 100 cal ybp (Figure 2.8). The timing of this apparent increase in ventilation coincides with flooding of the Beringian continental shelf and opening the connection to the Arctic Oceans via Bering Strait (*Elias et al.,* 1996). Today Dense Shelf Water (DSW), a primary component of well-ventilated North Pacific Intermediate Water

(NPIW) forms in winter, on the Sea of Okhotsk shelf (*Talley,* 1991; *Watanabe and Wakatsuchi,* 1998); northward export of buoyant low salinity surface waters via Bering Strait helps this process by decreasing stratification in the North Pacific (*Warren,* 1873; *Emile-Geay et al.,* 2003).

2.5 Conclusions

We conclude that the extremely high apparent ventilation ages implied by Age Model 3 during the deglacial interval, which co-vary in both benthic and planktonic foraminifera, and resemble those inferred at lower latitudes (*Marchitto et al.,* 2007; *Bryan et al.,* 2010) are likely an artifact of inappropriate age model tuning; they are unsupported by other sedimentological evidence and the timing of regional glacial retreat. We do not find evidence for rapid ventilation in the late glacial interval prior to 15 kyr BP, as has been inferred in the western Pacific based on calibrated planktonic ^{14}C age models similar to our Age Model 1 (*Okazaki et al.,* 2010), implying that such ventilation, if real, did not reach the intermediate waters of the Northeast Pacific. Based on Age Model 1, our inference of modest increases in ventilation ages during late glacial time relative to modern are consistent with previous findings of greater watercolumn stratification resulting from closure of Bering Strait (*Zahn et al*. 1991; *Sigman et al*, 2004). We conclude that the substantial retreat of Cordilleran ice, opening of Bering Strait as a gateway for northward export of low-salinity surface waters, and flooding of the Beringian shelf by ~10,300 cal yr BP conditioned the North Pacific for more effective ventilation of intermediate water during Holocene time.

2.6 Acknowledgements

The authors gratefully acknowledge the crew and sampling party of cruise EW0408-85JC, Jennifer McKay, Andy Ross, and the OSU Stable Isotope Facility, Bobbi Conard, Mysti Weber, and the OSU Marine Geology Repository, and John Southon and the staff of the UCI Keck AMS laboratory. We thank Ann Morey-Ross, Jessie Muratli, Sarah Strano, and Summer Praetorious for assistance with the radiocarbon dating. This work was funded by National Science Foundation Paleoclimate Grant ATM-0602395 to ACM, National Science Foundation Geophysics Grant EAR-0711584 to JSS and ACM, and National Science Foundation Ocean Drilling Grants OCE-0242084 to ACM and OCE-0351096 to JJ, BF, and JSS.

2.7 References

Adkins, J.F., and E.A. Boyle (1997), Changing atmospheric $\Delta^{14}C$ and the record of deep water paleoventilation ages, *Paleoceanography,* 12, 337-344.

Basak, C., E.E. Martin, K. Horikawa, and T. Marchitto (2010), Southern Ocean source of ^{14}C-depleted carbon in the North Pacific Ocean during the last deglaciation, *Nature Geoscience,* 3, 770-773.

Briner, J.P., D.S. Kaufman, W.F. Manley, R.C. Finkel, and M.W. Caffee (2005), Cosmogenic exposure dating of late Pleistocene moraine stabilization in Alaska, *Geological Society of America Bulletin*, doi: 10.1130/B25649.1

Broecker, W. (2009), The mysterious ^{14}C decline, *Radiocarbon,* 51, 109-119.

Broecker, W., and S. Barker (2007), A 190‰ drop in atmosphere's Δ14C during the 'Mystery Interval' (17.5–14.5 kyr), *Earth and Planetary Science Letters*, 256, 90-99.

Broecker, W., and E. Clark (2010), Search for a glacial-age ^{14}C-depleted ocean reservoir, *Geophysical Research Letters*, 37, LI3606, doi:10.1029/2010GL043969.

Broecker, W., T-H. Peng, S. Trumbore, G. Bonani (1990), The distribution of radiocarbon in the glacial ocean, *Global Biogeochemical Cycles,* 4, 103-117.

Broecker, W., E. Clark, and S. Barker (2008), Near constancy of the Pacific Ocean surface to mid-depth radiocarbon age difference over the last 20 kyr, *Earth and Planetary Science Letters,* 274, 322-326.

Bryan, S.P., T.M. Marchitto, and S.J. Lehman (2010), The release of ^{14}C-depleted carbon from the deep ocean during the last deglaciation: Evidence from the Arabian Sea, *Earth Planetary Science Letters,* 298, 244-254.

Cook, M.S., L.D. Keigwin, and C.A. Sancetta (2005), The deglacial history of surface and intermediate water of the Bering Sea, *Deep-Sea Research II*, 52, 2163-2173.

Cosma, T. and I.L. Hendy (2008), Pleistocene glacimarine sedimentation on the continental slope off Vancouver Island, British Columbia, *Marine Geology*, 255, 45-54.

Cowan, E.A. and R.D. Powell (1991), Ice-proximal sediment accumulation rates in a temperate glacial fjord, southeastern Alaska, in *Glacial Marine Sedimentation: Paleoclimatic Significance,* edited by J.B. Anderson and G.M. Ashley, *Geological Society of America Special Paper*, 261, 61–73.

Davies, M.H., A. C. Mix, J.S. Stoner, J.A. Addison, J. Jaeger, B. Finney, and J. Wiest (2011), The deglacial transition on the Southeastern Alaska Margin: meltwater input, sealevel rise, marine productivity, and sedimentary anoxia, *Paleoceanography*, in press.

Davies, M.H., J.S. Stoner, A.C. Mix, J. Jaeger, G.P. Rosen, J. Southon, J. Channell, C. Xuan (*in prep*), A 17,000 year paleomagnetic secular variation record from the Gulf of Alaska, *Geophysics, Geochemistry, Geosystems (G3).*

Dean, W.E., Y. Zheng, J.D. Ortiz, and A. van Geen (2006), Sediment Cd and Mo accumulation in the oxygen-minimum zone off western Baja California linked to global climate over the past 52kyr, *Paleoceanography*, 21, PA4209, doi:10.1029/2005PA001239.

de Boer, A.M., D. M. Sigman, J.R. Toggweiler, and J.L. Russell (2007), Effect of global ocean temperature on deep ocean ventilation, *Paleoceanography,* 22**,** PA2210, doi:10.1029/2005PA001242.

De Pol-Holz, R., L. Keigwin, J. Southon, D. Hebbeln, and M. Mohtadi (2010), No signature of abyssal carbon in intermediate waters off Chile during deglaciation, *Nature Geoscience,* 3, 192-195.

Elias, S.A., S.K. Short, C.H. Nelson, and H.H. Birks (1996), Life and times of the Bering land bridge, Nature, 382, 60-63.

Emile-Geay, J., M.A. Cane, N. Naik, R. Seager, A.C. Clement, and A. van Geen (2003), Warren revisited: Atmospheric freshwater fluxes and "Why is no deep water formed in the North Pacific", *Journal of Geophysical Research*, 108, 3178, doi:10.1029/2001JC001058.

Fischer, H., J. Schmitt, D. Lüthi, T.F. Stocker, T. Tschumi, P. Parekh, F. Joos, P. Köhler, C. Völker, R. Gersonde, C. Barbante, M. Le Floch, D. Raynaud, and E. Wolff (2010), The role of Southern Ocean processes in orbital and millennial CO_2 variations - A synthesis, *Quaternary Science Reviews, 29,* 193-205.

Hughen K.A., M.G.L. Baillie, E. Bard, J.W. Beck, C.J.H. Bertrand, P.G. Blackwell, C.E. Buck, G.S. Burr, K.B. Cutler, P.E. Damon, R.L. Edwards, R.G. Fairbanks, M. Friedrich, T.P. Guilderson, B. Kromer, G. McCormac, S. Manning, C.B. Ramsey, P.J. Reimer, R.W. Reimer, S. Remmele, J.R. Southon, M. Stuiver, S. Talamo, F.W. Taylor, J. van der Plicht, and C.E. Weyhenmeyer (2004), Marine04 marine radiocarbon age calibration, 0-26 cal kyr B,. *Radiocarbon,* 46**,** 1059-1086.

Hughen, K., J. Southon, S. Lehman, C. Bertrand, and J. Turnbull (2006), Marine-derived ^{14}C calibration and activity record for the past 50,000 years updated from the Cariaco Basin, *Quaternary Science Reviews,* 25, 3216–3227.

Kaufman, D.S., R.S. Anderson, F.S. Hu, E. Berg, and A. Werner (2010), Evidence for a variable and wet Younger Dryas in southern Alaska, Quaternary Science Reviews 29, 1445-1452.

Keeling, R.F. (2007), Deglaciation mysteries, *Science*, 316, 1440-1441.

Keigwin, L.D. (2002), Late Pleistocene-Holocene paleoceanography and ventilation of the Gulf of California, *Journal of Oceanography*, 58, 421-432.

Kennett, J.P., and B. L. Ingram (1995), A 20,000-year record of ocean circulation and climate change from the Santa Barbara basin, *Nature*, 377, 510-514.

Marchitto, T.M., S.J. Lehman, J.D. Ortiz, J. Flückiger, and A. van Geen (2007), Marine radiocarbon evidence for the mechanisms of deglacial atmospheric CO_2 rise, *Science*, 316, 1456-1459.

Matsumoto, K., T. Oba, J. Lynch-Stieglitz, and H. Yamamoto (2005), Interior hydrography and circulation of the glacial Pacific Ocean, *Quaternary Science Reviews,* 21, 1693-1704.

McKay, J.L., T. F. Pedersen, and J. Southon (2005), Intensification of the oxygen minimum zone in the northeast Pacific off Vancouver Island during the last deglaciation: Ventilation and/or export production?, *Paleoceanography*, 20, PA4002, doi:10.1029/2003PA000979.

McManus, J.F., R. Francois, J.-M. Gherardi, L.D. Keigwin, and S. Brown-Leger (2004), Collapse and rapid resumption of Atlantic meridional circulation linked to deglacial climate changes, *Nature,* 428, 834-837.

McNeely, R., A.S. Dyke, and J.R. Southon (2006), Canadian marine reservoir ages, preliminary data assessment, *Geological Survey Canada* Open File 5049, 3.

Mix, A.C., D.C. Lund, N.G. Pisias, P. Bodén, L. Bornmalm, M. Lyle, and J. Pike (1999),
Rapid climate oscillations in the Northeast Pacific during the last deglaciation reflect Northern and Southern Hemisphere sources, in *Mechanisms of global climate change at millennial time scales, American Geophysical Union*, edited by P.U. Clark et al.,

Geophysical Monograph 112, pp. 127-148.

Monnin, E., A. Indermühle, A. Dällenbach, J. Flückiger, B. Stauffer, T.F. Stocker, D. Raynaud, and J.-M. Barnola (2001), Atmospheric CO_2 concentrations over the Last Glacial Termination, *Science,* 291, 112–114.

Okazaki, Y., A. Timmermann, L. Menviel, N. Harada, A. Abe-Ouchi, M.O. Chikamoto, A. Mouchet, and A. Asahi (2010), Deepwater formation in the North Pacific during the Last Glacial Termination, *Science*, 329, 200-204.

Ortiz, J.D., S.B. O'Connell, J. Del Viscio, W. Dean, J.D. Carriquiry, T. Marchitto, Y. Zheng, and A. van Geen (2004), Enhanced marine productivity off western North America during warm climate intervals of the past 52 k.y., *Geology*, 32, 521-524.

Paillard, D., L. Labeyrie, and P. Yiou (1996), Macintosh program performs time-series analysis, *Eos Transactions,* 77, 379.

Peltier, W.R. (1994), Ice age paleotopography, *Science,* 265, 195-201.

Pena, L.D., I. Cacho, P. Ferretti, and M.A. Hall (2008), El Ninõ/Southern Oscillation-like variability during glacial terminations and interlatitudinal teleconnections, *Paleoceanography,* 23, PA3101, doi:10.1029/2008PA001620.

Porter, S. C. (1989), Late Holocene fluctuations of the fiord glacier system in Icy Bay, Alaska, U. S. A., *Arctic and Alpine Research,* 21, 364–379.

Porter, S.C. and T.W. Swanson (1998), Radiocarbon age constraints on rates of advance and retreat of the Puget Lobe of the Cordilleran Ice Sheet during the Lat Glaciation, *Quaternary Research*, 50, 205-213.

Primeau, F.W. and M. Holzer (2005), The ocean's memory of the atmosphere: residence-time and ventilation-rate distributions of water masses, *Journal of Physical Oceanography,* 36*,* 1439-1456.

Rasmussen, S.O., K.K. Andersen, A.M. Svensson, J.P. Steffensen, B.M. Vinther, H.B. Clausen, M.-L. Siggard-Andersen, S.J. Johnson, L.B. Larsen, D. Dahl-Jensen, M. Bigler, R. Röthlisberger, H. Fischer, K. Goto-Azuma, M.E. Hansson, and U. Ruth (2006), A new Greenland ice core chronology for the last glacial termination, *Journal of Geophysical Research,* 111**,** D06102, doi:10.1029/2005JD006079.
Reimer, P.J., M.G.L. Baillie, E. Bard, A. Bayliss, J.W. Beck, C.J.H. Bertrand, P.G. Blackwell, C.E. Buck, G.S. Burr, K.B. Cutler, P.E. Damon, R.L. Edwards, R.G. Fairbanks, M. Friedrich, T.P. Guilderson, A.G. Hogg, K.A. Hughen, B. Kromer, G. McCormac, S. Manning, C.B. Ramsey, R.W. Reimer, S. Remmele, J.R. Southon, M. Stuiver, S. Talamo, F.W. Taylor, J. van der Plicht, and C.E. Weyhenmeyer (2004), IntCal04 terrestrial radiocarbon age calibration, 0-26 cal kyr BP, *Radiocarbon*, 46, 1029-1058.

Rose, K. A., E.L. Sikes, T.P. Guilderson, P. Shane, T.M. Hill, R. Zahn, and H.J. Spero (2010), Upper-ocean-to-atmosphere radiocarbon offsets imply fast deglacial carbon dioxide release, *Nature*, 466, 1093-1097.

Sabine, C.L., R.M. Key, A. Kozyr, R.A. Feely, R. Wanninkhof, F.J. Millero, T.-H. Peng, J.L. Bullister, and K. Lee (2005), Global ocean data analysis project: Results and data, *Rep. ORNL/CDIAC-145/NDP-083*, Carbon Dioxide Inf. Anal. Cent., Oak Ridge Natl. Lab., U.S. Dep. of Energy, Oak Ridge, Tenn.

Sigman, D.M., and E.A. Boyle (2000), Glacial/interglacial variations in atmospheric carbon dioxide, *Nature,* 407, 859-869.

Sigman, D. M., S.L. Jaccard, and G.H. Haug (2004), Polar ocean stratification in a cold climate. *Nature*, 428, 59-63

Skinner, L.C., S. Fallon, C. Waelbroeck, E. Michel, and S. Barker (2010), Ventilation of the deep southern ocean and deglacial CO_2 rise, *Science,* 328, 1147-1151.

Skinner, L.C., and N.J. Shackleton (2004), Rapid transient changes in northeast Atlantic deep water ventilation age across Termination 1, *Paleoceanography,* 19, PA2005, doi:10.1029/2003PA000983.
Stott, L.D. (2010), No signs of Southern Ocean CO_2, *Nature Geoscience,* 3, 153-154.

Stephens, B.B., and R. F. Keeling (2000), The influence of Antarctic sea ice on glacial-interglacial CO_2 variations, *Nature,* 404**,** 171-173.

Stott, L., J. Southon, A. Timmermann, and A. Koutavas (2009), Radiocarbon age anomaly at intermediate water depth in the Pacific Ocean during the last deglaciation, *Paleoceanography,* 25, PA2223, doi:10.1029/2008PA001690.

Stuiver, M., and H.A. Polach (1977), Discussion: Reporting of ^{14}C data, *Radiocarbon,* 19, 355-363.

Stuiver, M., and T.F. Braziunas (1993), Modelling atmospheric ^{14}C influences and ^{14}C ages of marine samples to 10,000BC, *Radiocarbon,* 35, 137-189.

Stuiver, M., P.J. Reimer, and R. Reimer (2005), CALIB 5.0. [http://calib.qub.ac.uk/calib/].

Talley, L.D. (1991), An Okhotsk Sea water anomaly: implications for ventilation in the North Pacific, *Deep-Sea Research Part A,* 38, S171–S190.

Thiele, G., and J.L. Sarmiento (1990), Tracer dating and ocean ventilation, *Journal of Geophysical Research,* 95, 9377-9391.

Toggweiler, J.R. (1999), Variation of atmospheric CO_2 by ventilation of the ocean's deepest water, *Paleoceanography,* 14**,** 571-588.

van Geen, A., R.G. Fairbanks, P. Dartnell, M. McGann, J.V. Gardner, and M. Kashgarian (1996), Ventilation changes in the northeast Pacific during the Last Deglaciation, *Paleoceanography*, 11, 519-528.

Warren, B.A. (1983), Why is no deep water formed in the North Pacific?, *Journal of Marine Research*, 41, 327-347.

Watanabe, T., and M. Wakatsuchi (1998), Formation of 26.8–26.9 $\sigma\theta$ water in the Kuril Basin of the Sea of Okhotsk as a possible origin of North Pacific Intermediate Water, *Journal of Geophysical Research,* 103(C2), 2849–2865.

Zahn, R., T.F. Pedersen, B.D. Bornhold and A.C. Mix (1991), Water mass conversion in the glacial subarctic Pacific (54°N, 148°W). Physical constraints and the benthic-planktonic stable isotope record. *Paleoceanography*, 6, 543-560.

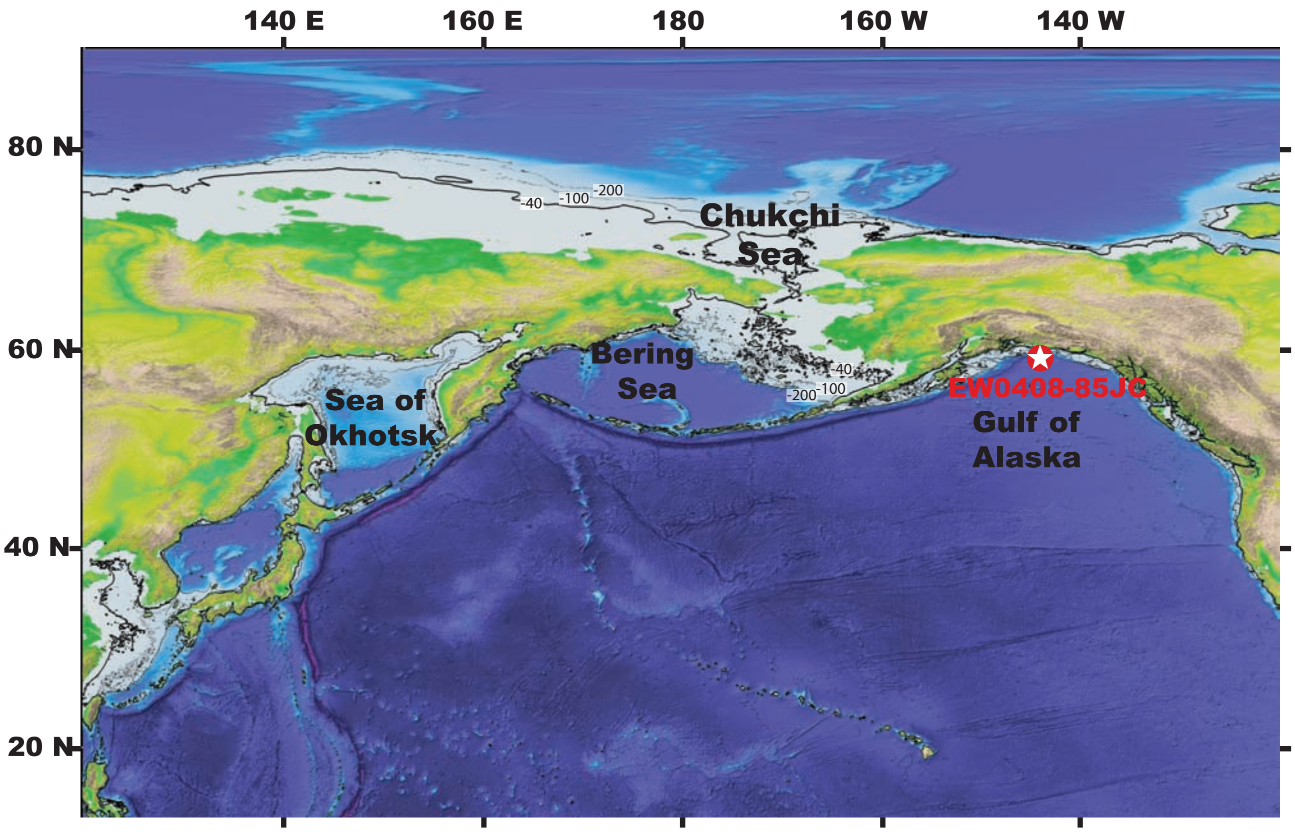

Figure 2.1 – Site map, showing location of jumbo piston core EW0408-85JC on the Southeastern Alaska margin. Bathymetry contours indicates -200 m (gray), -100 m (gray), and -40 m (black).

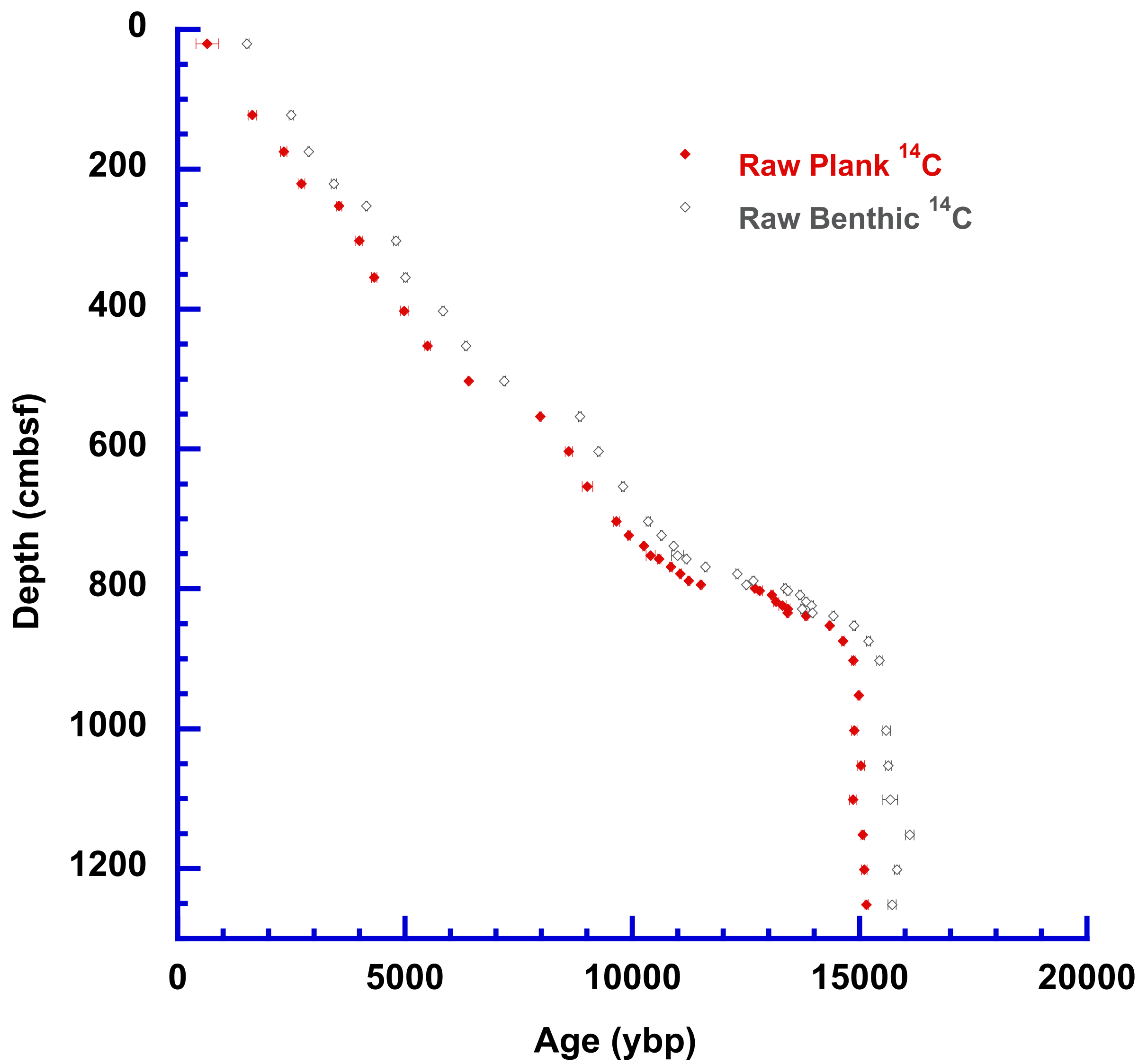

Figure 2.2 – Raw planktic (red diamonds) and benthic (blue diamonds) radiocarbon dates versus depth in core, plotted with 1-σ measurement error. Vertical resolution is ≤ 2 cm for all samples, and error bars fall within symbol size.

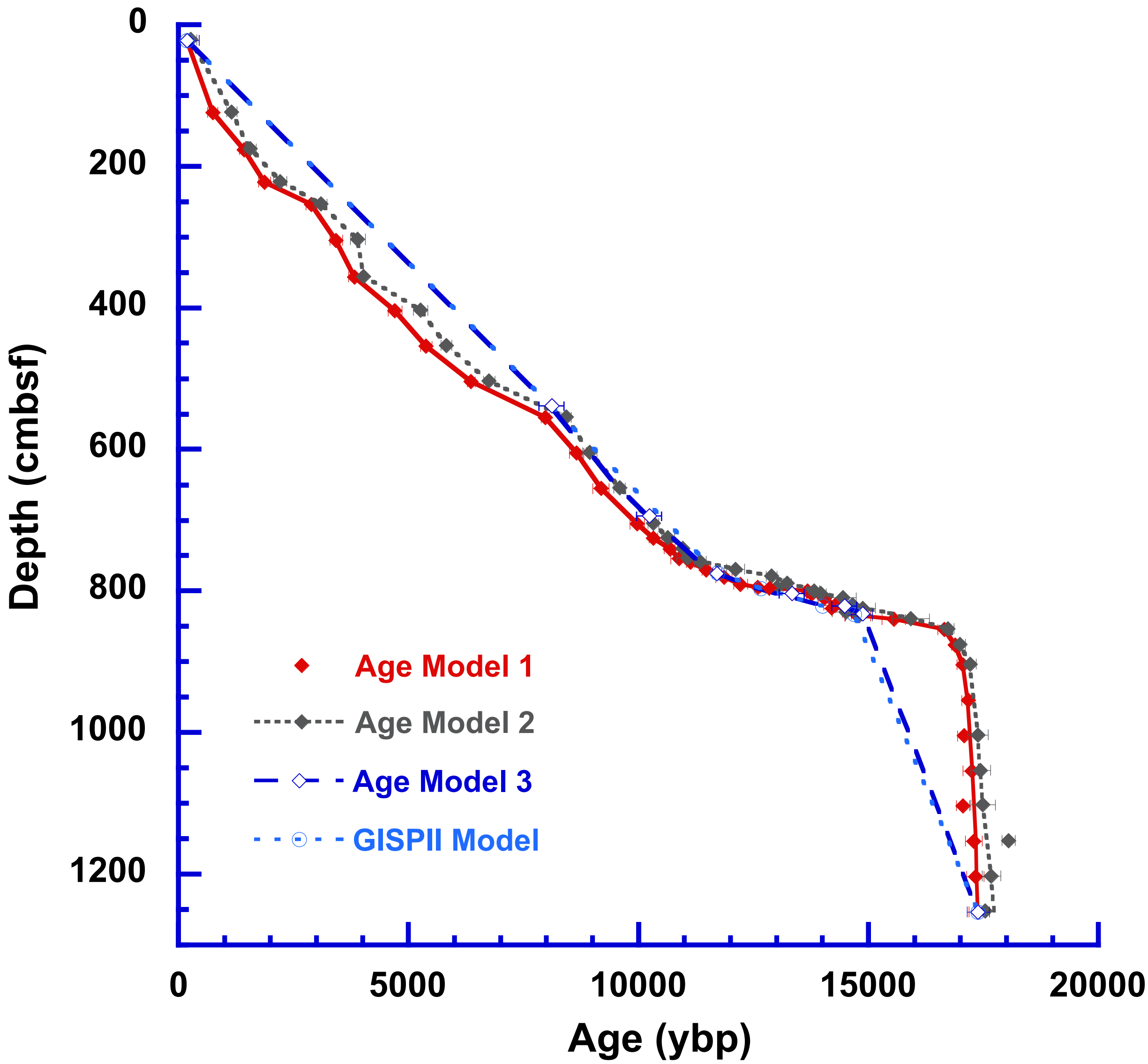

Figure 2.3 – Age-depth relationships given by calibrated planktic Age Model 1 (solid red line), calibrated benthic Age Model 2 (solid gray line), and NGRIP-tuned Age Model 3 (solid dark blue line), as well as from an alternative age model tuned to the GISPII ice core (dashed light blue line). Calibrated planktic (red diamonds) and benthic (blue diamonds) dates are shown with 1-σ errors for Age Models 1 and 2 respectively. Tie points used in generating Age Model 3 (solid blue diamonds) and the GISPII-tuned (hollow blue diamonds) age model, with estimated 1-σ errors, are also shown.

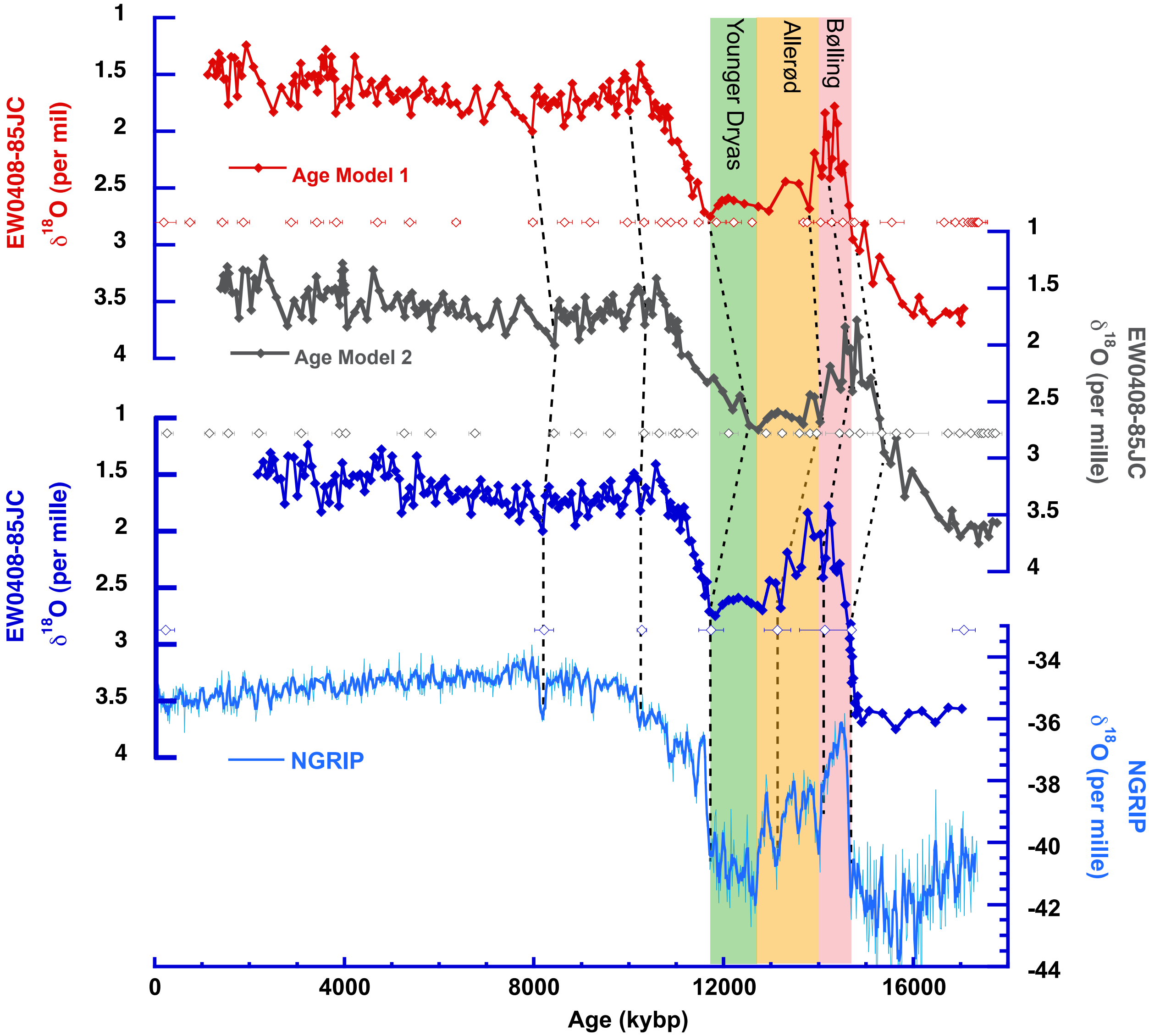

Figure 2.4 – EW0408-85JC *N. pachyderma* left-coiling $\delta^{18}O$ on Age Model 1 (solid red diamonds), Age Model 2 (solid gray diamonds), and Age Model 3 (solid blue diamonds). Dashed lines show temporal relationship between deglacial isotopic features on the different age models and the Bølling, Allerød, and Younger-Dryas climate events of the North Atlantic as expressed in NGRIP on the GICC05 timescale (dark blue line; Rasmussen et al., 2004). Age control points with 1-σ errors are shown for each age model. Age Model 1 is constrained by calibrated planktonic foraminiferal dates with a constant ΔR of 470 ± 80 yr (hollow red diamonds), Age Model 2 is constrained by calibrated benthic foraminiferal dates with a constant ΔR of 980 ± 100 yr (hollow gray diamonds), and Age Model 3 is constrained by 4 tie-points to NGRIP Greenland $\delta^{18}O$, similar to those used by Marchitto et al., (2007) (see Table 2S), with the top and bottom of the core pinned by calibrated planktic radiocarbon dates (hollow blue diamonds).

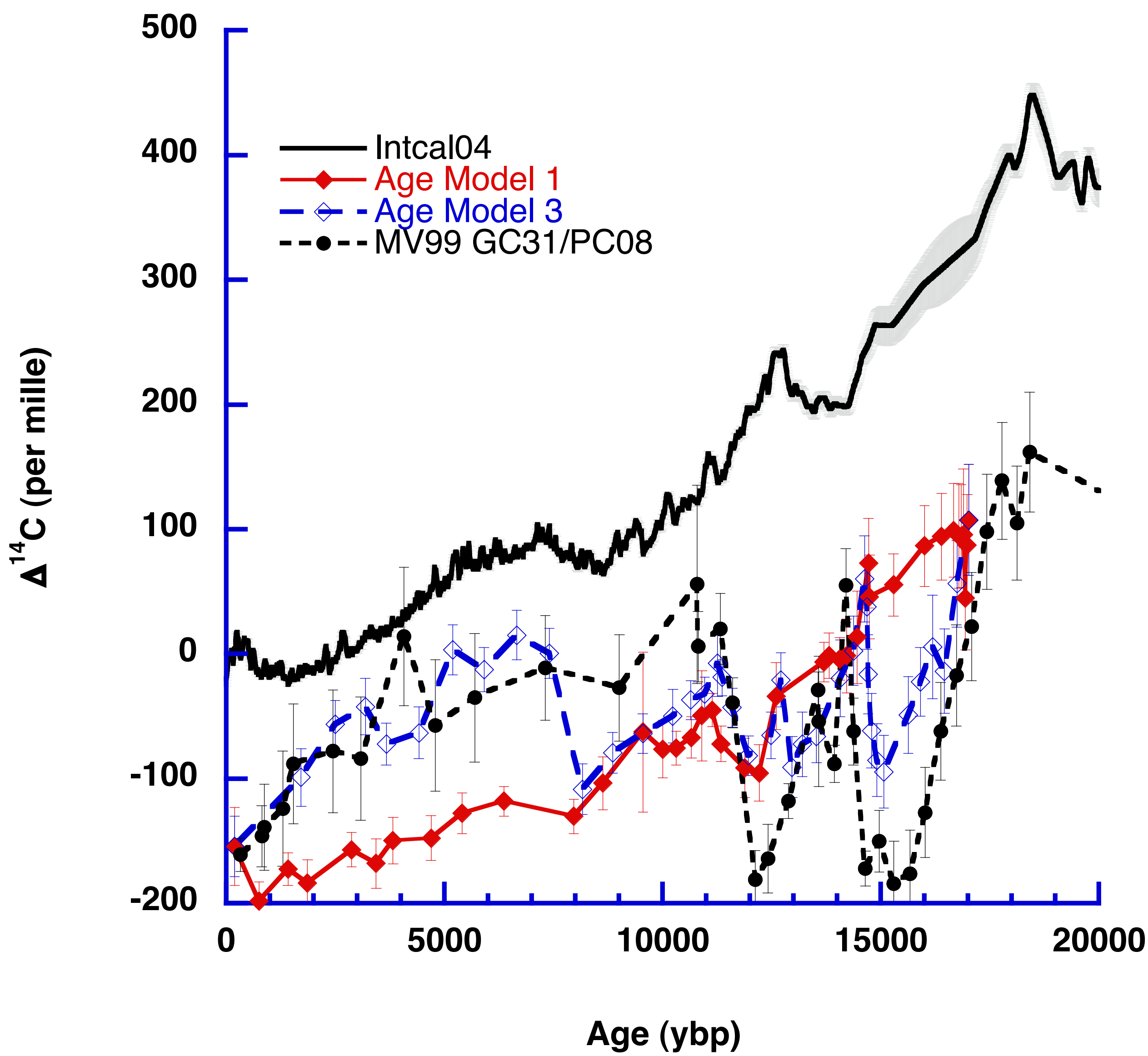

Figure 2.5 - $\Delta^{14}C$ deep values for Age Model 1 (red solid diamonds) and 3 (blue hollow diamonds), compared to results from MV99 GC31/PC08 (black solid circles; Marchitto et al., 2007), and atmospheric radiocarbon calibration dataset Intcal04 (solid black line). Plotted error bars are 1σ.

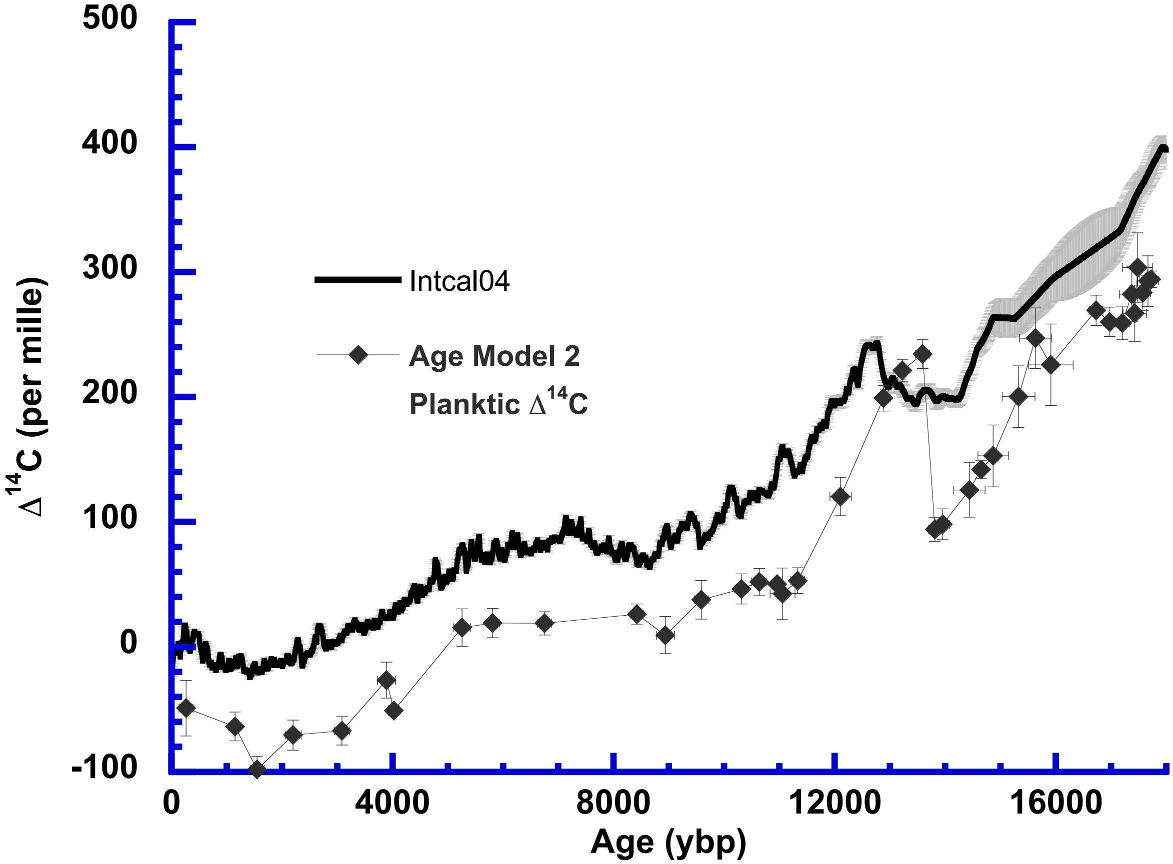

Figure 2.6 - $\Delta^{14}C$ planktic reservoir ages given by calibrated benthic Age Model 2 (black diamonds), compared to atmospheric radiocarbon calibration dataset Intcal04 (solid black line). Error bars shown are 1σ.

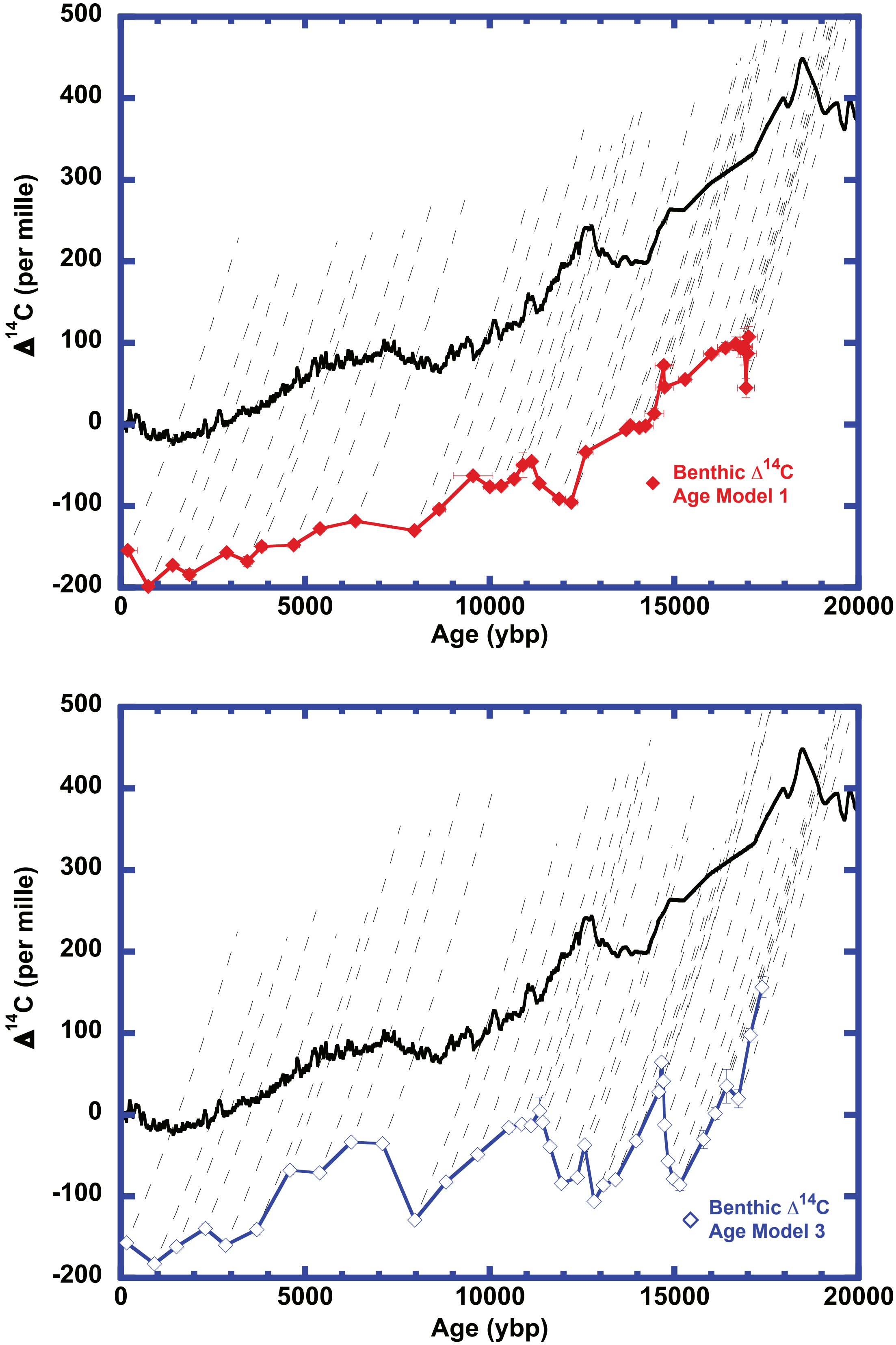

Figure 2.7 – The Δ14C values calculated from benthic foraminifera radiocarbon dates using a) Age Model 1 (solid red diamonds) and b) Age Model 3 (hollow blue diamonds), plotted with 1-σ error bars. The Intcal04 atmospheric radiocarbon calibration curve (black) is shown on both panels. Dashed lines indicate the radiocarbon decay path, used to calculate projection age values.

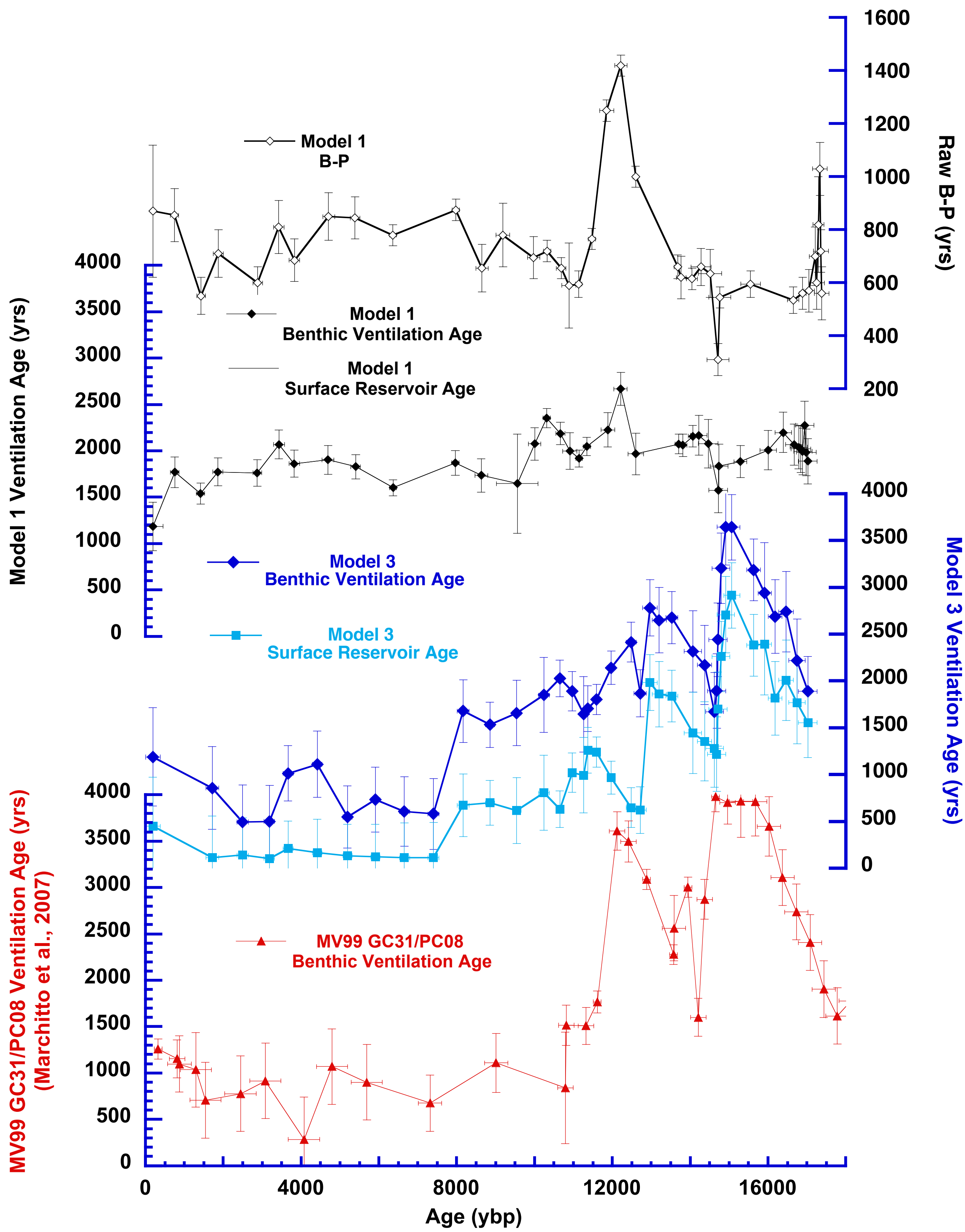

Figure 2.8 – Benthic less planktic foraminiferal radiocarbon ages (gray hollow diamonds), benthic reservoir ages reconstructed via the projection age method using Age Model 1 (black circles), surface and benthic reservoir ages reconstructed from Age Model 2 (light blue squares, dark blue circles), compared to results from MV99 GC31/PC08 (Marchitto et al., 2007) (red triangles).

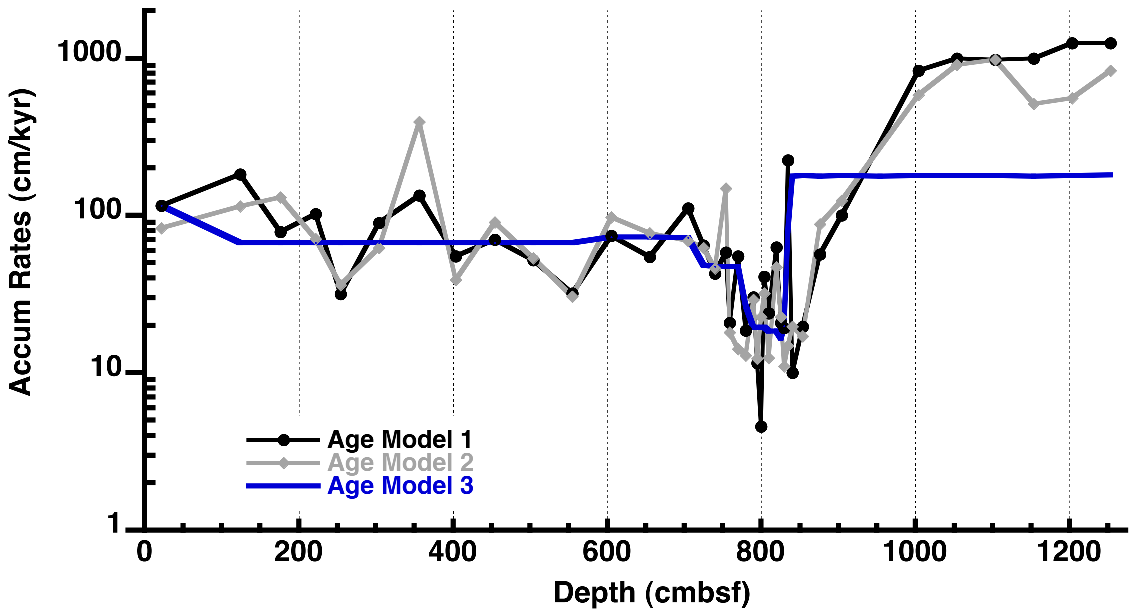

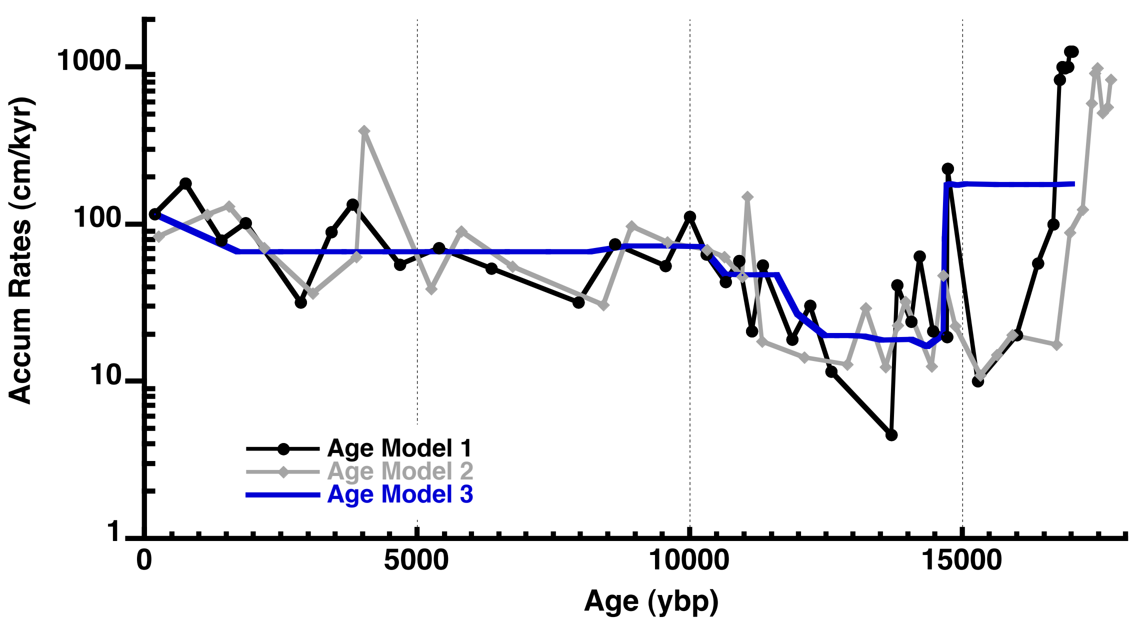

Figure 2.9 – Accumulation rates versus depth (a) and age (b) implied by Age Model 1 (black line w/circles), Age Model 2 (gray line w/circles), and Age Model 3 (blue line).

Table 2.1: Tie points used in EW0408-85JC Age Model 3

EW0408-85JC Depth (cmbsf)	Age (ybp)	Error (yrs)
22	190	190
555	8170	200
705	10230	100
774.5	11690	260
802	13090	280
820.5	14090	540
830	14650	70
1253	17020	240

Table 2.2: Raw radiocarbon data, age models, and calculated projection and ventilation ages for EW0408-85JC.

EW0408-85JC Depth (cmbsf)	Age Model 1 (ybp)	1σ	Age Model 3 (ybp)	1σ	Planktic Raw ^{14}C (yrs)	1σ	Benthic Raw ^{14}C (yrs)	1σ	Raw Benthic – Planktic (yrs)	1σ	Age Model 1 Benthic Proj Age (yrs)	1σ	Age Model 1 Benthic Vent Age (yrs)	1σ	Age Model 3 Benthic Proj Age (yrs)	1σ	Age Model 3 Benthic Vent Age (yrs)	1σ	Age Model 3 Planktic Proj Age (yrs)	1σ	Age Model 3 Planktic Vent Age (yrs)	1σ
22	190	260	190	190	660	250	1530	45	870	250	1380	40	1190	270	1380	40	1190	330	640	180	450	520
124	750	110	1717	161	1650	90	2505	50	855	100	2520	130	1770	170	2570	120	860	400	1830	150	110	440
176	1410	110	2495	145	2340	70	2890	20	550	70	2950	30	1540	120	2990	30	490	250	2640	130	140	400
222	1860	130	3183	134	2730	70	3440	60	710	90	3640	80	1780	150	3680	70	500	300	3290	140	100	380
254	2870	115	3662	128	3560	60	4160	20	600	60	4640	90	1770	150	4680	80	1010	290	3870	80	210	290
304	3430	135	4410	122	4000	80	4810	60	810	100	5500	80	2070	160	5520	70	1110	280	4580	130	170	360
356	3820	135	5188	120	4330	60	5015	45	685	80	5680	60	1860	150	5740	70	550	270	5320	120	130	330
404	4690	150	5906	123	4990	90	5840	25	850	90	6600	40	1910	160	6640	30	730	220	6030	120	120	350
454	5400	125	6655	130	5500	70	6345	30	845	80	7230	40	1830	130	7260	20	610	220	6770	130	110	370
504	6360	85	7403	141	6410	25	7190	25	780	40	7970	20	1610	90	7980	20	580	230	7510	130	110	380
555	7960	95	8164	153	7980	25	8855	35	875	40	9830	100	1870	140	9840	90	1680	350	8840	80	670	330
605	8630	165	8853	115	8610	80	9265	30	655	90	10370	70	1740	180	10390	70	1530	260	9550	60	700	240
655	9550	535	9541	109	9020	120	9800	30	780	120	11200	20	1650	540	11200	10	1660	170	10160	140	620	350
705	10000	160	10233	141	9660	70	10355	45	695	80	12080	70	2080	180	12080	60	1850	290	11040	140	810	400
725	10310	95	10648	107	9930	30	10650	25	720	40	12670	50	2360	110	12680	40	2030	200	11280	30	630	200
740	10660	120	10963	89	10260	25	10915	25	655	40	12850	10	2190	120	12850	10	1890	140	11990	60	1020	210
754	10900	180	11258	87	10410	100	11000	130	590	160	12900	80	2000	200	12900	80	1650	230	12250	200	990	400
759	11140	85	11363	91	10600	35	11195	30	595	50	13060	40	1920	100	13070	30	1700	170	12630	80	1260	240
770	11340	95	11594	104	10855	30	11620	30	765	40	13390	30	2050	100	13400	20	1800	180	12840	10	1240	160
780	11880	180	11968	108	11065	25	12315	35	1250	40	14110	40	2230	190	14110	30	2140	200	12940	20	970	180
790	12210	170	12480	129	11250	25	12670	35	1420	40	14880	60	2670	180	14900	50	2410	250	13130	20	650	210
794.5	12600	200	12711	153	11520	25	12520	30	1000	40	14570	110	1970	230	14580	100	1870	360	13330	20	620	250
799.5	13700	95	12967	186	12705	25	13365	35	660	45	15780	50	2080	110	15750	50	2780	330	14950	30	1980	300
804	13810	105	13199	184	12810	60	13430	45	620	80	15870	60	2060	130	15850	60	2650	350	15060	60	1860	350
810	14060	110	13526	154	13080	30	13695	30	615	40	16220	40	2160	120	16200	40	2680	270	15370	40	1840	280
820	14220	210	14069	222	13170	60	13830	35	660	70	16390	50	2170	220	16390	40	2320	380	15510	80	1450	430
825	14460	255	14370	182	13310	80	13945	45	635	90	16540	60	2080	270	16540	60	2170	340	15730	120	1360	420
830	14720	240	14622	232	13430	45	13740	35	310	60	16300	50	1580	250	16300	40	1670	390	15910	60	1280	420
834.5	14740	235	14678	238	13420	30	13965	30	545	40	16580	40	1840	240	16570	40	1890	390	15900	40	1220	400

Table 2.2 (Cont):

EW0408-85JC Depth (cmbsf)	Age Model 1 (ybp)	1σ	Age Model 3 (ybp)	1σ	Planktic Raw ^{14}C (yrs)	1σ	Benthic Raw ^{14}C (yrs)	1σ	Raw Benthic – Planktic (yrs)	1σ	Age Model 1 Benthic Proj Age (yrs)	1σ	Age Model 1 Benthic Vent Age (yrs)	1σ	Age Model 3 Benthic Proj Age (yrs)	1σ	Age Model 3 Benthic Vent Age (yrs)	1σ	Age Model 3 Planktic Proj Age (yrs)	1σ	Age Model 3 Planktic Vent Age (yrs)	1σ
840	15290	165	14709	235	13830	35	14425	30	595	50	17180	60	1890	180	17150	50	2440	400	16410	40	1700	390
854	16000	210	14787	228	14345	30	14880	35	535	50	18010	30	2010	220	17990	30	3200	360	17050	40	2260	380
876	16390	215	14911	217	14645	35	15205	45	560	60	18590	30	2200	220	18560	60	3650	390	17620	70	2710	410
904	16670	220	15348	186	14870	50	15440	60	570	80	18740	40	2070	230	18710	50	3640	360	17980	40	2910	350
1004	16790	225	15628	174	14890	60	15590	90	700	110	18830	60	2040	240	18810	50	3190	320	18010	60	2380	330
1054	16840	250	15908	171	15040	80	15640	60	600	100	18860	40	2020	260	18850	40	2940	290	18300	210	2390	540
1103	16890	235	16182	176	14860	80	15680	160	820	180	18890	90	2000	260	18870	90	2690	380	18000	100	1820	390
1153	16940	235	16463	190	15080	40	16110	90	1030	100	19220	120	2280	270	19200	110	2740	430	18470	110	2010	430
1203	16980	250	16743	210	15110	60	15830	60	720	80	18970	40	1990	260	18960	30	2220	340	18510	100	1770	440
1253	17020	240	17020	240	15160	35	15720	90	560	100	18910	50	1890	250	18910	50	1890	410	18570	20	1550	370

Chapter 3

The deglacial transition on the Southeastern Alaska Margin: meltwater input, sealevel rise, marine productivity, and sedimentary anoxia.

M.H. Davies[1], A.C. Mix[1], J.S. Stoner[1], J.A. Addison[2], J. Jaeger[3], B. Finney[4], J. Wiest[5]

1 – College of Oceanic and Atmospheric Sciences, Oregon State University, Corvallis OR 97331

2 – Department of Geology and Geophysics, University of Alaska, Fairbanks AK 99775

3 – Department of Geological Sciences, University of Florida, Gainesville, FL 32611

4 – Department of Biological Sciences, Idaho State University, Pocatello, ID 83209

5 – College of Veterinary Medicine, Oregon State University, Corvallis OR 97331

Paleoceanography

doi:10.1029/2010PA002051

2011

3.1 Abstract

Oxygen isotope data from planktonic and benthic foraminifera, on a high-resolution age model (44 ^{14}C dates spanning 17,400 years), document deglacial environmental change on the Southeast Alaska margin (59°33.32′ N, 144°9.21′ W, 682 m water depth). Surface freshening (i.e., $\delta^{18}O$ reduction of 0.8 ‰) began at 16,650 ± 170 cal ybp during an interval of ice proximal sedimentation, likely due to freshwater input from melting glaciers. A sharp transition to laminated hemipelagic sediments constrains retreat of regional outlet glaciers onto land circa 14,790 ± 380 cal ybp. Abrupt warming and/or freshening of the surface ocean (i.e., additional $\delta^{18}O$ reduction of 0.9 ‰) coincides with the Bølling Interstade of Northern Europe and Greenland. Cooling and/or higher salinities returned during the Allerød interval, coincident with the Antarctic Cold Reversal, and continue until 11,740 ± 200 cal ybp, when onset of warming coincides with the end of the Younger Dryas. An abrupt 1 ‰ reduction in benthic $\delta^{18}O$ at 14,250 ± 290 cal ybp likely reflects a decrease in bottom water salinity driven by deep mixing of glacial meltwater, a regional megaflood event, or brine formation associated with sea ice. Two laminated opal-rich intervals record discrete episodes of high productivity during the last deglaciation. These events, precisely dated here at 14,790 ± 380 to 12,990 ± 190 cal ybp and 11,160 ± 130 to 10,750 ± 220 cal ybp, likely correlate to similar features observed elsewhere on the margins of the North Pacific, and are coeval with episodes of rapid sealevel rise. Remobilization of iron from newly inundated continental shelves may have helped to fuel these episodes of elevated primary productivity and sedimentary anoxia.

3.2 Introduction

Both the North Atlantic and North Pacific Oceans experienced millennial-scale changes in climate during the last glacial-interglacial cycle [e.g., *Bond et al.*, 1993; *Kotilainen and Shackleton*, 1995; *Lund and Mix*, 1998; *Kiefer et al.*, 2001]. Establishing the relative timing of millennial-scale climate events in the North Pacific and Atlantic provides important insight into the mechanisms responsible for their generation and transmission. Hypotheses requiring in-phase behavior either invoke atmospheric teleconnections that rapidly transmit thermal anomalies from the Atlantic to the North Pacific [e.g. *Broecker*, 1994; *Mikolajewicz et al*., 1997; *Okumura et al*., 2008] with spatial variations in the response [*Hostetler et al*., 1999], or external forcing that affects both oceans synchronously [e.g. solar variability; *Bond et al.*, 2001]. Alternatively, if reorganization of thermohaline circulation and accompanying redistribution of heat in the ocean dominates transmission of these climate events, variations in North Pacific and Atlantic oceans could be out of phase [e.g. *Lund and Mix*, 1998; *Kiefer et al.*, 2001; *Saenko et al.*, 2004; *Okazaki et al.*, 2010], or lagged [e.g., *Schmittner and Stocker*, 1999] due to the response time of ocean adjustment. These are not mutually exclusive mechanisms; the possibility of responses to various remote forcings expressed in different parts of the North Pacific system [e.g., *Mix et al.*, 1999] has made it difficult to test specific hypotheses.

Here we investigate the mechanisms driving climate and environmental change in the high-latitude North Pacific by placing detailed isotopic and sedimentologic observations of upper ocean properties from the Gulf of Alaska (GoA) into a global context using a high-resolution radiocarbon-based age model. We focus on a site from the continental slope of SE Alaska, south of Kayak Island. Three cores, jumbo piston core

EW0408-85JC, its trigger core EW0408-85TC (59°33.32′ N, 144°9.21′ W, 682 m water depth), and an adjacent multicore EW0408-84MC2 (59°33.30′ N, 144°9.16′ W, 682 m water depth) provide a complete, high-resolution record of the last deglacial transition through the Holocene in this region (Figure 3.1).

3.3 Study Area

3.3.1 Regional Oceanography

Cyclonic motion of the subarctic gyre drives circulation in the Gulf of Alaska [*Stabeno et al.*, 2004]. The southern boundary of this gyre, the West Wind Drift, diverges as it approaches the continental shelf of North America and its northward branch becomes the Alaska Current (AC; Figure 3.1). The AC dominates flow along the southwestern Alaska continental slope and is eventually diverted south around the Kenai Peninsula, beyond which it is termed the Alaskan Stream.

Roughly parallel to the AC but largely confined to the continental shelf is the Alaska Coastal Current (ACC), a wind- and buoyancy-forced coastal jet with flow velocities occasionally in excess of 50 cm s^{-1} and mean annual transport of ~10^6 m^3 s^{-1} [*Royer*, 1982; *Johnson et al*, 1988; *Stabeno et al.*, 1995]. Although primarily wind driven, the ACC is enhanced by a baroclinic response to a coastal freshwater discharge to the Gulf with an annual average >23,000 m^3 s^{-1}, equivalent to the flow of the Mississippi River [*Royer* 1981; 1982]. This freshwater flux is delivered via a series of small, mountainous drainages, which experience high precipitation rates (2-6 m yr^{-1}) due to adiabatic cooling of warm moist air associated with the cyclonic storm systems of the Aleutian Low [*Weingartner et al*., 2005]. Runoff peaks in the fall, and this yields an abrupt, shallow (< 50 m) halocline of salinity contrast >3 over the shelf; the spring halocline is deeper (>100 m) and less abrupt (contrast of ~1) [*Stabeno et al.*, 2004].

During fall, winter, and spring, strong cyclonic winds promote onshore surface Ekman transport and downwelling on the shelf, along with storm-induced vertical mixing [*Childers et al.*, 2005]. During summer the onshore winds relax, allowing for brief periods of coastal upwelling in this dominantly downwelling system [*Stabeno et al.*, 2004].

Primary productivity in the Gulf of Alaska is limited by low light and deep surface mixed layers in the winter, but large algal blooms occur over the shelf with the return of the sun in the early spring. Productivity remains relatively high through early summer [*Stabeno et al.*, 2004]. Nitrate, silicic acid, and phosphate nutrients come mostly from the subsurface ocean, via open-ocean upwelling, onshore Ekman transport, tidal pumping, and storm or eddy mixing [*Childers et al.*, 2005]. Nutrients delivered by the fluvial system include iron and silicic acid [*Stabeno et al*., 2004]. Although reasonable estimates suggest that fluvial sources of reactive iron are sufficient to support shelf productivity, dissolved concentrations are limited (~1-3 nM) by a low availability of organic ligands, required to maintain iron in solution [*Lippiatt et al.*, 2010]. Relatively little data are available on the cycling of iron in this system, although it appears shelf processes and surface water discharge may play a role in regulating surface-ocean iron concentrations [*Stabeno et al.*, 2004; *Schroth et al.*, 2009; *Wu et al*., 2009].

In contrast to the productive coast, the central Gulf of Alaska is a high-nitrate low-chlorophyll (HNLC) region; primary productivity is likely limited by micronutrients such as iron [*Boyd et al*., 2004; *Tsuda et al.*, 2005]. Sources of iron to the central basin include curl-driven upwelling, aeolian dust [*Mahowald et al*., 2005], advection of dissolved iron from the continental shelf and slope [*Chase et al*., 2007; *Lam and Bishop*, 2008], and terrestrial runoff [*Stabeno et al*., 2004; *Royer*, 2005; *Milliman and Syvitsky*, 1992]. The core site studied here is off the shelf, and transitional between the productive nitrate-limited shelf system and the iron-limited open-ocean system.

3.3.2 Geologic Setting

The continental shelf in SE Alaska is about 25 km wide near Kayak Island. The mean depth is 140 m above a shelf break at ~220 m. Sediments exposed on the shelf include poorly sorted, glacially-derived diamicton, glacial-marine sand and silt, and hemipelagic mud [*Molnia and Carlson*, 1978; *Carlson*, 1989].

Core EW0408-85JC is located on the continental slope between two distinct sediment dispersal regions, the Copper River Shelf (59°30' - 60°15' N, 145° to 141°30' W) and the Bering-Malaspina Shelf (59°30' to 60° N, 147° to 145° W), and thus may be sensitive to fluctuations in terrestrial input from either source [*Jaeger et al*., 1998]. The Copper River Shelf includes the estuary and the delta of this large river, as well as regions north and west of Kayak Trough (~145° W); for example, Hinchinbrook Sea Valley and Prince William Sound are both distal depocenters of Copper River sediment [*Molnia*, 1986; *Milliman et al*., 1996; *Jaeger et al*., 1998]. The Bering-Malaspina Shelf is mostly supplied with sediment from smaller rivers draining the Bering and Malaspina piedmont glaciers.

In the late Pleistocene, the upper reaches of the Copper River basin were occupied by >9000 km^2 ice-dammed Glacial Lake Atna [*Nichols and Yehle*, 1969; *Williams and Galloway*, 1986]. During deglaciation, failure of the ice dam is thought to have produced freshwater megafloods in the Gulf of Alaska between ~26,000 and ~15,500 ybp, and perhaps additional younger events that are not yet well dated [*Wiedmer et al*., 2010]. The lake ultimately drained out the Copper River by 10,270-11,090 cal ybp [*Rubin and Alexander*, 1960].

The northwestern lobe of the Cordilleran Ice Sheet was present on the shelf during the Last Glacial Maximum (LGM), although the full extent of ice cover is poorly known [*Molnia*, 1986; *Manley and Kaufman*, 2002]. As recently as the early 1900's, the tidewater Guyot Glacier in Icy Bay released ice-rafted debris directly into the sea [*Molnia*, 1986]. Terrestrial records suggest that regional LGM expression lasted from 23,000 to 14,700 cal ybp, with evidence for millennial-scale cooling and transient glacial readvances during deglaciation [*Engstrom et al*., 1990; *Mann and Peteet*; 1994, *Briner et al*., 2002; *Hu et al.*, 2006]. Retreat of the Bering Glacier off the continental shelf following the LGM is not well dated, but peat was accumulating in parts of the Bering foreland as early as early as 16,000 cal ybp [*Peteet*, 2007]. Timing of advances and retreats of land-terminating valley and cirque glaciers in the early Holocene are also poorly constrained [*Barclay et al*., 2009]. Advances are estimated between 8,600 and 6,700 cal ybp in southwestern Alaska [*Ten Brink*, 1983; *Yehle et al*., 1983], and between 12,300 and 7,570 cal ybp in the Aleutian Islands [*Thorson and Hamilton*, 1986]. Regional late-Holocene glacial re-advances are dated at 3,300-2,900 cal ybp and 2,200-2,000 cal ybp [*Barclay et al*., 2009].

3.4 Methods

3.4.1 Sediment depths

The 1124 cm jumbo piston core EW0408-85JC (59°33.32′ N, 144°9.21′ W, 682 m water depth) was spliced to its 210 cm trigger core and to adjacent 56 cm multi-core EW0408-84MC2 (59°33.30′ N, 144°9.16′ W, 682 m water depth) using visual correlation of point-source magnetic susceptibility and gamma attenuation density data measured at sea. The sediment-water interface was recovered in the multicore. The trigger core over-penetrated the sea floor and did not recover an interval equivalent to 0-13 cm in the multicore. The jumbo piston failed to recover the uppermost 150 cm of sediment. Based on these observations, we define the centimeters-below-sea-floor (cmbsf) scale, which adds 150 cm to the nominal depths in EW0408-85JC and 13 cm to EW0408-85TC, but retains raw measured depths in EW0408-84MC2.

3.4.2 Radiocarbon

Benthic and planktonic foraminifera were picked from the >150 μm sediment fraction. The planktonic species *Neogloboquadrina pachyderma* (sinistral) and *Globigerina bulloides* were analyzed for radiocarbon using accelerator mass spectrometry (AMS). Although these two species were combined for most depths to increase sample size and minimize analytical error, the two species were dated separately at 759 cmbsf. The resulting age of *N. pachyderma* was 65 ± 50 years older than that of *G. bulloides*, close to the combined measurement uncertainty for the individual species. Benthic foraminiferal ^{14}C analyses were run as mixed species, although care was taken to avoid agglutinated and deep infaunal species such as *Globobulimina affinis*.

Radiocarbon analyses were performed at the Keck AMS facility, University of California at Irvine. A total of 44 measurements were performed for 40 samples: 3

benthic/planktonic pairs from core EW0408-85TC, 34 planktonic samples from core EW0408-85JC, and three benthic samples from core EW0408-84MC2. The raw radiocarbon dates were converted to a calendar age scale with using the Marine09 curve in CALIB 6.0 [*Stuiver and Reimer*, 1993; *Reimer et al*., 2009]. To account for regional surface-water reservoir ages [*McNeely et al.*, 2006], a constant reservoir age anomaly (ΔR) of 470 ± 80 years was applied to all planktonic foraminiferal dates. A value for ΔR of 990 ± 100 years was applied to the benthic foraminiferal dates, based on water column data at equivalent water density horizons in the Gulf of Alaska [*Sabine et al*., 2005]. These reservoir age corrections are consistent with the ^{14}C age differences observed in the paired benthic/planktonic dates within the trigger core. The calendar calibrated dates for the overlapping portions of the multi-, trigger, and jumbo piston core form a smooth progression without age reversals on the composite cmbsf scale derived in section 4.3.1.

3.4.3 CT Scans

Computerized tomographic (CT) density measurements were performed at the Oregon State University College of Veterinary Medicine using a Toshiba Aquilion 64 Slice. Scans were collected at 120 kVp and 200 mAs. For visualization purposes, the resulting images were processed with a “sharp” algorithm to generate sagittal and coronal images every 4mm across the core. Down-core and across core pixel resolution within each slice is 500 μm. The cores were scanned in ~60 cm segments and then joined into a composite image using Adobe Photoshop software (Figure 3.2). The pixel intensities of the resulting compilation were calibrated as a high-resolution proxy for sediment density by applying a 2nd order polynomial regression between the pixel values and the calibrated shipboard gamma-ray attenuation density measurements ($r = 0.91$, $n = 1122$, $p < 0.0001$; Figure 3.2).

3.4.4 Stable Isotope Measurements

Raw sediment sub-samples of 15 cc (1 cm thick, quarter-core) or 30 cc (2 cm thick, quarter core, for samples also subjected to ^{14}C analyses) were collected for stable isotopic measurements at 5 cm intervals (in bioturbated units) and 1 cm intervals (in laminated units) and wet-sieved at 125 µm. Planktonic foraminifera (*N. pachyderma,* sinistral coiling, and *G. bulloides*) and benthic foraminifera (*Uvigerina peregrina*, *Cibicidoides wuellerstorfi,* and *Nonionella sp.*) were picked from the >150 µm size fraction. Care was taken during hand-picking to select specimens that were as clean as possible, with no visual evidence for diagenetic overgrowths, which can sometimes be recognized by yellowish discoloration. Foraminiferal samples were ultrasonically cleaned prior to stable isotope analyses, but otherwise untreated.

Stable isotopic measurements were performed at the Oregon State University College of Oceanic and Atmospheric Sciences (OSU/COAS) Stable Isotope Mass Spectrometer Facility using a Kiel III carbonate preparation device connected to a Thermo-Finnigan MAT-252 mass spectrometer. The data were corrected to the accepted PDB scale using an internal lab calcite standard (Wiley) and the international calcite standard NIST-8544 (also known as NBS-19). External precision ($\pm$1 standard deviation) of the Wiley standard of similar weight to the foraminiferal samples, run on the same days, was ± 0.02 ‰ for $\delta^{13}C$ and ± 0.04 ‰ for $\delta^{18}O$ (n=230). Average NBS-19 values for these runs ($\delta^{13}C = +1.93 \pm 0.02$ ‰, $\delta^{18}O = -2.20 + 0.06$ ‰, n = 51) were comparable to the accepted VPDB values for NBS-19 ($\delta^{13}C$ = +1.95 $\delta^{13}C$, $\delta^{18}O$ = -2.20; National Institute of Standards and Technology, 1992). To allow direct comparison to *U. peregrina,* empirical species corrections of +0.64 and +0.1 were applied to the $\delta^{18}O$ values of *C. wuellerstorfi* and *Nonionella sp.*, respectively. Similarly, an empirical species correction of -0.2 was applied to the $\delta^{13}C$ values of C. *wuellerstorfi*.

3.5. Results

3.5.1 Chronology and accumulation rates

Based on the calendar-corrected radiocarbon chronology, the composite sediment sequence at site EW0408-85JC continuously spans the last >17,400 ybp in the Gulf of Alaska, and documents the Pleistocene/Holocene transition (Figure 3.3). The timings of the features described in the following sections are derived from this age model, with uncertainties propagated from the nearest bracketing radiocarbon dates.

Within the limitations of the dated increments, sediment accumulation rates vary from a low of 9 ± 2 cm/ky between 13,770-12,220 cal ybp, reflecting hemipelagic sedimentation during a time equivalent to the late Allerød and early Younger Dryas chronozones of Northern Europe, to values of >500 cm/ky prior to 17,050 cal ybp, during an interval of ice-proximal marine sedimentation composed dominantly of glacial silt with dropstones. Average post-glacial sedimentation rates are 56 cm/ka, and thus potential bioturbation-induced dating biases [e.g., Broecker et al., 1984] are expected to be <150 years (roughly one 10-cm mixed-layer depth) in most of the record. Within the interval of high sediment accumulation rates during deposition of the glacial-marine diamicts, two ^{14}C age reversals of <300 years occur with overlapping error bars; all other ages increase with depth (Table 3.1). We use direct linear interpolation between radiocarbon dates to generate the age model, except in the high-sedimentation rate interval, where we use a linear best fit through the dates that increased with depth, a compromise that falls within the 1σ uncertainties of all but one of the calibrated dates in this sedimentary unit (Figure 3.3). Sediment accumulation rates decrease by almost an order of magnitude (from >500 cm/kyr to ~90 cm/kyr) by 875 cmbsf (16,890 ± 90 cal ybp) within the interval of ice-proximal sedimentation, approximately 45 cm (2,100 ± 390 years) prior to the onset of hemipelagic sedimentation at the site.

3.5.2 Lithology

At depths >831 cmbsf, sediments are composed of terrigenous silt and clay with pebbles, which we infer to be glacial dropstones and other ice-rafted debris (Figures 2 and 3). Marine fossils, including benthic and planktonic foraminifera, are present in this interval and demonstrate the marine character of sedimentation. The radiocarbon chronology implies very rapid sediment accumulation in the oldest recovered interval, leading us to infer that this lithology represents ice-proximal glacial-marine sedimentation.

The glacial-marine unit is overlain at 831 cmbsf (interpolated to 14,790 ± 380 cal ybp) by a relatively low-density laminated unit 34-cm thick. The contact between these units is sharp, but with no visible evidence for erosion and no apparent discontinuity in the radiocarbon chronology. The preserved laminations (approximately 140 laminae of millimeter to sub-millimeter thickness based on CT scans and visual descriptions) span 1,800 ± 420 years in the calendar-corrected radiocarbon age model, and appear to reflect decadal-scale variability. Average sediment accumulation rates in this interval are ~ 25 ± 12 cm/kyr. The lithology of the laminated interval is diatom-rich mud; darker laminae are predominantly terrigenous silt, whereas lighter, lower density laminae have higher concentrations of siliceous and calcareous microfossils. Opal (biogenic silica) was measured using a spectrophotometric wet-alkali extraction method [*Mortlock and Froelich*, 1989], and is more thoroughly discussed by *Addison et al*. [submitted]. Opal content of the sediment increases during the laminated interval from ~3 wt % to 10 wt %, and it is likely that fluctuations in the ratio of biogenic to lithogenic sediment drive bulk density variability throughout EW0408-85JC (Figure 3.4a, b).

At 797 cmbsf (interpolated age 12,990 ± 190 cal ybp) the upper contact of the laminated unit is lightly bioturbated, grading into a 37 cm (~1,830 year) interval of higher density. This interval contains mottled terrigenous silt and clay, with opal and calcium carbonate. A secondary, sub-laminated unit (with light burrow mottling) of low density and with opal content of 10 wt % occurs between 745-760 cmbsf (11,160 ± 130 to 10,750 ± 220 cal ybp). At depths <745 cm, sediment composition is bioturbated hemipelagic mud for the remainder of the Holocene; fine-scale variations in the lithology of this sediment is described by *Addison et al.,* [submitted].

3.5.3 Stable isotopes

Benthic foraminiferal (*U. peregrina*) $\delta^{18}O$ ranges from maximum values of 4.9 ‰ (17,050 ± 350 cal ybp) to minimum values of 3.1 ‰, a range of 1.8 ‰ (Figure 3.4d). Mean glacial and late Holocene values (4.66 ± 0.05 ‰ and 3.27 ± 0.02 ‰, respectively, n=7, standard error of the mean) are essentially identical to values reported from the same laboratory at 980 m depth from the Oregon margin [*Mix et al.*, 1999] suggesting that this site captures the full glacial-interglacial transition. The decrease from Pleistocene values of benthic foraminiferal $\delta^{18}O$ begins at 16,650 ± 170 cal ybp, with a transient -1 ‰ excursion to minimum values centered at 14,250 ± 240 ybp (Figure 3.4d). The $\delta^{18}O$ variations recorded by *U. peregrina* are reproduced by analyses of both *C. wuellerstorfi* and *Nonionella sp.* in 18 samples between 720 and 820 cmbsf.

Planktonic foraminiferal $\delta^{18}O$ values range from 3.7 ‰ (17,330 ± 270 cal ybp) to 1.3 ‰ (3,600 ± 190 cal ybp; Figure 3.4c). This glacial-to-interglacial range of 2.4 ‰ is substantially larger than that measured in the benthic foraminifera. The decrease from Pleistocene values begins at 16,650 ± 170 cal ybp, and as in the benthic record, includes an approximately -1 ‰ $\delta^{18}O$ excursion between 14,710 ± 280 and 13,770 ± 120 cal ybp. Both the onset of and recovery of the event are abrupt, and the peak of expression is centered at 14,250 ± 240 cal ybp. The planktonic event includes two episodes of $\delta^{18}O$ depletion, reproduced in both planktonic species and centered at 822.5 cmbsf (14,340 ± 390 cal ybp) and 814.5 cmbsf (14,150 ± 290 cal ybp) respectively. The benthic $\delta^{18}O$ excursion occurs between these planktonic events (Figure 5). This fine-structure is likely not an artifact of bioturbation, as the event occurs within the laminated interval.

The two planktonic species, *N. pachyderma* and *G. bulloides*, reproduce $\delta^{18}O$ values within 0.3 ‰ for most of the record, with two exceptions (Figure 3.4c). The first is during the interval of high $\delta^{18}O$ between 12,940 ± 190 and 10,850 ± 220 cal ybp. Following the shift to low $\delta^{18}O$ values of ~1.5 ‰ in the early Holocene, $\delta^{18}O$ increases in both species to 2.0 ‰ by 7,770 ± 120 cal ybp, followed by a decrease to the most depleted values in the record (1.3 ‰) at 3,600 ± 190 cal ybp. Planktonic foraminiferal

$\delta^{18}O$ values then increase, reaching 1.8 ‰ by 2,520 ± 180 cal ybp, after which the values from *N. pachyderma* and *G. bulloides* again diverge (Figures 4c and 5a).

Detailed interpretation of the benthic $\delta^{13}C$ values is complicated by the shallow infaunal behavior of *U. peregrina*, the species for which a complete record exists (Figure 4g). Other stable isotope records from the North Pacific are typically dominated by this species, and their $\delta^{13}C$ values have been evaluated cautiously as benthic watermass tracers, with possible productivity overprints [e.g., *Lund and Mix*, 1998; *Mix et al*., 1999; *Okazaki et al*., 2010]. Although *C. wuellerstorfi* is relatively rare, where present its $\delta^{13}C$ values approximately reproduce those of *U. peregrina*, with an average offset of 0.2 ‰. Benthic $\delta^{13}C$ in core EW0408-85JC is relatively high (-0.7 ‰) in the glacial interval (~17,400 cal ybp), falling to a low of ~ -1.2 ‰ between 16,720 ± 170 and 15,340 ± 380 cal ybp. Values then climb to a high of ~ -1.05 ‰ centered at 14,710 ± 280 cal ybp, before falling to the most depleted interval of the deglacial (-1.4 ‰) between 13,770 ± 120 and 11,550 ± 200 cal ybp. By 10,310 ± 180 cal ybp, benthic $\delta^{13}C$ has rebounded to > -0.7 ‰, and then gradually declines until 7,420 ± 120 cal ybp (-1.3 ‰). From this point, benthic $\delta^{13}C$ slowly increases throughout the remainder of the Holocene, reaching > -0.8 ‰ by 1,090 ± 160 cal ybp.

The $\delta^{13}C$ values of *N. pachyderma* are consistently elevated (average offset of 0.51 ± .15 ‰) relative to those of *G. bulloides* (Figure 3.4f). The lowest $\delta^{13}C$ values of the record (-0.8 ‰ for *G. bulloides*, -0.17 ‰ for *N. pachyderma)* occur at 16,640 ± 150 cal ybp. Values increase to maxima at 14,710 ± 280 ybp (0.06 ‰ for *G. bulloides*, 0.3 ‰ for *N. pachyderma*), before decreasing again. Both species return to high $\delta^{13}C$ values between 11,850 ± 240 and 10,880 ± 180 cal ybp before falling to a depleted plateau (~

-0.55 ‰ for *G. bulloides*, ~ 0.09 ‰ for *N. pachyderma*) between 10,380 ± 150 and 9,120 ± 240 cal ybp. Recovery from these $\delta^{13}C$ minima occurs by 6,630 cal ybp (0.34 ‰ for *G. bulloides*, 0.78 ‰ for *N. pachyderma*). The highest $\delta^{13}C$ values of the record are observed in the late Holocene; 0.57 ‰ for *G. bulloides*, and 0.96 ‰ for *N. pachyderma.*

3.6. Discussion

3.6.1 Regional deglaciation of the Northwest Cordilleran Ice Sheet

Decreasing sedimentation rate within the interval of glacial-marine sedimentation likely documents early stages of glacial stagnation or retreat near 16,900 cal ybp. Starting at 16,650 ± 170 cal ybp, planktonic foraminiferal $\delta^{18}O$ decreases rapidly (and benthic foraminiferal $\delta^{18}O$ decreases more slowly), consistent with warming temperatures and the input of meltwater from retreating outlet glaciers. The abrupt contact between ice-proximal sediments and the overlying diatom-rich laminated interval at 14,790 ± 380 cal ybp records the retreat of Pleistocene tidewater glaciers onto land or behind fjord sills as global sealevel rose.

The abundance of opal, mostly from diatoms, and relatively high biogenic flux in the laminated intervals implicates high surface productivity as a cause of the laminations, which are preserved by benthic anoxia (also reflected by high molybdenum concentrations [*Barron et al.*, 2009; *Addison et al*., submitted]). Benthic foraminiferal $\delta^{13}C$ changed very little at the onset of laminations, suggesting no major changes in benthic watermasses (Figure 3.5), implying that sedimentary anoxia was due primarily to changing productivity rather than changes in subsurface ocean circulation.

By subtracting the benthic $\delta^{18}O$ record from the *N. pachyderma* planktonic $\delta^{18}O$, we remove the potential isotopic signature of global ice volume that is common to both records and are left with the regional signature of isotopic gradients ($\delta^{18}O_{P-B}$; Figure 3.4e) associated with local temperature and salinity stratification between surface and local bottom water [*Lopes and Mix*, 2009]. Anomalously low $\delta^{18}O_{P-B}$ values of –0.8 ‰ from 14,710 ± 280 to 12,950 ± 190 cal ybp, indicate strong upper-ocean stratification, likely associated with high freshwater input during deglaciation. Superimposed upon this structure, the abrupt planktonic $\delta^{18}O$ depletions centered at 14,340 ± 390 cal ybp and 14,150 ± 290 cal ybp (Figure 3.5) may reflect two discrete episodes of very high freshwater input to the Gulf of Alaska.

Assuming meltwater $\delta^{18}O$ of ~-30 to -40 ‰ (SMOW), consistent with the isotopic values recorded in the Mount Logan ice-core during the last termination [Fisher et al., 2008], and no temperature change, a -0.8 ‰ $\delta^{18}O$ excursion would be equivalent to lowering the surface ocean salinity by ~0.7. Today, a halocline of >2 exists between the sea surface and 680 m depth at the site (Figure 3.1) driven by high freshwater input along the margin of 23,000 $m^3\ s^{-1}$ [annual average; *Royer,* 1982], so as a first approximation, the surface-ocean $\delta^{18}O$ excursion during deglaciation could have been induced by modest additional freshwater inputs of half to one third the modern freshwater flux (i.e., ~8000-12000 $m^3\ s^{-1}$). The laminated interval is not uniquely associated with the interval of inferred high freshwater input, as the laminations continue for ~800 years after the end of the planktonic $\delta^{18}O$ excursion (Figure 3.5).

An abrupt low $\delta^{18}O$ excursion in the benthic foraminifera at 14,250 ± 290 cal ybp occurs within the laminated interval, between the two low $\delta^{18}O$ events in the planktonic foraminifera (Figure 3.5b). This event is unlikely to be explained solely as a subsurface temperature excursion, as it would require an implausible 5°C increase in bottom water temperature at a paleodepth of 580 m (accounting for ~100 m lowered sealevel). Following the assumptions above, the benthic $\delta^{18}O$ excursion implies a salinity reduction of ~1 at the sea floor. Three possible mechanisms for this observation include: deepening of the modern halocline associated with the Alaska Coastal Current, hyperpycnal flow associated with an abrupt meltwater event, and/or local formation of isotopically depleted brines associated with sea-ice expansion.

Deepening of the modern halocline at this site (Figure 3.1), which presently reaches a spring maximum of between 100 and 200 m depth, to more than 580 m paleodepth, would require a very large increase in freshwater inputs. Although the amount is difficult to quantify, deepening of the regional halocline by a factor of 4 implies at least a proportional increase in freshwater flux of that amount, and perhaps much more (i.e., a factor of 16 to account for a factor of 4 depth increase coupled to a factor of 4 offshore extension). Given modern freshwater inputs of 23,000 $m^3 s^{-1}$ [*Royer,* 1982], driving the benthic foraminiferal $\delta^{18}O$ excursion via halocline depression would imply a seasonal increase of this flux to at least 92,000 $m^3 s^{-1}$, and perhaps as much as 370,000 $m^3 s^{-1}$. To produce an event of the duration observed in the laminated sediments, ice sheet melting would have to intermittently reach this rate for a period of >300 years. Rates of melting on the low end of this range have been observed off South Greenland [*Rignot and Kanagaratnam*, 2006], which may be a fair analog for the retreating NW Cordilleran at the end of the Pleistocene. Runoff of this magnitude (~10^5 $m^3 s^{-1}$) sustained for six months per year over the period of laminations, would imply a loss of 6-30% of the Cordilleran Icesheet volume [*Peltier*, 1994].

Benthic foraminiferal $\delta^{18}O$ is lowest during a period of relatively high planktonic $\delta^{18}O$ between the transient lows centered at 14,340 ± 390 cal ybp and 14,150 ± 290 cal ybp (Figure 3.5). Differences in the fine structure of the benthic and planktonic $\delta^{18}O$ anomalies suggest that local meltwater and thickening of the halocline did not cause of the benthic anomaly. Other potential mechanisms include non-local hyperpycnal flows, or brine formation. To reach depths of >580 m, a low-salinity hyperpycnal flow must be charged with sediment [*Imran and Syvitski*, 2000; *Aharon*, 2006]. Although the radiocarbon dates indicate a transient increase in sedimentation rate at the time of the benthic $\delta^{18}O$ anomaly, there is no sedimentological evidence for an increase in the fraction of lithogenic sedimentation associated with the event. A plausible source for freshwater inputs capable of generating hyperpycnal flows is the Copper River, a known conduit for mega-floods associated with draining of glacial Lake Atna as recently as ~10,000 ybp [*Ferrians*, 1989; *Shimer*, 2009; *Wiedmer et al*., 2010]. If this is the source of the low benthic $\delta^{18}O$ anomaly at Site EW0408-85JC, the silt-rich portion of the flow must have been focused in the submarine canyons near the source, allowing some of the entrained low-salinity, low $\delta^{18}O$ waters to diffuse across the slope to the location of the core without an accompanying sediment load.

Formation of brine water on the shelf by salt rejection from seasonal sea-ice has been invoked to explain negative benthic $\delta^{18}O$ excursions of similar magnitude observed in the Nordic Seas [*Bauch and Bauch*, 2001] and in the Northwest Pacific [*Gebhardt et al.*, 2008], although this inference is controversial [*Rasmussen and Thomsen*, 2009]. As sea level at the time of the benthic excursion was ~100 m lower, it follows that ocean salinities were ~0.8 higher than modern values. The planktonic isotopic excursion in this interval suggests that regional freshwater input decreased surface salinities by ~0.7 at this time, so surface water salinities during the excursion were roughly similar to today. In order to sink to the depths of the core site, brine-enhanced water would have had to reach salinities of ~35, implying ~8% surface-water conversion to sea ice. An abrupt increase in winter sea-ice formation in the Gulf of Alaska may have been facilitated by the decrease in surface salinity associated with regional meltwater input. Sea-ice related diatoms peak in EW0408-85JC (30-40% of the total diatom assemblage) during the Bølling period [Figure 3.5, *Barron et al*., 2009]. *Caissie et al.* [2010] also note high abundance of sea-ice diatoms in the SE Bering Sea at about this time. Cooler surface temperatures associated with sea-ice formation may also help to explain the concurrent minor enrichment in the planktonic $\delta^{18}O$ at the height of the benthic excursion. Thus, either the hyperpycnal flow or the brine rejection mechanisms remain as plausible explanations of the low benthic foraminiferal $\delta^{18}O$ anomaly near 14,250 ± 290 cal ybp.

By 12,990 ± 190 cal ybp, laminations were no longer preserved and accumulation of authigenic manganese increased [*Addison et al.*, submitted], implying that oxygen was again present at the sea floor. The increase in bulk density of the sediment at this time, accompanied by an increase in sedimentation rate (Figure 2) and a visually apparent increase in the >150 μm lithologic size-fraction, imply increased ice-rafted debris at the site. These multiple lines of evidence suggest regional glacial readvance. $\delta^{18}O$ values in both planktonic species reach their greatest post-Pleistocene enrichment in this interval, suggesting that the annual mean temperature of the surface ocean was colder and/or more saline than at any time following the initial retreat of the Northwest Cordilleran ice sheet off the continental shelf. These findings are congruent with other terrestrial/lacustrine evidence for cooling and alpine glacial readvance in Alaska during the Younger Dryas interval [*Engstrom et al*., 1990; *Hadjas et al*., 1998; *Briner et al*., 2002; *Hu et al*, 2006].

Neogloboquadrina pachyderma $\delta^{18}O$ values are relatively constant, 2.65 ± 0.05‰, between 12,940 ± 200 and 11,740 ± 200 cal ybp. In contrast, *G. bulloides* $\delta^{18}O$ values decrease by ~0.3 ‰ through the same interval. At high latitudes today, *N. pachyderma* blooms at the height of summer and thus cannot shift to a warmer growth season, making them a faithful recorder of the summer conditions [*Fraile et al*., 2009]. In contrast, *G. bulloides* is sensitive to food availability [*Ortiz et al*. 1995; *Tedesco et al*., 2007; *Fraile et al*., 2009], and thus may shift its seasonal preferences to track phytoplankton blooms. The delay in $\delta^{18}O$ increase in *G. bulloides*, and earlier return to lower $\delta^{18}O$ values relative to *N. pachyderma*, may reflect a shift in the seasonality of the *G. bulloides* bloom. Thus we hypothesize the $\delta^{18}O$ signature of *G. bulloides* in this interval reflects a combination of environmental and physiological shifts, and will favor *N. pachyderma* as a proxy of regional summer surface ocean salinity/temperature. Based on this species, the period from 12,940 ± 200 and 11,740 ± 200 cal ybp was a time of fairly stable cold and/or saline surface conditions. This observation is further supported by an increase in cold-water microfossil groups in EW0408-85JC [*Barron et al*., 2009].

A return to sub-laminated conditions occurs from 11,160 ± 130 to 10,750 ± 220 cal ybp (Figure 5a). This sub-laminated interval has high opal content similar to the older fully laminated interval, although sediment accumulation rates during the younger event are lower, within the range of Holocene variability. High concentrations of biogenic opal, along with diatom species assemblages and the synchronous high concentrations of molybdenum and uranium [*Barron et al*., 2009; *Addison et al*., submitted] show that high surface-ocean productivity drove benthic anoxia during this event, similar to the earlier event. The $\delta^{18}O$ and $\delta^{13}C$ data again indicate no major changes in bottom water masses. The onset of sedimentary anoxia occurred a few hundred years prior to significant surface-water warming or freshening (decrease in planktonic $\delta^{18}O$ relative to benthic foraminiferal $\delta^{18}O$) suggesting primary production was not uniquely linked to local freshwater runoff.

The Holocene interval of core EW0408-85JC records more modest environmental changes; planktonic $\delta^{18}O$ suggests that the surface ocean gradually cooled or increased in salinity until 7,770 ± 120 cal ybp, followed by warming and/or freshening through the late Holocene. The late Holocene (<4000 cal ybp) displays greater millennial-scale variability than the mid-Holocene. During this time $\delta^{18}O_{P-B}$ increased for ~600 years centered at 2,500 ± 180 cal ybp, accompanied by a minor but concomitant increase in benthic $\delta^{18}O$, possibly associated with regional terrestrial glacial advances dated between 3,300-2,900 cal ybp and 2,200-2,000 cal ybp [*Barclay et al*., 2009].

3.6.2 Links to regional and global climate

Warming and freshening of surface waters in the subarctic Northeastern Pacific at 14,710 ± 280 cal ybp coincides within analytical uncertainty with the current layer-count chronology for the onset of Bølling-warmth in the Greenland NGRIP ice core records (14,740 ± 60 cal ybp; *Rasmussen et al*., [2006]), and is consistent with a rapid atmospheric teleconnection between the North Pacific and Atlantic [*Broecker*, 1994; *Mikolajewicz et al*., 1997; *Hostetler et al*., 1999]. The increase of $\delta^{18}O_{P-B}$ at 13,770 ± 120 cal ybp likely reflects the end of anomalous freshwater inputs, and perhaps cooling and/or drying conditions in the Northeast Pacific. This occurs within the Allerød interstadial event, preceding the onset of the Younger Dryas (Y-D) event of the North Atlantic by almost a millennium (12,890 ± 140 cal ybp; *Rasmussen et al*. [2006]).

The early termination of the Bolling-Allerod warm interval observed in EW0408-85JC appears in a number of high-latitude North Pacific records. In Figure 3.6 we compare the planktic oxygen isotopic records from this study to Gulf of Alaska cores MD02-2489 (54°23.4' N, 148°55.26' W, 3640 m) [*Gebhardt et al*., 2008] and PAR87A-10 (54°21.8' N, 148°28.0' W, 3664 m) [*Zahn et al*., 1991], and Northwest Pacific core Vinogradov GGC-37 (50°25.2' N, 167°43.2' E, 3,300 m) [*Keigwin et al.*, 1998; on the chronology of *Galbraith et al*., 2007] through Termination 1. The low resolution of the isotopic data and age model of PAR87A-10 [*Zahn et al.*, 1991] makes direct comparison with EW0408-85JC difficult, but represents a pioneering effort for the region. Similarly, although planktonic oxygen isotope records have been generated for Gulf of Alaska ODP Site 887 [*McDonald et al.*, 1999; *Galbraith et al.*, 2007], these provide little additional insight due to their low resolution through Termination 1.

To facilitate comparison with EW0408-85JC, radiocarbon dates from PAR87A-10 and MD02-2489 have been recalibrated with CALIB 6.0 using a constant ΔR of 550 ± 250, following the logic applied to nearby ODP Site 887 by *Galbraith et al*., [2007]. In the case of MD02-2489, four age reversals (Figure 3.6) were excluded from the resultant age-model, derived by linear interpolation between calibrated dates. Within dating uncertainties, all three high-resolution, high-latitude North Pacific records (GGC-37, MD02-2489, EW0408-85JC) show warming/freshening of the surface ocean coincident with the onset of the Bølling warm interval in the North Atlantic (Figure 6), providing support for a rapid atmospheric teleconnection between the two basins [*Broecker*, 1994; *Mikolajewicz et al*., 1997; *Okumura et al.*, 2008]. However, these same records on their independent radiocarbon-based chronologies lack evidence for a warm/fresh surface ocean during the Allerød (Figure 3.6).

An apparent North Pacific lead, relative to the North Atlantic, in the post-Bølling return to conditions typical of the Younger Dryas has been found elsewhere in the North Pacific [e.g., *Mix et al.*, 1999; *Ortiz et al*., 2004, *Cook et al*., 2005, *Dean et al*., 2006], although these records are less well dated than core EW0408-85JC. If the lead of North Pacific cooling is an artifact of dating, it would imply a significantly higher reservoir age at that time, on the order of ~1,600 years for the surface ocean. This is implausible during a time of strong freshwater input and upper ocean stratification; if anything, the high input of freshwater with a reservoir age near zero would support a lower oceanic reservoir age at that time, implying that the apparent lead of North Pacific cooling prior to the onset of Younger Dryas conditions in the North Atlantic is a real phenomenon.

The post-Bølling increase in $\delta^{18}O$ in the North Pacific may reflect the blended influences of Northern Hemisphere (i.e., the Allerød and Younger Dryas) and Southern Hemisphere (i.e., the Antarctic Cold Reversal, ACR; [*Blunier et al*., 1997]) climates in the region. The influence of the ACR was previously inferred in subsurface North Pacific paleotemperature records [e.g., *Mix et al*., 1999]. The Southern Ocean is the formation site of North Pacific Deep Water, and recent evidence suggests that changes in Antarctic source water properties may be propagated rapidly to the high-latitude North Pacific via internal waves [*Fukasawa et al.,* 2004*; Masuda et al.,* 2010]. In this model, changes in the location and rate of deep water formation in the Southern Ocean reorganize isopycnal surfaces throughout the interior of the Pacific Basin, impacting the high-latitude North Pacific within a few decades [*Masuda et al., 2010*]. This suggests the potential for a geologically instantaneous teleconnection between the Antarctic and sub-surface North Pacific, perhaps superimposed upon a Northern Hemisphere atmospheric teleconnection [*Broecker*, 1994; *Mikolajewicz et al*., 1997; *Okumura et al.*, 2008]. When compared to the $\delta^{18}O$ records from the EDML ice core in Antarctica [*Ruth et al.*, 2007] and the NGRIP ice core in Greenland [*Andersen et al.*, 2006; *Rasmussen et al*., 2006; *Svensson et al*., 2006], we find the planktonic oxygen isotope pattern of EW0408-85JC bears some similarity to both of these records (Figure 3.6), lending support to the idea that North Pacific climate records reflect both North Atlantic and Southern Ocean forcing [*Mix et al.*, 1999].

3.6.3 Mechanisms for the deglacial productivity events

The two events of high productivity recorded at site EW0408-85JC from 14,790 ± 380 to 12,990 ± 190 and 11,160 ± 130 to 10,750 ± 220 (also see *Addison et al*., [*submitted*]) may be associated with the less well-dated strengthening of the oxygen minimum zone (OMZ) in the North Pacific [*Behl and Kennett*, 1996; *Ortiz et al*., 2004; *Hendy and Pederson*, 2006; *Okazaki et al*., 2010], and perhaps also to similar paleoceanographic changes throughout the Pacific and Atlantic Oceans [*Zheng et al*., 2000; *Dean*, 2007]. Inferences of two deglacial high productivity events at approximately the same time as those at site EW0408-85JC have been made on the Mexican Pacific margin [*Dean et al*., 2006; *Ortiz et al*., 1997; *Van Geen et al*., 2003], the Santa Barbara Basin [*Hendy and Kennett*, 2003], the Gulf of California [*Barron et al*., 2005; *Keigwin*, 2002], the northern California margin [*Barron et al.*, 2003; *Lund and Mix*, 1998; *Mix et al*., 1999], the Canadian Vancouver margin [*Hendy and Cosma*, 2008; *McKay et al*., 2004], the Bering Sea [*Okazaki et al*., 2005; *Cook et al*., 2005; *Okazaki et al.*, 2010, *Cassie et al.*, 2010], the continental slope of the Kamchatka Peninsula [*Keigwin et al*., 1992], the Sea of Okhotsk [*Gorbarenko et al*., 2004], the Japanese margin [*Crusius et al*., 2004; *Shibahara et al.*, 2007] and the western Pacific [*Brunelle et al.*, 2010].

Hypotheses to explain the apparently synchronous onset of short-lived high-productivity events during the Bølling-Allerød interstadial event and in the early Holocene around the margin of the North Pacific include: (1) basin-wide enhanced upwelling [e.g., *Dean* 2007; *Barron et al*. 2009], (2) nutricline adjustment related to variability in the strength of the Atlantic Meridional Overturning Circulation (AMOC) [e.g. *Schmittner*, 2005; *Galbraith et al.*, 2007; *Schmittner and Galbraith*, 2008], (3) eolian fertilization associated with increased dust or volcanic ash delivery [e.g. *Martin*, 1990], (4) freshwater fertilization associated with deglacial meltwater flux to the North Pacific, and/or (5) fertilization associated with enhanced benthic iron flux from shelf sediments driven by deglacial sea-level rise [e.g. *Mix et al*., 1999].

In Hypothesis 1, the increase in oceanic fertility is attributed to bio-available macro- and micronutrients associated with enhanced upwelling. *Dean* [2007] hypothesized that the B-A warming in Greenland was transmitted from the Atlantic to the Pacific Ocean via more energetic Hadley and Walker circulations, which strengthen subtropical high-pressure cells, potentially increasing upwelling at the edges of the subtropical high. This wind-driven upwelling hypothesis, however, is difficult to apply to the SE Alaska margin, an area of coastal downwelling, and is not supported by the planktonic $\delta^{13}C$ records. Upwelling zones typically have low $\delta^{13}C$ in planktonic foraminifera such as *G. bulloides* [*Sautter and Thunell*, 1991; *Gansen and Kroon*, 2000]. Although this in part reflects the presence of enhanced contribution of waters with low-$\delta^{13}C$ dissolved inorganic carbon during upwelling, *Ortiz et al*. [1996] attributed some of the $\delta^{13}C$ data in foraminifera to metabolic disequilibrium effects related to temperature (warmth yielding lower $\delta^{13}C$ relative to equilibrium) or food supply (high biomass yielding lower $\delta^{13}C$ relative to equilibrium). For both reasons, the upwelling hypothesis for high productivity on the margins predicts a decrease in planktonic foraminiferal $\delta^{13}C$ during the events. This interpretation is consistent with other deglacial planktonic $\delta^{13}C$ foraminiferal datasets from the North Pacific [e.g. *Hendy et al., 2004*]. In core EW0408-85JC, both measured species of planktonic foraminifera, *N. pachyderma* and *G. bulloides*, record a 0.4 ‰ increase of $\delta^{13}C$ during the deglacial productivity events, which appears to preclude the upwelling hypothesis as a general driver.

In Hypothesis 2, the collapse of the Atlantic meridional overturning circulation at the end of the last ice age (during Heinrich Event 1, prior to Bølling-Allerød warmth) and again during the Younger Dryas cold event [*McManus et al.*, 2004] traps nutrients in the North Atlantic, and depletes them in the rest of the upper ocean, which in turn decreases ocean productivity in the North Pacific [*Schmittner et al*., 2007]. In this biogeochemical model, phosphate and nitrate accumulate in the interior ocean and productivity rebounds about 600 years after the initial reduction as the nutrient inventory adjusts to the change in circulation. Accompanying the accumulation of nutrients in the interior Pacific predicted by this model, benthic $\delta^{13}C$ should be depleted leading up to the rebound in productivity. In contrast, the benthic $\delta^{13}C$ record of EW0408-85JC shows enrichment in $\delta^{13}C$ associated with the onset of both the Bølling-Allerød and early Holocene productive intervals, seeming to contradict the global nutricline adjustment hypothesis as a cause of these events.

In Hypothesis 3, the driver of the deglacial productivity events would be an enhanced supply of micronutrients such as iron to the marine environment via eolian dust or volcanic eruptions. Dust is thought to be an important source of dissolved iron to surface waters in most areas of the open ocean [*Martin*, 1990; *Duce and Tindale*, 1991]. However, dust concentrations in marine sediment and ice core records suggest that dust fluxes were higher during glacial and stadial intervals, and lower in warmer interstadial or interglacial intervals; atmospheric supply during the Last Glacial Maximum may have been 5-50 times greater than modern day [*de Angelis et al*., 1987; *Winckler et al*, 2008; *Martinez-Garcia* et al., 2009]. This offset in timing between observations of high atmospheric dust content and the deglacial productivity highs of the North Pacific makes increased eolian iron supply an unlikely driver of these particular events. Alternatively, volcanic ash may be a source of iron. This would require a period of enhanced volcanic activity sufficiently prolonged to drive anomalously high productivity for up to two millennia. We found no evidence for the presence of volcanic ash in the laminated silica-rich sediments of the high production intervals, so local ash fertilization cannot be invoked. *Huybers and Langmuir* [2009] infer a 200-600% increase in volcanism in areas experiencing deglaciation following the LGM, possibly related to decompression of the mantle associated with ablating ice sheets. However their inferred increase in global volcanism does not begin until 12,000 cal ybp, and peaks near 7,000 cal ybp before subsiding to near-glacial levels in the modern day. This significantly post-dates the larger B-A productivity event and has no convincing relationship to the shorter early-Holocene productivity event. The enhanced volcanic fertilization scenario is unlikely to explain the abrupt onset of high productivity and anoxia associated with the deglacial laminated intervals.

In Hypothesis 4, the deglacial retreat of the Cordilleran Ice Sheet would increase the supply of meltwater-delivered dissolved nutrients and glacial flour. Fluvial input today delivers both iron and silicic acid to the Gulf of Alaska [*Stabeno et al*., 2004] and iron in Alaskan glacial rock flour is ten times more soluble than iron in Chinese Loess or Saharan Dust [*Schroth et al*., 2009]. Mega-floods associated with the draining of glacial lake Atna reached the Gulf of Alaska via the Copper River as recently as ~10,000 ybp [*Ferrians*, 1989; *Shimer*, 2009], and could have transported glacial rock flour from the retreating Cordilleran Ice Sheet. However, regional increases in glacial flour delivery to the Gulf of Alaska cannot explain the apparently coincident productivity maxima around the margins of the North Pacific, and far from glaciated coastlines.

In Hypothesis 5, the deglacial sea-level rise could increase the supply of iron via remobilization of iron from sediments deposited on previously subaerial shelves. Dissolved iron is transported today from shelves in shallow subsurface waters [*Johnson et al*., 1999; *Lam and Bishop*, 2008]. These sub-surface particulate iron maxima contain a relatively high proportion of reduced iron (Fe^{2+} comprises up to 25% of the total Fe; *Lam and Bishop* [2008]). Primary mineral phases dominated by Fe^{2+} are soluble in oxidizing water conditions [*Moffett*, 2001], increasing their bioavailability in the upper ocean. The large phytoplankton blooms artificially induced during the SERIES iron addition experiments in the Gulf of Alaska were seeded with ferrous sulphate ($Fe^{2+}SO_4$) [*Boyd et al.*, 2004].

Mix et al. [1999] first hypothesized remobilization of shelf-sources of iron during sealevel rise as an explanation for deglacial productivity events observed off of Oregon, citing resuspension of particulate iron as a potential fertilization mechanism. More recently, *Severmann et al*. [2006; 2008; 2010] described dissolved iron flux from suboxic continental shelf sediments. Combining these ideas, we suggest that abrupt sea-level rise during deglaciation inundated previously exposed coastal plains on the continental shelf, which were depocenters of glacial, fluvial, and aeolian sediment. Suspension of these sediments would provide iron (and other) nutrients, which would in turn increase regional biological productivity near the ocean margins and drive anoxia in the shelf sediments. Iron release would then be further enhanced within these suboxic sediments [*Severmann et al*., 2008; 2010], fueling production in a positive feedback mechanism. Remobilization of sedimentary iron associated with sea-level rise may be a particularly potent mechanism in the North Pacific, a region with volcanic margins, vast continental shelves and two large, shallow marginal seas (the Bering and Okhotsk).

In support of this hypothesis, the onset of both North Pacific productivity highs are coincident with periods of rapid sea-level rise. For example, Meltwater Pulse 1A, which was initiated at 14,690 ± 85 cal ybp [*Weaver et al*., 2003, *Kienast et al.,* 2003, *Deschamps et al*., 2009] was coincident, within analytical error, with the onset of the older Gulf of Alaska laminated interval (14,790 ± 380 cal ybp). A less abrupt sealevel rise known as Meltwater Pulse 1B at ~11,300 cal ybp [*Fairbanks,* 1989; *Bard et al*., 1990, 1993] but reduced in rate by *Bard et al*., [2010]), coincides (within dating uncertainties) with the onset of the younger laminated interval in the Gulf of Alaska (11,140 ± 85 cal ybp) .

An attractive feature of sea-level rise as a major driver of North Pacific productivity pulses is that this provides a plausible mechanism to link the events described in the Gulf of Alaska with apparently simultaneous observations from continental margin environments throughout the North Pacific [*Keigwin et al*., 1992; *Ortiz et al*., 1997; *Lund and Mix*, 1998; *Mix et al*., 1999; *Keigwin*, 2002; *Barron et al.*, 2003; *Hendy and Kennett*, 2003; *Van Geen et al*., 2003; *Crusius et al*., 2004; *Gorbarenko et al*., 2004; *McKay et al*., 2004; *Barron et al*., 2005; *Cook et al*., 2005; *Okazaki et al*., 2005; *Dean et al*., 2006; *Shibahara et al.*, 2007; *Hendy and Cosma*, 2008; *Okazaki et al.*, 2010, *Cassie et al.*, 2010]. This hypothesis is further supported by the recent findings of *Klinkhammer et al*. [2009], who report elevated Mn/Ca ratios in foraminiferal tests from the Eastern Tropical North Pacific as evidence for dissolved terrestrial input to coastal waters being higher during intervals of sealevel rise.

3.7. Conclusions

The detailed radiocarbon chronology of high-accumulation rate jumbo piston core EW0408-85JC and its associated trigger core and multicore provide an opportunity to place high-latitude North Pacific climate changes into a global chronological framework.

Retreat of glaciers in the region of the northeastern Gulf of Alaska began by 16,650 ± 170 cal ybp, based on apparent salinity reductions recorded in planktonic foraminiferal $\delta^{18}O$ and a decrease in the rate of glacial-marine sediment accumulation. The transition from the ice-proximal to laminated hemipelagic sediments at 14,790 ± 380 ybp marks the retreat of glaciers either behind sills or onto land.

An interval of low $\delta^{18}O$ in planktonic foraminifera reflects regional freshwater input from retreating glaciers between 16,650 ± 210 cal ybp and 13,770 ± 120 cal ybp ± 200 cal ybp. A more abrupt low $\delta^{18}O$ event in the benthic foraminifera at 14,250 ± 290 cal ybp likely reflects an injection of low-salinity water to 580 m paleodepth driven by rapid glacial melt, perhaps due to low surface salinities that enhanced winter sea-ice cover and attendant brine formation on the shelf. Alternatively, the benthic foraminiferal oxygen isotopic excursion could reflect hyperpycnal flows or a transient deepening of the halocline.

Radiocarbon dates constrain the timing of deglacial warming and freshening of the Gulf of Alaska as coeval with the onset of Bølling interstadial warmth of the North Atlantic and Greenland. North Pacific cooling and/or an increase in surface salinities during Allerød interstadial time may reflect the influence of the Antarctic Cold Reversal, likely transmitted via the subsurface ocean.

Productivity maxima drove sedimentary anoxia and laminated sediments occur between 14,790 ± 380 to 12,990 ± 190 cal ybp and between 11,160 ± 130 to 10,750 ± 220 cal ybp. These events are similar to and likely correlative with, less precisely dated events observed around the rim of the North Pacific. The high-resolution chronology links these events to episodes of global sealevel rise. We evaluate several hypotheses to explain these events, and conclude that remobilization of iron and other limiting nutrients from continental shelves and inundated estuaries during sealevel rise may help to explain synchronous increases in productivity and anoxia that preserved laminated sediments in many places around the margins of the North Pacific.

3.8 Acknowledgments

The authors gratefully acknowledge the crew and science party of cruise EW0408, Nick Pisias for valuable commentary and insight, John Southon and the staff of the UCI Keck AMS laboratory, Jennifer McKay, Andy Ross, and the OSU Stable Isotope Facility. We thank Maziet Cheseby, Bobbi Conard, Mysti Weber, and the OSU Marine Geology Repository. We thank Eric Galbraith and Ingrid Hendy for their assistance in assembling the planktic stable isotope data from extant North Pacific records. We also thank the two anonymous reviewers, whose thoughtful comments substantially improved the manuscript. This work was funded by National Science Foundation Paleoclimate Grant ATM-0602395 to ACM, National Science Foundation Geophysics Grant EAR-0711584 to JSS and ACM, and National Science Foundation Ocean Drilling Grants OCE-0242084 to ACM and OCE-0351096 to JJ, BF, and JSS.

3.9 References:

Addison J.A., B.P. Finney, W.E. Dean, M.H. Davies, A.M. Mix, J.M. Jaeger, Productivity maxima and sedimentary $\delta^{15}N$ during the Last Glacial Maximum termination in the Gulf of Alaska, *Paleoceanography,* submitted.

Aharon, P. (2006), Entrainment of meltwaters in hyperpycnal flows during deglaciation superfloods in the Gulf of Mexico, *Earth Planet. Sci. Lett.*, *241,* 260-270.

Andersen, K.K., A. Svensson, S.J. Johnsen, S.O. Rasmussen, M. Bigler, R. Rothlisberger, U.Ruth, M.-L. Siggaard-Andersen, J.P. Steffensen (2006), The Greenland Ice Core Chronology 2005, 15-42 ka, Part 1: Constructing the time scale. *Quat. Sci. Rev. (25), Shackleton Special Issue 24.*

Barclay, D.J., G.C. Wiles and P.E. Calkin (2009), Holocene glacier fluctuations in Alaska, *Quat. Sci. Rev, 28,* 2034-2048.

Bard, E., B. Hamelin, and D. Delanghe-Sabatier (2010), Deglacial Meltwater Pulse 1B and Younger Dryas sea levels revisited with boreholes at Tahiti, *Science*, 1-4.

Bard, E. , B. Hamelin, and R.G. Fairbanks (1990), U-Th ages obtained by mass spectrometry in corals from Barbados: sea-level during the past 130,000 years. *Nature, 346*, 456-458.

Bard, E., M. Arnold, R.G. Fairbanks and B. Hamelin (1993), $^{230}Th/^{234}U$ and ^{14}C ages obtained by mass spectrometry on corals, *Radiocarbon, 35,* 191-199.

Barron, J. A., L. Heusser, T. Herbert, and M. Lyle (2003), High-resolution climatic evolution of coastal northern California during the past 16,000 years, *Paleoceanography*, *18*(1).

Barron, J. A., D. Bukry, and W.E. Dean (2005), Paleoceanographic history of the Guaymas Basin, Gulf of California, during the past 15,000 years based on diatoms, silicoflagellates, and biogenic sediments, *Marine Micropaleontology*, *56*(3-4), 81-102.

Barron, J. A., D., Bukry, W.E.. Dean, J.A. Addison, and B. Finney (2009), Paleoceanography of the Gulf of Alaska during the past 15,000 years: results from diatoms, silicoflagellates, and geochemistry, *Marine Micropaleontology*, *72*, 176-195.

Bauch, D., and H. A. Bauch (2001), Last glacial benthic foraminiferal $\delta^{18}O$ anomalies in the polar North Atlantic: A modern analogue evaluation, *J. Geophys, Res., 106*, 9135-9143.

Behl, R. J., and J. P. Kennett (1996), Evidence for brief interstadial events in the Santa Barbara Basin, NE Pacific during the past 60 Kyr, *Nature, 379,* 243-246.

Blunier, T., and E. Brook, Timing of millennial-scale climate change in Antarctica and Greenland during the Last Glacial Period, *Science, 5,*109-112.

Blunier, T., J. Schwander, B. Stauffer, T. Stocker, A. Dallenbach, A. Indermuhle, J. Tschumi, J. Chappellaz, D. Raynaud, J.-M. Barnola (1997), Timing of the Antarctic cold reversal and the atmospheric CO_2 increase with respect to the Younger Dryas Event, *Geophys. Res. Lett., 24*(21), 2683-2686.

Bond, G., W. Showers, M. Cheseby, R. Lotti, P. Almasi, P. deMenocal, P. Priore, H. Cullen, I. Hajdas, G. Bonani (1993), A pervasive millennial-scale cycle in North Atlantic Holocene and Glacial climates, *Science, 278,* 1257-1266.

Bond, G., B. Kromer, J. Beer, R. Muscheler, M. N. Evans, W. Showers, S. Hoffmann, R. Lotti-Bond, I. Hajdas, G. Bonani (2001), Persistent solar influence on North Atlantic climate during the Holocene, *Science, 294*, 2130-2136.

Boyd, P. W., C.S. Law, C.S. Wong, Y. Nojiri, A. Tsuda, M. Levasseur, S. Takeda, R. Rivkin, P.J. Harrison, R. Strzepek, J. Gower, R.M. McKay, E. Abraham, M. Arychuk, J. Barwell-Clarke, W. Crawford, D. Crawford, M. Hale, K. Harada, K. Johnson, H.

Kiyosawa, I. Kudo, A. Marchetti, W. Miller, J. Needoba, J. Nishioka, H. Ogawa, J. Page, M. Robert, J. Saito, A. Sastri, N. Sherry, T. Soutar, N. Sutherland, Y. Taira, F. Whitney, S.-K. E. Wong, and T. Yoshimura (2004), The decline and fate of an iron-induced subarctic phytoplankton bloom, *Nature, 428*(6982), 549-553.

Briner, J.P., D.S. Kaufman, A. Werner, M. Caffee, L. Levy, W.F. Manley, M.R. Kaplan, and R. Finkel (2002). Glacier readvance during the late glacial (Younger Dryas?) in the Ahklun Mountains, southwestern Alaska, *Geology, 30*, 679-682.

Broecker, W.S. (1994) Massive iceberg discharges as triggers for global climate change. *Nature, 372*, 421-424.

Broecker, W., S. A. Mix, M. Andree, and H. Oeschger (1984), Radiocarbon measurements on co-existing benthic and planktonic foraminiferal shells: Potential for reconstructing ocean ventilation times over the past 20,000 years, *Nuclear Instruments and Methods in Physics Research, B5,* 340-345.

Brunelle, B.G., D.M. Sigman , S.L. Jaccard , L.D. Keigwin, B. Plessen, G. Schettler, M.S. Cook, G.H. Haug (2010) Glacial/interglacial changes in nutrient supply and stratification in the western subarctic North Pacific since the penultimate glacial maximum, Quaternary Science Reviews, 29, 2579-2590.

Caissie, B.E., J. Brigham-Grette, K.T. Lawrence, T.D. Herbert, and M.S. Cook (2010), Last Glacial Maximum to Holocene sea surface conditions at Umnak Plateau, Bering Sea, as inferred from diatom, alkenone, and stable isotope records, *Paleoceanography, 25,* doi:10.1029/2008PA001671.

Carlson, P. R. (1989), Seismic reflection characteristics of glacial and glacimarine sediment in the Gulf of Alaska and adjacent fjords, *Mar. Geol., 85,* 391-416.

Chase, Z., P. Strutton, and B. Hales (2007), Iron links river runoff and shelf width to phytoplankton biomass along the U.S. West Coast, *Geophys. Res. Lett. 34,* doi:10.1029/2006GL028069.

Childers, A. R., T.E. Whitledge, and D.A. Stockwell (2005), Seasonal and interannual variability in the distribution of nutrients and chlorophyll *a* across the Gulf of Alaska shelf: 1998-2000. *Deep-Sea Res. II, 52,* 193-216.

Cook, M. S., L.D. Keigwin, and C.A. Sancetta (2005), The deglacial history of surface and intermediate water of the Bering Sea, *Deep-Sea Res., Part II*, *52*(16-18), 2163-2173.

Crusius, J., T. Pedersen, S. Kienast, L. Keigwin, and L. Labeyrie (2004), Influence of northwest Pacific productivity on North Pacific Intermediate Water oxygen concentrations during the Boiling-Allerød interval (14.7-12.9 ka), *Geology*, *32*(7), 633-636.

Dean, W. E. (2007), Sediment geochemical records of productivity and oxygen depletion along the margin of western North America during the past 60,000 years: teleconnections with Greenland Ice and the Cariaco Basin, *Quat. Sci. Rev.*, *26*(1-2), 98-114.

Dean, W. E., Y. Zhen, J.D. Ortiz, A. van Geen (2006), Sediment Cd and Mo accumulation in the oxygen-minimum zone off western Baja California linked to global climate over the past 52 kyr, *Paleoceanography*, *21*(4), 13.

De Angelis, M., N.I. Barkov, and V.N. Petrov, (1987): Aerosol concentrations over the last climatic cycle (160 kyr) from an Antarctic ice core, *Nature, 325*, 318-321.

Deschamps, P., N. Durand, E. Bard, B. Hamelin, G. Camoin, A.L. Thomas, G.M. Henderson, and Y. Yokoyama (2009), Synchroneity of Meltwater Pulse 1A and the Bolling onset: New evidence from IODP "Tahiti Sea-Level" expedition, Geophysical Research Abstracts, Vol. 11, EGU2009-10233, EGU General Assembly 2009, Vienna, Austria.

Duce, R. A., and N. W. Tindale (1991), Atmospheric transport of iron and its deposition in the ocean, *Limn. Oceanogr., 36(8),* 1715-1726.

Engstrom, D. R., B.C.S. Hansen, and H.E. Wright, Jr. (1990), A possible Younger Dryas record in Southeastern Alaska, *Science 7,* doi:10.1126/science.250.4986.1383.

Fairbanks, R.G. (1989). A 17,000 year glacio-eustatic sea level record: influence of glacial melting rates on the Younger Dryas event and deep ocean circulation, *Nature, 260*, 962-968.

Ferrians, O. J. (1989), Glacial Lake Atna, Copper River Basin, Alaska. In: Carter, L.D., Hamilton, T.D., and Galloway, J.P. (Eds.), *Late Cenezoic History of the Interior Basins of Alaska and the Yukon,* US Geological Survey Circular 1026, 85-89.

Fisher, D., E. Osterberg, A. Dyke, D. Dahl-Jensen, M. Demuth, C. Zdanowicz, J. Bourgeois, R.M. Koerner, P. Mayewski, C. Wake, K. Kreutz, E. Steig, J. Zheng, K. Yalcin, K. Goto-Azuma, B. Luckman, and S. Rupper (2008), The Mount Logan late Wisconsonian isotope record: tropical Pacific Yukon connections. *The Holocene 18,* 667-677.

Fraile, I., S. Mulitza, and M. Schulz (2009), Modeling planktonic foraminiferal seasonality: Implications for sea-surface temperatures. *Marine Micropaleontology, 72,* doi:10.1016/j.marmicro.2009.01.003.

Fukasawa, M., H. Freeland, R. Perkin, T. Watanabe, H. Uchida, A. Nishina (2004), Bottom water warming of the North Pacific Ocean, *Nature, 427,* 825-827.

Galbraith, E.D., S.J. Jaccard, T.F. Pedersen, D.M. Sigman, G.H. Haug, M. Cook, J.R. Southon, and R. Francois (2007), Carbon dioxide release from the North Pacific abyss during the last deglaciation, *Nature, 449*, 890-893.

Gansen G., and D. Kroon (2000), The isotopic signature of planktonic foraminifera from NE Atlantic surface sediments: implications for the reconstruction of past oceanic conditions, *J. Geol. Soc. London, 157,* 639-699.

Gebhardt, H, M. Sarnthein, P.M. Grootes, T. Kiefer, H. Keuhn, F. Schmieder, and U. Rohl (2008), Paleonutrient and productivity records from the subarctic North Pacific for Pleistocene glacial terminations I to V, *Paleoceanography 23*, PA4212, doi:10.1029/2007PA001513.

Gorbarenko, S. A., J.R. Southon, L.D. Keigwin, M.V. Cherepanova, and I.G. Gvozdeva (2004), Late Pleistocene-Holocene oceanographic variability in the Okhotsk Sea: geochemical, lithological and paleontological evidence, *Palaeogeography Palaeoclimatology Palaeoecology 209*(1-4), 281-301.

Hendy, I. L., and T. N. Cosma (2008) Vulnerability of the Cordilleran Ice Sheet to iceberg calving during late Quaternary rapid climate change events, *Paleoceanography*, *23*, PA2101, doi:2110.1029/2008PA001606.

Hendy, I. L., and J. P. Kennett (2003), Tropical forcing of North Pacific intermediate water distribution during Late Quaternary rapid climate change?, *Quat. Sci. Rev, 22*(5-7), 673-689.

Hendy, I.K., T.F. Pedersen, J.P. Kennett, and R. Tada (2004), Intermittent existence of a southern Californian upwelling cell during submillennial climate change of the last 60 kyr, *Paleoceanography, 19,* PA3007, doi:10.1029/2003PA000965.

Hendy, I. L., and T. F. Pedersen (2006), Oxygen miminum zone expansion in the eastern tropical North Pacific during deglaciation, *Geophys. Res. Lett., 33,* L20602, doi:10.1029/2006GL025975.

Hajdas, I., G. Bonani, P. Bodén, D. M. Peteet, and D.H. Mann (1998), Cold reversal on Kodiak Island, Alaska, correlated with the European Younger Dryas by using variations in atmospheric ^{14}C content. *Geology, 26*, 1047-1050.

Hostetler, S.W., P.U. Clark, P.J. Bartlein, A.C. Mix, and N.J. Pisias (1999), Atmospheric transmission of North Atlantic Heinrich events, *J. Geophys. Res., 104,* 3947-3952.

Hu, F.S., D. M. Nelson, G. H. Clarke, K.M. Rühland, Y. Huang, D.S. Kaufman, and J.P. Smol (2006), Abrupt climate events during the last glacial-interglacial transition in Alaska, *Geophys. Res. Lett. 33,* doi:10.1029/2006GL027261

Huybers, P. and C. Langmuir (2009), Feedback between deglaciation, volcanism, and atmospheric CO2, *Earth Planet. Sci. Lett., 286* 479-491.

Imran, J., and J.P.M. Syvitski (2000), Impact of extreme river events on the coastal ocean, *Oceanography, 13,* 85-92.

Jaeger, J. M., C.A. Nittrouer, N.D. Scout, and J.D. Milliman (1998), Sediment accumulation along a glacially impacted mountainous coastline: North-east Gulf of Alaska, *Basin Res.*, *10*(1), 155-173.

Johnson, W.R., T.C. Royer, and J.L. Luick (1988), On the seasonal variability of the Alaska Coastal Current. *J. Geophys. Res. 93*, 12423–12437.

Johnson, K.S., F.P. Chavez, and G.E. Friederich (1999), Continental-shelf sediment as a primary source of iron for coastal phytoplankton, *Nature, 398*, 697-700.

Kiefer, T., M. Sarnthein, H. Erlenkeuser, P.M. Grootes, A.P. Roberts (2001). North Pacific response to millennial-scale changes in ocean circulation over the last 60 ky. *Paleoceanography* 16, 179-189.

Keigwin, L. D. (2002), Late Pleistocene-Holocene paleoceanography and ventilation of the Gulf of California, *J. Oceanogr.*, *58*(2), 421-432.

Keigwin, L. D., G.A. Jones, and P.N. Froelich (1992), A 15,000 year paleoenvironmental record from Meiji Seamount, Far Northwestern Pacific, *Earth Planet. Sci. Lett.*, *111*(2-4), 425-440.

Keigwin, L.D. (1998), Glacial-age hydrography of the far northwest Pacific Oceani, *Paleoceanography, 13,* 323-339.

Kienast, M., T.J.J. Hanebuth, C. Pelejero, and S. Steinke (2003), Synchroneity of Meltwater Pulse 1A and the Bølling warming: new evidence from the South China Sea, *Geology*, *31*(1), 67-70.

Klinkhammer, G. P., A.C. Mix, and B.A. Haley (2009), Increased dissolved terrestrial input to the coastal ocean during the last deglaciation, *Geochem. Geophys. Geosyst.,*10, Q03009, doi: 10.1029/2008GC002219.

Kotilainen, A. T. and N .J. Shackleton, (1995), Rapid climate variability in the North Pacific Ocean during the past 95,000 years, *Nature* 377, 323-326.

Lam, P.J., and J.K.B. Bishop (2008), The continental margin is a key source of iron to the HNLC North Pacific Ocean, *Geophys. Res. Lett., 35,* L07608, doi:10.1029/2008GL033294.

Lippiatt, S.M., M.C. Lohan, K.W. Bruland (2010), The distribution of reactive iron in northern Gulf of Alaska coastal waters, *Marine Chemistry, 121,* doi:/10.1016/j.marchem.2010.04.007.

Lopes, C. and A. C. Mix (2009), Pleistocene megafloods in the northeast Pacific, *Geology*, *37(1),* 79-82.

Lund, D. C., and A. C. Mix (1998), Millenial-scale deep water oscillations: reflections of the North Atlantic in the deep Pacific from 10 to 60 ka, *Paleoceanography*, *13*(1), 10-19.

Mahowald, N.M., A. R. Baker, G. Bergametti, N. Brooks, R.A. Duce, T.D. Jickells, N. Kubilay, J.M. Prospero, and I. Tegen (2005), Atmospheric global dust cycle and iron inputs to the ocean, *Global Biogeochem. Cycles, 19,* GB4024, doi:10.1029/2004GB002402.

Manley, W.F., and D.S. Kaufman (2002), Alaska PaleoGlacier Atlas, Institute of Arctic and Alpine Research (INSTARR), University of Colorado, http://instaar.colorado.edu/QGISL/ak_paleoglacier_atlas, v. 1.

Mann, D.H., and D.M. Peteet (1994), Extent and timing of the Last Glacial Maximum in Southwestern Alaska, *Quat. Res., 42(2),*136-148.

Martin, J.H. (1990), Glacial-Interglacial CO_2 Change: The Iron Hypothesis, *Paleoceanography*, *5(1),* 1-13.

Martinez-Garcia, A., A. Rosell-Mele, W. Geibert, R. Gersonde, P. Masqué, V. Gaspari, and C. Barbante (2009), Links between iron supply, marine productivity, sea surface temperature, and CO_2 over the last 1.1 Ma, *Paleoceanography, 24,* PA1207, doi:10.1029/2008PA001657.

Masuda, S., T. Awaji, N. Sugiura, J.P. Matthews, T. Toyoda, Y. Kawai, T. Doi, S. Kouketsu, H. Igarashi, K. Katsumata, H. Uchida, T. Kawano, M. Fukasawa (2010), Simulated rapid warming of the abyssal North Pacific waters, *Science, 329*, 319-322.

McDonald, D., T.F. Pedersen, and J. Crusius, Multiple late Quaternary episodes of exceptional diatom production in the Gulf of Alaska, *Deep-Sea Res., Part II*, *46(11-12)*, 2993-3017.

McKay, J.L., T.F. Pedersen, and S.S. Kienast (2004), Organic carbon accumulation over the last 16 kyr off Vancouver Island, Canada: Evidence for increased marine productivity during the deglacial, *Quat. Sci. Rev., 23,* 261-281.

McManus, J. F., R. Francois, J.-M. Gherardi, L.D. Keigwin, and S. Brown-Leger (2004), Collapse and rapid resumption of Atlantic meridional circulation linked to deglacial climate changes, *Nature 428*, 834-837.

McNeely, R., A.S. Dyke, and J.R. Southon (2006), Canadian marine reservoir ages, preliminary data assessment, *Geological Survey Canada*, Open File 5049.

Mikolajewicz, U., T.J. Crowley, A. Schiller, and R. Voss (1997), Modelling teleconnections between the North Atlantic and North Pacific during the Younger Dryas. *Nature, 387,* 384-387.

Milliman, J. D., and J. P. M. Syvitski (1992), Geomorphic tectonic control of sediment discharge to the ocean - the importance of small mountainous rivers, *Geology*, *100*(5), 525-544.

Milliman , J. D., D. Stocks, J.M. Jaeger, and C.A. Nittrouer (1996), Prince William Sound, Alaska: distal depocenter for Copper River sediment. *EOS Trans., 77,* OS202.

Mix, A.C., D.C. Lund, N.G. Pisias, P. Bodén, L. Bornmalm, M. Lyle, and J. Pike (1999), Rapid climate oscillations in the Northeast Pacific during the last deglaciation reflect Northern and Southern Hemisphere sources, In: Clark, P.U., et al. (Eds), *Mechanisms of global climate change at millennial time scales,* Am. Geophys. Union Geophysical Monograph 112, 127-148.

Moffett, J. W. (2001), Transformations among different forms of iron in the ocean, In: D. R. Turner and K. A. Hunter (Eds), *The biogeochemistry of iron in seawater*, edited by D. R. Turner and K. A. Hunter, pp. 343-372, John Wiley & Sons, Ltd., West Sussex, England.

Molnia, B. F. (1986), Late Wisconsin glacial history of the Alaskan continental margin. In: Hamilton, T.D., Reed, K.M., Thorson, R.M. (Eds), *Glaciation in Alaska-the Geologic Record*, 99-144. Plenum, New York.

Molnia, B. F., and P. R. Carlson (1978), Surface sedimentary units of the northern Gulf of Alaska continental shelf. *Bull. Am. Assoc. Petrol. Geol., 62,* 633-643.

Mortlock, R.A., and P.N. Froelich (1989), A simple method for the rapid determination of biogenic opal in pelagic marine sediments, *Deep-Sea Res., 36(9),*1415–1426.

Nichols, D.R., and L.A. Yehle (1969), Engineering geologic map of the southeastern Copper River Basin, Alaska, *U.S. Geological Survey Miscellaneous Investigations 524*, 1 sheet scale 1:125,000.

National Institute of Standards and Technology (1992), Report of Investigation, Reference Materials 8543-8546, US Department of Commerce, Gaithersburg, MD, 3pp.

Okazaki, Y., K. Takahashi, H. Asahi, K. Katsuki, J. Hori, H. Yasuda, Y. Sagawa, and H. Tokuyama (2005), Productivity changes in the Bering Sea during the late Quaternary, *Deep-Sea Res., Part II*, *52*(16-18), 2150-2162.

Okazaki, Y., A. Timmermann, K. Menviel, N. Harada, A. Abe-Ouchi, M.O. Chikamoto, A. Mouchet, H. Asahi (2010), Deepwater formation in the North Pacific during the Last Glacial Termination, *Science, 329*, 200-204.

Okumura, Y.M., C. Deser, A. Hu, A. Timmermann, S-P Xie (2008) North Pacific Climate Response to Freshwater Forcing in the Subarctic North Atlantic: Oceanic and Atmospheric Pathways. *J. Clim.* , 22, 1424-1445.

Ortiz, J.D., A. Mix, R.W. Collier (1995), Environmental control of living symbiotic and asymbiotic foraminifera of the California Current, *Paleoceanography, 10,* 987-1009.

Ortiz, J.D., A.C. Mix, W. Ruch, J.M. Watkins, and R.W. Collier (1996), Deep-dwelling planktonic foraminifera of the northeastern Pacific Ocean reveal environmental control of oxygen and carbon isotopic disequilibria, *Geochimica et Cosmochimica Acta, 60,* 4509-4523.

Ortiz, J., A. Mix, S. Hostetler, and M. Kashgarian (1997), The California current of the last glacial maximum: Reconstruction at 42 degrees N based on multiple proxies, *Paleoceanography*, *12*(2), 191-205.

Ortiz, J.D., S.B. O'Connell, J. DelViscio, W. Dean, J.D. Carriquiry, T. Marchitto, Y. Zheng, and A. van Geen (2004), Enhanced marine productivity off western North America during warm climate intervals of the past 52 k.y., *Geology, 32(6)*, doi:10.1130/G20234.1.

Peltier, W.R. (1994), Ice Age Paleotopography, *Science, 256,* 195-201.

Peteet, D. (2007), Muskeg archives of vegetation, migration, and climate history in the Gulf of Alaskan arc. Paper 9–8. In: *Abstracts – Geological Society of America, Cordilleran Section – 103rd Annual Meeting*. http://gsa.confex.com/gsa/2007CD/finalprogram/abstract_120879.htm, Bellingham, Washington.

Rasmussen, S. O., Andersen, K. K., Svensson, A. M., Steffensen, J. P., Vinther, B., Clausen, H. B., Siggaard-Andersen, M.-L., Johnsen, S. J., Larsen, L. B., Dahl- Jensen, D., Bigler, M., R ̈othlisberger, R., Fischer, H., Goto-Azuma, K., Hansson, M., Ruth, U. (2006), A new Greenland ice core chronology for the last glacial termination. *J. Geophys. Res. 111*, D06102.

Rasmusen, T.L., and E. Thomsen (2009) Stable isotope signals from brines in the Barents Sea: Implications for brine formation during the last glaciation, *Geology 37*, 903-906.

Reimer, P.J., M.G.L. Baillie, E. Bard, A. Bayliss, J.W. Beck, P.G. Blackwell, C. Bronk Ramsey, C.E. Buck, G.S. Burr, R.L. Edwards, M. Friedrich, P.M. Grootes, T.P. Guilderson, I. Hajdas, T.J. Heaton, A.G. Hogg, K.A. Hughen, K.F. Kaiser, B. Kromer, F.G. McCormac, S.W. Manning, R.W. Reimer, D.A. Richards, J.R. Southon, S. Talamo, C.S.M. Turney, J. van der Plicht, and C.E. Weyhenmeyer (2009), INTCAL09 and MARINE09 radiocarbon age calibration curves, 0-50,000 years cal BP, *Radiocarbon 51*, 1111-1150.

Rignot, E., and P. Kanagaratnam (2006), Changes in the velocity structure of the Greenland Ice Sheet, *Science 311*, doi: 10.1126/science.1121381.f

Royer, T.C. (1981). Baroclinic transport in the Gulf of Alaska. Part II. Fresh water driven coastal current. *Journal of Marine Research 39*, 251–266.

Royer, T.C. (1982). Coastal fresh water discharge in the northeast Pacific. *J. Geophys.*

Res. 87, 2017–2021.

Royer, T.C. (2005), Hydrographic responses at a coastal site in the northern Gulf of Alaska to seasonal and interannual forcing. *Deep-sea Res. II Top. Stud. Oceanogr., 52(1-2),* 267-288.

Rubin, M., and C. Alexander (1960), U.S. Geological Survey radiocarbon dates V, *Radiocarbon 2*, 129-185.

Ruth, U., J-M Barnola, J. Beer, M. Bigler, T. Blunier, E. Castellano, H. Fischer, F. Fundel, P. Huybrechts, P.R. Kaufmann, J. Kipfstuhl, A. Lambrecht, A. Morganti, H. Oerter, F Parrenin, O. Rybak, M. Severi, R. Udisti, F. Wilhelms, E.W. Wolff (2007): EDML1: a chronology for the EPICA deep ice core from Dronning Maud Land, Antarctica, over the last 150 000 years. Climate of the Past, 3, 475-484, doi:10.5194/cp-3-475-2007

Sabine, C.L., R.M. Key, A. Kozyr, R.A. Feely, R. Wanninkhof, F.J. Millero, T.-H. Peng, J.L. Bullister, and K. Lee (2005), Global Ocean Data Analysis Project: Results and Data. *ORNL/CDIAC-145, NDP-083,* doi: 10.3334/CDIAC/otg.ndp0833.

Saenko, O.A., A. Schmittner, and A.J. Weaver (2004), The Atlantic-Pacific Seesaw, *J. Clim. , 17,* 2033-2038.

Sautter, L.R. and R.C. Thunell (1991) Seasonal variability in the $\delta^{18}O$ and $\delta^{13}C$ of planktonic foraminifera from an upwelling environment: Sediment trap results from the San Pedro Basin, Southern California. *Paleoceanography, 6*, 307-334.

Schmittner, A. (2005), Decline of the marine ecosystem caused by a reduction in the Atlantic overturning circulation, *Nature, 434,* 628-633.

Schmittner, A., and E.D. Galbraith (2008), Glacial greenhouse-gas fluctuations controlled by ocean circulation changes, *Nature 456,* doi:10.1038/nature07531.
Schmittner, A., and T. F. Stocker (1999), The stability of the thermohaline circulation in global warming experiments, *J. Clim. 12,* 1117-1133.

Schmittner, A., E. D. Galbraith, S. W. Hostetler, T. F. Pedersen, and R. Zhang (2007) Large fluctuations of dissolved oxygen in the Indian and Pacific oceans during Dansgaard-Oeschger oscillations caused by variations of North Atlantic Deep Water subduction, *Paleoceanography, 22, PA3207,* doi:10.1029/2006PA001384.

Schroth, A. W., J. Crusius, E.R. Sholkovitz, and B.C. Bostick (2009), Iron solubility driven by speciation in dust sources to the ocean, *Nat. Geosci.*, *2*, 337-340.

Severmann S., Johnson C. M., Beard B. L. and McManus J. (2006) The effect of early diagenesis on the Fe isotope compositions of porewaters and authigenic minerals in continental margin sediments. *Geochim.Cosmochim.Acta* 70, 2006-2022.

Severmann S., Lyons T.W., Anbar A., McManus J. and Gordon G (2008) Modern iron isotope perspective on the benthic iron shuttle and the redox evolution of ancient ocean, *Geology* 36, 487-490.

Severmann S., J. McManus, W.M. Berelson, and D.E. Hammond (2010), The continental shelf benthic iron flux and its isotope composition, *Geochim. Cosmochim. Acta,* doi:10.1016/j.gca.2010.04.022.

Shibahara, A., K. Ohkushi, J.P. Kennett, K. Ikehara (2007), Late Quaternary changes in intermediate water oxygenation and oxygen minimum zone, northern Japan: A benthic foraminiferal perspective, *Paleoceanography, 22,* PA3213, doi:10.1029/2005PA001234.

Shimer, G. (2009), Holocene vegetation and climate change at Canyon Lake, Copper River basin, Alaska, M.S., Dep. Of Geol.and Geophys., Univ. of Alaska, Fairbanks, Alaska, USA.

Svensson, A., K.K. Andersen, M. Bigler, H.B. Clausen, D. Dahl-Jensen, S.M. Davies, S.J. Johnsen, R. Muscheler, S.O. Rasmussen, R. Rothlisberger, J.P. Steffensen, and B.M. Vinther (2006) The Greenland Ice Core Chronology 2005, 15-42 ka. Part 2: Comparison to other records. *Quat. Sci. Rev.(25), Shackleton special issue 24.*

Stabeno, P.J., R.K. Reed, and J.D. Schumacher (1995). The Alaska Coastal Current: continuity of transport and forcing. *J. Geophys. Res. 100*, 2477–2485.

Stabeno, P.J., N.A. Bond, A.J. Hermann, N.B. Kachel, C.W. Mordy, J.E. Overland (2004), Meteorology and oceanography of the Northern Gulf of Alaska, *Continental Shelf Research, 24*, 859-897.

Stuiver, M., and P.J. Reimer (1993), Extended 14C database and revised CALIB radiocarbon calibration program, *Radiocarbon*, *35*, 137-189.

Ten Brink, N.W. (1983), Glaciation of the northern Alaska Range, In: Thorson, R.M., and Hamilson, T.D. (Eds), *Glaciation in Alaska: Extended abstracts from a workshop*. Alaskan Quaternary Center, Univ. of Alaska Museum Occasional Paper 2, 82-91.

Tedesco, K., R. Thunell, Y. Astor, and F. Muller-Karger (2007), The oxygen isotope composition of planktonic foraminifera from the Cariaco Basin, Venezuela: Seasonal and interannual variations. *Marine Micropaleontology 62,* 180-193.

Thorson, R.M., and T.D. Hamilton (1986), Glacial geology of the Aleutian Islands, In: Hamilton, T.D., Reed, K.M., Thorson, R.M. (Eds), *Glaciation in Alaska-the Geologic Record*, 171-192. Plenum, New York.

Tsuda, A., H. Kiyosawa, A. Kuwata, M. Mochizuki, N. Shiga, H. Saito, S. Chiba, K. Imal, J. Nishioka, and T. Ono (2005), Responses of diatoms to iron-enrichment (SEEDS) in the western subarctic Pacific, temporal and special comparisons, *Prog. Oceanogr., 64*(2-4), 189-205.

Van Geen, A., Y. Zheng, J.M. Bernhard, K.G. Cannariato, J. Carriquiry, W.E. Dean, B.W. Eakins, J.D. Ortiz, J. Pike (2003), On the preservation of laminated sediments along the western margin of North America, *Paleoceanography*, *18*(4), 18.

Weaver, A.J., O.A. Saenko, P.U. Clark, and J.X. Mitrovica (2003), Meltwater Pulse 1A from Antarctica as a trigger of the Bølling-Allerød Warm Interval, *Science, 299,* 1709-1713.

Weingartner, T. J., S. K. Danielson, and T.C. Royer (2005) Freshwater variability and predictability in the Alaskan Coastal Current, *Deep Sea Res., Part II, 52*, 161– 191.

Wiedmer, M., D.R. Montgomery, A.R. Gillespie, and H. Greenberg (2010), Late Quaternary megafloods from Glacial Lake Atna, Southcentral Alaska U.S.A., *Quat. Res.,* doi: 10.1016/j.yqres.2010.02.005.

Williams, J.R., and J.P. Galloway (1986), Map of western Copper River Basin, Alaska, showing lake sediments and shorelines, glacial moraines, and location of stratigraphic sections and radiocarbon-dated samples. *U.S. Geological Survey Open-File Report* 86-390, 1 sheet, scale 1:250,000.

Winckler, G., R.F. Anderson, M.Q. Fleisher, D. McGee, N. Mahowald (2008), Covariant glacial-interglacial dust fluxes in the Equatorial Pacific and Antarctica, *Science, 320,* 93-96.

Wu, J., A. Aguilar-Islas, R. Rember, T. Weingertner, S. Danielson, and T. Whitledge (2009), Size-fractionation iron distribution on the northern Gulf of Alaska, *Geophys. Res. Lett., 36,* L11606, doi:10.1029/2009GL038304.

Yehle, L.A., H.R. Schmoll, and A.F. Chleborad (1983), Preliminary surficial geologic map of the southwestern part of the Tyonek B-5 quadrangle, south-central Alaska. *U.S. Geological Survey Miscellaneous Field Investigations Map* MF-1161-B, scale 1:31,680.

Zahn, R., Pedersen, T. F., Bornhold, B. D., and Mix, A. C. (1991), Water mass conversion in the glacial subarctic Pacific [54°N, 148°W]: Physical constraints and the benthic-planktonic stable isotope record, *Paleoceanography, 6*, 543–560.

Zheng, Y., A. van Geen, R.F. Anderson, J.V. Gardner, and W.E. Dean (2000), Intensification of the northeast Pacific oxygen minimum zone during the Bølling-Allerød warm period, *Paleoceanography*, *15*(5), 528-536.

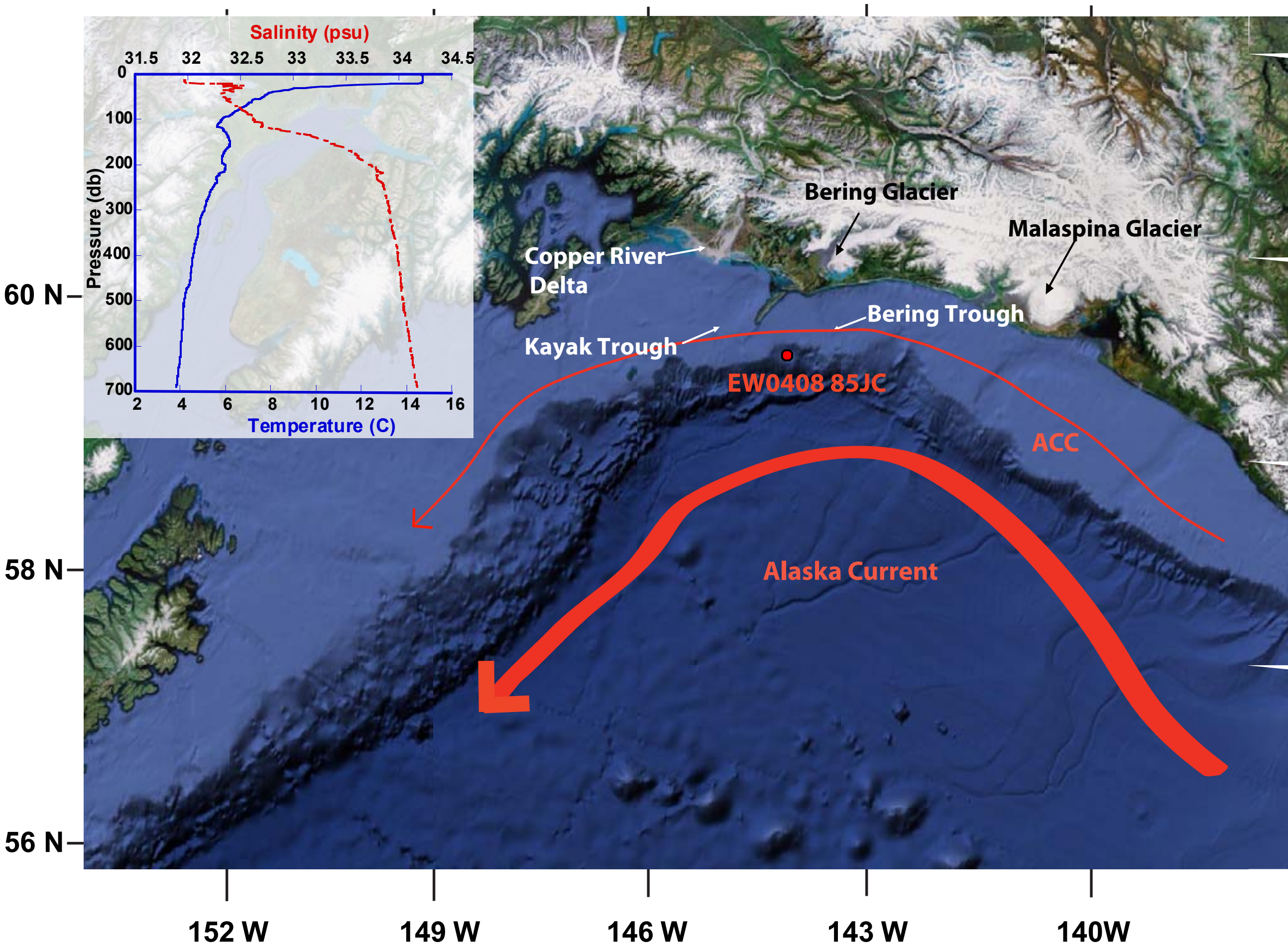

Figure 3.1. Google Earth image (©Google, 2009) of the Gulf of Alaska showing the location of site EW0408-85JC on shaded bathymetry. ACC is the Alaska Coastal Current. The salinity and temperature profiles collected at the core site via CTD cast during August 2004 are shown inset on the upper-left.

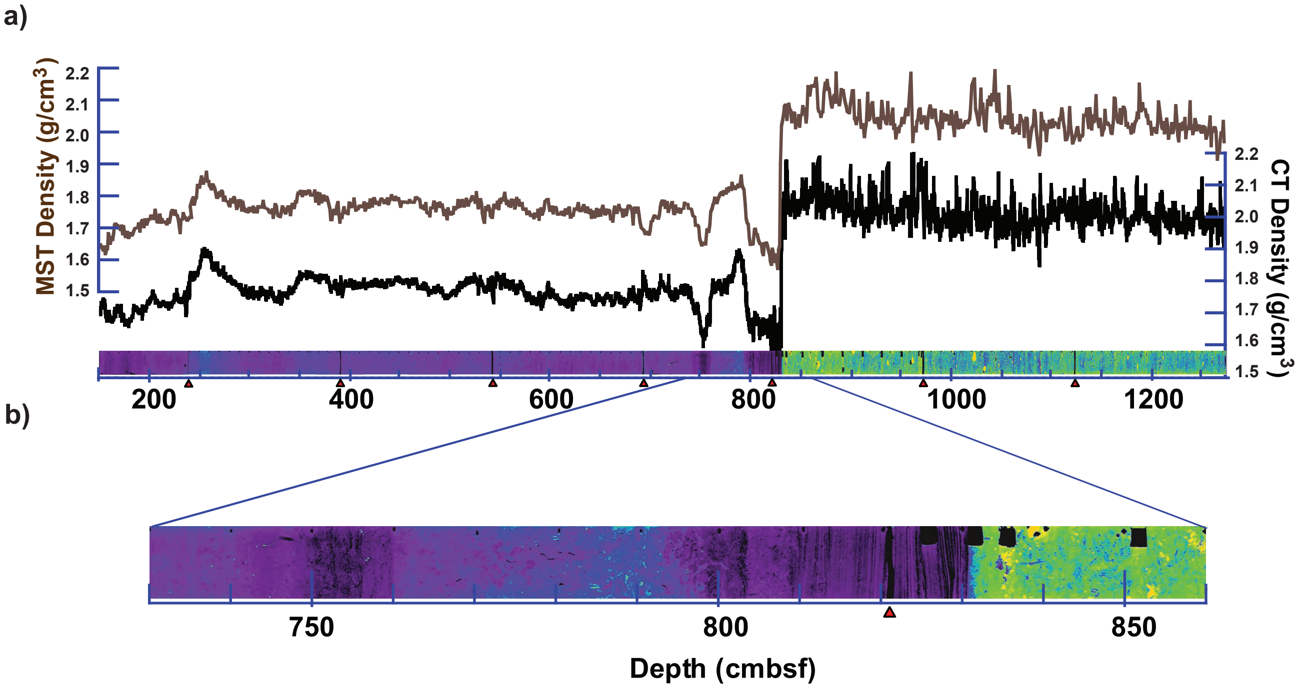

Figure 3.2. a) Computerized tomographic (CT) scans of core EW0408-85JC. Warmer colors (yellow and red) indicate higher densities, and cooler colors (blue and purple) indicate lower densities. CT scan densities (black line) are extracted from the images in a line 100 pixels (~5 mm) wide down the center of the core, and compared to shipboard gamma-ray attenuation densities (gray line) that integrate across the full core before opening. b) The abrupt transition from coarse glacial-marine sediments to finely laminated interval at 831 cmbsf is inferred to represents the time at which the tidewater glaciers of the northwest Cordilleran retreated onto land, or behind regional fjord sills that trapped much of their lithogenic sediment load. Locations of core section breaks are delineated by red triangles below the depth axis.

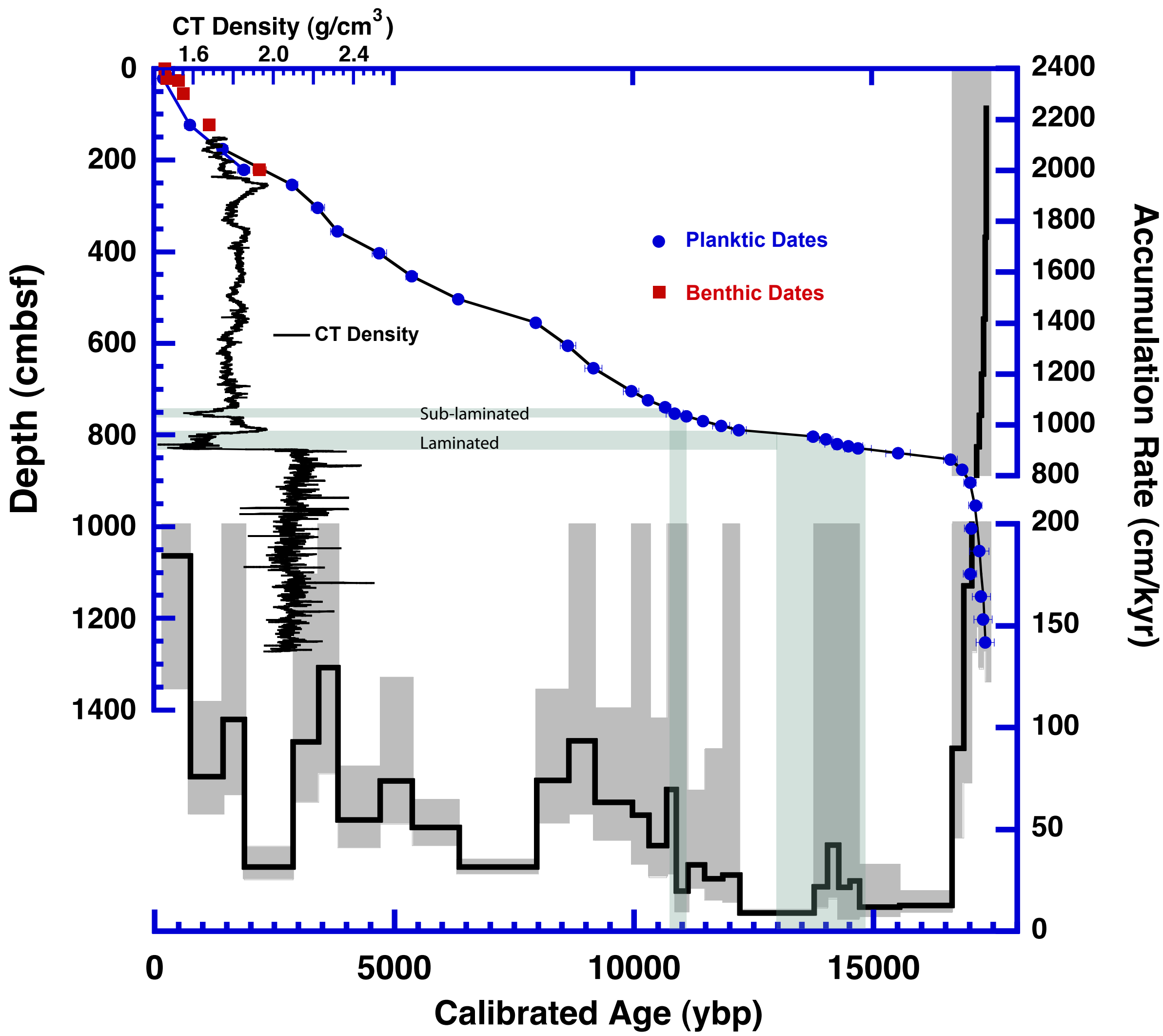

Figure 3.3. Calibrated planktonic (blue circles) and benthic (red squares) radiocarbon dates (shown with 1σ error bars) used to generate the age model for site EW0408-85JC (solid line). Density values from the CT scans are shown against depth on the left, with the laminated and sub-laminated intervals highlighted relative to the age model. Sediment accumulation rates from the age model are shown along the bottom of the figure, with the gray bars indicating the 1σ uncertainties.

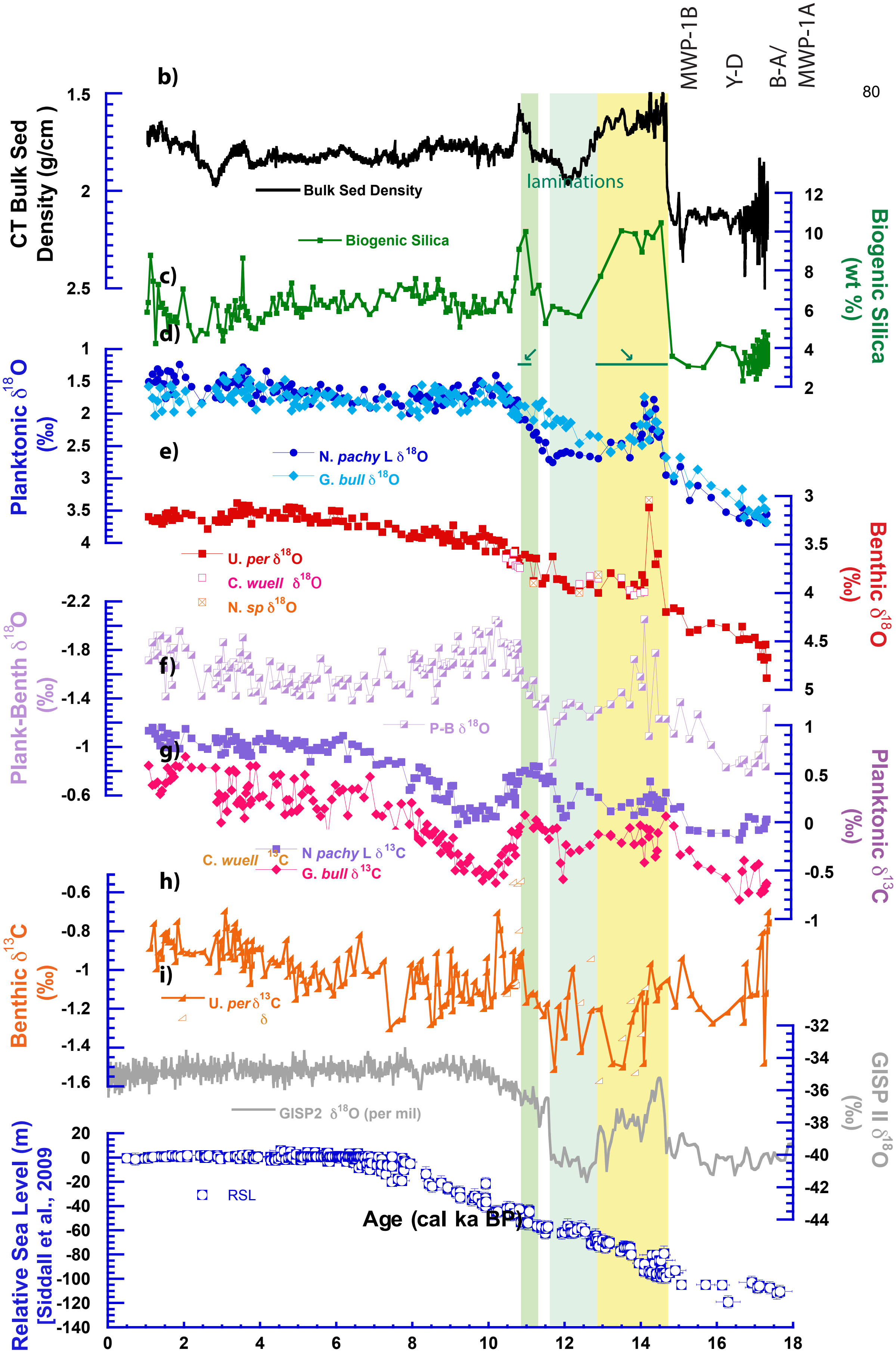
MWP-1B
Y-D
B-A/
MWP-1A
b)
c)
d)
e)
f)
g)
h)
i)
CT Bulk Sed Density (g/cm)
Bulk Sed Density
laminations
Biogenic Silica
Biogenic Silica (wt %)
Planktonic δ18O (‰)
N. pachy L δ18O
G. bull δ18O
U. per δ18O
C. wuell δ18O
N. sp δ18O
Benthic δ18O (‰)
Plank-Benth δ18O (‰)
P-B δ18O
Planktonic δ13C (‰)
C. wuell 13C
N pachy L δ13C
G. bull δ13C
Benthic δ13C (‰)
U. per δ13C
GISP2 δ18O (per mil)
GISP II δ18O (‰)
Relative Sea Level (m) [Siddall et al., 2009
RSL
Age (cal ka BP)

Figure 3.4. (a) The EW0408-85JC CT-derived bulk density data (black line). (b) Opal (green squares; periods of lamination are delineated below the record by green bars). (c) Planktonic $\delta^{18}O$ (*N. pachyderma sinistral* in dark blue circles and *G. bulloides* in light blue diamonds). (d) Benthic $\delta^{18}O$ (*U. peregrina* in solid red squares, *C. wuellerstorfi +0.64* in open red squares, *Nonionella sp.* +0.10 in crossed orange squares). (e) Planktonic – benthic $\delta^{18}O$ (orange squares). (f) Planktonic $\delta^{13}C$ (*N. pachyderma sinistral* in purple squares and *G. bulloides* in pink diamonds). (g) Benthic $\delta^{13}C$ (*U. peregrina* +0.20 in solid orange canted triangles, *C. wuellerstorfi* in open orange canted triangles). For global context these data are presented next to (h) the Greenland ice core $\delta^{18}O$ record (NGRIP; gray line) [*Andersen et al.*, 2006; *Rasmussen et al*., 2006; Svensson et al., 2006] and (i) the sealevel curve compiled in Siddall et al. [2009] (blue hollow squares). Timing of the North Atlantic Bølling-Allerød (B-A) and Younger Dryas (Y-D) climate anomalies is highlighted in yellow and blue, respectively, as well as meltwater pulse (MWP) 1A (yellow, coeval with the B-A), and 1B (green).

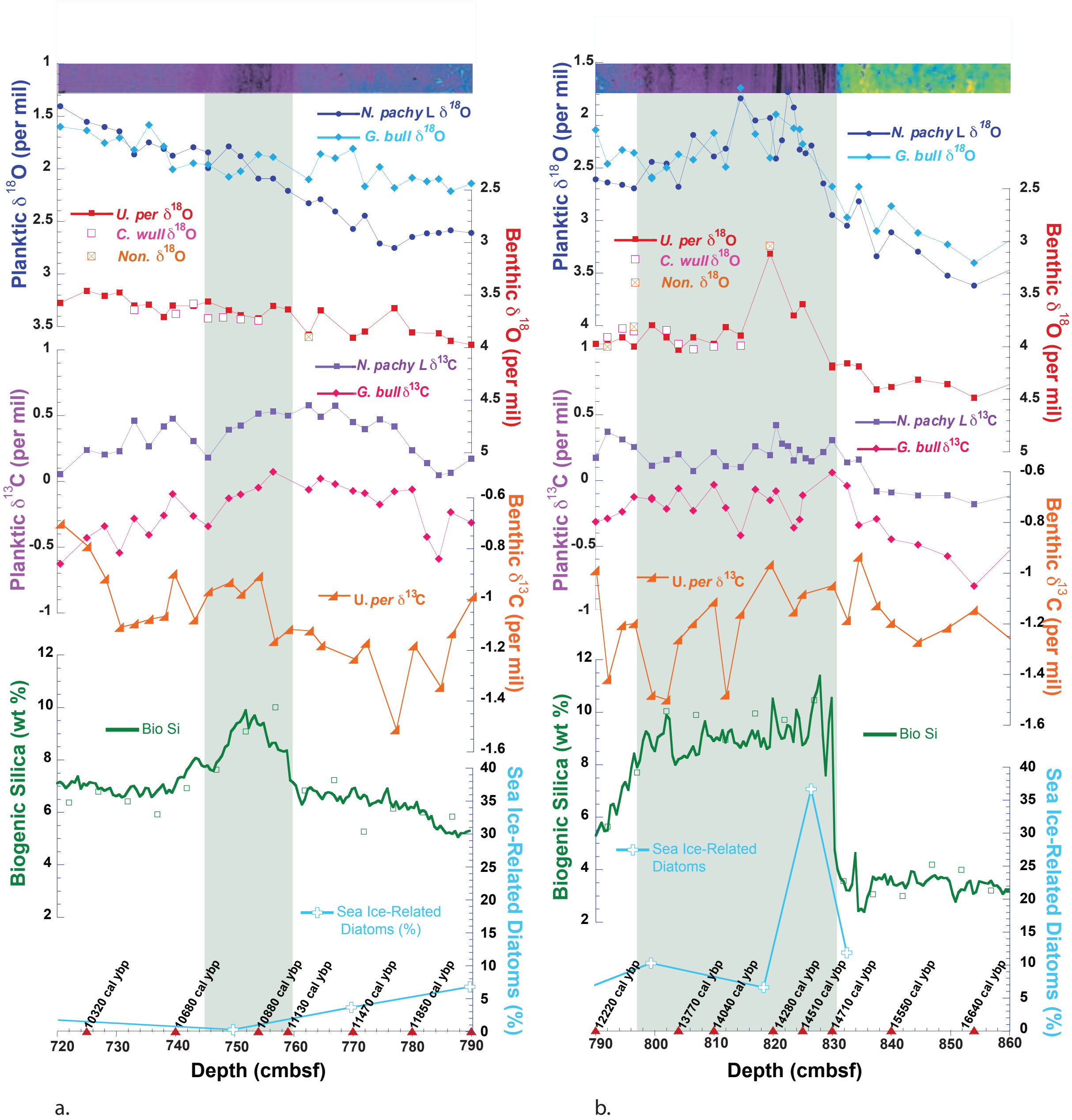

Figure 3.5. Detail of sub-laminated (a) and laminated (b) intervals with stable isotopic records and CT scan results. Planktonic $\delta^{18}O$ (*N. pachyderma sinistral* in dark blue circles and G. bulloides in light blue diamonds), benthic δ18O (*U. peregrina* in solid red squares, *C. wuellerstorfi* in open red squares, Nonionella sp. in crossed orange squares), and planktonic $\delta^{13}C$ (*N. pachyderma sinistral* in purple squares and *G. bulloides* in pink diamonds) are shown versus depth. Benthic $\delta^{13}C$ (*U. peregrina*) is shown in canted orange triangles. Measured opal weight percent is shown (open green squares), superimposed upon a high-resolution opal reconstruction (solid green line) derived from a linear regression between measured silica content and CT scan density ($r^2 = 0.87$). The relative abundance of sea ice and sea ice-related diatoms (*B. fragilis, F. cylindrus, F. oceanica, T. gravida, and T. hyalina*) is also plotted (light blue), from *Barron et al.*, [2009]. The laminated and sub-laminated sections identified in the text are highlighted. Calendar-corrected planktonic foraminiferal radiocarbon dates are shown along the x-axis as labeled red triangles; see Table 1 for calibration precision.

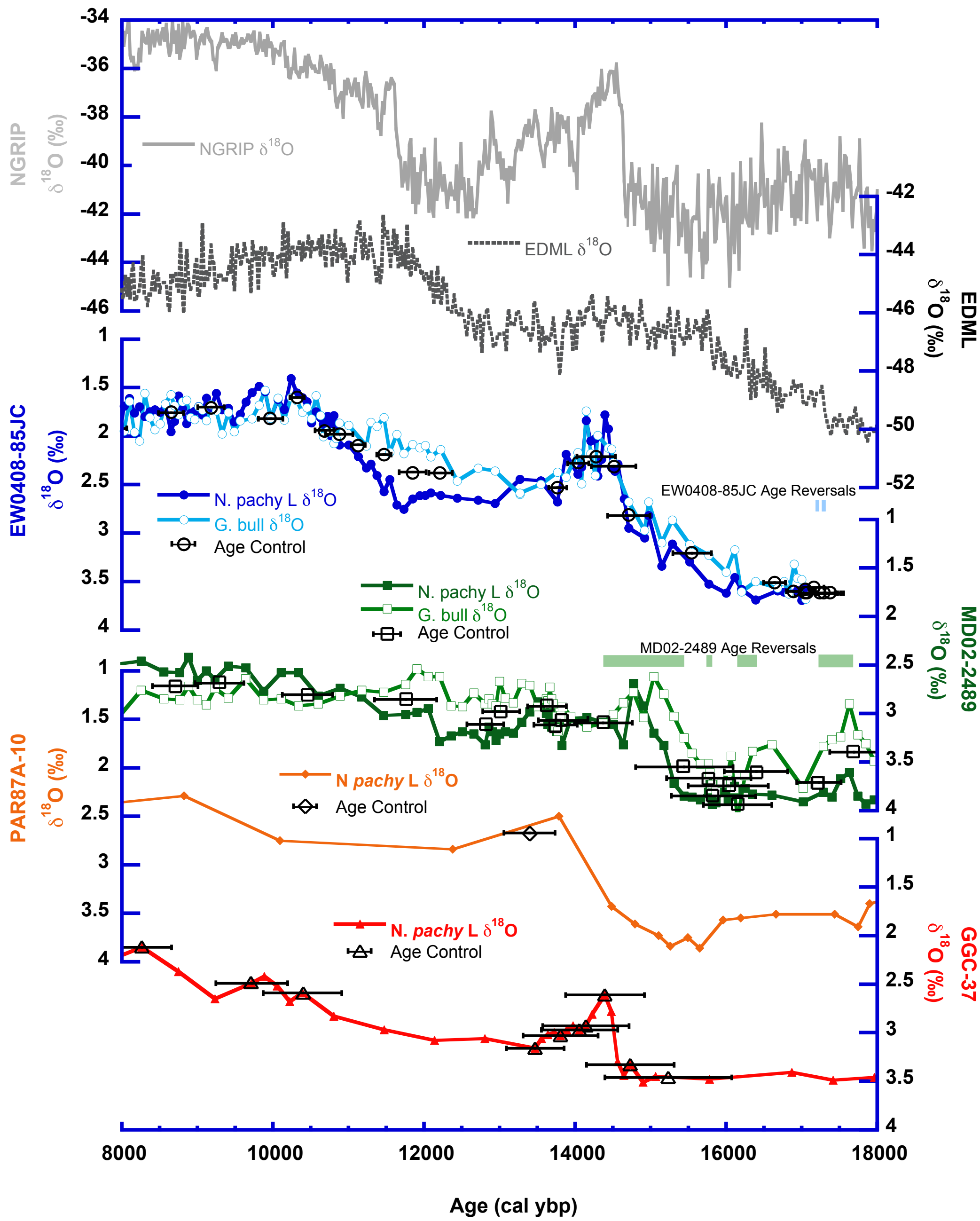

Figure 3.6. Ice-core oxygen isotope records from NGRIP in Greenland (gray solid line) [*Andersen et al.*, 2006; *Rasmussen et al.*, 2006; *Svensson et al.*, 2006] and EDML in Antarctica (black dotted line) [*Ruth et al.*, 2007], compared to planktonic δ18O records from four high-latitude North Pacific sites: Gulf of Alaska cores EW0408 -85JC (blue circles), MD02-2489 (green squares) [*Gebhardt et al.*, 2008], PAC87A-10 (orange diamonds) [*Zahn et al.*, 1991], and Northwest Pacific site GGC-37 (red triangles) (*Keigwin*, [1998]; presented on the chronology of *Galbraith*, [2007]). The location of two age reversals are shown for EW0408-85JC (blue bars; see also Figure 3). Radiocarbon-age control points for each core are delineated by hollow symbols superimposed on the oxygen isotope data, and plotted with 1σ errors. The radiocarbon dates published for PAC87A-10 and MD02-2489 are re-calibrated via CALIB 6.0 using a ΔR of 550 ± 250 as justified in *Galbraith et al.* [2007] for ODP Site 887. The age models shown here are based on linear interpolation between these re-calibrated dates, excluding four periods of age reversal (green bars) from the radiocarbon data of MD02-2489.

Table 3.1: Benthic and planktic radiocarbon dates

Core Type	Core Depth (cm)	Depth Below Seafloor (cmbsf)	Planktic ^{14}C Age (yr)	+/-	Benthic ^{14}C Age (yr)	+/-	Calendar Age (yr)[a]	+/-
MC	0	0	n/a		1490	20	200	120
MC	26	26	n/a		1795	35	520	90
MC	54	54	n/a		1930	45	600	85
TC	8	21	660	250	1530	45	190	260
TC	110	123	1650	90	2505	50	750	110
TC	208	221	2730	70	3440	60	1860	130
JC	25	175	2340	70			1410	110
JC	103	253	3560	60			2870	115
JC	153	303	4000	80			3430	135
JC	205	355	4330	60			3820	135
JC	253	403	4990	90			4690	150
JC	303	453	5500	70			5400	125
JC	353	503	6410	25			6360	85
JC	404	554	7980	25			7960	95
JC	454	604	8610	80			8630	165
JC	504	654	9020	120			9550	535
JC	554	704	9660	70			10000	160
JC	574	724	9930	30			10310	95
JC	589	739	10260	25			10660	120
JC	603	753	10410	100			10900	180
JC	608	758	10600	35			11140	85
JC	619	769	10855	30			11340	95
JC	629	779	11065	25			11880	180
JC	639	789	11250	25			12210	170
JC	653	803	12810	60			13810	105
JC	659	809	13080	30			14060	110
JC	669	819	13170	60			14220	210
JC	674	824	13310	80			14460	255
JC	679	829	13430	45			14720	240
JC	689	839	13830	35			15290	165
JC	703	853	14345	30			16000	210
JC	725	875	14645	35			16390	215
JC	753	903	14870	50			16680	220
JC	803	953	14985	35			16830	220
JC	853	1003	14890	60			16710	225
JC	903	1053	15040	80			16900	250
JC	952	1102	14860	80			16670	235
JC	1002	1152	15080	40			16950	235
JC	1052	1202	15110	60			17010	250
JC	1102	1252	15160	35			17100	240

[a] Calculated from mean planktic 14C ages using Calib v.6.0 (Stuiver et al., 2005) with the Marine09 calibration curve and $\Delta R = 470 \pm 80$ yr for all samples.

Chapter 4

A 17,000 year paleomagnetic secular variation record from the Gulf of Alaska

M.H. Davies[1], J.S. Stoner[1], A.C. Mix[1], J. Jaeger[2], G.P. Rosen[2], J. Southon[3], J. Channell[2], C. Xuan[1]

1 – College of Oceanic and Atmospheric Sciences, Oregon State University, Corvallis OR 97331

2 – Department of Geological Sciences, University of Florida, Gainesville, FL 32611

3 – Earth System Science, University of California, Irvine, CA 97331

Geochemistry, Geophysics, Geosystems (G3)

In Preparation

4.1 Abstract

High-resolution paleomagnetic secular variation (PSV) records from the Gulf of Alaska margin constrain regional field behavior, and expand the observation of coherent Holocene geomagnetic behavior from North America into the Northeastern Pacific. Natural and laboratory remanent magnetizations were studied by progressive alternating field (AF) demagnetization of u-channel samples. Chronologies for these cores are constrained by foraminiferal radiocarbon dates, with 11 dated horizons in core EW0408-79JC and 38 dated horizons in core EW0408-85JC. Undisturbed sediment at Core 79JC extends back >6,000 cal ybp, while 85JC reaches >17,000 cal ybp. Sedimentation rates in 85JC range from ~ 20 to 80 cm kyr in the Holocene through the Bølling warm interval, to more than 500 cm/kyr (85JC) during regional deglaciation. Sedimentation rates at 79JC are much higher on average, ranging from ~100 up to ~500 cm/kyr in the last 1000 cal ybp. Both cores preserve a generally strong and relatively stable (MAD < 5°) magnetization for the period of overlap, though the quality of the magnetization at 85JC declines beyond 8,000 cal ybp as deglacial and early Holocene climatic and environmental shifts influence magnetic mineralogy. Component inclinations from both sites are consistent with historical predictions for the site location and vary around geocentric axial dipole (GAD) values through the length of the record. Declinations show variations consistent with PSV, and both inclination and declination are consistent with continuous global field model predictions through 7,000 cal ybp. However, normalized remanence, even in the late Holocene, cannot be clearly demonstrated to be free of lithologic contamination and therefore cannot be interpreted as reflecting relative paleointensity variations in the absence of additional records. Comparison with newly

available high-resolution archeomagnetic data from the Southwestern US and global templates over the last 4000 yrs through a virtual geomagnetic pole transformation of the PSV data shows that the Gulf of Alaska PSV captures regional variability consistent with North America, but with features distinct from global variations. Extending the PSV comparison back in time, though with greater dating and data uncertainties, shows similarities with both North American and Hawaiian records over most of the last 17,000 yrs. This indicates that consistent directional variability is persistent over an almost hemispheric scale and through the entire Holocene.

4. 2 Introduction

Averaged over tens of thousands of years, the earth's magnetic field can be approximated by a geocentric axial dipole (GAD) [Merrill, et al., 1996; Jackson et al., 2000]. However, at any given moment the geomagnetic field expressed at the Earth's surface deviates substantially from this simple morphology, displaying variable tilt of the best-fitting dipole relative to the axis of rotation, as well as non-dipole structures. Our incomplete understanding of what drives deviation from GAD, in conjunction with the unresolved temporal and spatial scales over which non-dipolar structures persist, complicates accurate prediction of geomagnetic field behavior both forward and into the past. Historical reconstructions indicate the existence of persistent concentrations of geomagnetic flux, such as the Canadian and Siberia flux lobes, that may result from organizing structure imposed on the geomagnetic field by lower mantle heterogeneity [Bloxham and Gubbins, 1987; Bloxham 2002]. If so, patterns of paleomagnetic secular variation are unlikely to be random, and the interplay of dipolar and non-dipolar components of the field may allow us to one day understand the dynamics of geomagnetic change.

An understanding of pre-historic geomagnetic variability on paleomagnetic secular variation (PSV, or sub-reversal) scales is important for modeling production rates of cosmogenic nuclides such as ^{14}C and ^{10}Be [e.g. St-Onge et al. 2003; Snowball and Muscheler, 2007], understanding the convective behavior of the outer core and core/mantle boundary interactions [e.g. Gubbins, 1988], and offers the potential to correlate moments in time across substantial distances independent of climate proxies [e.g. Stoner and St-Onge, 2007; Ortiz et al., 2009]. To this end, efforts are underway to reconstruct the historical [e.g. Jackson et al., 2000] and paleo field [e.g., Korte and Constable., 2005, Korte et al., 2009] through spherical harmonic models constrained by historical data and paleo-records of geomagnetic variability. These paleomagnetic reconstructions include both detrital remanent magnetization (DRM) records from sediments and thermal remanent magnetization (TRM) data from lava flows and archeological sites [Korte and Constable, 2005; Korte et al., 2009]. In practice the spatial and temporal resolution of these descriptive models are limited by the present distribution and quality of extant PSV data, in turn restricting their capacity to evaluate the longevity of non-dipolar geomagnetic structures. Additionally, these observations themselves are concentrated in the Atlantic hemisphere [Korte et al., 2005]; the paleomagnetic behavior of the Pacific is comparatively poorly constrained, and it remains unresolved whether the subdued secular variation inferred for this basin reflects the resolution of extant records or actual geomagnetic behavior.

The Gulf of Alaska is a tectonically active, glaciated margin. The mean shelf depth is ~140 m and is <40 km wide in the study area, with a shelf break depth of ~220 m. Sediments exposed on the margin include poorly sorted, glacially-derived diamicton, glacial-marine sand and silt, and hemipelagic mud [Molnia and Carlson, 1978; Carlson, 1989]. Sedimentation is overwhelmingly terrigenous, with the major sources including the drainages of the Bering and Malaspina Glaciers, as well as the Copper River (Figure 1). Together, these distribution systems form the greatest source of terrigenous material ($>200\times10^{6}$ tons yr^{-1}) to the Pacific Ocean from either American continent [Jaeger et al., 1998; Jaeger and Nittrouer, 2006]. Due to local shelf subsidence, there has been ample accommodation space for Holocene sediment accumulation [Zellers, 1995], with modern accumulation rates on the shelf of ~0.1 – 3 cm/yr [Jaeger and Nittrouer, 2006]. Thus the expanded lithogenic depositional sequences of the Alaskan shelf potentially allow for PSV reconstructions of a resolution impossible to capture in slowly-accumulating deep-ocean and even lacustrine sedimentary environments.

Although there is significant opportunity to capture the geomagnetic field at high-resolution, marine continental margin records are prone to a variety of complications. The Gulf of Alaska shelf and slope are fairly energetic depositional environments, exposed to rapid near-bed currents associated with strong wind-driven downwelling and tides, as well as large winter storm events associated with the Aleutian Low [Weingartner et al., 2002]. Winter significant wave heights on the shelf, as recorded by NOAA buoy 46082 (59.69° N 143.4° W) between 2002-2011, can exceed 15 m. The sediment supply associated with the proximal erosion of the St. Elias Range Bering and Malaspina glaciers, combined with more distal delivery from the catchment basin of the Copper River, is highly variable in both magnetic lithology and grain-size, potentially complicating interpretations of normalized remanence [Cowen et al., 2006]. The shelf is also highly productive, with annual organic carbon production rates of ~300 g C m^2 [Sambrotto and Lorenzen, 1987]. While benthic oxygen levels have been increasing on the open shelf through the Holocene, the early Holocene and late deglacial are known to have experienced episodes of benthic hypoxia [Addison et al., submitted; Davies et al., 2011]. This could allow for the degradation of paleomagnetic records via microbial destruction of primary iron-bearing magnetic remanence carriers during bacterially-mediated anaerobic sulphate reduction [Karlin and Levi, 1983; Karlin and Levi, 1985; Karlin, 1990].

In this study we evaluate Holocene paleomagnetic secular variation records generated for the Gulf of Alaska from jumbo piston, trigger, and multi-cores cores collected during the 2004 R/V Ewing cruise EW0408 (Figure 4.1). Site EW0408-79JC (59.53° N, 141.76° W, 158 m depth) is located on the open continental shelf, while site EW0408-85JC (59.56° N, 144.15° W, 682 m depth) is located in a small depositional basin on the adjacent Kayak slope. As the sites are proximal to each other, although in different depositional environments, they are expected to have experienced identical geomagnetic variability. We thus interpret the records on marine radiocarbon chronologies of sub-millennial scale resolution and in the context of detailed sedimentology, in an effort to deconvolve high-latitude Pacific geomagnetic behavior from lithologic and depositional variability.

4.3 Methods

4.3.1 Bulk Sediment Properties

Magnetic susceptibility and gamma-ray attenuation bulk-density data were measured shipboard on whole cores on a GEOTEK MSCL-S multi-sensor track. Point-source magnetic susceptibility was measured at 0.5 cm intervals in the multi-core, trigger-core, and uppermost sections of jumbo piston cores EW0408-85JC via Bartington MS2 dual-frequency magnetic susceptibility meter (Figure 4.2).

4.3.2 Computerized tomographic (CT) scanning

Computerized tomographic (CT) density measurements were performed at the Oregon State University College of Veterinary Medicine using a Toshiba Aquilion 64 Slice. Scans were collected at 120 kVp and 200 mAs. For visualization purposes, the resulting images were processed with a "sharp" algorithm to generate sagittal and coronal images every 4mm across the core. Down-core and across core pixel resolution within each slice is 500 µm. The cores were scanned in ~60 cm segments and then joined into a composite image using Adobe Photoshop software (Figures 4.3 and 4.4; Davies et al., 2011).

4.3.3 Radiocarbon Dating

Planktonic foraminifera were picked from the >150 µm sediment fraction. The two predominant planktonic species for the sites, *N. pachyderma* (sinistral) and *G. bulloides*, were analyzed separately at 604 cmbsf in core EW0408-79JC, and at 555 cmbsf in core EW0408-85JC. The resultant *N. pachyderma* radiocarbon age is 10 ± 50 years younger than that for the *G.bulloides* in core EW0408-79JC, and 65 ± 50 years greater than that for the *G. bulloides* in core EW0408-85JC (Davies et al., 2011). As these differences approximate the measurement uncertainty for the individual samples, for all other depths the species were combined to increase sample size and reduce analytical error.

Radiocarbon analyses were performed at the UC Irvine Keck AMS facility. A total of 38 radiocarbon measurements were performed for 37 stratigraphic horizons in core EW0408-85JC: 3 planktonic samples from the trigger core, and 35 planktonic samples from the jumbo piston core (Table 4.1). A total of 11 radiocarbon measurements were performed for 10 stratigraphic horizons in core EW0408-79JC (Table 4.1). The raw radiocarbon dates were converted to a calendar age scale using the Marine09 curve in CALIB 6.0 [Stuiver and Reimer, 1993]. To account for regional surface-water reservoir ages, a constant ΔR of 470 ± 80 years was applied to all planktonic foraminiferal dates [McNeely et al, 2006]. To generate the age model, we use direct linear interpolation between planktic radiocarbon dates, except in the high sedimentation-rate interval of the late Pleistocene in core EW0408-85JC, where we use a linear best fit through the dates that increased with depth (Figure 4.5). This compromise falls within the 1σ uncertainties of all but one of the calibrated dates in this sedimentary unit, as outlined in Davies et al. [2011].

4.3.4 Remanent Magnetizations

Natural remanent magnetization (NRM) of u-channel samples was measured using a 2G Enterprises cryogenic magnetometer at the Paleomagnetism and Environmental Magnetism Laboratory at University of Florida. NRM measurements were performed at 1-cm spacing, though the data are smoothed to a resolution of ~4.5

cm, dictated by the Gaussian half-width of the response function of the magnetometer's pickup coils [Weeks et al., 1993]. Measurements were made before demagnetization and after 14 alternating-field (AF) demagnetization steps in the 10-100 mT range (5 mT increments between 10-50 mT, 10 mT increments between 50-100 mT). Declination, inclination, and intensity data were processed using the excel program Macro-Uch-1.xls [Mazaud, 2005] and component magnetic directions and their maximum angular deviation (MAD) were calculated from the 10-60 mT steps using the principal component method [Kirschvink, 1980] to establish their characteristic remanent magnetization (ChRM).

Low-field volumetric magnetic susceptibility (κ) measurements of u-channel samples were performed using a SI2 magnetic susceptibility meter, with a pickup-loop response function affording a resolution of measurement similar to the u-channel magnetometer [Thomas et al., 2003]. Anhysteretic remanent magnetization (ARM), also expressed as a susceptibility of ARM (κ_{ARM}), was applied to each u-channel in a peak alternating field of 100 mT, with a 50 μT DC bias field, and measured at 1-cm intervals prior to and after AF demagnetization at the same steps used for NRM up to 80 mT. Isothermal remanent magnetizations (IRM) were produced using 0.95 T and reversed 0.3 T pulsed magnetic fields. The $IRM_{0.95T}$ and $IRM_{0.3T}$ were measured prior to and after demagnetization at the same steps used for ARM. S-ratios were calculated according to Bloemendal et al., [1992], via normalization of the backfield IRM applied at 0.3T by the $IRM_{0.95T}$, assumed to represent a saturating field. Figures 6 – 9 show the NRM, component directions, MAD values, κ, ARM, IRM, κ_{ARM}/κ values and accumulation rates for the multi-cores, trigger cores, and jumbo piston cores for both sites.

To isolate the signature of geomagnetic behavior, NRM is normalized for lithologic variability using either ARM or IRM laboratory-induced magnetizations. The resulting normalized remanence can be interpreted as a proxy for relative paleointensity if the sediments pass a specific set of quality and uniformity criteria [Levi and Banerjee, 1976; King et al., 1983; Tauxe, 1993].

4.4 Results

4.4.1 Generation of composite depth scale

Sediment depths in centimeters-below-sea-floor (cmbsf) were established using visual correlation of point-source magnetic susceptibility and gamma density data to align the jumbo piston cores with their trigger cores and attendant multi-cores (Figure 4.2). For site EW0408-79JC, the jumbo piston core did not detectably lose sediment at the top of the core. Trigger core EW0408-79TC lost 13 cm due to over-penetration, while multi-core EW0408-78MC7 captured the sediment/water interface. The resultant cmbsf scale for site EW0408-79JC therefore includes a 13 cm correction to all trigger core depths. For site EW0408-85JC, the jumbo piston core was found to have lost 150 cm of core top due to over-penetration. Trigger core EW0408-85TC lost 13 cm of core top, while the multi-core EW0408-84MC8 successfully captured the sediment/water interface. Therefore, to generate a composite cmbsf scale for site EW0408-85JC, 150 cm were added to all jumbo core depths and 13 cm were added to all trigger core depths.

4.4.2 Stratigraphy

The CT-scan imagery of shelf core EW0408-79JC shows strong vertical deformation structures in the sediment below 1350 cm (Figure 4.3b), apparently reflecting sediment drawn rapidly into the core barrel following the penetration of several cohesive, sandy layers. As this portion of the recovery reflects an extreme distortion of primary deposition, it has been excluded from analytical interpretation. The remainder of core EW0408-79JC is predominantly dark greenish-gray bioturbated silty clay, with interbedded sand/silt beds ranging from sub-millimeter to several centimeters in thickness. A massive sandy-silt unit with anomalously high κ beginning with a sharp basal contact at 705 cmbsf and extending through ~ 600 cmbsf (Figure 4.3a), representing either an increase in depositional energy or an abrupt decrease in fine-grained lithogenic sediment supply. This deposit is lithologically distinct and likely incomparable to the remainder of the sediment sequence; as such we exclude it from paleomagnetic interpretation.

Slope core EW0408-85JC captures distinct changes in lithology reflecting the retreat of the Cordilleran ice sheet and the transition to Holocene climate conditions (Figure 4.4b) [Davies et al., 2011]. The deepest unit, from the base of the core to 831 cmbsf, consists of a massive dark gray diamict, and has been interpreted as reflecting ice-proximal glacial-marine sedimentation [Davies et al., 2011]. Above 831 cmbsf, there is a sharp contact with a relatively low-density laminated unit 34 cm in thickness, reflecting high primary productivity and low bottom-water oxygen content, an interpretation supported by excess concentrations of Mo and U [Barron et al., 2009; Davies et al., 2011; Addison et al., submitted]. There is a resurgence in glacially-sourced terrestrial sediment deposition between 797 and 745 cmbsf, with an accompanying decrease in primary productivity and renewed bottom-water oxygen [Davies et al., 2011; Addison et al., submitted]. Above 745 cmbsf to the top of the core, sedimentation at the site is broadly characterized by bioturbated dark-gray silty clays, although the lowest 15 cm of this unit present weak laminations and excess Mo and U contents, indicating a secondary episode of low bottom-water oxygen in the early Holocene [Barron et al., 2009; Davies et al., 2011; Addison et al., submitted].

4.4.3 Chronology

Assuming constant accumulation rates below the lowest dated interval (1204 cmbsf), the undeformed portion of shelf core EW0408-79JC spans 6,260 cal ybp [Figure 4.5]. Accumulation rates range from ~100 to 2000 cm/kyr in the jumbo piston core. The depth at which ^{210}Pb drops to supported level in multi-core EW0408-78MC indicates modern sediment accumulation of 290 cm/kyr [G. Rosen, Personal Communication], similar to the radiocarbon-based accumulation rate of 320 cm/kyr in the late Holocene. To preserve primary depositional structures such as documented in the CT-scan images of the core, accumulation rates would need to be in excess of 2 cm/yr [Jaeger and Nittrouer, 2006]. As the long-term accumulation rates observed in the core average less than half this value, we infer that the bulk of sediment deposition was episodic.

Slope core EW0408-85JC spans 17,400 cal ybp (Figure 4.5), and documents the most recent deglaciation of the Northeast Pacific [Davies et al., 2011]. Accumulation rates range from ~10 cm/kyr, associated with hemipelagic sedimentation, to >500 cm/kyr during the period of ice-proximal marine sedimentation. The ^{210}Pb results from multi-core EW0408-84MC indicate that modern sediment accumulation is ~320 cm/kyr [G. Rosen, Personal Communication], over twice the highest accumulation rates observed from the radiocarbon data in the Holocene. The difference between accumulation rates observed in the multi-core versus the jumbo/piston cores at site EW0408-85JC may reflect a recent three-fold increase in sedimentation. Alternatively, the surface sediments deposited at the sediment-water interface over the last few decades may remain vulnerable to episodes of erosion and redeposition on longer time-scales resulting in a net reduction in sediment accumulation rates.

4.4.4 Natural Remanent Magnetization

Figures 4.6 – 4.9 show the component directions and MAD values for the multi-cores, trigger cores, and jumbo piston cores for both sites. Due to lack of absolute azimuthal orientation, the mean declinations of the TC and JC records were set to zero. Component inclination values from both cores are close to the expected inclination (74°) for the coring sites' latitude, based on a GAD assumption. MAD values are generally lower than 3° for both cores, with the exception of the interval between 716-793 cmbsf in EW0408-85JC. This period, spanning large fluctuations in sediment lithology and organic carbon content associated with regional deglaciation, and with a higher proportion of high-coercivity magnetic minerals, exhibited MAD values of up to 40°. In an attempt to recover the best possible paleomagnetic results through this interval, we applied an optimized approach to determining characteristic magnetization, selecting the most consistent 7 of 14 demagnetization steps. For most of the record this produced component directions indistinguishable from those calculated using the 10-60 mT steps, however in the early Holocene/late Pleistocene portion of the record the optimized principal component analysis lessened several deep inclination lows and reduced MAD values from >40 to <10 (Figure 4.10).

4.4.5 Magnetic mineralogy and grain-size

The high-sediment accumulation rates from the Gulf of Alaska cores suggest the possibility for well-resolved records of paleomagnetic behavior, however the heterogeneous lithologies in these glacial-proximal sequences require cautious interpretation. Therefore, prior to interpreting measured magnetic remanence as reflective of geomagnetic input, we evaluate variability in concentration, grain-size and mineralogy of magnetic remanence carriers as indicated by ARM, IRM, S-ratios and κ_{ARM}/κ values.

Pseudo-single domain magnetite is often considered the optimal sedimentary recorder of geomagnetic input [Tauxe, 1993]. Mean S-ratios are ~0.95 in the Holocene section of the cores, suggesting a low-coercivity (e.g. magnetite) magnetic mineralogy [Thompson and Oldfield, 1986]. However, values decrease to ~0.8 during the early Holocene and late glacial in EW0408-85JC (Figure 4.10), suggesting a higher proportion of high-coercivity minerals (e.g. hematite) during the most recent glacial/interglacial transition [Thompson and Oldfield, 1986].

Although directional records are somewhat forgiving of variability in magnetic grain-size, there is a grain-size dependence in the relationship between depositional and laboratory-applied magnetization [Amerigian, 1977; King et al., 1983]. The κ_{ARM}/κ ratio can be used as a proxy for magnetic grain-size [King et al., 1982; Stoner et al., 1996], and the lower values indicate a coarser remanence carrier at shelf site EW0408-79JC relative to EW0408-85JC, consistent with their depositional environments. Small-scale chatter in κ_{ARM}/κ at EW0408-79JC is likely due to the episodic nature of deposition at the site, although variance over the length of the record remains low at 0.03 SI^2 (Figure 4.6 and 4.7). EW0408-85JC displays a smoother κ_{ARM}/κ record, although variance in the overall record is comparatively high at 0.22 SI^2 (Figures 4.8 and 4.9), associated with a long-term shift to coarser magnetic mineralogy in the early Holocene/late Pleistocene.

4.4.6. Normalized Remanence and Relative Paleointensity

The intensity of detrital remanent magnetization reflects the convolved influences of geomagnetic field intensity at the time of sediment deposition as well as the concentration and magnetic characteristics of the remanence-carrying grains, along with a variety of other environmental factors. In theory normalizing the NRM using a laboratory magnetization may allow separation of lithologic from geomagnetic effects. In practice this only works when sediments are restricted to a relatively narrow range of variability. In EW0408-79JC, the NRM/ARM ratios through the 10-60mT demagnetization range are more consistent than the NRM/IRM ratios (Figures 4.11 and 4.12), although both methods produce similar patterns of normalized remanence in EW0408-79JC. This would seem to support a relative paleointensity interpretation for the normalized remanence. Comparison of NRM, ARM, and IRM demagnetization behavior, however, reveals that both the ARM and IRM magnetizations activate a similar lower-coercivity component of the magnetic mineralogy that is somewhat distinct from the coercivity of the NRM (Figure 4.13a). Additionally, coherent spectral power between κ and both NRM/ARM and NRM/IRM ratios suggest a lithologic component to the normalized remanence (Figure 4.14a) that is not removed through normalization. For these reasons we refrain from interpreting the normalized remanence at this site as reflective of relative paleointensity.

For slope core EW0408-85JC, the pattern of normalized remanence produced by NRM/ARM appreciably deviates from that of NRM/IRM (Figure 4.12). As in EW0408-79JC, the similarity of NRM/ARM ratios through progressive AF-demagnetization indicates are similar coercivity spectrum, while the ARM/IRM ratios show greater overall variance with higher demagnetization steps, indicating that IRM is activating a softer component of the magnetic mineralogy than is reflected in the NRM intensities. This is alternatively illustrated by an examination of the demagnetization behavior of NRM, ARM, and IRM; as in EW0408-79JC, both laboratory induced magnetizations are activating lower-coercivity component of the magnetic mineralogy. In the case of EW0408-85JC, the ARM demagnetization more closely approximates the NRM observations (Figure 4.13b), suggesting that ARM is a more appropriate normalizer for reconstructions of geomagnetic paleointensity. However, there remains a troubling correlation between κ and the ARM normalized remanence, again as reflected in the squared spectral coherence of the normalizer and the normalized product (Figure 4.14b).

If the magnetic mineralogy is consistent down core, ARM/IRM ratios on a bivariate plot should cluster, evolving into increasingly elliptical distributions with variance in the dilution of the remanence-bearing material. Core EW0408-79JC displays closely clustered ARM/IRM ratios, indicating stability in the magnetic remanence carrier activated by the laboratory magnetizations throughout the record (Figure 4.15). However, EW0408-85JC appears to show distinct magnetic mineral populations, complicating interpretations of normalized remanence. To circumvent this problem, we clean the data for a single population of ARM/IRM behavior, consistent with the behavior of the trigger core. The discarded population of ARM/IRM ratios is shown in blue in Figure 4.15, and represent a mid-Holocene population between 420-547 cmbsf (~5050 – 7750 cal ybp), as well as the glacial-proximal diamicton unit below 830 cmbsf (~14,750 cal ybp). However, even this treatment fails to completely remove the portion of the record enriched in the high-coercivity component of the magnetic remanence carrier as indicated by S-ratio proxy (Figure 4.10). For these reasons, in the absence of a well-constrained homogeneous regional record for comparison, we determine that the magnetic mineralogy in these sites is too heterogeneous for a robust interpretation of RPI.

4.5. Discussion

4.5.1 Gulf of Alaska records compared to the CALS7k.2 model

When placed on their independent age models, component inclinations and declinations (rotated to a mean of zero) from the EW0408 sites support the Holocene secular variation predicted for the northern Gulf of Alaska from the CALS7k.2 geomagnetic model (Figure 4.16). This supports both the capacity of these Gulf of Alaska sites to preserve Holocene PSV and the ability of the directional output of CALS7k.2 model to accurately reconstruct geomagnetic behavior in the poorly-constrained North Pacific [Korte and Constable, 2005]. The far-right panel of Figure 4.16 shows the processed normalized remanence from EW0408-79JC as well as EW0408 85TC/JC plotted over the local paleointensity product of the CALS7k.2 model, normalized to the mean and standard deviation of the overlapping portion of the Gulf of

Alaska DRM records to facilitate comparison. Although the normalized remanence reconstructions of EW0408-79JC and EW0408-85TC/JC are internally consistent, they deviate substantially from the predictions of the CALS7K.2 model. As discussed in section 4.4.6, this could reflect the failure of the normalized remanence to reflect geomagnetic intensity at the Gulf of Alaska sites due to variability in the magnetic remanence carriers. However, the accuracy of the CALS7k.2 paleointensity output may also be compromised by the sparse distribution of high-quality paleointensity reconstructions available to tune the model, particularly in the Pacific sector [Korte et al., 2005].

4.5.2 Northeast Pacific Holocene PSV

Evidence for coherent North American Holocene PSV was pioneered by the work of Lund (1996), who correlated 9 mid-latitude (35 - 50° N) records spanning from ~120°W to 70°W via 14 inclination and 17 declination PSV features. This concept has since been extended using marine records from the St. Lawrence Estuary in Eastern Canada [St Onge et al., 2003; Barletta et al., 2010], and tentatively to the Arctic Alaskan margin [Lise-Pronovost et al., 2009], however the spatial extent of North-American type PSV behavior remains relatively unconstrained in the Pacific sector.

Evaluation of North Pacific PSV, where almost all records are sedimentary, is complicated by the sediment recording process even if age models are well-constrained. Natural compaction and even the coring process can lead to inclination flattening [Anson and Kodama, 1987; Verosub, 1977]. Barrel rotation, flow-in (as seen in the CT cans from EW0408-79JC), compression, and extension during coring can all generate deformation difficult to diagnose even with high-resolution imaging [Snowball and Sandgren, 2004; Bowles, 2007]. Diagenesis can lead to magnetic mineral destruction and signal overprinting [Karlin and Levi, 1983; Karlin and Levi, 1985; Karlin, 1990]. Additionally, the process of detrital remanence acquisition remains poorly understood; the gradual acquisition of magnetization below the sediment-water interface acts to smooth the paleomagnetic record as well as imparts a negative age offset to the PSV record relative to the sediment [Verosub, 1977; Tauxe et al., 1993].

To check the accuracy of our directional reconstructions, we convert the component inclination and declination data (calibrated via rotation to the historical prediction for the sites from GUFM1; [Jackson et al., 2000]) of the Gulf of Alaska sites to virtual geomagnetic pole (VGP) latitudes and longitudes to facilitate comparison with the PSV record from well-dated Western US archeomagnetic stack of Hagstrum and Blinman [2010] (Figure 4.17). This has the advantage of taking site locations into account by mapping a geocentric dipole that would cause the observed PSV record. Though changes in VGP latitudes and longitudes between EW0408-85TC/JC and the Hagstrum and Blinman [2010] archeomagnetic stack are observed at similar times, supporting the PSV reconstruction, the difference in amplitude and mean latitude may reflect sedimentary noise or greater non-dipole variability at these higher latitudes [Verosub, 1982]. VGP latitudes are lower in EW0408-79JC, possibly reflecting inclination flattening. There is also apparent temporal offset (~200 yr) to younger ages in VGP features for the upper 1,500 years recorded in EW0408-79JC. This offset is in the opposite direction expected from post-depositional lock-in that at the measured sedimentation rates would only be, at most, on the order of decades, and likely reflects the inability of radiocarbon to resolve sediment accumulation rates of this magnitude (~ 6 m of deposition in ~1,500 years).

A comparison of these North American VGP directional predictions to the global stack VGP dipole model of Nilsson et al., [2010] indicates broad similarity in millennial-scale structure (Figure 4.17). Yet a number of smaller-scale features identified in the robust Western US archeomagnetic stack and supported in the Gulf of Alaska sedimentary records (i.e. the centennial-scale structures identified by tie-points over the last 2000 ybp in the VGP inclination records) appear out of phase with the prediction of the best-fitting global dipole. This could be due to poor magnetic quality and/or insufficient age control on the part of the North American PSV records [Nilsson et al., 2010]. However. as the Western US archeomagnetic stack and Gulf of Alaska detrital remanence data are separated by a substantial distance, reflect different magnetic acquisition processes, and are independently dated, we hypothesize that this misfit reflects the non-dipolar component of Holocene North American PSV.

Figure 18 presents component inclination records from a number of independently-dated Northeast Pacific/Western Arctic sites, arranged from South to North: Lake Waiau, Hawaii (Core 82-2; 19.8° N, 155.5° W) on an updated age model using the published dates recalibrated via Calib 6.0 [Peng and King, 1992; Stuiver and Reimer, 1993], Fish Lake, Oregon [42.7° N, 118.7°W; Verosub al., 1986], on the adjusted chronology proposed by Hagstrum and Champion [2002], EW0408-85JC, and Grandfather Lake, Alaska [59.8°, 158.6° W; Geiss and Banerjee., 2003].

Although the age models are of varying resolution and accuracy, a number of sub-millennial scale inclination features appear common to most records. EW0408-85JC shows 10 of the 14 inclination features identified in Fish Lake and across North America by Lund [1996], with early shift to low inclination values relative to feature 5, and features 10-12 (a period of high North American inclinations) missing due to a data gap. The low inclination feature present in the Gulf of Alaska between ~10,000 -13,000 cal ybp may be correlative with a similarly-timed low-frequency feature in the Hawaiian and Alaskan lacustrine records, within timing offset due to poorly-resolved age models or unconstrained radiocarbon reservoir effects [St-Onge et al., 2003].

We generate a simple geomagnetic stack of inclination from these Northeast Pacific records (Figure 18) via averaging the GAD latitude-normalized inclinations of all 5 records, interpolated to a constant 50 year resolution and accompanied by a 3-point smooth to remove high-frequency (<150 years) directional variability unlikely to reflect true geomagnetic behavior (e.g. Finlay, 2008). We postulate that, although detail is likely lost due to varying magnetic acquisition processes and age-model errors in the individual records, this stack reflects the Western end member of North American flux lobe behavior.

Figure 19 presents declination records from the same Northeast Pacific cores, with the exception of Grandfather Lake, due to lack of azimuthal orientation on the discrete samples. For comparison, we present these records alongside the Western US volcanic/archeomagnetic stack [adjusted to 35.3°N; 105.5°W; Hagstrum and Blinman, 2010], Lake St Crois [45°N, 267.2°E; Lund and Banerjee, 1985], and St. Lawrence Estuary core MD99-2220 [48.76°N, 68.6°W; St-Onge et al., 2003]. While every Holocene North American declination feature identified by Lund [1996] is a period of change in the EW0408-85JC core, these features are out of phase with eastern declination records prior to ~5,000 ybp, becoming in phase deeper in the core. Due to the agreement of the VGP projections derived from EW0408-85JC and the archeomagnetic stack of Hagstrum and Blinman [2010], in conjunction with the predictions of the CALS7k.2 model, we hypothesize that this out-of-phase behavior may be driven by variability in the intensity of the North American flux lobe. When the flux lobe bundle tightens, or increases in intensity, inclinations steepen and western sites experience eastward declination shifts, while eastward sites experience westward ones. The converse would be true for episodes of low North American flux lobe intensity, with inclinations decreasing and declinations relaxing away from the common attractor.

The mostly consistent directional behavior of these dispersed Pacific and North American sites indicates a common geomagnetic driver on secular variation timescales, potentially related to fluctuations in the intensity of the North American flux lobe. If so, the persistence of this geomagnetic feature through the Holocene supports lower mantle control of geodynamo structure, possibly via regulation of diffusive heat flux from the core [Bloxham and Gubbins, 1987; Bloxham, 2002].

4.6. Conclusions

Two independently-dated sedimentary records from the shelf (EW0408-79JC) and slope (EW0408-85JC) of the Gulf of Alaska margin have reproducibly recorded geomagnetic field variability at sub-millenial resolution through the last 6,000 ybp, with the slope core record extending through ~17,000 ybp with somewhat greater uncertainty. Normalized remanence is not robustly interpretable as RPI in the absence of supporting regional records, due to heterogeneity in magnetic remanence-bearing mineralogy.

However, paleosecular variation reconstructions agree well with the predictions of CALS7k.2 for the sites [Korte and Constable, 2005]. Directional data from EW0408-85JC rotated to a virtual geomagnetic pole vary at similar times as the well-dated archeomagnetic Western US stack of Hagstrum and Blinman [2010]. Both North American PSV reconstructions agree with predictions from a simple dipole model of global VGP position (Nilsson et al., 2010) on millennial timescales. Sub-millennial scale variability in VGP latitude present in the well-constrained Western US Archeomagnetic stack (Hagstrum and Blinman, 2010) and reproduced in the Gulf of Alaska may reflect the non-dipolar component of Holocene PSV. VGP predictions from EW0408-79JC suggests an ~200 year negative offset over the last 1,500 years relative to site EW0408-85JC and the Western US stack, likely due to the limitations of radiocarbon dating on this scale. EW0408-85JC reproduces many of the North American directional features identified by Lund [1996], extending the spatial and temporal observations of coherent North American PSV behavior to the sub-Arctic North Pacific and back >13,000 ybp, and supporting the long-term persistence of the North American flux lobe.

4.7 Acknowledgements

The authors gratefully acknowledge the crew and science party of cruise EW0408, the research center for Paleomagnetism and Environmental magnetism at the University of Florida, John Southon and the staff of the UCI Keck AMS laboratory, and the National Science Foundation.

4.8 References

Addison, J.A., B.P. Finney, W.E. Dean, M.H. Davies, A.M. Mix, and J.M. Jaeger, Productivity maxima and sedimentary $\delta^{15}N$ during the Last Glacial Maximum termination in the Gulf of Alaska, *Paleoceanography,* submitted.

Amerigian, C. (1977), Measurement of the effect of particle size variation on the detrital remanent magnetization to anhysteretic remanent magnetization ratio in some abyssal sediments, *Earth and Planetary Science Letters,* 36, 434-442.

Anson, G.L., and K.P. Kodama (1987), Compaction-induced inclination shallowing of the post-depositional remanent magnetization in a synthetic sediment, *Geophysical Journal of the Royal Astronomical Society,* 88, 673-692.

Barletta, F., G. St-Onge, J.S. Stoner, P. Lajeunesse, and J. Locat (2010), A high-resolution Holocene paleomagnetic secular variation and relative paleointensity stack from eastern Canada, *Earth and Planetary Science Letters,* 298, 162-174.

Barron, J.A., D. Bukry, W.E. Dean, J.A. Addison, and B. Finney (2009), Paleoceanography of the Gulf of Alaska during the past 15,000 years: Results from diatoms, silicoflagellates, and geochemistry, *Marine Micropaleontology,* 72, 176-195.

Bloemendal, J., J.W. King, F.R. Hall, and S.J. Doh (1992), Rock magnetism of Late Neogene and Pleistocene deep-sea sediments: relationship to sediment source, diagenetic processes, and sediment lithology, *Journal of Geophysical Research,* 97, 4361-4375.

Bloxham, J. (2002), Time-independent and time-dependent behaviour of high-latitude flux bundles at the core-mantle boundary, *Geophysical Research Letters*, 29, 1854, doi:10,1029/2001GBLO14543.

Bloxham, J., and D. Gubbins (1985), The secular variation of Earth's magnetic field, *Nature*, 317, 777-781.

Bowles, J. (2007), Coring-related deformation of Leg 208 sediments from Walvis Ridge: Implications for paleomagnetic data, *Physics of the Earth and Planetary Interiors,* 161, 161-169.

Carlson, P.R. (1989), Seismic reflection characteristics of glacial and glacimarine sediment in the Gulf of Alaska and adjacent fjords, *Marine Geology,* 85, 391-416.

Cowan, E.A., S.A. Brachfeld, R.D. Powell, and S.C. Schoolfield (2006), Terrane-specific rock magnetic characteristics preserved in glacimarine sediment from southern coastal Alaska, *Canadian Journal of Earth Sciences,* 43, 1269-1282.

Davies, C.J., D. Gubbins, A.P. Willis, and P.K. Jimack (2008), Time-averaged paleomagnetic field and secular variation: Predictions from dynamo solutions based on lower mantle seismic tomography, *Physics of the Earth and Planetary Interiors,* 169, 194-203.

Davies, M.H., A.C. Mix, J.S. Stoner, J.A. Addison, J. Jaeger, B. Finney, J. Wiest, The deglacial transition on the Southeastern Alaska Margin: meltwater input, sealevel rise, marine productivity, and sedimentary anoxia, *Paleoceanography,* in press.

Finlay, C. (2008), Historical variation of the geomagnetic axial dipole, *Physics of the Earth and Planetary Interiors,* 170, 1-14.

Geiss, C.E., and S.K. Banerjee (2003), A Holocene–Late Pleistocene geomagnetic inclination record from Grandfather lake, SW Alaska, *Geophysical Journal International,* 153, 497-507.

Gubbins, D. (1988), Thermal core-mantle interactions and time-averaged paleomagnetic field., *J. Geophys. Res.,* 93, 3413-3420.

Hagstrum, J.T., and D.E. Champion (2002), A Holocene paleosecular variation record from 14C-dated volcanic rocks in western North America, *Journal of Geophysical Research*, 107(B1), 2025, doi:10.1029/2001JB000524.

Hagstrum, J.T., and E. Blinman (2010), Archeomagnetic dating in western North America: an updated reference curve based on paleomagnetic and archeomagnetic data sets, *Geochemistry, Geophysics, Geosystems,* 11, Q06009, doi:10.1029/2009/GC002979

Jackson, A., A.R.T. Jonkers, and M.R. Walker (2000), Four centuries of geomagnetic secular variation from historical records, *Philosophical Transactions of the Royal Society of London. Series A: Mathematical, Physical and Engineering Sciences,* 358, 957-990.

Jaeger, J.M., and C.A. Nittrouer (2006), A quantitative examination of modern sedimentary lithofacies formation on the glacially influenced Gulf of Alaska continental shelf, *Continental Shelf Research,* 26, 2178-2204.

Jaeger, J.M., C.A. Nittrouer, N.D. Scott, and J.D. Milliman (1998), Sediment accumulation along a glacially impacted mountainous coastline: Northeast Gulf of Alaska, *Basin Research,* 10, 155-173.

Karlin, R. (1990), Magnetite diagenesis in marine sediments from the Oregon continental margin, *Journal of Geophysical Research,* 95, 4405-4419.

Karlin, R., and S. Levi (1983), Diagenesis of magnetic minerals in recent haemipelagic sediments, *Nature,* 303, 327-330.

Karlin, R., and S. Levi (1985), Geochemical and sedimentological control of the magnetic properties of hemipelagic sediments, *Journal of Geophysical Research,* 90, 373-392.

King, J., S.K. Banerjee, J. Marvin, and O. Ozdemir (1982), A comparison of different magnetic methods for determining the relative grain size of magnetite in natural materials: some results from lake sediments, *Earth and Planetary Science Letters,* 59, 404-419.

King, J.W., S.K. Banerjee, and J. Marvin (1983), A new rock-magnetic approach to selecting sediments for geomagnetic paleointensity studies: application to paleointensity for the last 4000 years, *Journal of Geophysical Research,* 88, 5911-5921.

Kirschvink, J.L. (1980), The least-squares line and plane and the analysis of palaeomagnetic data, *Geophysical Journal of the Royal Astronomical Society,* 62, 699-718.

Korte, M., A. Genevey, C.G. Constable, U. Frank, and E. Schnepp (2006), Continuous geomagnetic field models for the past 7 millenniaI: a new global data compilation, *Geochemistry, Geophysics, Geosystems,* 6, Q02H15.

Korte, M., and C.G. Constable (2005), Continuous geomagnetic field models for the past 7 millennia: 2, CALS7K*, Geochemistry, Geophysics, Geosystems,* 6, Q02H16, doi:10.1029/2004GC000801

Korte, M., F. Donadini, and C.G. Constable (2009), The geomagnetic field for 0-3 ka, Part II: a new series of time-varying global models, *Geochemistry, Geophysics, Geosystems,* 10, Q06008, doi:10.1029/2008GC002297

Levi, S., and S.K. Banerjee (1976), On the possibility of obtaining relative paleointensities from lake sediments, *Earth and Planetary Science Letters,* 29, 219-226.

Lisé-Pronovost, A., G. St-Onge, S. Brachfeld, F. Barletta, and D. Darby (2009), Paleomagnetic constraints on the Holocene stratigraphy of the Arctic Alaskan margin, *Global and Planetary Change,* 68, 85-99.

Lund, S.P. (1996), A comparison of Holocene paleomagnetic secular variation records from North America, *Journal of Geophysical Research,* 101, 8007-8024.

Lund, S.P., and S.K. Banerjee (1985), Late Quaternary paleomagnetic field secular variation from two Minnesota lakes, *Journal of Geophysical Research,* 90(B1), 803-825.

Mazaud, A. (2005), User-friendly software for vector analysis of the magnetization of long sediment cores, *Geochemistry Geophysics Geosystems,* 6, Q12006, doi:10.1029/2005GC001036.

McNeely, R., A.S. Dyke, and J.R. Southon (2006), Canadian marine reservoir ages, preliminary data assessment, *Geological Survey Canada, Open File* 5049

Merril, R., M. McElhinny, P. McFadden (1996), *The Magnetic Field of the Earth*, Academic Press, San Diego, CA, 531 pp.

Molnia, B.F., and P.R. Carlson (1978), Surface sedimentary units of northern Gulf of Alaska continental shelf, *Bull. Am. Assoc. Petrol. Geol*., 62, 633-643.

Nilsson, A., I. Snowball, R. Muscheler, C. Bertacchi Uvo (2010), Holocene geocentric dipole tile model constrained by sedimentary paleomagnetic data. *Geochemistry Geophysics Geosystems,* 11, doi: 10.1029/2010GC003118.

Ortiz, J.D., L. Polyak, J.M. Grebmeier, D.A. Darby, D.D. Eberl, S. Naidu, and D. Nof (2009), Provenance of Holocene sediment on the Chukchi-Alaskan margin based on combined diffuse spectral reflectance and quantitative X-Ray Diffraction analysis, *Global and Planetary Change,* 68, 73-84.

Peng, L., and J.W. King (1992), A late Quaternary geomagnetic secular variation record from Lake Waiau, Hawaii, and the question of the Pacific nondipole low, *Journal of Geophysical Research,* 97(B2), 4407-4424.

Sambrotto, R.N., and C.J. Lorenzen (1987), Phytoplankton and primary production, in *The Gulf of Alaska,* Edited by Hood, D.W., and S.T. Zimmerman, pp. 249-282, U.S. Department of Commerce, USA.

Snowball, I., and R. Muscheler (2007), Palaeomagnetic intensity data: an Achilles heel of solar activity reconstructions, *Holocene,* 17(6), 851-859, doi:10.1177/0959683607080531.

Snowball, I., and P. Sandgrena (2002), Geomagnetic field variations in northern Sweden during the Holocene quantified from varved lake sediments and their implications for cosmogenic nuclide production rates, *Holocene,* 12(5), 517-530

Stoner, J.S. And G. St-Onge (2007), Magnetic stratigraphy: Reversals, excursions, paleointensity and secular variation, in *Development in Marine Geology: Volume 1, Proxies in Late-Cenezoic Paleoceanography,* Edited by Hillaire-Marcel, C., and A. de Vernal, pp. 99-138.

Stoner, J.S., J.E.T. Channell, and C. Hillaire-Marcel (1996), The magnetic signature of rapidly deposited detrital layers from the deep Labrador Sea: Relationship to North Atlantic Heinrich layers, *Paleoceanography*, 11(3), 309-325

St-Onge, G., J.S. Stoner, and C. Hillaire-Marcel (2003), Holocene paleomagnetic records from the St. Lawrence Estuary, eastern Canada: centennial-to millennial-scale geomagnetic modulation of cosmogenic isotopes, *Earth and Planetary Science Letters,* 209, 113-130.

Stuiver, M., and P.J. Reimer (1993), Extended 14C database and revised CALIB radiocarbon calibration program, *Radiocarbon,* 35, 137-189.

Tauxe, L. (1993), Sedimentary records of relative paleointensity of the geomagnetic field: theory and practice, *Reviews of Geophysics,* 31, 319-354.

Thomas, R.G., Y. Guyodo, and J.E.T. Channell (2003), U-channel track for susceptibility measurements, *Geochemistry, Geophysics, Geosystems,* 4, doi:10.1029/2002GC000454.

Thompson, R. and F. Oldfield (1986), *Environmental Magnetism*, Allen & Unwin, London.

Verosub, K.L. (1977), Depositional and postdepositional processes in the magnetization of sediments, *Reviews of Geophysics,* 15, 129-143.

Verosub, K.L. (1982), A paleomagnetic record from Tangle Lakes, Alaska: Large amplitude secular variation at high latitudes, *Geophysical Research Letters,* 9, 823-826.

Verosub, K.L., P.J. Mehringer Jr, and P. Waterstraat (1986), Holocene secular variation in western North America: paleomagnetic record from Fish Lake, Harney County, Oregon, *Journal of Geophysical Research,* 91, 3609-3623.

Weeks, R.J., C. Laj, L. Endignoux, M.D. Fuller, A.P. Robert, R. Manganne, E. Blanchard, and W. Goree (1993), Improvements in long core measurement techniques: applications in paleomagnetism and paleoceanography, *Geophysical Journal International*, 114, 651–662.

Weingartner, K. Coyle, B. Finney, R. Hopcroft, T. Whitledge, R. Brodeur, M. Dagg, E. Farley, D. Haidvogel, L. Haldorson, A. Hermann, S. Hinckley, J. Napp, P. Stabeno, T. Kline, C. Lee, E. Lessard, T. Royer and S. Strom (2002), The Northeast Pacific GLOBEC Program: Coastal Gulf of Alaska, *Oceanography,* 15(2), 10–35.

Zellers, S.D. (1995), Foraminiferal sequence biostratigraphy and seismic stratigraphy of a tectonically active margin; the Yakataga Formation, northeastern Gulf of Alaska, *Marine Micropaleontology,* 26, 255-271.

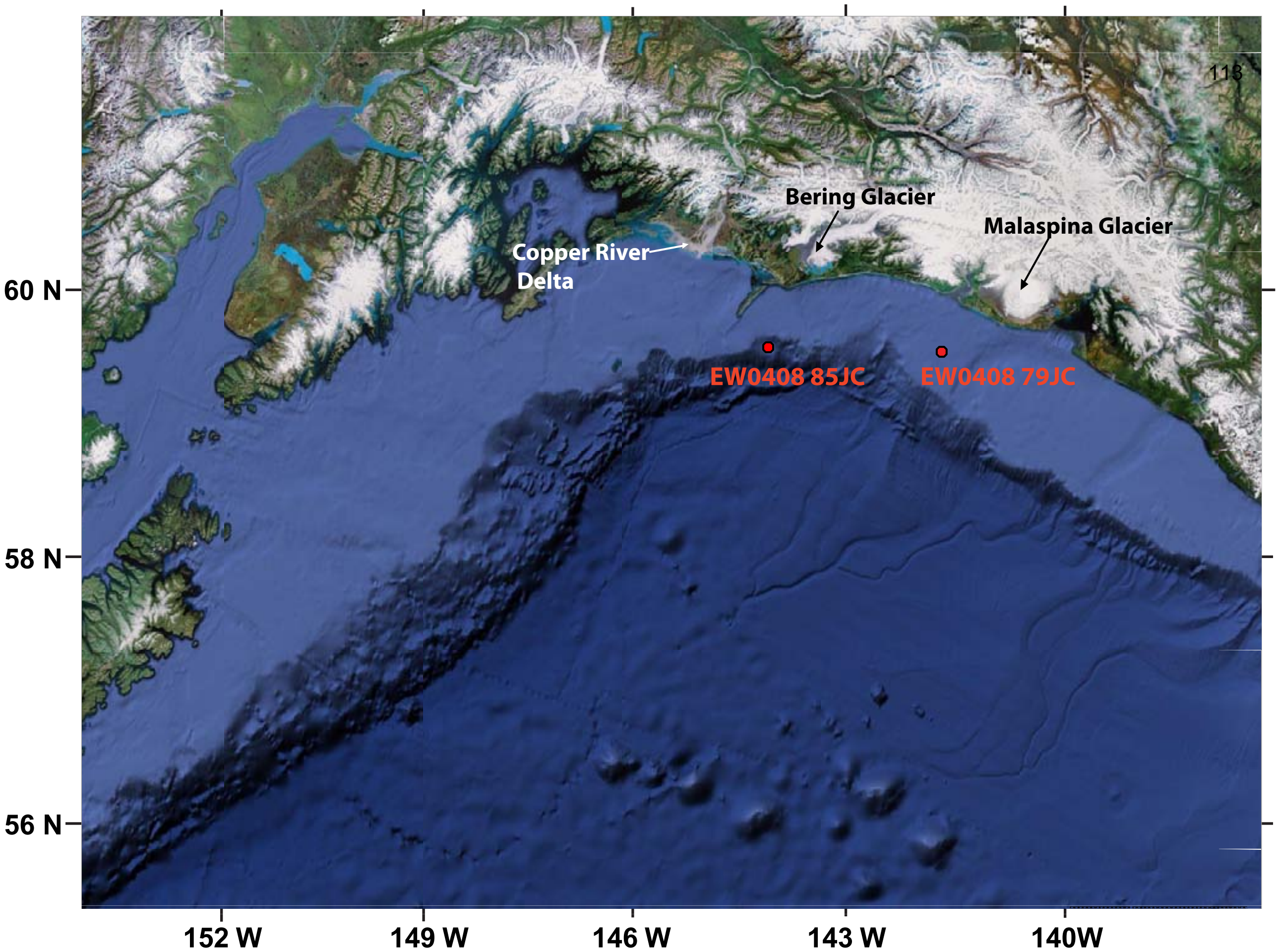

Figure 4.1: Site map showing the bathymetry of the Gulf of Alaska, as well as the locations of shelf core EW0408-79JC and slope core EW0408-85JC. The locations of the major sediment sources to the margin, which include drainages from the Bering and Malaspina glaciers as well as the Copper River, are labeled.

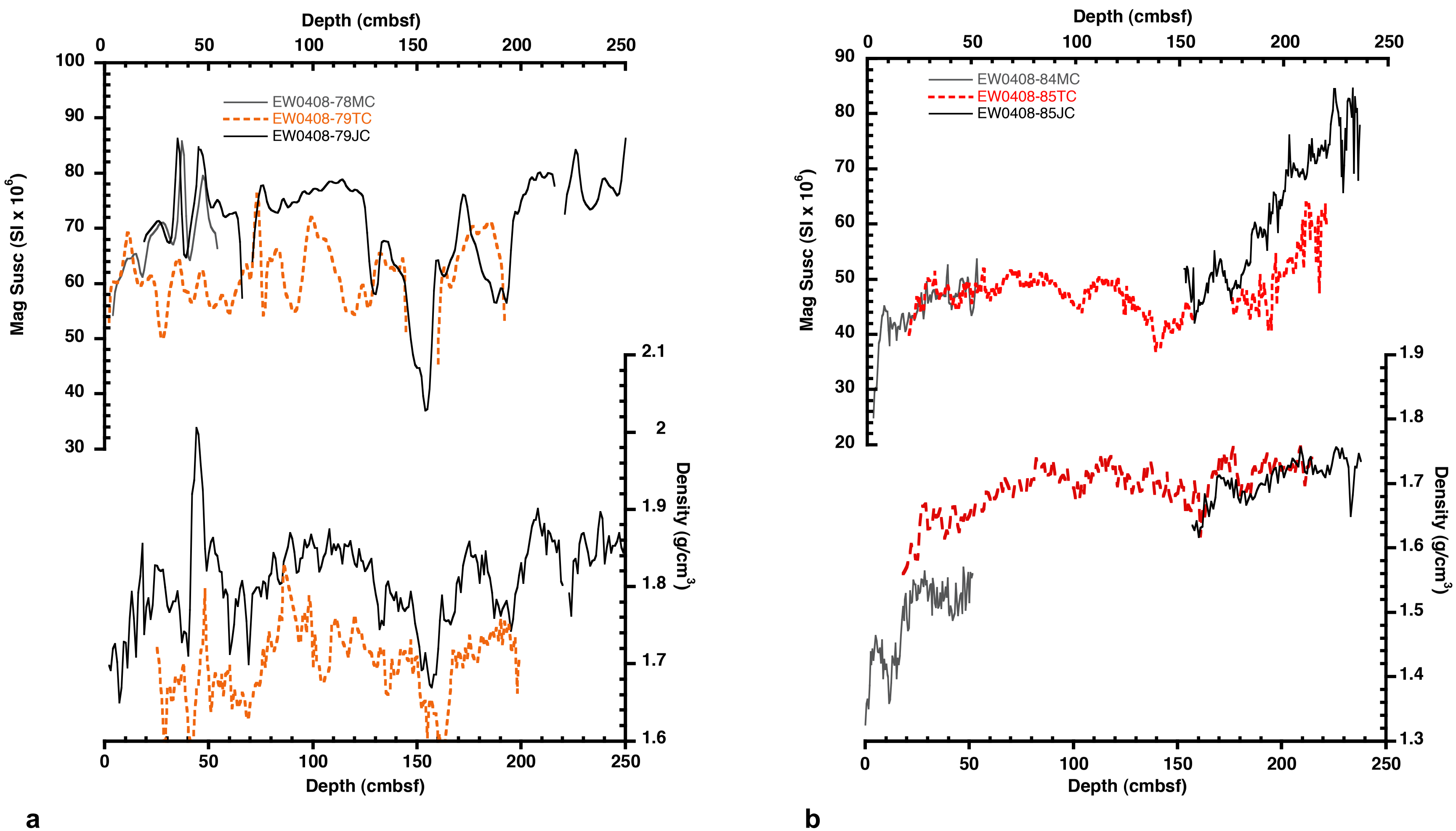

Figure 4.2: Point source magnetic susceptibility and gamma-ray attenuation density data illustrating generation of cmbsf scale for EW0408-79JC (a, b) and EW0408-79JC (c, d).

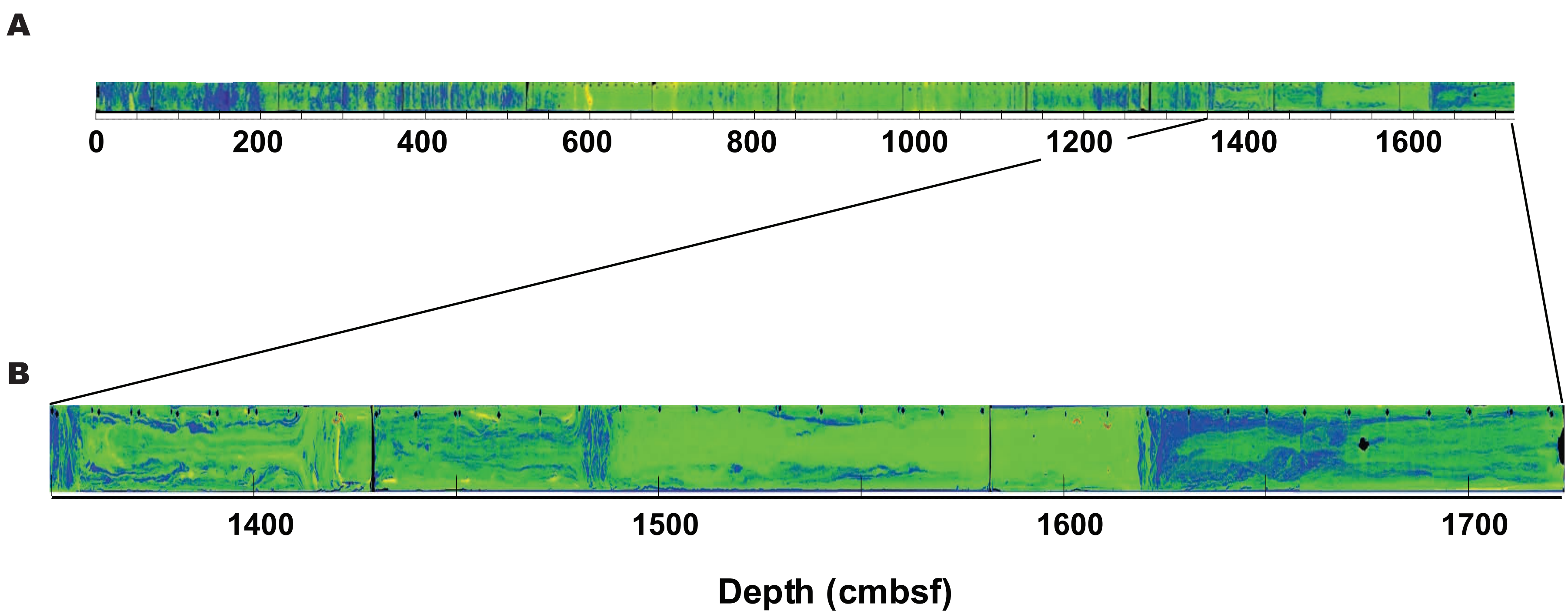

Figure 4.3: a) Computerized tomographic (CT) scan of EW0408-79JC, shown in false color to highlight density changes. Warmer (green, yellow) colors indicate high densities associated with larger lithogenic grains, while cooler (blue, purple) colors indicate lower densities associated with finer clays and biogenic sedimentation. b) The section below 1350 cmbsf in the core shows vertical flow structures meters in scale, indicative of extreme coring deformation.

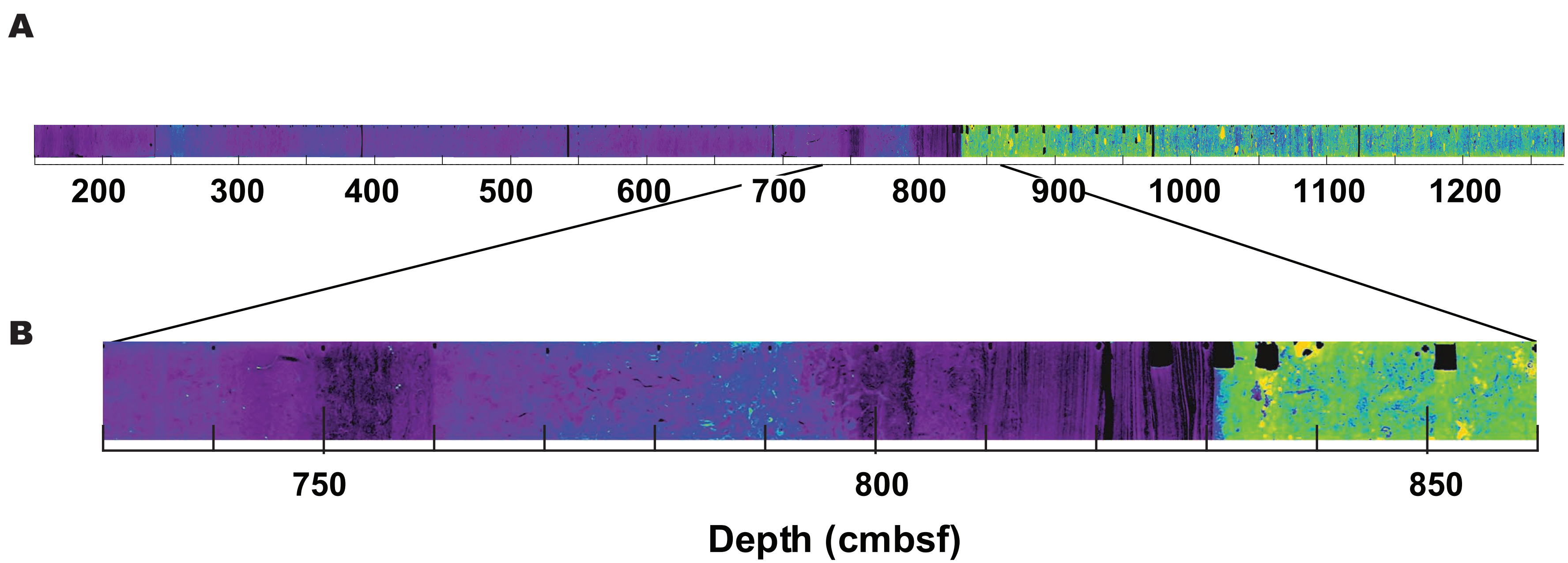

Figure 4.4: a) Computerized tomographic (CT) scan of EW0408-85JC, shown in false color to highlight density changes. Warmer (green, yellow) colors indicate high densities associated with larger lithogenic grains, while cooler (blue, purple) colors indicate lower densities associated with finer clays and biogenic sedimentation. b) The deglacial transition is characterized by abrupt shifts in lithology, as well as intermittent laminae preservation associated with high organic carbon content and low bottom water oxygen content.

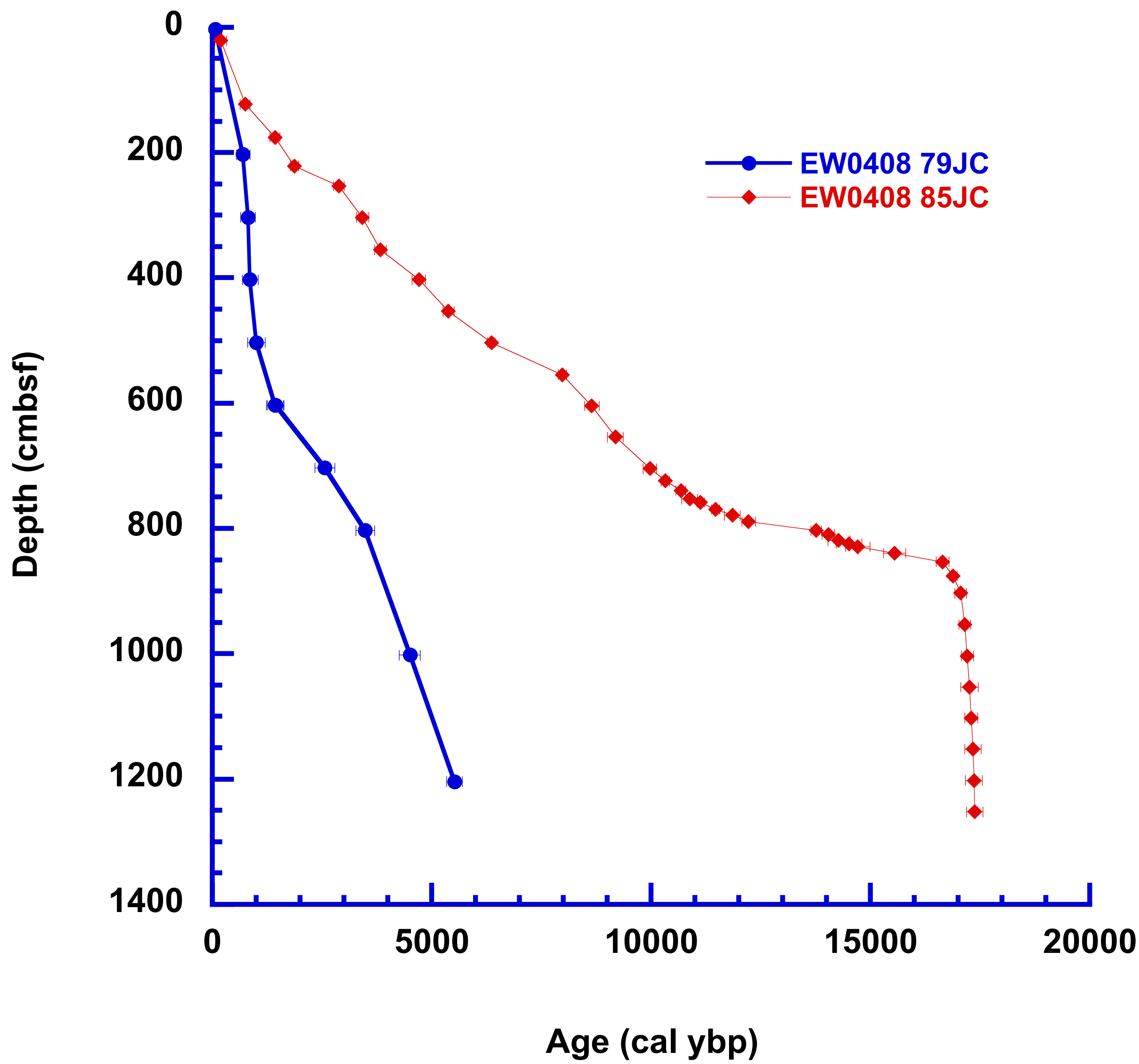

Figure 4.5: Calibrated planktonic foraminiferal dates used to generate the age models for EW0408-79JC (blue circles) and EW0408-85JC (red diamonds). Plotted error bars represent 1-sigma uncertainty.

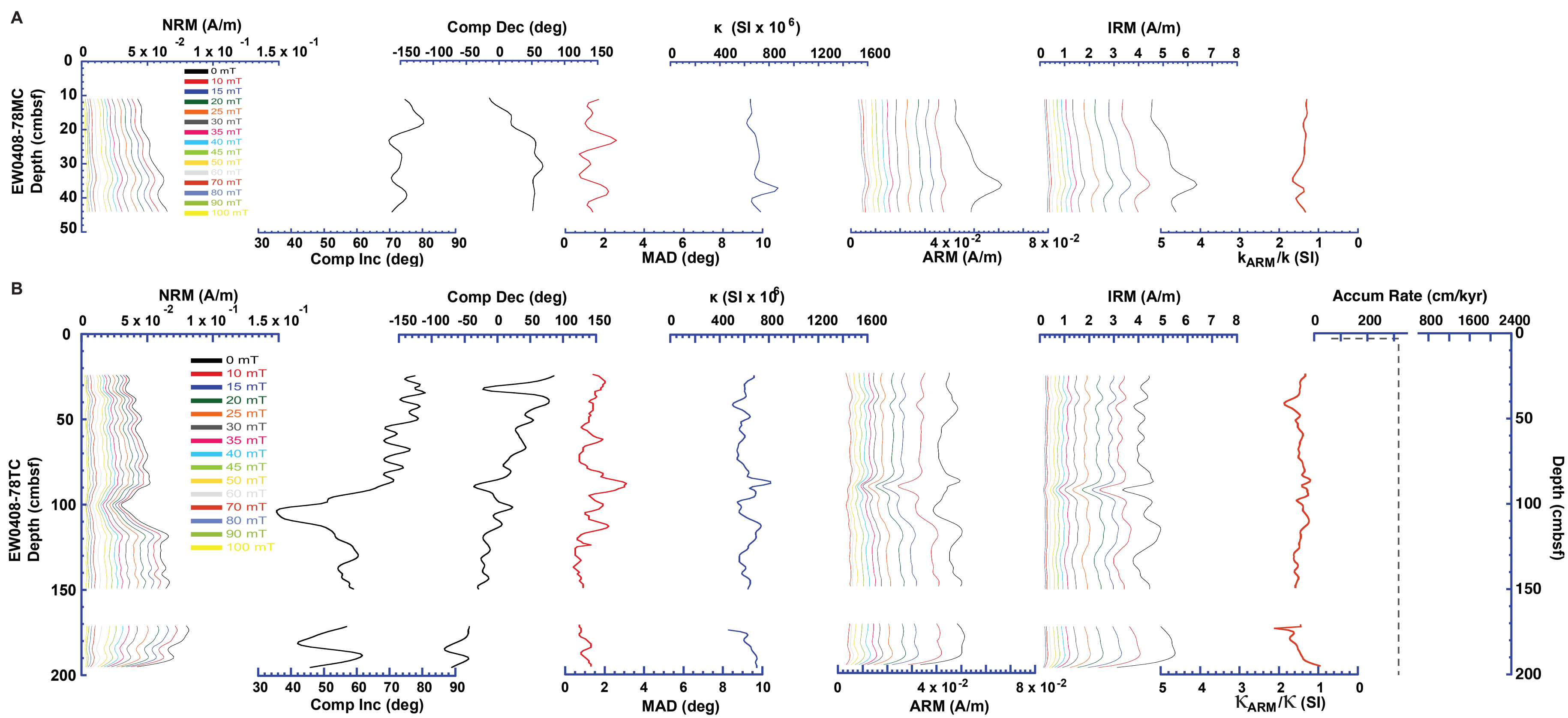

Figure 4.6: a) Bulk magnetic parameters from EW0408-78MC7, indicating natural remanent magnetization (NRM) intensities for AF-demagnetization steps from 0-100 mT, component inclinations, declinations, and mean angular deviation (MAD) values calculated from the 10-60 mT steps, magnetic susceptibility (κ), laboratory-applied anhysteretic (ARM) and 0.3 T isothermal (IRM) remanent magnetization intensities for AF-demagnetization steps from 0-80 mT, and the down-core κ_{ARM}/κ ratio. b) The above properties measured for EW0408-79TC, as well as accumulation rates derived from radiocarbon dates on equivalent depths in associated jumbo piston core EW0408-79JC.

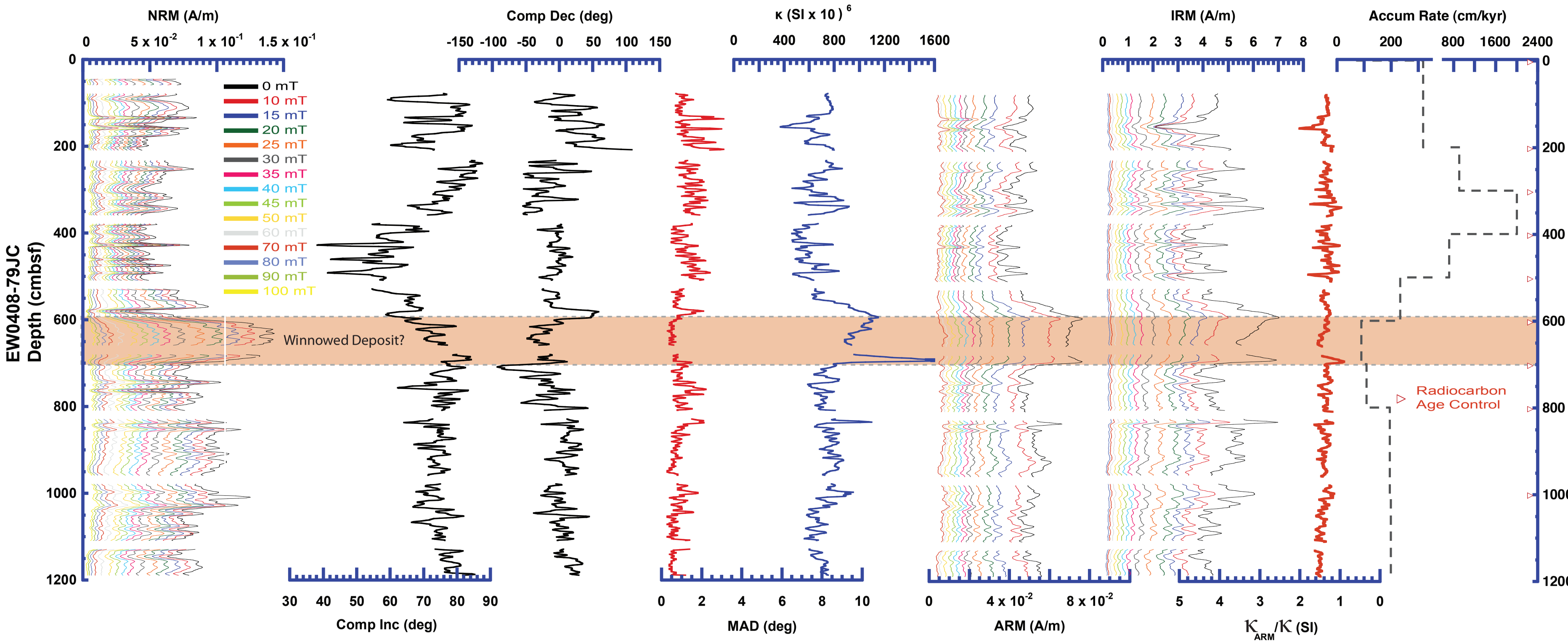

Figure 4.7: Bulk magnetic parameters from EW0408-79JC, indicating natural remanent magnetization (NRM) intensities for AF-demagnetization steps from 0-100 mT, component inclinations, declinations, and mean angular deviation (MAD) values calculated from the 10-60 mT steps, magnetic susceptibility (κ), laboratory-applied anhysteretic (ARM) and 0.3 T isothermal (IRM) remanent magnetization intensities for AF-demagnetization steps from 0-80 mT, the down-core κ_{ARM}/κ ratio, and sediment accumulation rates derived from the planktonic radiocarbon dates (red triangles).

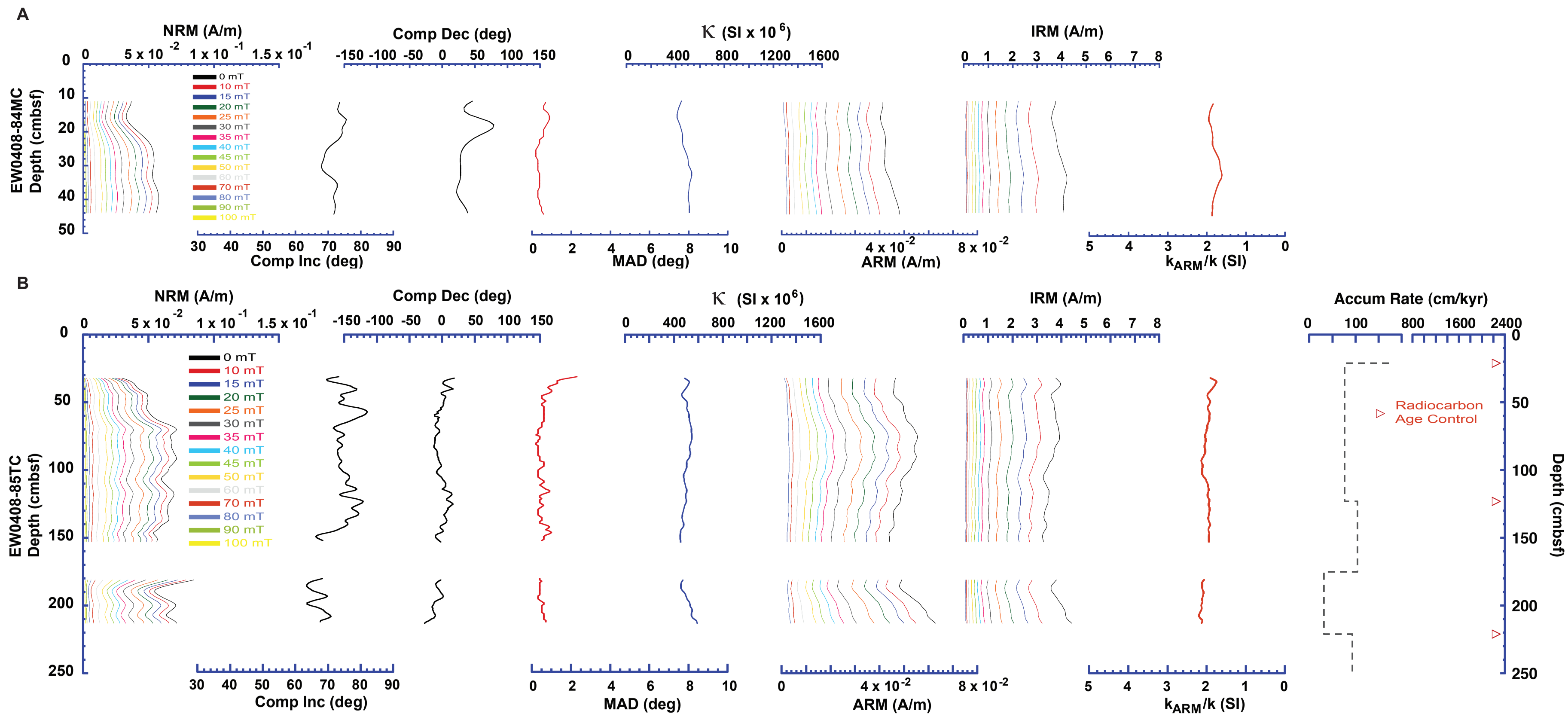

Figure 4.8

Figure 4.8: a) Bulk magnetic parameters from EW0408-84MC8, indicating natural remanent magnetization (NRM) intensities for AF-demagnetization steps from 0-100 mT, component inclinations, declinations, and mean angular deviation (MAD) values calculated from the 10-60 mT steps, magnetic susceptibility (κ), laboratory-applied anhysteretic (ARM) and 0.3 T isothermal (IRM) remanent magnetization intensities for AF-demagnetization steps from 0-80 mT, and the down-core κ_{ARM}/κ ratio. b) The above properties measured for EW0408-85TC, as well as accumulation rates derived from radiocarbon dates in the core (red triangles).

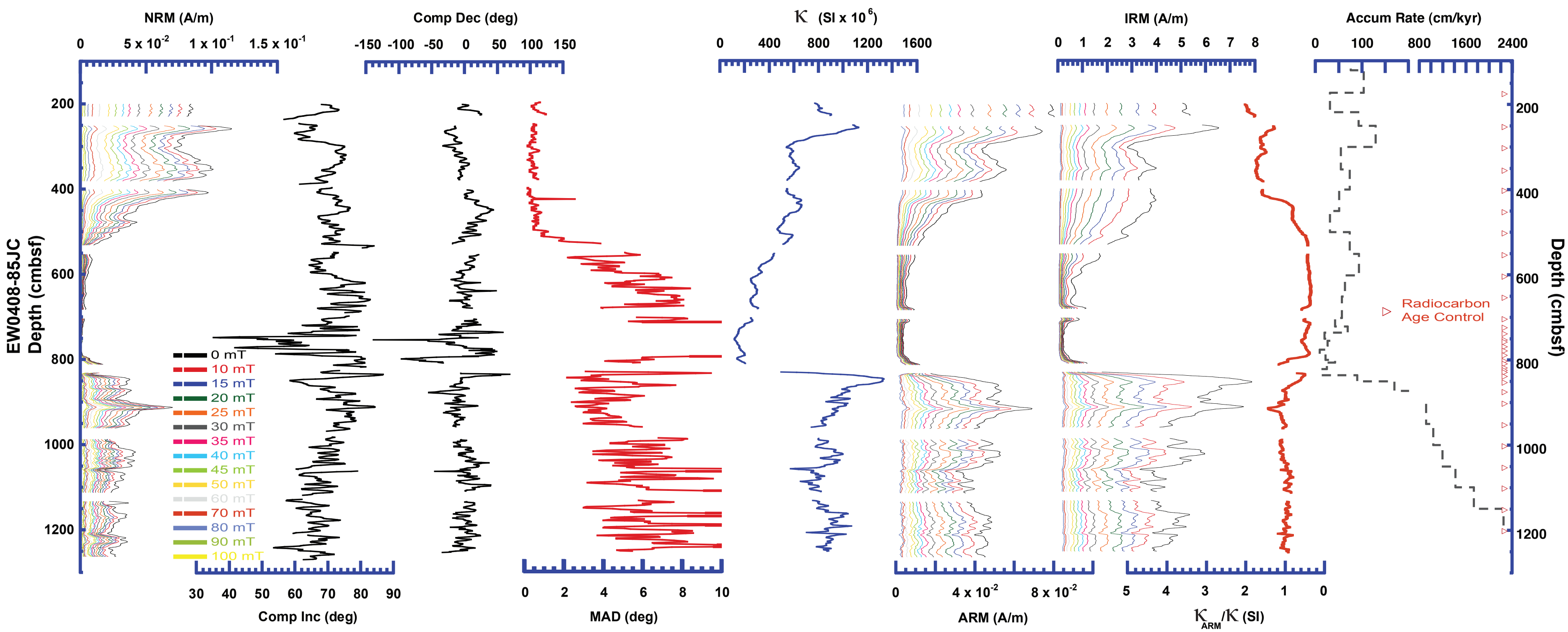

Figure 4.9: Bulk magnetic parameters from EW0408-85JC, indicating natural remanent magnetization (NRM) intensities for AF-demagnetization steps from 0-100 mT, component inclinations, declinations, and mean angular deviation (MAD) values calculated from the 10-60 mT steps, magnetic susceptibility (κ), laboratory-applied anhysteretic (ARM) and 0.3 T isothermal (IRM) remanent magnetization intensities for AF-demagnetization steps from 0-80 mT, the down-core κ_{ARM}/κ ratio, and sediment accumulation rates derived from the planktonic radiocarbon dates (red triangles).

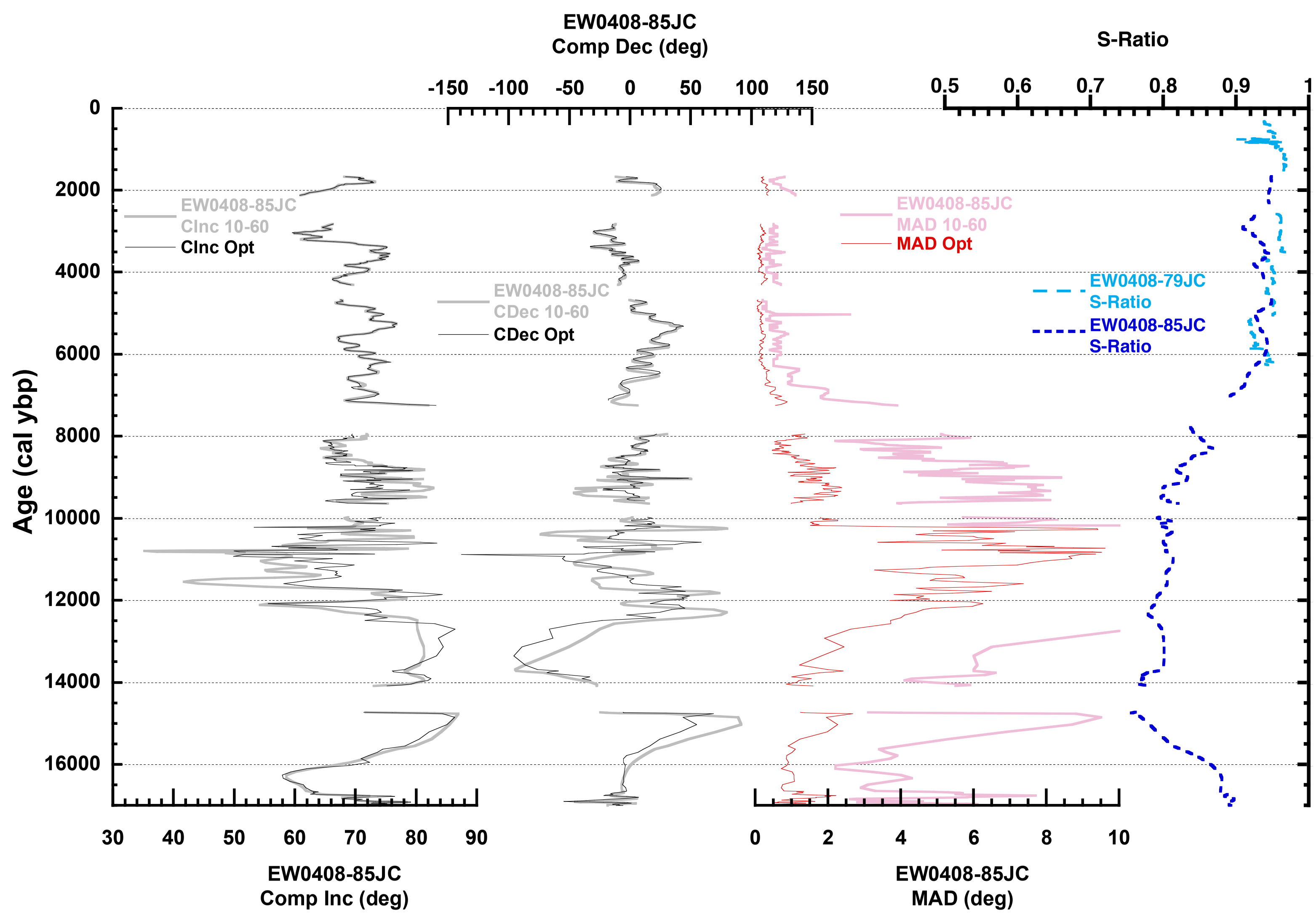

Figure 4.10: Component inclinations and declinations, as well as mean angular deviation (MAD) values calculated using the 10-60 mT AF demagnetization steps (gray, pink), as well as using the optimized demagnetization step selection approach described in the text (black, red). S-ratio values indicates that magnetite is the dominant remanence carrier in both EW0408-79JC (light blue) and EW0408-85JC (dark blue), however the increase in MAD values in the early Holocene and during deglaciation appears to be associated with an increase in the proportion of high-coercivity magnetic minerals.

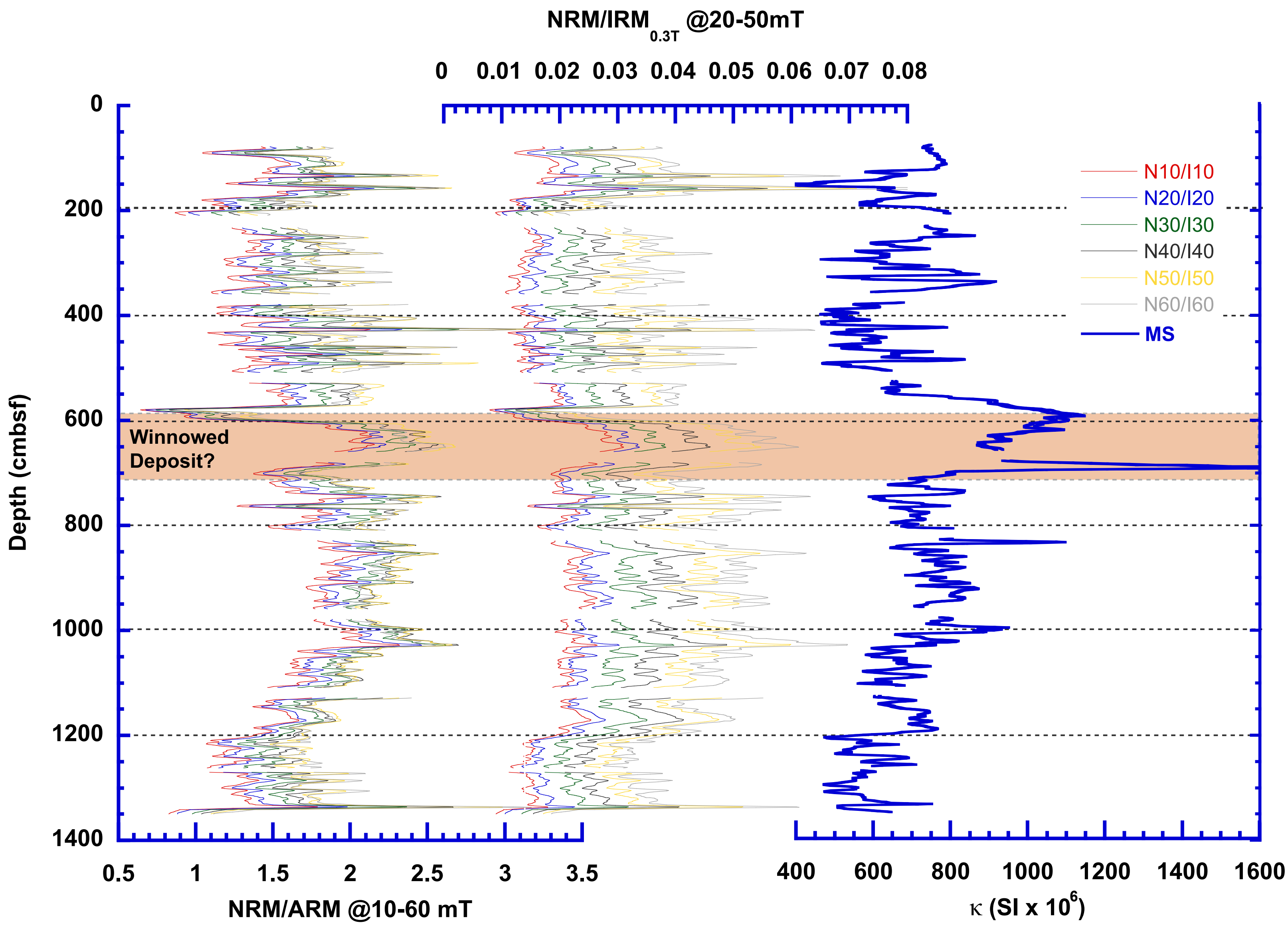

Figure 4.11: Natural remanent magnetization intensities from EW0408-79JC normalized by both laboratory-applied anhysteretic remanent magnetization (NRM/ARM), as well as by the 0.3 T isothermal remanent magnetization (NRM/IRM0.3T) plotted at the 10-60 mT AF-demagnetization steps. Magnetic susceptibility (κ) is shown on the far right (blue).

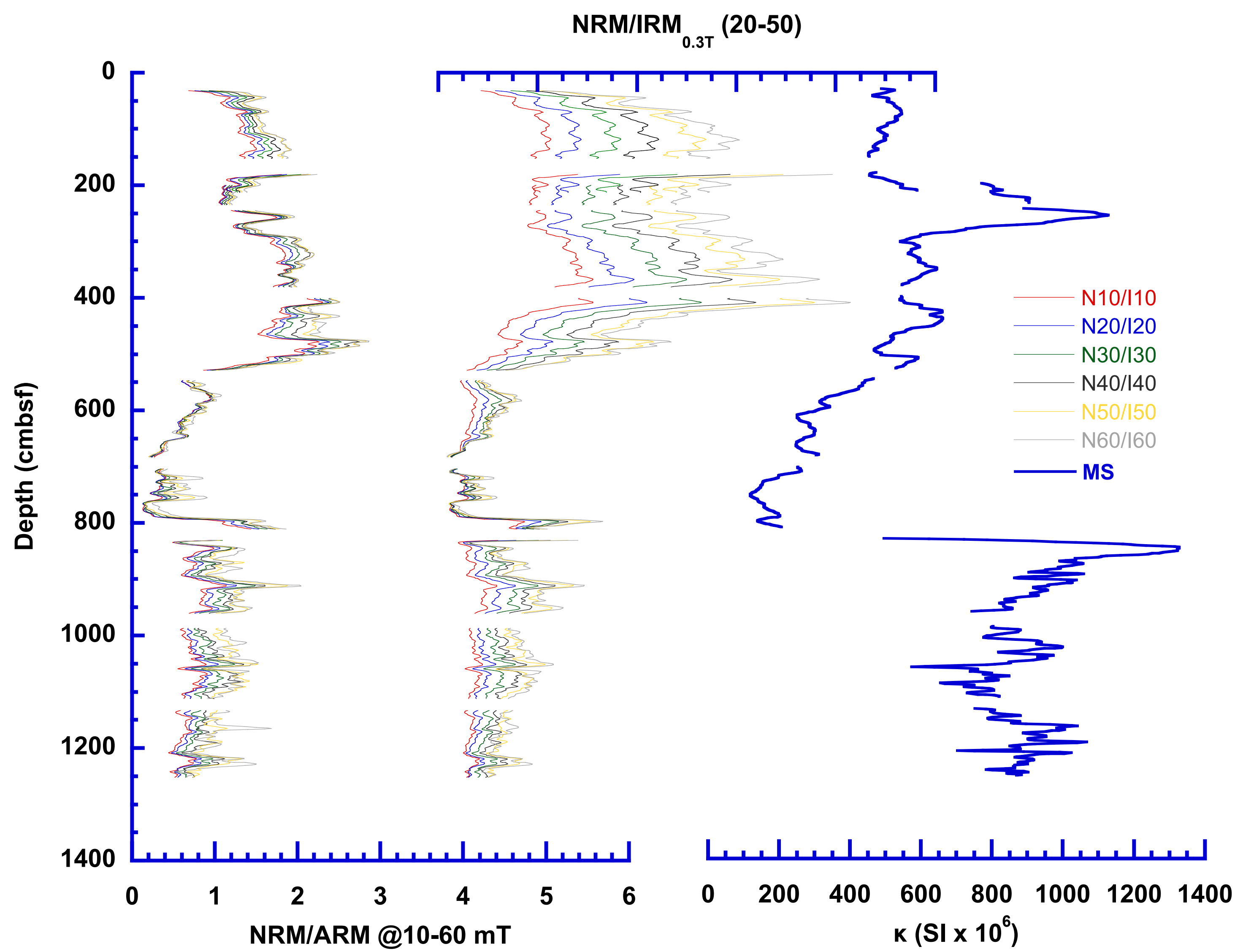

Figure 4.12: Natural remanent magnetization intensities from EW0408-85TC/JC normalized by both laboratory-applied anhysteretic remanent magnetization (NRM/ARM), as well as by the 0.3 T isothermal remanent magnetization (NRM/IRM0.3T) plotted at the 10 -60 mT AF-demagnetization steps. Magnetic susceptibility (κ) is shown on the far right (blue).

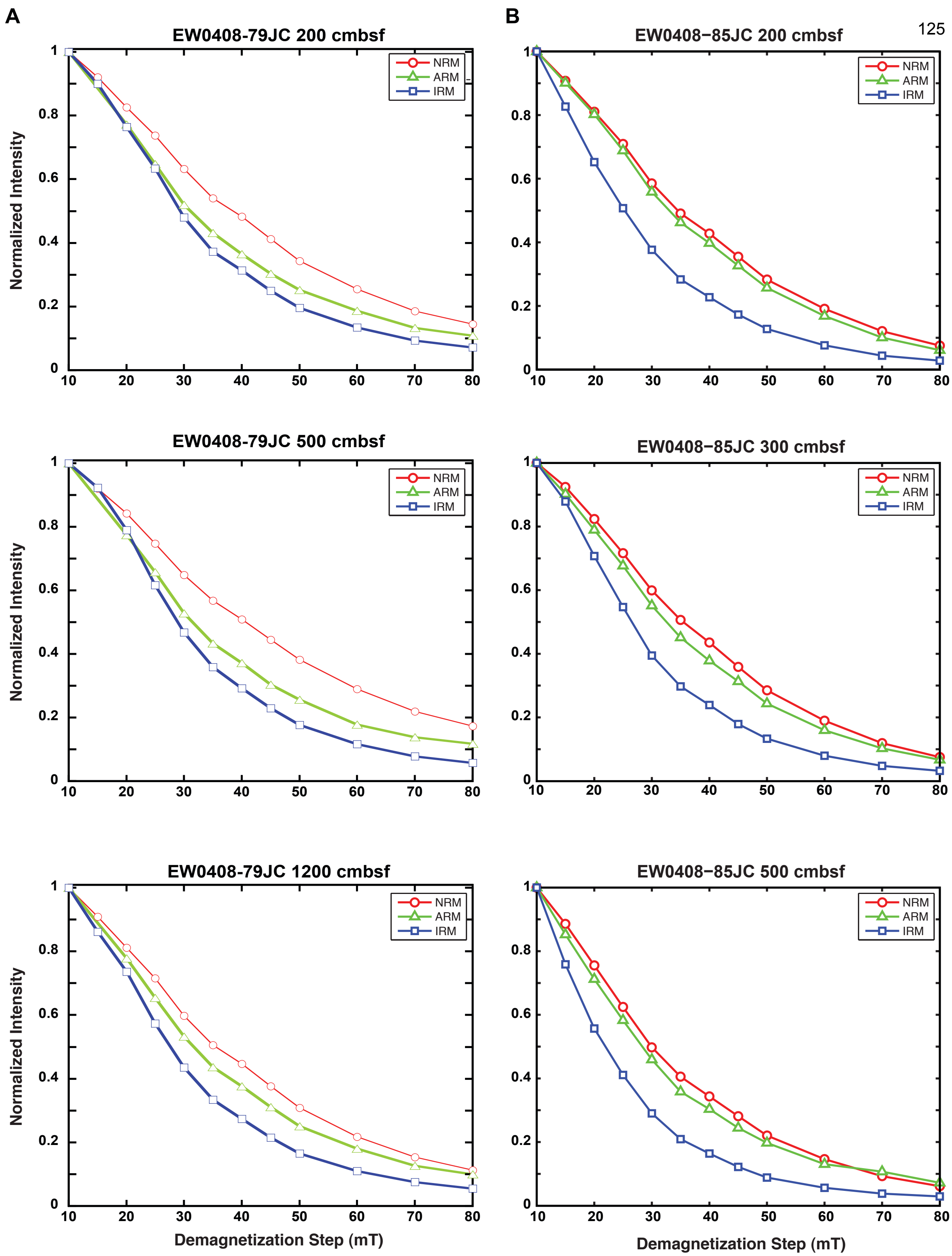

Figure 4.13: AF-demagnetization behavior of natural (NRM; red), anhysteretic (ARM; green), and isothermal (IRM; blue) remanent magnetizations, normalized to the 10 mT step for the 200, 500, and 1200 cmbsf samples in EW0408-79JC (column a), and the 200, 300, and 500 cmbsf samples in EW0408-85JC (column b).

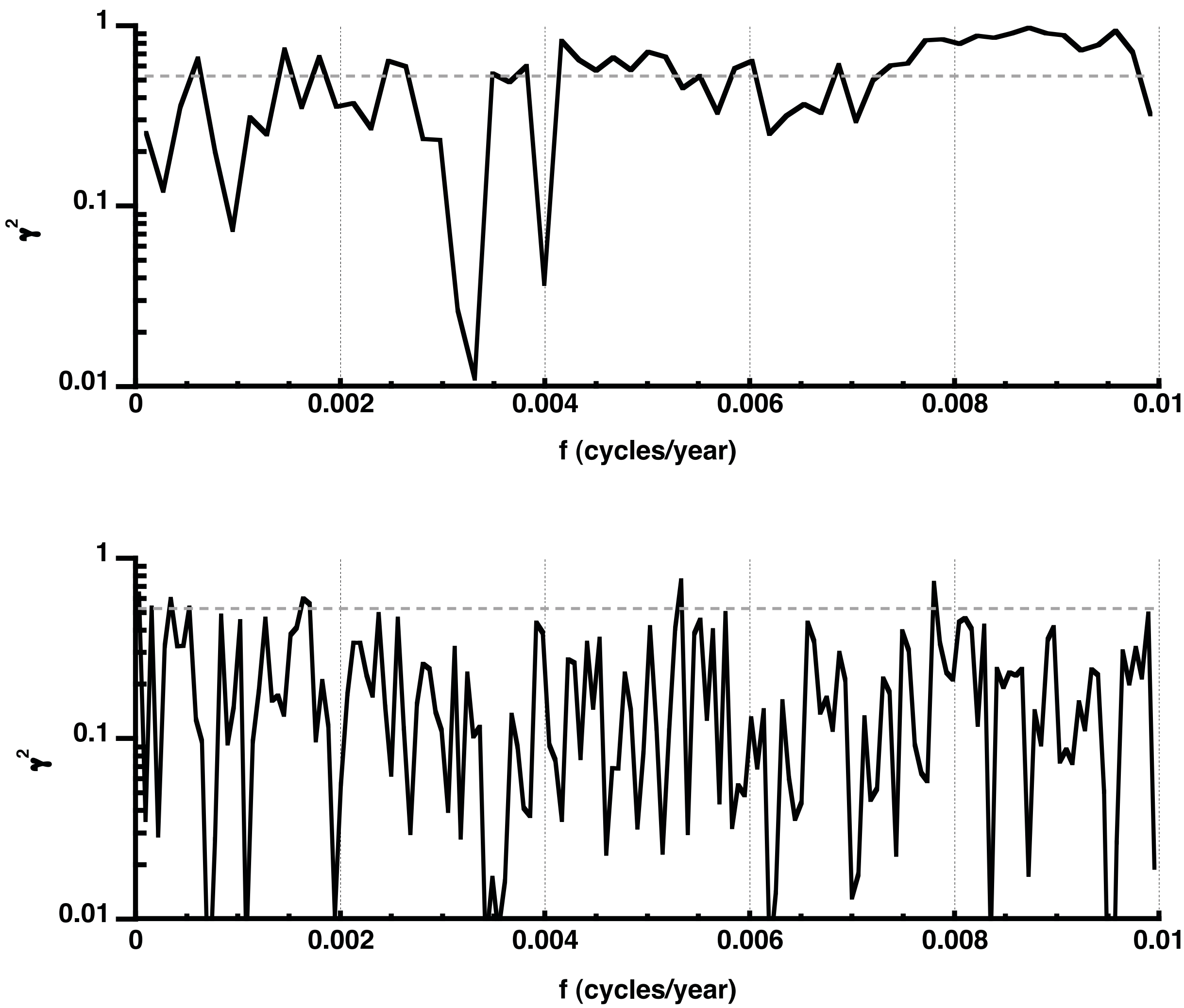

Figure 4.14: Plot of squared coherence (γ2) between natural remanent magnetization intensity normalized by anhysteretic remanent magnetization (NRM/ARM) versus anhysteretic remanent magnetization (ARM) intensity at the 30 mT AF-demagnetization step for a) EW0408-79JC and b) EW0408-85JC. The 95% significance level of squared coherence is denoted via dashed line.

a

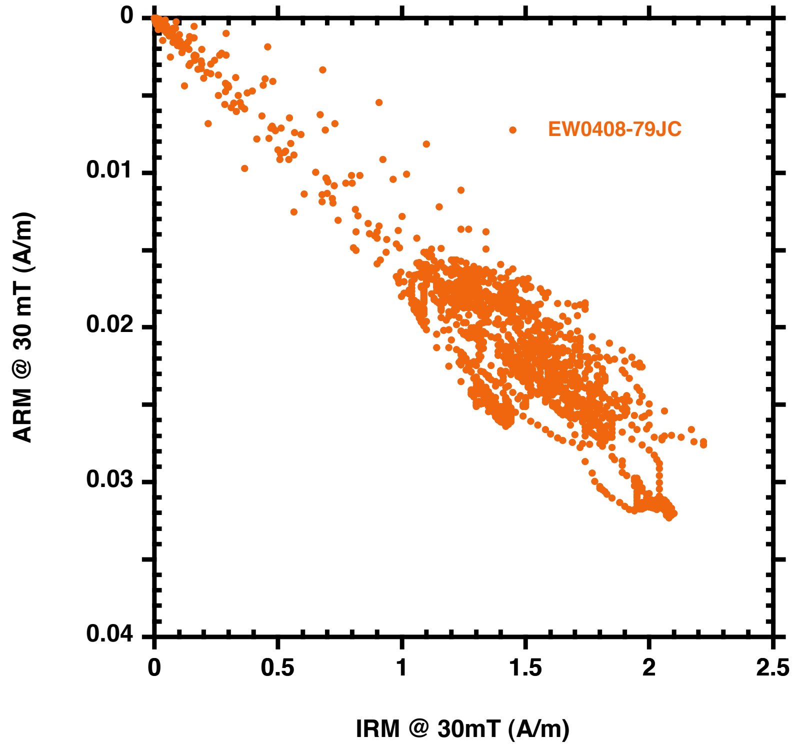

b

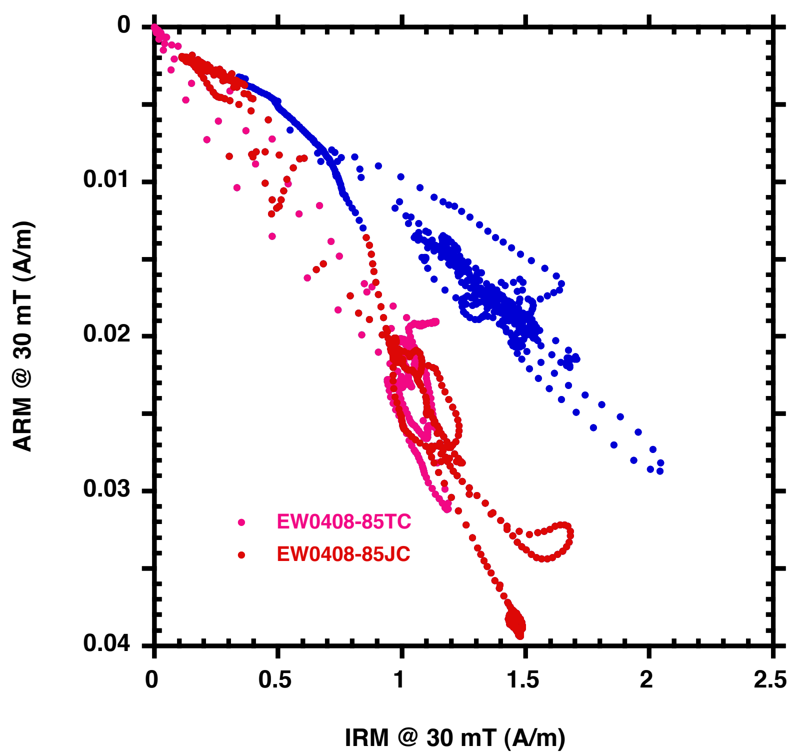

Figure 4.15: Bivariate scatter plot comparing ARM to IRM intensities at the 30 mT demagnetization step for a) EW0408-79JC and b) EW0408-85JC. The blue values in the plot indicate data that has been discarded from RPI reconstructions, due to a shift in the magnetic remanence carrier.

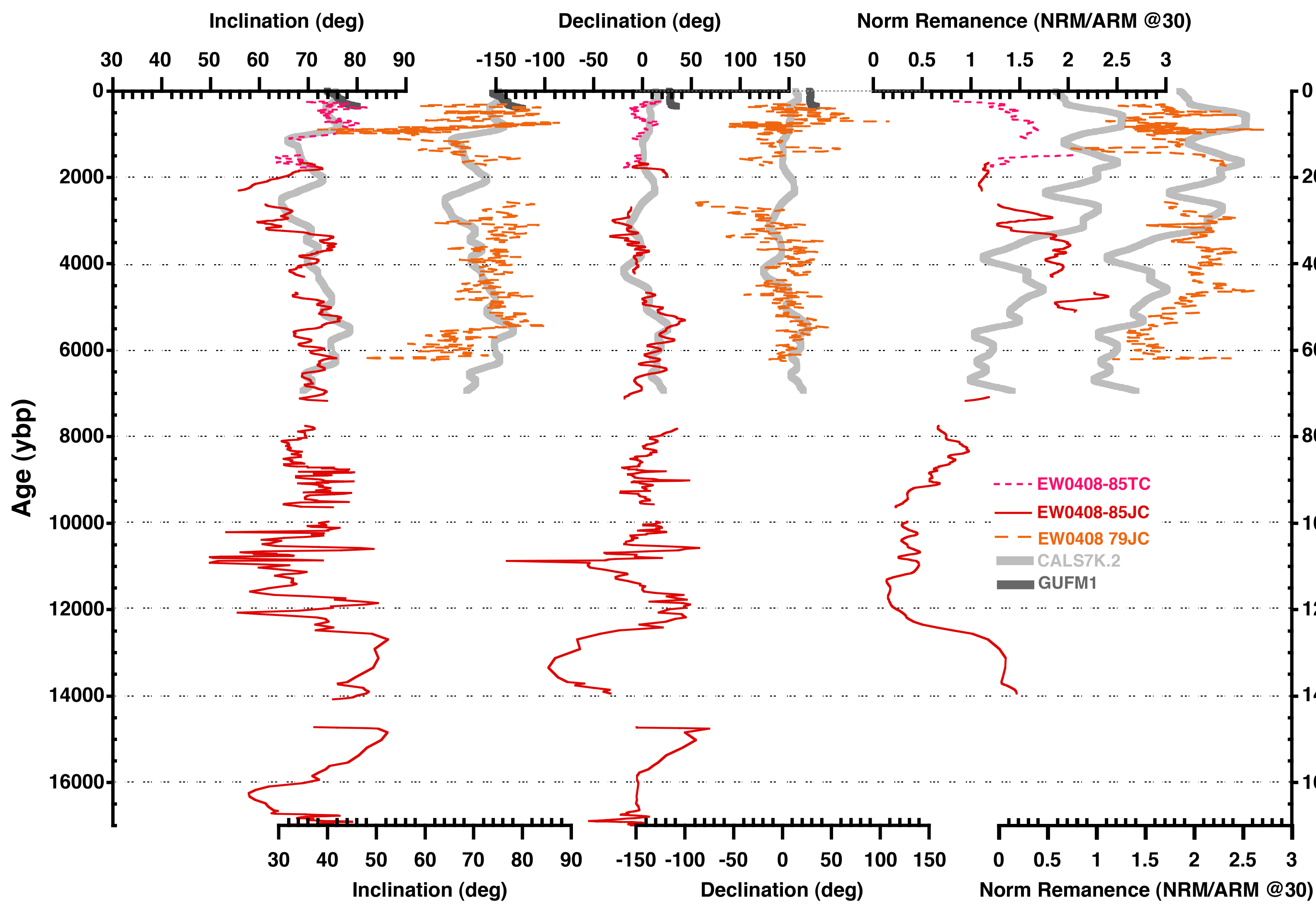

Figure 4.16: Component Inclinations, Declinations, and Normalized Remanence (NRM/ARM @ 30mT demagnetization) from EW0408-85TC/JC (red/pink) and EW0408-79JC (orange), superimposed on the site predictions from the Holocene CALS7K.2 (light gray, Korte and Constable, 2005) and historic GUFM1 (dark gray, Jackson et al., 2000) field models.

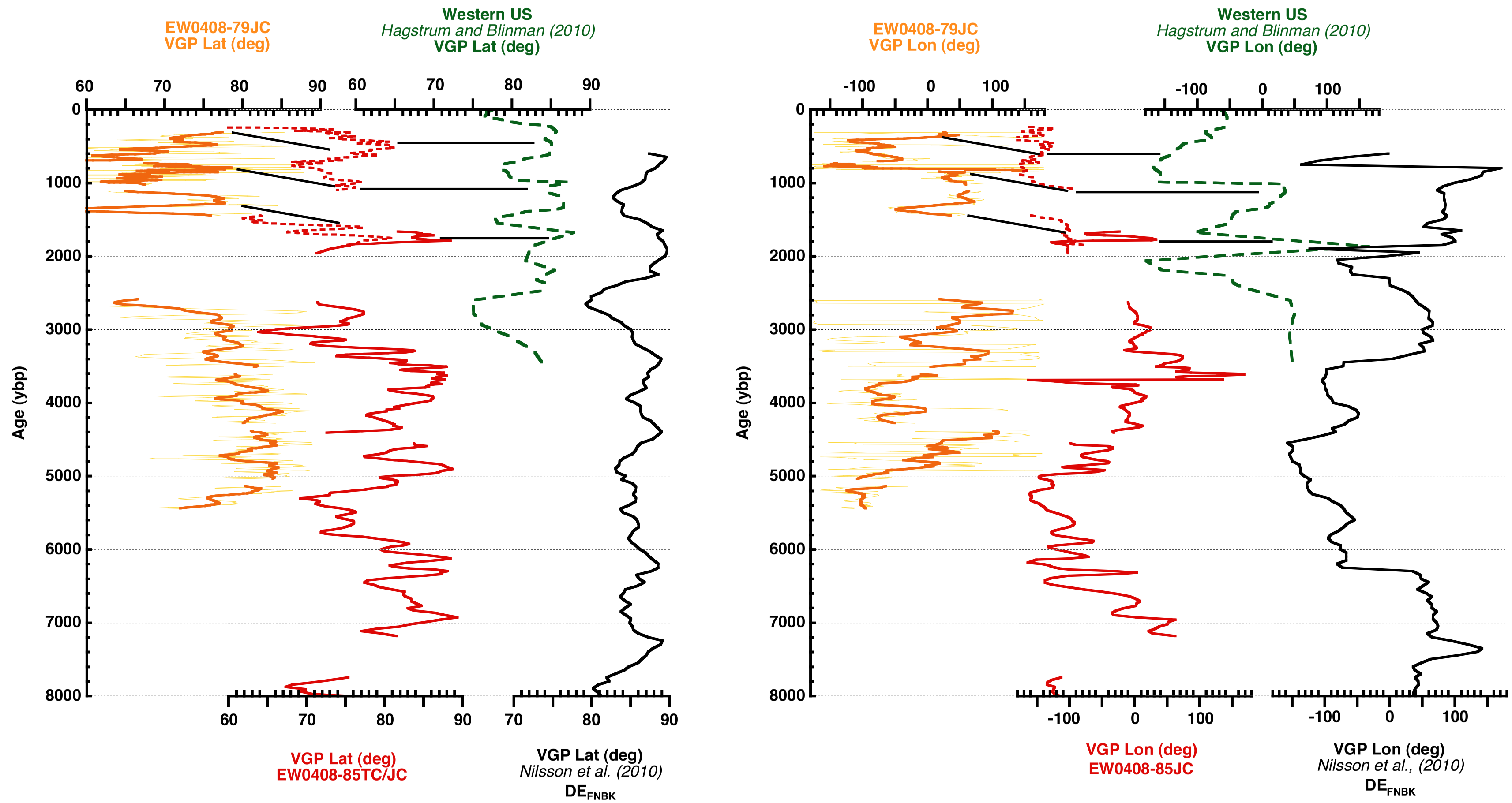

Figure 4.17: Component directional data from the Gulf of Alaska cores EW0408-79JC (orange), EW0408-85JC (red) compared to the Western US Archeomagnetic stack (green circles; Hagstrum and Blinman,2010), corrected for site location via transformation to virtual geomagnetic pole (VGP) inclinations (a) and declinations (b). Tie points for correlative features in EW0408-79JC, EW0408-85JC, and the Western US stack are shown as solid black lines.

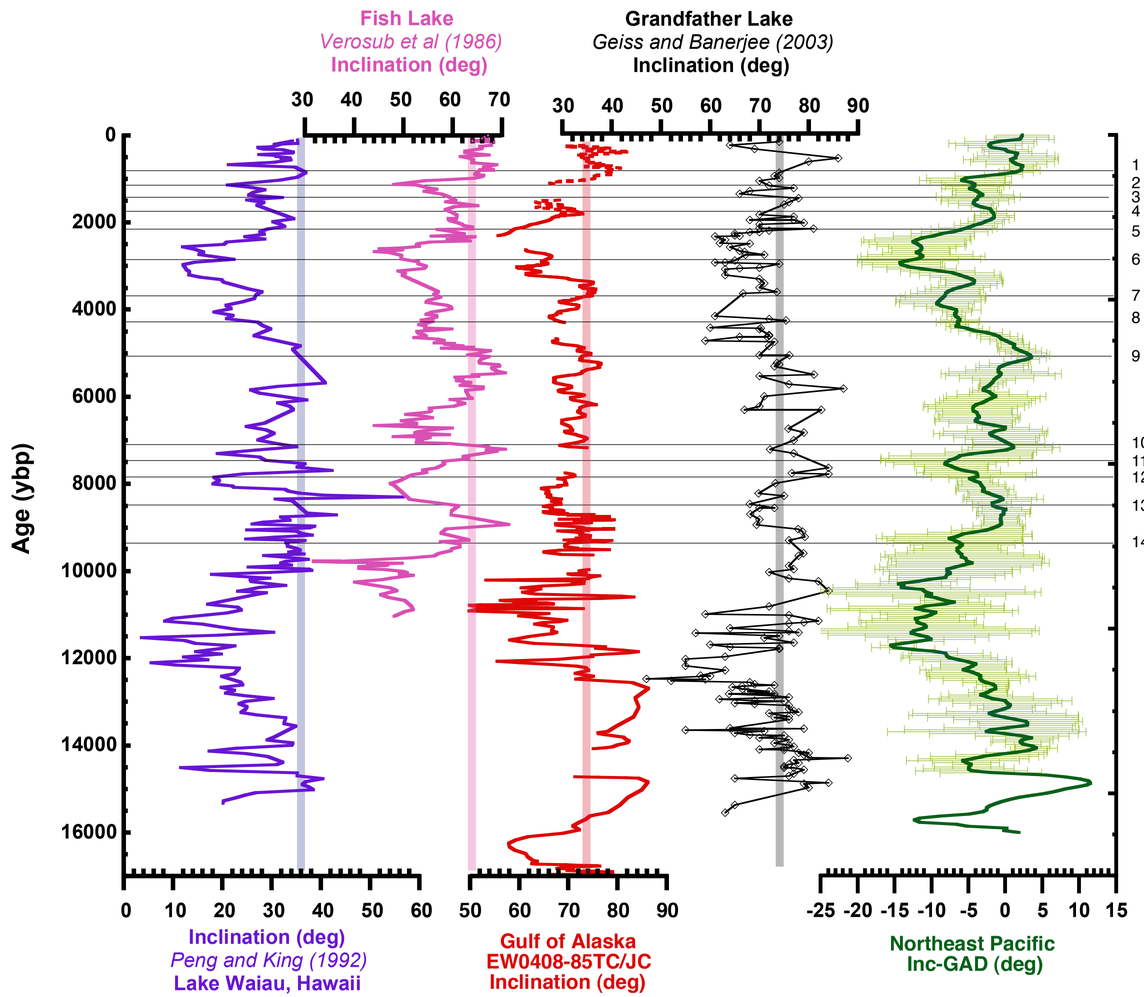

Figure 4.18: North Pacific Holocene inclination records, compared on independent chronologies. From left to right: Lake Waiau, Hawaii (solid purple line, Peng and King, 1992), Fish Lake (solid pink line, Verosub et al., 1986), Gulf of Alaska record EW0408-85TC/JC (dashed/ solid red line), and Grandfather Lake, Alaska (hollow black diamonds, Geiss and Banerjee, 2003). Predicted GAD inclinations for site latitude are shown as bars on each record. A simple GAD latitude-corrected Northeast Pacific inclination stack, derived by averaging these 4 records, is shown to the far right in green, with 1-σ errors. Inclination features identified by Lund (1996) are labeled on the right y-axis.

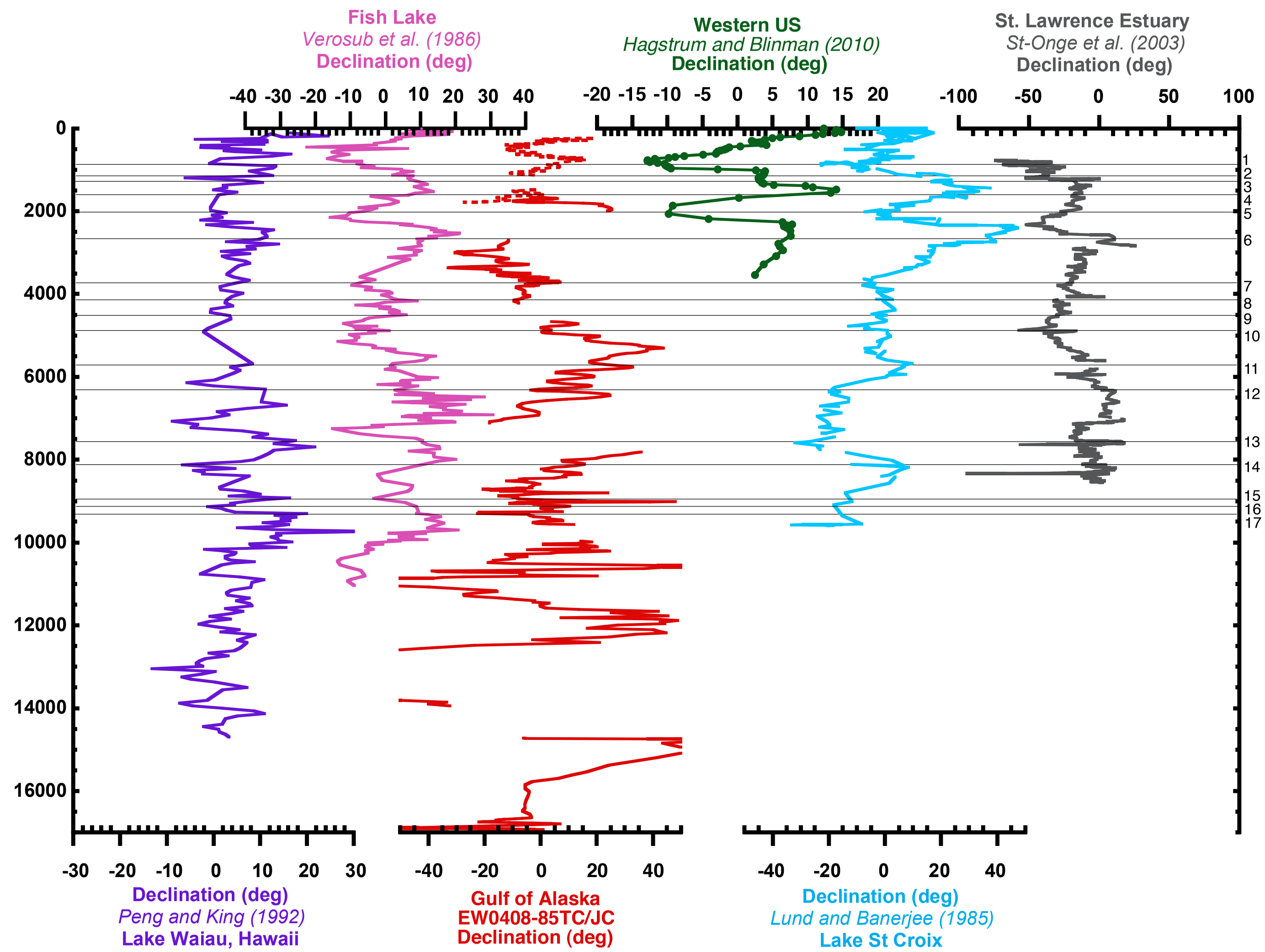

Figure 4.19: North Pacific Holocene declination records, compared on independent chronologies. From left to right: From left to right: Lake Waiau, Hawaii (solid purple line, Peng and King, 1992), Fish Lake (solid pink line, Verosub et al., 1986), Gulf of Alaska record E W0408-85TC/JC (dashed/solid red line), the Western US archeomagnetic stack (green circles; Hagstrum and Blinman, 2010), Lake St. Croix (solid light blue line, Lund and Banerjee, 1985), and the St. Lawrence Estuary (solid gray line; St. Onge et al., 2003). Declination features identified by Lund (1996) are marked by solid gray bars, and labeled on the right y-axis.

Chapter 5

Conclusions

The detailed radiocarbon chronology of high-accumulation rate jumbo piston core EW0408-85JC and its associated trigger core and multicore provide an opportunity to place high-latitude North Pacific climate changes into a global chronological framework.

Retreat of glaciers in the region of the northeastern Gulf of Alaska began by 16,650 ± 170 cal ybp, based on apparent salinity reductions recorded in planktonic foraminiferal $\delta^{18}O$ and a decrease in the rate of glacial-marine sediment accumulation. The transition from the ice-proximal to laminated hemipelagic sediments at 14,790 ± 380 ybp marks the retreat of glaciers either behind sills or onto land.

An interval of low $\delta^{18}O$ in planktonic foraminifera reflects regional freshwater input from retreating glaciers between 16,650 ± 210 cal ybp and 13,770 ± 120 cal ybp ± 200 cal ybp. A more abrupt low $\delta^{18}O$ event in the benthic foraminifera at 14,250 ± 290 cal ybp likely reflects an injection of low-salinity water to 580 m paleodepth driven by rapid glacial melt, perhaps due to low surface salinities that enhanced winter sea-ice cover and attendant brine formation on the shelf. Alternatively, the benthic foraminiferal oxygen isotopic excursion could reflect hyperpycnal flows or a transient deepening of the halocline.

Radiocarbon dates constrain the timing of deglacial warming and freshening of the Gulf of Alaska as coeval with the onset of Bølling interstadial warmth of the North Atlantic and Greenland. North Pacific cooling and/or an increase in surface salinities during Allerød interstadial time may reflect the influence of the Antarctic Cold Reversal, likely transmitted via the subsurface ocean.

Productivity maxima drove sedimentary anoxia and laminated sediments occur between 14,790 ± 380 to 12,990 ± 190 cal ybp and between 11,160 ± 130 to 10,750 ± 220 cal ybp. These events are similar to and likely correlative with, less precisely dated events observed around the rim of the North Pacific. The high-resolution chronology links these events to episodes of global sealevel rise. We evaluate several hypotheses to explain these events, and conclude that remobilization of iron and other limiting nutrients from continental shelves and inundated estuaries during sealevel rise may help to explain synchronous increases in productivity and anoxia that preserved laminated sediments in many places around the margins of the North Pacific.

We conclude that the extremely high apparent ventilation ages implied by Age Model 3 during the deglacial interval, which co-vary in both benthic and planktonic foraminifera, and resemble those inferred at lower latitudes (*Marchitto et al.,* 2007; *Bryan et al.,* 2010) are likely an artifact of inappropriate age model tuning; they are unsupported by other sedimentological evidence and the timing of regional glacial retreat. We do not find evidence for rapid ventilation in the late glacial interval prior to 15 kyr BP, as has been inferred in the western Pacific based on calibrated planktonic ^{14}C age models similar to our Age Model 1 (*Okazaki et al.,* 2010), implying that such ventilation, if real, did not reach the intermediate waters of the Northeast Pacific. Based on Age Model 1, our inference of modest increases in ventilation ages during late glacial time relative to modern are consistent with previous findings of greater watercolumn stratification resulting from closure of Bering Strait (*Zahn et al*. 1991; *Sigman et al*, 2004). We conclude that the substantial retreat of Cordilleran ice, opening of Bering Strait as a gateway for northward export of low-salinity surface waters, and flooding of the Beringian shelf by ~10,300 cal yr BP conditioned the North Pacific for more effective ventilation of intermediate water during Holocene time.

Two independently-dated sedimentary records from the shelf (EW0408-79JC) and slope (EW0408-85JC) of the Gulf of Alaska margin have reproducibly recorded geomagnetic field variability at sub-millenial resolution through the last 6,000 ybp, with the slope core record extending through ~17,000 ybp with somewhat greater uncertainty. Normalized remanence is not robustly interpretable as RPI in the absence of supporting regional records, due to heterogeneity in magnetic remanence-bearing mineralogy. However, paleosecular variation reconstructions agree well with the predictions of CALS7k.2 for the sites [Korte and Constable, 2005]. Directional data from EW0408-85JC rotated to a virtual geomagnetic pole vary at similar times as the well-dated archeomagnetic Western US stack of Hagstrum and Blinman [2010]. Both North American PSV reconstructions agree with predictions from a simple dipole model of global VGP position (Nilsson et al., 2010) on millennial timescales. Sub-millennial scale variability in VGP latitude present in the well-constrained Western US Archeomagnetic stack (Hagstrum and Blinman, 2010) and reproduced in the Gulf of Alaska may reflect the non-dipolar component of Holocene PSV. VGP predictions from EW0408-79JC suggests an ~200 year negative offset over the last 1,500 years relative to site EW0408-85JC and the Western US stack, likely due to the limitations of radiocarbon dating on this scale. EW0408-85JC reproduces many of the North American directional features identified by Lund [1996], and agrees well with records from Hawaii to eastern Canada, extending the spatial and temporal observations of coherent North American PSV behavior to the sub-Arctic North Pacific and back >13,000 ybp, and supporting the long-term persistence of the North American flux lobe.

Bibliography

Chapter 1:
Broecker, W.S. (1982), Glacial to interglacial changes in ocean chemistry. *Progress in Oceanography,* 11, 151–197.

Broecker, W., E. Clark, and S. Barker (2008), Near constancy of the Pacific Ocean surface to mid-depth radiocarbon age difference over the last 20 kyr, *Earth and Planetary Science Letters,* 274, 322-326.

Gubbins, D. (1988), Thermal core-mantle interactions and time-averaged paleomagnetic field., *J. Geophys. Res.,* 93, 3413-3420.

Hughen, K., J. Southon, S. Lehman, C. Bertrand, and J. Turnbull (2006), Marine-derived ^{14}C calibration and activity record for the past 50,000 years updated from the Cariaco Basin, *Quaternary Science Reviews,* 25, 3216–3227.

Lund, S.P. (1996), A comparison of Holocene paleomagnetic secular variation records from North America, *Journal of Geophysical Research,* 101, 8007-8024.

Manabe, S. and R.J. Stouffer (1980), Sensitivity of a global climate model to an increase of CO2 concentration in the atmosphere. J Geophys Res 85: 5529–5554

Olsen, N. and M. Mandea (2007), Will the magnetic north Pole move to Siberia?, *Eos*, 88, 293-300.

Sigman, D.M., and E.A. Boyle (2000), Glacial/interglacial variations in atmospheric carbon dioxide, *Nature,* 407, 859-869.

Snowball, I., and R. Muscheler (2007), Palaeomagnetic intensity data: an Achilles heel of solar activity reconstructions, *Holocene,* 17(6), 851-859, doi:10.1177/0959683607080531.

Stoner, J.S. And G. St-Onge (2007), Magnetic stratigraphy: Reversals, excursions, paleointensity and secular variation, in *Development in Marine Geology: Volume 1, Proxies in Late-Cenezoic Paleoceanography,* Edited by Hillaire-Marcel, C., and A. de Vernal, pp. 99-138.
Addison J.A., B.P. Finney, W.E. Dean, M.H. Davies, A.M. Mix, J.M. Jaeger, Productivity maxima and sedimentary $\delta^{15}N$ during the Last Glacial Maximum termination in the Gulf of Alaska, *Paleoceanography,* submitted.

Chapter 2:
Adkins, J.F., and E.A. Boyle (1997), Changing atmospheric $\Delta^{14}C$ and the record of deep water paleoventilation ages, *Paleoceanography,* 12, 337-344.

Basak, C., E.E. Martin, K. Horikawa, and T. Marchitto (2010), Southern Ocean source of

^{14}C-depleted carbon in the North Pacific Ocean during the last deglaciation, *Nature Geoscience,* 3, 770-773.

Briner, J.P., D.S. Kaufman, W.F. Manley, R.C. Finkel, and M.W. Caffee (2005), Cosmogenic exposure dating of late Pleistocene moraine stabilization in Alaska, *Geological Society of America Bulletin*, doi: 10.1130/B25649.1

Broecker, W. (2009), The mysterious ^{14}C decline, *Radiocarbon,* 51, 109-119.

Broecker, W., and S. Barker (2007), A 190‰ drop in atmosphere's Δ14C during the 'Mystery Interval' (17.5–14.5 kyr), *Earth and Planetary Science Letters*, 256, 90-99.

Broecker, W., and E. Clark (2010), Search for a glacial-age ^{14}C-depleted ocean reservoir, *Geophysical Research Letters*, 37, LI3606, doi:10.1029/2010GL043969.

Broecker, W., T-H. Peng, S. Trumbore, G. Bonani (1990), The distribution of radiocarbon in the glacial ocean, *Global Biogeochemical Cycles,* 4, 103-117.

Broecker, W., E. Clark, and S. Barker (2008), Near constancy of the Pacific Ocean surface to mid-depth radiocarbon age difference over the last 20 kyr, *Earth and Planetary Science Letters,* 274, 322-326.

Bryan, S.P., T.M. Marchitto, and S.J. Lehman (2010), The release of ^{14}C-depleted carbon from the deep ocean during the last deglaciation: Evidence from the Arabian Sea, *Earth Planetary Science Letters,* 298, 244-254.

Cook, M.S., L.D. Keigwin, and C.A. Sancetta (2005), The deglacial history of surface and intermediate water of the Bering Sea, *Deep-Sea Research II*, 52, 2163-2173.

Cosma, T. and I.L. Hendy (2008), Pleistocene glacimarine sedimentation on the continental slope off Vancouver Island, British Columbia, *Marine Geology*, 255, 45-54.

Cowan, E.A. and R.D. Powell (1991), Ice-proximal sediment accumulation rates in a temperate glacial fjord, southeastern Alaska, in *Glacial Marine Sedimentation: Paleoclimatic Significance,* edited by J.B. Anderson and G.M. Ashley, *Geological Society of America Special Paper*, 261, 61–73.

Davies, M.H., A. C. Mix, J.S. Stoner, J.A. Addison, J. Jaeger, B. Finney, and J. Wiest (2011), The deglacial transition on the Southeastern Alaska Margin: meltwater input, sealevel rise, marine productivity, and sedimentary anoxia, *Paleoceanography*, in press.

Davies, M.H., J.S. Stoner, A.C. Mix, J. Jaeger, G.P. Rosen, J. Southon, J. Channell, C. Xuan (*in prep*), A 17,000 year paleomagnetic secular variation record from the Gulf of Alaska, *Geophysics, Geochemistry, Geosystems (G3).*

Dean, W.E., Y. Zheng, J.D. Ortiz, and A. van Geen (2006), Sediment Cd and Mo accumulation in the oxygen-minimum zone off western Baja California linked to global climate over the past 52kyr, *Paleoceanography*, 21, PA4209, doi:10.1029/2005PA001239.

de Boer, A.M., D. M. Sigman, J.R. Toggweiler, and J.L. Russell (2007), Effect of global ocean temperature on deep ocean ventilation, *Paleoceanography,* 22**,** PA2210, doi:10.1029/2005PA001242.

De Pol-Holz, R., L. Keigwin, J. Southon, D. Hebbeln, and M. Mohtadi (2010), No signature of abyssal carbon in intermediate waters off Chile during deglaciation, *Nature Geoscience,* 3, 192-195.

Elias, S.A., S.K. Short, C.H. Nelson, and H.H. Birks (1996), Life and times of the Bering land bridge, Nature, 382, 60-63.

Emile-Geay, J., M.A. Cane, N. Naik, R. Seager, A.C. Clement, and A. van Geen (2003), Warren revisited: Atmospheric freshwater fluxes and "Why is no deep water formed in the North Pacific", *Journal of Geophysical Research*, 108, 3178, doi:10.1029/2001JC001058.

Fischer, H., J. Schmitt, D. Lüthi, T.F. Stocker, T. Tschumi, P. Parekh, F. Joos, P. Köhler, C. Völker, R. Gersonde, C. Barbante, M. Le Floch, D. Raynaud, and E. Wolff (2010), The role of Southern Ocean processes in orbital and millennial CO_2 variations - A synthesis, *Quaternary Science Reviews, 29,* 193-205.

Hughen K.A., M.G.L. Baillie, E. Bard, J.W. Beck, C.J.H. Bertrand, P.G. Blackwell, C.E. Buck, G.S. Burr, K.B. Cutler, P.E. Damon, R.L. Edwards, R.G. Fairbanks, M. Friedrich, T.P. Guilderson, B. Kromer, G. McCormac, S. Manning, C.B. Ramsey, P.J. Reimer, R.W. Reimer, S. Remmele, J.R. Southon, M. Stuiver, S. Talamo, F.W. Taylor, J. van der Plicht, and C.E. Weyhenmeyer (2004), Marine04 marine radiocarbon age calibration, 0-26 cal kyr B,. *Radiocarbon,* 46**,** 1059-1086.

Hughen, K., J. Southon, S. Lehman, C. Bertrand, and J. Turnbull (2006), Marine-derived ^{14}C calibration and activity record for the past 50,000 years updated from the Cariaco Basin, *Quaternary Science Reviews,* 25, 3216–3227.

Kaufman, D.S., R.S. Anderson, F.S. Hu, E. Berg, and A. Werner (2010), Evidence for a variable and wet Younger Dryas in southern Alaska, Quaternary Science Reviews 29, 1445-1452.

Keeling, R.F. (2007), Deglaciation mysteries, *Science*, 316, 1440-1441.

Keigwin, L.D. (2002), Late Pleistocene-Holocene paleoceanography and ventilation of the Gulf of California, *Journal of Oceanography*, 58, 421-432.

Kennett, J.P., and B. L. Ingram (1995), A 20,000-year record of ocean circulation and climate change from the Santa Barbara basin, *Nature*, 377, 510-514.

Marchitto, T.M., S.J. Lehman, J.D. Ortiz, J. Flückiger, and A. van Geen (2007), Marine radiocarbon evidence for the mechanisms of deglacial atmospheric CO_2 rise, *Science*, 316, 1456-1459.

Matsumoto, K., T. Oba, J. Lynch-Stieglitz, and H. Yamamoto (2005), Interior hydrography and circulation of the glacial Pacific Ocean, *Quaternary Science Reviews,* 21, 1693-1704.

McKay, J.L., T. F. Pedersen, and J. Southon (2005), Intensification of the oxygen minimum zone in the northeast Pacific off Vancouver Island during the last deglaciation: Ventilation and/or export production?, *Paleoceanography*, 20, PA4002, doi:10.1029/2003PA000979.

McManus, J.F., R. Francois, J.-M. Gherardi, L.D. Keigwin, and S. Brown-Leger (2004), Collapse and rapid resumption of Atlantic meridional circulation linked to deglacial climate changes, *Nature,* 428, 834-837.

McNeely, R., A.S. Dyke, and J.R. Southon (2006), Canadian marine reservoir ages, preliminary data assessment, *Geological Survey Canada* Open File 5049, 3.

Mix, A.C., D.C. Lund, N.G. Pisias, P. Bodén, L. Bornmalm, M. Lyle, and J. Pike (1999), Rapid climate oscillations in the Northeast Pacific during the last deglaciation reflect Northern and Southern Hemisphere sources, in *Mechanisms of global climate change at millennial time scales, American Geophysical Union*, edited by P.U. Clark et al., Geophysical Monograph 112, pp. 127-148.

Monnin, E., A. Indermühle, A. Dällenbach, J. Flückiger, B. Stauffer, T.F. Stocker, D. Raynaud, and J.-M. Barnola (2001), Atmospheric CO_2 concentrations over the Last Glacial Termination, *Science,* 291, 112–114.

Okazaki, Y., A. Timmermann, L. Menviel, N. Harada, A. Abe-Ouchi, M.O. Chikamoto, A. Mouchet, and A. Asahi (2010), Deepwater formation in the North Pacific during the Last Glacial Termination, *Science*, 329, 200-204.

Ortiz, J.D., S.B. O'Connell, J. Del Viscio, W. Dean, J.D. Carriquiry, T. Marchitto, Y. Zheng, and A. van Geen (2004), Enhanced marine productivity off western North America during warm climate intervals of the past 52 k.y., *Geology*, 32, 521-524.

Paillard, D., L. Labeyrie, and P. Yiou (1996), Macintosh program performs time-series analysis, *Eos Transactions,* 77, 379.

Peltier, W.R. (1994), Ice age paleotopography, *Science,* 265, 195-201.

Pena, L.D., I. Cacho, P. Ferretti, and M.A. Hall (2008), El Ninõ/Southern Oscillation-like variability during glacial terminations and interlatitudinal teleconnections, *Paleoceanography,* 23, PA3101, doi:10.1029/2008PA001620.

Porter, S. C. (1989), Late Holocene fluctuations of the fiord glacier system in Icy Bay, Alaska, U. S. A., *Arctic and Alpine Research,* 21, 364–379.

Porter, S.C. and T.W. Swanson (1998), Radiocarbon age constraints on rates of advance and retreat of the Puget Lobe of the Cordilleran Ice Sheet during the Lat Glaciation, *Quaternary Research*, 50, 205-213.

Primeau, F.W. and M. Holzer (2005), The ocean's memory of the atmosphere: residence-time and ventilation-rate distributions of water masses, *Journal of Physical Oceanography,* 36*,* 1439-1456.

Rasmussen, S.O., K.K. Andersen, A.M. Svensson, J.P. Steffensen, B.M. Vinther, H.B. Clausen, M.-L. Siggard-Andersen, S.J. Johnson, L.B. Larsen, D. Dahl-Jensen, M. Bigler, R. Röthlisberger, H. Fischer, K. Goto-Azuma, M.E. Hansson, and U. Ruth (2006), A new Greenland ice core chronology for the last glacial termination, *Journal of Geophysical Research,* 111**,** D06102, doi:10.1029/2005JD006079.
Reimer, P.J., M.G.L. Baillie, E. Bard, A. Bayliss, J.W. Beck, C.J.H. Bertrand, P.G. Blackwell, C.E. Buck, G.S. Burr, K.B. Cutler, P.E. Damon, R.L. Edwards, R.G. Fairbanks, M. Friedrich, T.P. Guilderson, A.G. Hogg, K.A. Hughen, B. Kromer, G. McCormac, S. Manning, C.B. Ramsey, R.W. Reimer, S. Remmele, J.R. Southon, M. Stuiver, S. Talamo, F.W. Taylor, J. van der Plicht, and C.E. Weyhenmeyer (2004), IntCal04 terrestrial radiocarbon age calibration, 0-26 cal kyr BP, *Radiocarbon*, 46, 1029-1058.

Rose, K. A., E.L. Sikes, T.P. Guilderson, P. Shane, T.M. Hill, R. Zahn, and H.J. Spero (2010), Upper-ocean-to-atmosphere radiocarbon offsets imply fast deglacial carbon dioxide release, *Nature*, 466, 1093-1097.

Sabine, C.L., R.M. Key, A. Kozyr, R.A. Feely, R. Wanninkhof, F.J. Millero, T.-H. Peng, J.L. Bullister, and K. Lee (2005), Global ocean data analysis project: Results and data, *Rep. ORNL/CDIAC-145/NDP-083*, Carbon Dioxide Inf. Anal. Cent., Oak Ridge Natl. Lab., U.S. Dep. of Energy, Oak Ridge, Tenn.

Sigman, D.M., and E.A. Boyle (2000), Glacial/interglacial variations in atmospheric carbon dioxide, *Nature,* 407, 859-869.

Sigman, D. M., S.L. Jaccard, and G.H. Haug (2004), Polar ocean stratification in a cold climate. *Nature*, 428, 59-63

Skinner, L.C., S. Fallon, C. Waelbroeck, E. Michel, and S. Barker (2010), Ventilation of the deep southern ocean and deglacial CO_2 rise, *Science,* 328, 1147-1151.

Skinner, L.C., and N.J. Shackleton (2004), Rapid transient changes in northeast Atlantic

deep water ventilation age across Termination 1, *Paleoceanography,* 19, PA2005, doi:10.1029/2003PA000983.
Stott, L.D. (2010), No signs of Southern Ocean CO_2, *Nature Geoscience,* 3, 153-154.

Stephens, B.B., and R. F. Keeling (2000), The influence of Antarctic sea ice on glacial-interglacial CO_2 variations, *Nature,* 404**,** 171-173.

Stott, L., J. Southon, A. Timmermann, and A. Koutavas (2009), Radiocarbon age anomaly at intermediate water depth in the Pacific Ocean during the last deglaciation, *Paleoceanography,* 25, PA2223, doi:10.1029/2008PA001690.

Stuiver, M., and H.A. Polach (1977), Discussion: Reporting of ^{14}C data, *Radiocarbon,* 19, 355-363.

Stuiver, M., and T.F. Braziunas (1993), Modelling atmospheric ^{14}C influences and ^{14}C ages of marine samples to 10,000BC, *Radiocarbon,* 35, 137-189.

Stuiver, M., P.J. Reimer, and R. Reimer (2005), CALIB 5.0. [http://calib.qub.ac.uk/calib/].

Talley, L.D. (1991), An Okhotsk Sea water anomaly: implications for ventilation in the North Pacific, *Deep-Sea Research Part A,* 38, S171–S190.

Thiele, G., and J.L. Sarmiento (1990), Tracer dating and ocean ventilation, *Journal of Geophysical Research,* 95, 9377-9391.

Toggweiler, J.R. (1999), Variation of atmospheric CO_2 by ventilation of the ocean's deepest water, *Paleoceanography,* 14**,** 571-588.

van Geen, A., R.G. Fairbanks, P. Dartnell, M. McGann, J.V. Gardner, and M. Kashgarian (1996), Ventilation changes in the northeast Pacific during the Last Deglaciation, *Paleoceanography*, 11, 519-528.

Warren, B.A. (1983), Why is no deep water formed in the North Pacific?, *Journal of Marine Research*, 41, 327-347.

Watanabe, T., and M. Wakatsuchi (1998), Formation of 26.8–26.9 $\sigma\theta$ water in the Kuril Basin of the Sea of Okhotsk as a possible origin of North Pacific Intermediate Water, *Journal of Geophysical Research,* 103(C2), 2849–2865.

Zahn, R., T.F. Pedersen, B.D. Bornhold and A.C. Mix (1991), Water mass conversion in the glacial subarctic Pacific (54°N, 148°W). Physical constraints and the benthic-planktonic stable isotope record. *Paleoceanography*, 6, 543-560.

Chapter 3:

Aharon, P. (2006), Entrainment of meltwaters in hyperpycnal flows during deglaciation superfloods in the Gulf of Mexico, *Earth Planet. Sci. Lett.*, *241,* 260-270.

Andersen, K.K., A. Svensson, S.J. Johnsen, S.O. Rasmussen, M. Bigler, R. Rothlisberger, U.Ruth, M.-L. Siggaard-Andersen, J.P. Steffensen (2006), The Greenland Ice Core Chronology 2005, 15-42 ka, Part 1: Constructing the time scale. *Quat. Sci. Rev. (25), Shackleton Special Issue 24.*

Barclay, D.J., G.C. Wiles and P.E. Calkin (2009), Holocene glacier fluctuations in Alaska, *Quat. Sci. Rev, 28,* 2034-2048.

Bard, E., B. Hamelin, and D. Delanghe-Sabatier (2010), Deglacial Meltwater Pulse 1B and Younger Dryas sea levels revisited with boreholes at Tahiti, *Science*, 1-4.

Bard, E. , B. Hamelin, and R.G. Fairbanks (1990), U-Th ages obtained by mass spectrometry in corals from Barbados: sea-level during the past 130,000 years. *Nature, 346*, 456-458.

Bard, E., M. Arnold, R.G. Fairbanks and B. Hamelin (1993), ^{230}Th/^{234}U and ^{14}C ages obtained by mass spectrometry on corals, *Radiocarbon, 35,* 191-199.

Barron, J. A., L. Heusser, T. Herbert, and M. Lyle (2003), High-resolution climatic evolution of coastal northern California during the past 16,000 years, *Paleoceanography*, *18*(1).

Barron, J. A., D. Bukry, and W.E. Dean (2005), Paleoceanographic history of the Guaymas Basin, Gulf of California, during the past 15,000 years based on diatoms, silicoflagellates, and biogenic sediments, *Marine Micropaleontology*, *56*(3-4), 81-102.

Barron, J. A., D., Bukry, W.E.. Dean, J.A. Addison, and B. Finney (2009), Paleoceanography of the Gulf of Alaska during the past 15,000 years: results from diatoms, silicoflagellates, and geochemistry, *Marine Micropaleontology*, *72*, 176-195.

Bauch, D., and H. A. Bauch (2001), Last glacial benthic foraminiferal δ^{18}O anomalies in the polar North Atlantic: A modern analogue evaluation, *J. Geophys, Res., 106*, 9135-9143.

Behl, R. J., and J. P. Kennett (1996), Evidence for brief interstadial events in the Santa Barbara Basin, NE Pacific during the past 60 Kyr, *Nature, 379,* 243-246.

Blunier, T., and E. Brook, Timing of millennial-scale climate change in Antarctica and Greenland during the Last Glacial Period, *Science, 5,*109-112.

Blunier, T., J. Schwander, B. Stauffer, T. Stocker, A. Dallenbach, A. Indermuhle, J. Tschumi, J. Chappellaz, D. Raynaud, J.-M. Barnola (1997), Timing of the Antarctic cold reversal and the atmospheric CO_2 increase with respect to the Younger Dryas Event, *Geophys. Res. Lett., 24*(21), 2683-2686.

Bond, G., W. Showers, M. Cheseby, R. Lotti, P. Almasi, P. deMenocal, P. Priore, H. Cullen, I. Hajdas, G. Bonani (1993), A pervasive millennial-scale cycle in North Atlantic Holocene and Glacial climates, *Science, 278,* 1257-1266.

Bond, G., B. Kromer, J. Beer, R. Muscheler, M. N. Evans, W. Showers, S. Hoffmann, R. Lotti-Bond, I. Hajdas, G. Bonani (2001), Persistent solar influence on North Atlantic climate during the Holocene, *Science, 294*, 2130-2136.

Boyd, P. W., C.S. Law, C.S. Wong, Y. Nojiri, A. Tsuda, M. Levasseur, S. Takeda, R. Rivkin, P.J. Harrison, R. Strzepek, J. Gower, R.M. McKay, E. Abraham, M. Arychuk, J. Barwell-Clarke, W. Crawford, D. Crawford, M. Hale, K. Harada, K. Johnson, H. Kiyosawa, I. Kudo, A. Marchetti, W. Miller, J. Needoba, J. Nishioka, H. Ogawa, J. Page, M. Robert, J. Saito, A. Sastri, N. Sherry, T. Soutar, N. Sutherland, Y. Taira, F. Whitney, S.-K. E. Wong, and T. Yoshimura (2004), The decline and fate of an iron-induced subarctic phytoplankton bloom, *Nature, 428*(6982), 549-553.

Briner, J.P., D.S. Kaufman, A. Werner, M. Caffee, L. Levy, W.F. Manley, M.R. Kaplan, and R. Finkel (2002). Glacier readvance during the late glacial (Younger Dryas?) in the Ahklun Mountains, southwestern Alaska, *Geology, 30*, 679-682.

Broecker, W.S. (1994) Massive iceberg discharges as triggers for global climate change. *Nature, 372*, 421-424.

Broecker, W., S. A. Mix, M. Andree, and H. Oeschger (1984), Radiocarbon measurements on co-existing benthic and planktonic foraminiferal shells: Potential for reconstructing ocean ventilation times over the past 20,000 years, *Nuclear Instruments and Methods in Physics Research, B5,* 340-345.

Brunelle, B.G., D.M. Sigman , S.L. Jaccard , L.D. Keigwin, B. Plessen, G. Schettler, M.S. Cook, G.H. Haug (2010) Glacial/interglacial changes in nutrient supply and stratification in the western subarctic North Pacific since the penultimate glacial maximum, Quaternary Science Reviews, 29, 2579-2590.

Caissie, B.E., J. Brigham-Grette, K.T. Lawrence, T.D. Herbert, and M.S. Cook (2010), Last Glacial Maximum to Holocene sea surface conditions at Umnak Plateau, Bering Sea, as inferred from diatom, alkenone, and stable isotope records, *Paleoceanography, 25,* doi:10.1029/2008PA001671.

Carlson, P. R. (1989), Seismic reflection characteristics of glacial and glacimarine sediment in the Gulf of Alaska and adjacent fjords, *Mar. Geol., 85,* 391-416.

Chase, Z., P. Strutton, and B. Hales (2007), Iron links river runoff and shelf width to phytoplankton biomass along the U.S. West Coast, *Geophys. Res. Lett. 34,* doi:10.1029/2006GL028069.

Childers, A. R., T.E. Whitledge, and D.A. Stockwell (2005), Seasonal and interannual variability in the distribution of nutrients and chlorophyll *a* across the Gulf of Alaska shelf: 1998-2000. *Deep-Sea Res. II, 52,* 193-216.

Cook, M. S., L.D. Keigwin, and C.A. Sancetta (2005), The deglacial history of surface and intermediate water of the Bering Sea, *Deep-Sea Res., Part II*, *52*(16-18), 2163-2173.

Crusius, J., T. Pedersen, S. Kienast, L. Keigwin, and L. Labeyrie (2004), Influence of northwest Pacific productivity on North Pacific Intermediate Water oxygen concentrations during the Boiling-Allerød interval (14.7-12.9 ka), *Geology*, *32*(7), 633-636.

Dean, W. E. (2007), Sediment geochemical records of productivity and oxygen depletion along the margin of western North America during the past 60,000 years: teleconnections with Greenland Ice and the Cariaco Basin, *Quat. Sci. Rev.*, *26*(1-2), 98-114.

Dean, W. E., Y. Zhen, J.D. Ortiz, A. van Geen (2006), Sediment Cd and Mo accumulation in the oxygen-minimum zone off western Baja California linked to global climate over the past 52 kyr, *Paleoceanography*, *21*(4), 13.

De Angelis, M., N.I. Barkov, and V.N. Petrov, (1987): Aerosol concentrations over the last climatic cycle (160 kyr) from an Antarctic ice core, *Nature, 325*, 318-321.

Deschamps, P., N. Durand, E. Bard, B. Hamelin, G. Camoin, A.L. Thomas, G.M. Henderson, and Y. Yokoyama (2009), Synchroneity of Meltwater Pulse 1A and the Bolling onset: New evidence from IODP "Tahiti Sea-Level" expedition, Geophysical Research Abstracts, Vol. 11, EGU2009-10233, EGU General Assembly 2009, Vienna, Austria.

Duce, R. A., and N. W. Tindale (1991), Atmospheric transport of iron and its deposition in the ocean, *Limn. Oceanogr., 36(8),* 1715-1726.

Engstrom, D. R., B.C.S. Hansen, and H.E. Wright, Jr. (1990), A possible Younger Dryas record in Southeastern Alaska, *Science 7,* doi:10.1126/science.250.4986.1383.

Fairbanks, R.G. (1989). A 17,000 year glacio-eustatic sea level record: influence of glacial melting rates on the Younger Dryas event and deep ocean circulation, *Nature, 260*, 962-968.

Ferrians, O. J. (1989), Glacial Lake Atna, Copper River Basin, Alaska. In: Carter, L.D., Hamilton, T.D., and Galloway, J.P. (Eds.), *Late Cenezoic History of the Interior Basins of Alaska and the Yukon,* US Geological Survey Circular 1026, 85-89.

Fisher, D., E. Osterberg, A. Dyke, D. Dahl-Jensen, M. Demuth, C. Zdanowicz, J. Bourgeois, R.M. Koerner, P. Mayewski, C. Wake, K. Kreutz, E. Steig, J. Zheng, K. Yalcin, K. Goto-Azuma, B. Luckman, and S. Rupper (2008), The Mount Logan late Wisconsonian isotope record: tropical Pacific Yukon connections. *The Holocene 18,* 667-677.

Fraile, I., S. Mulitza, and M. Schulz (2009), Modeling planktonic foraminiferal seasonality: Implications for sea-surface temperatures. *Marine Micropaleontology, 72,* doi:10.1016/j.marmicro.2009.01.003.

Fukasawa, M., H. Freeland, R. Perkin, T. Watanabe, H. Uchida, A. Nishina (2004), Bottom water warming of the North Pacific Ocean, *Nature, 427,* 825-827.

Galbraith, E.D., S.J. Jaccard, T.F. Pedersen, D.M. Sigman, G.H. Haug, M. Cook, J.R. Southon, and R. Francois (2007), Carbon dioxide release from the North Pacific abyss during the last deglaciation, *Nature, 449*, 890-893.

Gansen G., and D. Kroon (2000), The isotopic signature of planktonic foraminifera from NE Atlantic surface sediments: implications for the reconstruction of past oceanic conditions, *J. Geol. Soc. London, 157,* 639-699.

Gebhardt, H, M. Sarnthein, P.M. Grootes, T. Kiefer, H. Keuhn, F. Schmieder, and U. Rohl (2008), Paleonutrient and productivity records from the subarctic North Pacific for Pleistocene glacial terminations I to V, *Paleoceanography 23*, PA4212, doi:10.1029/2007PA001513.

Gorbarenko, S. A., J.R. Southon, L.D. Keigwin, M.V. Cherepanova, and I.G. Gvozdeva (2004), Late Pleistocene-Holocene oceanographic variability in the Okhotsk Sea: geochemical, lithological and paleontological evidence, *Palaeogeography Palaeoclimatology Palaeoecology 209*(1-4), 281-301.

Hendy, I. L., and T. N. Cosma (2008) Vulnerability of the Cordilleran Ice Sheet to iceberg calving during late Quaternary rapid climate change events, *Paleoceanography*, *23*, PA2101, doi:2110.1029/2008PA001606.

Hendy, I. L., and J. P. Kennett (2003), Tropical forcing of North Pacific intermediate water distribution during Late Quaternary rapid climate change?, *Quat. Sci. Rev, 22*(5-7), 673-689.

Hendy, I.K., T.F. Pedersen, J.P. Kennett, and R. Tada (2004), Intermittent existence of a southern Californian upwelling cell during submillennial climate change of the last 60 kyr, *Paleoceanography, 19,* PA3007, doi:10.1029/2003PA000965.

Hendy, I. L., and T. F. Pedersen (2006), Oxygen miminum zone expansion in the eastern tropical North Pacific during deglaciation, *Geophys. Res. Lett., 33,* L20602, doi:10.1029/2006GL025975.

Hajdas, I., G. Bonani, P. Bodén, D. M. Peteet, and D.H. Mann (1998), Cold reversal on Kodiak Island, Alaska, correlated with the European Younger Dryas by using variations in atmospheric ^{14}C content. *Geology, 26*, 1047-1050.

Hostetler, S.W., P.U. Clark, P.J. Bartlein, A.C. Mix, and N.J. Pisias (1999), Atmospheric transmission of North Atlantic Heinrich events, *J. Geophys. Res., 104,* 3947-3952.

Hu, F.S., D. M. Nelson, G. H. Clarke, K.M. Rühland, Y. Huang, D.S. Kaufman, and J.P. Smol (2006), Abrupt climate events during the last glacial-interglacial transition in Alaska, *Geophys. Res. Lett. 33,* doi:10.1029/2006GL027261

Huybers, P. and C. Langmuir (2009), Feedback between deglaciation, volcanism, and atmospheric CO2, *Earth Planet. Sci. Lett., 286* 479-491.

Imran, J., and J.P.M. Syvitski (2000), Impact of extreme river events on the coastal ocean, *Oceanography, 13,* 85-92.

Jaeger, J. M., C.A. Nittrouer, N.D. Scout, and J.D. Milliman (1998), Sediment accumulation along a glacially impacted mountainous coastline: North-east Gulf of Alaska, *Basin Res.*, *10*(1), 155-173.

Johnson, W.R., T.C. Royer, and J.L. Luick (1988), On the seasonal variability of the Alaska Coastal Current. *J. Geophys. Res. 93*, 12423–12437.

Johnson, K.S., F.P. Chavez, and G.E. Friederich (1999), Continental-shelf sediment as a primary source of iron for coastal phytoplankton, *Nature, 398*, 697-700.

Kiefer, T., M. Sarnthein, H. Erlenkeuser, P.M. Grootes, A.P. Roberts (2001). North Pacific response to millennial-scale changes in ocean circulation over the last 60 ky. *Paleoceanography* 16, 179-189.

Keigwin, L. D. (2002), Late Pleistocene-Holocene paleoceanography and ventilation of the Gulf of California, *J. Oceanogr.*, *58*(2), 421-432.

Keigwin, L. D., G.A. Jones, and P.N. Froelich (1992), A 15,000 year paleoenvironmental record from Meiji Seamount, Far Northwestern Pacific, *Earth Planet. Sci. Lett.*, *111*(2-4), 425-440.

Keigwin, L.D. (1998), Glacial-age hydrography of the far northwest Pacific Oceani, *Paleoceanography, 13,* 323-339.

Kienast, M., T.J.J. Hanebuth, C. Pelejero, and S. Steinke (2003), Synchroneity of Meltwater Pulse 1A and the Bølling warming: new evidence from the South China Sea, *Geology*, *31*(1), 67-70.

Klinkhammer, G. P., A.C. Mix, and B.A. Haley (2009), Increased dissolved terrestrial input to the coastal ocean during the last deglaciation, *Geochem. Geophys. Geosyst.,*10, Q03009, doi: 10.1029/2008GC002219.

Kotilainen, A. T. and N .J. Shackleton, (1995), Rapid climate variability in the North Pacific Ocean during the past 95,000 years, *Nature* 377, 323-326.

Lam, P.J., and J.K.B. Bishop (2008), The continental margin is a key source of iron to the HNLC North Pacific Ocean, *Geophys. Res. Lett., 35,* L07608, doi:10.1029/2008GL033294.

Lippiatt, S.M., M.C. Lohan, K.W. Bruland (2010), The distribution of reactive iron in northern Gulf of Alaska coastal waters, *Marine Chemistry, 121,* doi:/10.1016/j.marchem.2010.04.007.

Lopes, C. and A. C. Mix (2009), Pleistocene megafloods in the northeast Pacific, *Geology*, *37(1),* 79-82.

Lund, D. C., and A. C. Mix (1998), Millenial-scale deep water oscillations: reflections of the North Atlantic in the deep Pacific from 10 to 60 ka, *Paleoceanography*, *13*(1), 10-19.

Mahowald, N.M., A. R. Baker, G. Bergametti, N. Brooks, R.A. Duce, T.D. Jickells, N. Kubilay, J.M. Prospero, and I. Tegen (2005), Atmospheric global dust cycle and iron inputs to the ocean, *Global Biogeochem. Cycles, 19,* GB4024, doi:10.1029/2004GB002402.

Manley, W.F., and D.S. Kaufman (2002), Alaska PaleoGlacier Atlas, Institute of Arctic and Alpine Research (INSTARR), University of Colorado, http://instaar.colorado.edu/QGISL/ak_paleoglacier_atlas, v. 1.

Mann, D.H., and D.M. Peteet (1994), Extent and timing of the Last Glacial Maximum in Southwestern Alaska, *Quat. Res., 42(2),*136-148.

Martin, J.H. (1990), Glacial-Interglacial CO_2 Change: The Iron Hypothesis, *Paleoceanography*, *5(1),* 1-13.

Martinez-Garcia, A., A. Rosell-Mele, W. Geibert, R. Gersonde, P. Masqué, V. Gaspari, and C. Barbante (2009), Links between iron supply, marine productivity, sea surface temperature, and CO_2 over the last 1.1 Ma, *Paleoceanography, 24,* PA1207, doi:10.1029/2008PA001657.

Masuda, S., T. Awaji, N. Sugiura, J.P. Matthews, T. Toyoda, Y. Kawai, T. Doi, S. Kouketsu, H. Igarashi, K. Katsumata, H. Uchida, T. Kawano, M. Fukasawa (2010), Simulated rapid warming of the abyssal North Pacific waters, *Science, 329*, 319-322.

McDonald, D., T.F. Pedersen, and J. Crusius, Multiple late Quaternary episodes of exceptional diatom production in the Gulf of Alaska, *Deep-Sea Res., Part II*, *46(11-12)*, 2993-3017.

McKay, J.L., T.F. Pedersen, and S.S. Kienast (2004), Organic carbon accumulation over the last 16 kyr off Vancouver Island, Canada: Evidence for increased marine productivity during the deglacial, *Quat. Sci. Rev., 23,* 261-281.

McManus, J. F., R. Francois, J.-M. Gherardi, L.D. Keigwin, and S. Brown-Leger (2004), Collapse and rapid resumption of Atlantic meridional circulation linked to deglacial climate changes, *Nature 428*, 834-837.

McNeely, R., A.S. Dyke, and J.R. Southon (2006), Canadian marine reservoir ages, preliminary data assessment, *Geological Survey Canada*, Open File 5049.

Mikolajewicz, U., T.J. Crowley, A. Schiller, and R. Voss (1997), Modelling teleconnections between the North Atlantic and North Pacific during the Younger Dryas. *Nature, 387,* 384-387.

Milliman, J. D., and J. P. M. Syvitski (1992), Geomorphic tectonic control of sediment discharge to the ocean - the importance of small mountainous rivers, *Geology*, *100*(5), 525-544.

Milliman , J. D., D. Stocks, J.M. Jaeger, and C.A. Nittrouer (1996), Prince William Sound, Alaska: distal depocenter for Copper River sediment. *EOS Trans., 77,* OS202.

Mix, A.C., D.C. Lund, N.G. Pisias, P. Bodén, L. Bornmalm, M. Lyle, and J. Pike (1999), Rapid climate oscillations in the Northeast Pacific during the last deglaciation reflect Northern and Southern Hemisphere sources, In: Clark, P.U., et al. (Eds), *Mechanisms of global climate change at millennial time scales,* Am. Geophys. Union Geophysical Monograph 112, 127-148.

Moffett, J. W. (2001), Transformations among different forms of iron in the ocean, In: D. R. Turner and K. A. Hunter (Eds), *The biogeochemistry of iron in seawater*, edited by D. R. Turner and K. A. Hunter, pp. 343-372, John Wiley & Sons, Ltd., West Sussex, England.

Molnia, B. F. (1986), Late Wisconsin glacial history of the Alaskan continental margin. In: Hamilton, T.D., Reed, K.M., Thorson, R.M. (Eds), *Glaciation in Alaska-the Geologic Record*, 99-144. Plenum, New York.

Molnia, B. F., and P. R. Carlson (1978), Surface sedimentary units of the northern Gulf of Alaska continental shelf. *Bull. Am. Assoc. Petrol. Geol., 62,* 633-643.

Mortlock, R.A., and P.N. Froelich (1989), A simple method for the rapid determination of biogenic opal in pelagic marine sediments, *Deep-Sea Res., 36(9),*1415–1426.

Nichols, D.R., and L.A. Yehle (1969), Engineering geologic map of the southeastern Copper River Basin, Alaska, *U.S. Geological Survey Miscellaneous Investigations 524*, 1 sheet scale 1:125,000.

National Institute of Standards and Technology (1992), Report of Investigation, Reference Materials 8543-8546, US Department of Commerce, Gaithersburg, MD, 3pp.

Okazaki, Y., K. Takahashi, H. Asahi, K. Katsuki, J. Hori, H. Yasuda, Y. Sagawa, and H. Tokuyama (2005), Productivity changes in the Bering Sea during the late Quaternary, *Deep-Sea Res., Part II*, *52*(16-18), 2150-2162.

Okazaki, Y., A. Timmermann, K. Menviel, N. Harada, A. Abe-Ouchi, M.O. Chikamoto, A. Mouchet, H. Asahi (2010), Deepwater formation in the North Pacific during the Last Glacial Termination, *Science, 329*, 200-204.

Okumura, Y.M., C. Deser, A. Hu, A. Timmermann, S-P Xie (2008) North Pacific Climate Response to Freshwater Forcing in the Subarctic North Atlantic: Oceanic and Atmospheric Pathways. *J. Clim.* , 22, 1424-1445.

Ortiz, J.D., A. Mix, R.W. Collier (1995), Environmental control of living symbiotic and asymbiotic foraminifera of the California Current, *Paleoceanography, 10,* 987-1009.

Ortiz, J.D., A.C. Mix, W. Ruch, J.M. Watkins, and R.W. Collier (1996), Deep-dwelling planktonic foraminifera of the northeastern Pacific Ocean reveal environmental control of oxygen and carbon isotopic disequilibria, *Geochimica et Cosmochimica Acta, 60,* 4509-4523.

Ortiz, J., A. Mix, S. Hostetler, and M. Kashgarian (1997), The California current of the last glacial maximum: Reconstruction at 42 degrees N based on multiple proxies, *Paleoceanography*, *12*(2), 191-205.

Ortiz, J.D., S.B. O'Connell, J. DelViscio, W. Dean, J.D. Carriquiry, T. Marchitto, Y. Zheng, and A. van Geen (2004), Enhanced marine productivity off western North America during warm climate intervals of the past 52 k.y., *Geology, 32(6)*, doi:10.1130/G20234.1.

Peltier, W.R. (1994), Ice Age Paleotopography, *Science, 256,* 195-201.

Peteet, D. (2007), Muskeg archives of vegetation, migration, and climate history in the Gulf of Alaskan arc. Paper 9–8. In: *Abstracts – Geological Society of America, Cordilleran Section – 103rd Annual Meeting*. http://gsa.confex.com/gsa/2007CD/finalprogram/abstract_120879.htm, Bellingham, Washington.

Rasmussen, S. O., Andersen, K. K., Svensson, A. M., Steffensen, J. P., Vinther, B., Clausen, H. B., Siggaard-Andersen, M.-L., Johnsen, S. J., Larsen, L. B., Dahl- Jensen, D., Bigler, M., R¨othlisberger, R., Fischer, H., Goto-Azuma, K., Hansson, M., Ruth, U. (2006), A new Greenland ice core chronology for the last glacial termination. *J. Geophys. Res. 111*, D06102.

Rasmusen, T.L., and E. Thomsen (2009) Stable isotope signals from brines in the Barents Sea: Implications for brine formation during the last glaciation, *Geology 37*, 903-906.

Reimer, P.J., M.G.L. Baillie, E. Bard, A. Bayliss, J.W. Beck, P.G. Blackwell, C. Bronk Ramsey, C.E. Buck, G.S. Burr, R.L. Edwards, M. Friedrich, P.M. Grootes, T.P. Guilderson, I. Hajdas, T.J. Heaton, A.G. Hogg, K.A. Hughen, K.F. Kaiser, B. Kromer, F.G. McCormac, S.W. Manning, R.W. Reimer, D.A. Richards, J.R. Southon, S. Talamo, C.S.M. Turney, J. van der Plicht, and C.E. Weyhenmeyer (2009), INTCAL09 and MARINE09 radiocarbon age calibration curves, 0-50,000 years cal BP, *Radiocarbon 51*, 1111-1150.

Rignot, E., and P. Kanagaratnam (2006), Changes in the velocity structure of the Greenland Ice Sheet, *Science 311*, doi: 10.1126/science.1121381.f

Royer, T.C. (1981). Baroclinic transport in the Gulf of Alaska. Part II. Fresh water driven coastal current. *Journal of Marine Research 39*, 251–266.

Royer, T.C. (1982). Coastal fresh water discharge in the northeast Pacific. *J. Geophys. Res. 87*, 2017–2021.

Royer, T.C. (2005), Hydrographic responses at a coastal site in the northern Gulf of Alaska to seasonal and interannual forcing. *Deep-sea Res. II Top. Stud. Oceanogr., 52(1-2),* 267-288.

Rubin, M., and C. Alexander (1960), U.S. Geological Survey radiocarbon dates V, *Radiocarbon 2*, 129-185.

Ruth, U., J-M Barnola, J. Beer, M. Bigler, T. Blunier, E. Castellano, H. Fischer, F. Fundel, P. Huybrechts, P.R. Kaufmann, J. Kipfstuhl, A. Lambrecht, A. Morganti, H. Oerter, F Parrenin, O. Rybak, M. Severi, R. Udisti, F. Wilhelms, E.W. Wolff (2007): EDML1: a chronology for the EPICA deep ice core from Dronning Maud Land, Antarctica, over the last 150 000 years. Climate of the Past, 3, 475-484, doi:10.5194/cp-3-475-2007

Sabine, C.L., R.M. Key, A. Kozyr, R.A. Feely, R. Wanninkhof, F.J. Millero, T.-H. Peng, J.L. Bullister, and K. Lee (2005), Global Ocean Data Analysis Project: Results and Data. *ORNL/CDIAC-145, NDP-083,* doi: 10.3334/CDIAC/otg.ndp0833.

Saenko, O.A., A. Schmittner, and A.J. Weaver (2004), The Atlantic-Pacific Seesaw, *J. Clim. , 17,* 2033-2038.

Sautter, L.R. and R.C. Thunell (1991) Seasonal variability in the $\delta^{18}O$ and $\delta^{13}C$ of planktonic foraminifera from an upwelling environment: Sediment trap results from the San Pedro Basin, Southern California. *Paleoceanography, 6*, 307-334.

Schmittner, A. (2005), Decline of the marine ecosystem caused by a reduction in the Atlantic overturning circulation, *Nature, 434,* 628-633.

Schmittner, A., and E.D. Galbraith (2008), Glacial greenhouse-gas fluctuations controlled by ocean circulation changes, *Nature 456,* doi:10.1038/nature07531.

Schmittner, A., and T. F. Stocker (1999), The stability of the thermohaline circulation in global warming experiments, *J. Clim. 12,* 1117-1133.

Schmittner, A., E. D. Galbraith, S. W. Hostetler, T. F. Pedersen, and R. Zhang (2007) Large fluctuations of dissolved oxygen in the Indian and Pacific oceans during Dansgaard-Oeschger oscillations caused by variations of North Atlantic Deep Water subduction, *Paleoceanography, 22, PA3207,* doi:10.1029/2006PA001384.

Schroth, A. W., J. Crusius, E.R. Sholkovitz, and B.C. Bostick (2009), Iron solubility driven by speciation in dust sources to the ocean, *Nat. Geosci.*, *2*, 337-340.

Severmann S., Johnson C. M., Beard B. L. and McManus J. (2006) The effect of early diagenesis on the Fe isotope compositions of porewaters and authigenic minerals in continental margin sediments. *Geochim.Cosmochim.Acta* 70, 2006-2022.

Severmann S., Lyons T.W., Anbar A., McManus J. and Gordon G (2008) Modern iron isotope perspective on the benthic iron shuttle and the redox evolution of ancient ocean, *Geology* 36, 487-490.

Severmann S., J. McManus, W.M. Berelson, and D.E. Hammond (2010), The continental shelf benthic iron flux and its isotope composition, *Geochim. Cosmochim. Acta,* doi:10.1016/j.gca.2010.04.022.

Shibahara, A., K. Ohkushi, J.P. Kennett, K. Ikehara (2007), Late Quaternary changes in intermediate water oxygenation and oxygen minimum zone, northern Japan: A benthic foraminiferal perspective, *Paleoceanography, 22,* PA3213, doi:10.1029/2005PA001234.

Shimer, G. (2009), Holocene vegetation and climate change at Canyon Lake, Copper River basin, Alaska, M.S., Dep. Of Geol.and Geophys., Univ. of Alaska, Fairbanks, Alaska, USA.

Svensson, A., K.K. Andersen, M. Bigler, H.B. Clausen, D. Dahl-Jensen, S.M. Davies, S.J. Johnsen, R. Muscheler, S.O. Rasmussen, R. Rothlisberger, J.P. Steffensen, and B.M. Vinther (2006) The Greenland Ice Core Chronology 2005, 15-42 ka. Part 2: Comparison to other records. *Quat. Sci. Rev.(25), Shackleton special issue 24.*

Stabeno, P.J., R.K. Reed, and J.D. Schumacher (1995). The Alaska Coastal Current: continuity of transport and forcing. *J. Geophys. Res. 100*, 2477–2485.

Stabeno, P.J., N.A. Bond, A.J. Hermann, N.B. Kachel, C.W. Mordy, J.E. Overland (2004), Meteorology and oceanography of the Northern Gulf of Alaska, *Continental Shelf Research, 24*, 859-897.

Stuiver, M., and P.J. Reimer (1993), Extended 14C database and revised CALIB radiocarbon calibration program, *Radiocarbon*, *35*, 137-189.

Ten Brink, N.W. (1983), Glaciation of the northern Alaska Range, In: Thorson, R.M., and Hamilson, T.D. (Eds), *Glaciation in Alaska: Extended abstracts from a workshop*.

Alaskan Quaternary Center, Univ. of Alaska Museum Occasional Paper 2, 82-91.

Tedesco, K., R. Thunell, Y. Astor, and F. Muller-Karger (2007), The oxygen isotope composition of planktonic foraminifera from the Cariaco Basin, Venezuela: Seasonal and interannual variations. *Marine Micropaleontology 62,* 180-193.

Thorson, R.M., and T.D. Hamilton (1986), Glacial geology of the Aleutian Islands, In: Hamilton, T.D., Reed, K.M., Thorson, R.M. (Eds), *Glaciation in Alaska-the Geologic Record*, 171-192. Plenum, New York.

Tsuda, A., H. Kiyosawa, A. Kuwata, M. Mochizuki, N. Shiga, H. Saito, S. Chiba, K. Imal, J. Nishioka, and T. Ono (2005), Responses of diatoms to iron-enrichment (SEEDS) in the western subarctic Pacific, temporal and special comparisons, *Prog. Oceanogr., 64*(2-4), 189-205.

Van Geen, A., Y. Zheng, J.M. Bernhard, K.G. Cannariato, J. Carriquiry, W.E. Dean, B.W. Eakins, J.D. Ortiz, J. Pike (2003), On the preservation of laminated sediments along the western margin of North America, *Paleoceanography*, *18*(4), 18.

Weaver, A.J., O.A. Saenko, P.U. Clark, and J.X. Mitrovica (2003), Meltwater Pulse 1A from Antarctica as a trigger of the Bølling-Allerød Warm Interval, *Science, 299,* 1709-1713.

Weingartner, T. J., S. K. Danielson, and T.C. Royer (2005) Freshwater variability and predictability in the Alaskan Coastal Current, *Deep Sea Res., Part II, 52*, 161– 191.

Wiedmer, M., D.R. Montgomery, A.R. Gillespie, and H. Greenberg (2010), Late Quaternary megafloods from Glacial Lake Atna, Southcentral Alaska U.S.A., *Quat. Res.,* doi: 10.1016/j.yqres.2010.02.005.

Williams, J.R., and J.P. Galloway (1986), Map of western Copper River Basin, Alaska, showing lake sediments and shorelines, glacial moraines, and location of stratigraphic sections and radiocarbon-dated samples. *U.S. Geological Survey Open-File Report* 86-390, 1 sheet, scale 1:250,000.

Winckler, G., R.F. Anderson, M.Q. Fleisher, D. McGee, N. Mahowald (2008), Covariant glacial-interglacial dust fluxes in the Equatorial Pacific and Antarctica, *Science, 320,* 93-96.

Wu, J., A. Aguilar-Islas, R. Rember, T. Weingertner, S. Danielson, and T. Whitledge (2009), Size-fractionation iron distribution on the northern Gulf of Alaska, *Geophys. Res. Lett., 36,* L11606, doi:10.1029/2009GL038304.

Yehle, L.A., H.R. Schmoll, and A.F. Chleborad (1983), Preliminary surficial geologic map of the southwestern part of the Tyonek B-5 quadrangle, south-central Alaska. *U.S. Geological Survey Miscellaneous Field Investigations Map* MF-1161-B, scale 1:31,680.

Zahn, R., Pedersen, T. F., Bornhold, B. D., and Mix, A. C. (1991), Water mass conversion in the glacial subarctic Pacific [54°N, 148°W]: Physical constraints and the benthic-planktonic stable isotope record, *Paleoceanography, 6*, 543–560.

Zheng, Y., A. van Geen, R.F. Anderson, J.V. Gardner, and W.E. Dean (2000), Intensification of the northeast Pacific oxygen minimum zone during the Bølling-Allerød warm period, *Paleoceanography*, *15*(5), 528-536.

Chapter 4:

Addison, J.A., B.P. Finney, W.E. Dean, M.H. Davies, A.M. Mix, and J.M. Jaeger, Productivity maxima and sedimentary $\delta^{15}N$ during the Last Glacial Maximum termination in the Gulf of Alaska, *Paleoceanography,* submitted.

Amerigian, C. (1977), Measurement of the effect of particle size variation on the detrital remanent magnetization to anhysteretic remanent magnetization ratio in some abyssal sediments, *Earth and Planetary Science Letters,* 36, 434-442.

Anson, G.L., and K.P. Kodama (1987), Compaction-induced inclination shallowing of the post-depositional remanent magnetization in a synthetic sediment, *Geophysical Journal of the Royal Astronomical Society,* 88, 673-692.

Barletta, F., G. St-Onge, J.S. Stoner, P. Lajeunesse, and J. Locat (2010), A high-resolution Holocene paleomagnetic secular variation and relative paleointensity stack from eastern Canada, *Earth and Planetary Science Letters,* 298, 162-174.

Barron, J.A., D. Bukry, W.E. Dean, J.A. Addison, and B. Finney (2009), Paleoceanography of the Gulf of Alaska during the past 15,000 years: Results from diatoms, silicoflagellates, and geochemistry, *Marine Micropaleontology,* 72, 176-195.

Bloemendal, J., J.W. King, F.R. Hall, and S.J. Doh (1992), Rock magnetism of Late Neogene and Pleistocene deep-sea sediments: relationship to sediment source, diagenetic processes, and sediment lithology, *Journal of Geophysical Research,* 97, 4361-4375.

Bloxham, J. (2002), Time-independent and time-dependent behaviour of high-latitude flux bundles at the core-mantle boundary, *Geophysical Research Letters*, 29, 1854, doi:10,1029/2001GBLO14543.

Bloxham, J., and D. Gubbins (1985), The secular variation of Earth's magnetic field, *Nature*, 317, 777-781.

Bowles, J. (2007), Coring-related deformation of Leg 208 sediments from Walvis Ridge: Implications for paleomagnetic data, *Physics of the Earth and Planetary Interiors,* 161, 161-169.

Carlson, P.R. (1989), Seismic reflection characteristics of glacial and glacimarine sediment in the Gulf of Alaska and adjacent fjords, *Marine Geology,* 85, 391-416.

Cowan, E.A., S.A. Brachfeld, R.D. Powell, and S.C. Schoolfield (2006), Terrane-specific rock magnetic characteristics preserved in glacimarine sediment from southern coastal Alaska, *Canadian Journal of Earth Sciences,* 43, 1269-1282.

Davies, C.J., D. Gubbins, A.P. Willis, and P.K. Jimack (2008), Time-averaged paleomagnetic field and secular variation: Predictions from dynamo solutions based on lower mantle seismic tomography, *Physics of the Earth and Planetary Interiors,* 169, 194-203.

Davies, M.H., A.C. Mix, J.S. Stoner, J.A. Addison, J. Jaeger, B. Finney, J. Wiest, The deglacial transition on the Southeastern Alaska Margin: meltwater input, sealevel rise, marine productivity, and sedimentary anoxia, *Paleoceanography,* in press.

Finlay, C. (2008), Historical variation of the geomagnetic axial dipole, *Physics of the Earth and Planetary Interiors,* 170, 1-14.

Geiss, C.E., and S.K. Banerjee (2003), A Holocene–Late Pleistocene geomagnetic inclination record from Grandfather lake, SW Alaska, *Geophysical Journal International,* 153, 497-507.

Gubbins, D. (1988), Thermal core-mantle interactions and time-averaged paleomagnetic field., *J. Geophys. Res.,* 93, 3413-3420.

Hagstrum, J.T., and D.E. Champion (2002), A Holocene paleosecular variation record from 14C-dated volcanic rocks in western North America, *Journal of Geophysical Research*, 107(B1), 2025, doi:10.1029/2001JB000524.

Hagstrum, J.T., and E. Blinman (2010), Archeomagnetic dating in western North America: an updated reference curve based on paleomagnetic and archeomagnetic data sets, *Geochemistry, Geophysics, Geosystems,* 11, Q06009, doi:10.1029/2009/GC002979

Jackson, A., A.R.T. Jonkers, and M.R. Walker (2000), Four centuries of geomagnetic secular variation from historical records, *Philosophical Transactions of the Royal Society of London. Series A: Mathematical, Physical and Engineering Sciences,* 358, 957-990.

Jaeger, J.M., and C.A. Nittrouer (2006), A quantitative examination of modern sedimentary lithofacies formation on the glacially influenced Gulf of Alaska continental shelf, *Continental Shelf Research,* 26, 2178-2204.

Jaeger, J.M., C.A. Nittrouer, N.D. Scott, and J.D. Milliman (1998), Sediment accumulation along a glacially impacted mountainous coastline: Northeast Gulf of Alaska, *Basin Research,* 10, 155-173.

Karlin, R. (1990), Magnetite diagenesis in marine sediments from the Oregon continental margin, *Journal of Geophysical Research,* 95, 4405-4419.

Karlin, R., and S. Levi (1983), Diagenesis of magnetic minerals in recent haemipelagic sediments, *Nature,* 303, 327-330.

Karlin, R., and S. Levi (1985), Geochemical and sedimentological control of the magnetic properties of hemipelagic sediments, *Journal of Geophysical Research,* 90, 373-392.

King, J., S.K. Banerjee, J. Marvin, and O. Ozdemir (1982), A comparison of different magnetic methods for determining the relative grain size of magnetite in natural materials: some results from lake sediments, *Earth and Planetary Science Letters,* 59, 404-419.

King, J.W., S.K. Banerjee, and J. Marvin (1983), A new rock-magnetic approach to selecting sediments for geomagnetic paleointensity studies: application to paleointensity for the last 4000 years, *Journal of Geophysical Research,* 88, 5911-5921.

Kirschvink, J.L. (1980), The least-squares line and plane and the analysis of palaeomagnetic data, *Geophysical Journal of the Royal Astronomical Society,* 62, 699-718.

Korte, M., A. Genevey, C.G. Constable, U. Frank, and E. Schnepp (2006), Continuous geomagnetic field models for the past 7 millenniaI: a new global data compilation, *Geochemistry, Geophysics, Geosystems,* 6, Q02H15.

Korte, M., and C.G. Constable (2005), Continuous geomagnetic field models for the past 7 millennia: 2, CALS7K*, Geochemistry, Geophysics, Geosystems,* 6, Q02H16, doi:10.1029/2004GC000801

Korte, M., F. Donadini, and C.G. Constable (2009), The geomagnetic field for 0-3 ka, Part II: a new series of time-varying global models, *Geochemistry, Geophysics, Geosystems,* 10, Q06008, doi:10.1029/2008GC002297

Levi, S., and S.K. Banerjee (1976), On the possibility of obtaining relative paleointensities from lake sediments, *Earth and Planetary Science Letters,* 29, 219-226.

Lisé-Pronovost, A., G. St-Onge, S. Brachfeld, F. Barletta, and D. Darby (2009), Paleomagnetic constraints on the Holocene stratigraphy of the Arctic Alaskan margin, *Global and Planetary Change,* 68, 85-99.

Lund, S.P. (1996), A comparison of Holocene paleomagnetic secular variation records from North America, *Journal of Geophysical Research,* 101, 8007-8024.

Lund, S.P., and S.K. Banerjee (1985), Late Quaternary paleomagnetic field secular variation from two Minnesota lakes, *Journal of Geophysical Research,* 90(B1), 803-825.

Mazaud, A. (2005), User-friendly software for vector analysis of the magnetization of long sediment cores, *Geochemistry Geophysics Geosystems,* 6, Q12006, doi:10.1029/2005GC001036.

McNeely, R., A.S. Dyke, and J.R. Southon (2006), Canadian marine reservoir ages, preliminary data assessment, *Geological Survey Canada, Open File* 5049

Merril, R., M. McElhinny, P. McFadden (1996), *The Magnetic Field of the Earth*, Academic Press, San Diego, CA, 531 pp.

Molnia, B.F., and P.R. Carlson (1978), Surface sedimentary units of northern Gulf of Alaska continental shelf, *Bull. Am. Assoc. Petrol. Geol*., 62, 633-643.

Nilsson, A., I. Snowball, R. Muscheler, C. Bertacchi Uvo (2010), Holocene geocentric dipole tile model constrained by sedimentary paleomagnetic data. *Geochemistry Geophysics Geosystems,* 11, doi: 10.1029/2010GC003118.

Ortiz, J.D., L. Polyak, J.M. Grebmeier, D.A. Darby, D.D. Eberl, S. Naidu, and D. Nof (2009), Provenance of Holocene sediment on the Chukchi-Alaskan margin based on combined diffuse spectral reflectance and quantitative X-Ray Diffraction analysis, *Global and Planetary Change,* 68, 73-84.

Peng, L., and J.W. King (1992), A late Quaternary geomagnetic secular variation record from Lake Waiau, Hawaii, and the question of the Pacific nondipole low, *Journal of Geophysical Research,* 97(B2), 4407-4424.

Sambrotto, R.N., and C.J. Lorenzen (1987), Phytoplankton and primary production, in *The Gulf of Alaska,* Edited by Hood, D.W., and S.T. Zimmerman, pp. 249-282, U.S. Department of Commerce, USA.

Snowball, I., and R. Muscheler (2007), Palaeomagnetic intensity data: an Achilles heel of solar activity reconstructions, *Holocene,* 17(6), 851-859, doi:10.1177/0959683607080531.

Snowball, I., and P. Sandgrena (2002), Geomagnetic field variations in northern Sweden during the Holocene quantified from varved lake sediments and their implications for cosmogenic nuclide production rates, *Holocene,* 12(5), 517-530

Stoner, J.S. And G. St-Onge (2007), Magnetic stratigraphy: Reversals, excursions, paleointensity and secular variation, in *Development in Marine Geology: Volume 1, Proxies in Late-Cenezoic Paleoceanography,* Edited by Hillaire-Marcel, C., and A. de Vernal, pp. 99-138.

Stoner, J.S., J.E.T. Channell, and C. Hillaire-Marcel (1996), The magnetic signature of rapidly deposited detrital layers from the deep Labrador Sea: Relationship to North Atlantic Heinrich layers, *Paleoceanography*, 11(3), 309-325

St-Onge, G., J.S. Stoner, and C. Hillaire-Marcel (2003), Holocene paleomagnetic records from the St. Lawrence Estuary, eastern Canada: centennial-to millennial-scale geomagnetic modulation of cosmogenic isotopes, *Earth and Planetary Science Letters,* 209, 113-130.

Stuiver, M., and P.J. Reimer (1993), Extended 14C database and revised CALIB radiocarbon calibration program, *Radiocarbon,* 35, 137-189.

Tauxe, L. (1993), Sedimentary records of relative paleointensity of the geomagnetic field: theory and practice, *Reviews of Geophysics,* 31, 319-354.

Thomas, R.G., Y. Guyodo, and J.E.T. Channell (2003), U-channel track for susceptibility measurements, *Geochemistry, Geophysics, Geosystems,* 4, doi:10.1029/2002GC000454.

Thompson, R. and F. Oldfield (1986), *Environmental Magnetism*, Allen & Unwin, London.

Verosub, K.L. (1977), Depositional and postdepositional processes in the magnetization of sediments, *Reviews of Geophysics,* 15, 129-143.

Verosub, K.L. (1982), A paleomagnetic record from Tangle Lakes, Alaska: Large amplitude secular variation at high latitudes, *Geophysical Research Letters,* 9, 823-826.

Verosub, K.L., P.J. Mehringer Jr, and P. Waterstraat (1986), Holocene secular variation in western North America: paleomagnetic record from Fish Lake, Harney County, Oregon, *Journal of Geophysical Research,* 91, 3609-3623.

Weeks, R.J., C. Laj, L. Endignoux, M.D. Fuller, A.P. Robert, R. Manganne, E. Blanchard, and W. Goree (1993), Improvements in long core measurement techniques: applications in paleomagnetism and paleoceanography, *Geophysical Journal International*, 114, 651–662.

Weingartner, K. Coyle, B. Finney, R. Hopcroft, T. Whitledge, R. Brodeur, M. Dagg, E. Farley, D. Haidvogel, L. Haldorson, A. Hermann, S. Hinckley, J. Napp, P. Stabeno, T. Kline, C. Lee, E. Lessard, T. Royer and S. Strom (2002), The Northeast Pacific GLOBEC Program: Coastal Gulf of Alaska, *Oceanography,* 15(2), 10–35.

Zellers, S.D. (1995), Foraminiferal sequence biostratigraphy and seismic stratigraphy of a tectonically active margin; the Yakataga Formation, northeastern Gulf of Alaska, *Marine Micropaleontology,* 26, 255-271.

Appendix 1: Stable isotope data from EW0408-85JC

PACL Depth (cmbsf)	PACL δ13C (‰)	PACL d18O (‰)
153	0.95	1.5
161	0.98	1.39
166	0.91	1.51
171	0.86	1.47
176	0.79	1.37
181	0.98	1.54
186	0.87	1.54
191	0.77	1.76
196	0.92	1.34
204	0.82	1.35
209	0.76	1.69
214	0.9	1.41
219	0.9	1.51
224	0.76	1.24
229	0.96	1.43
234	0.86	1.58
242.5	0.77	1.83
247.5	0.75	1.61
254	0.87	1.75
257.5	0.82	1.58
262.5	0.84	1.51
267.5	0.69	1.78
272.5	0.86	1.4
277.5	0.72	1.57
282.5	0.81	1.59
287.5	0.93	1.51
293.5	0.84	1.52
297.5	0.84	1.5

BULL Depth (cmbsf)	Bull δ13C (‰)	Bull d18O (‰)
153	0.58	1.58
161	0.38	1.76
166	0.39	2.03
171	0.41	1.81
176	0.29	1.6
181	0.32	1.96
186	0.4	1.74
191	0.56	1.72
196	0.43	1.56
204	0.5	1.59
209	0.46	1.97
214	0.58	1.7
219	0.57	1.81
224	0.68	1.65
229	0.56	1.98
234	0.56	1.84
242.5	0.56	1.6
254	0.21	1.65
257.5	0.29	1.71
262.5	-0.01	1.76
267.5	0.25	1.46
272.5	0.27	1.49
277.5	0.11	1.5
282.5	0.53	1.76
287.5	0.33	1.71
293.5	0.54	1.82
297.5	0.51	1.66
304	0.19	1.43

UVI Depth (cmbsf)	UVI δ13C (‰)	UVI δ18O (‰)
153	-0.89	3.21
161	-0.76	3.25
166	-0.99	3.26
171	-0.91	3.23
176	-0.94	3.24
181	-0.81	3.29
186	-0.84	3.26
191	-0.8	3.19
196	-0.86	3.18
204	-0.85	3.23
209	-0.88	3.25
214	-0.96	3.15
219	-0.75	3.2
224	-0.9	3.23
229	-0.91	3.18
234	-0.91	3.19
242.5	-0.9	3.25
247.5	-0.96	3.34
254	-0.81	3.25
257.5	-1.01	3.25
262.5	-0.85	3.27
267.5	-0.93	3.19
272.5	-0.69	3.23
277.5	-0.78	3.26
282.5	-0.91	3.27
287.5	-0.93	3.24
293.5	-0.79	3.17
297.5	-0.94	3.16

CIB Depth (cmbsf)	CIB δ13C (‰)	CIB δ18O (‰)
733	-0.92	3.64
740	-0.34	3.68
743	-0.86	3.58
745.5	-0.87	3.72
748	-0.35	3.71
751	-0.59	3.73
754	-0.33	3.74
792	-0.96	3.91
794.5	-0.74	3.83
796.5	-1.37	3.85
802	-1.15	3.84
804	-0.95	3.97
806.5	-1.33	4.02
810	-1.13	4
814.5	-0.89	3.99

NON Depth (cmbsf)	NON δ13C (‰)	NON δ18O (‰)
762.5	-0.82	3.9
792	-0.99	4
796.5	-1.03	3.81
819.5	-1.37	3.04

Appendix 1 (Cont): Stable isotope data from EW0408-85JC

PACL Depth (cmbsf)	PACL δ13C (‰)	PACL δ18O (‰)	BULL Depth (cmbsf)	Bull δ13C (‰)	Bull δ18O (‰)	UVI Depth (cmbsf)	UVI δ13C (‰)	UVI δ18O (‰)
304	0.88	1.65	307.5	0.21	1.47	297.5	-0.76	3.2
307.5	0.75	1.51	312.5	0.23	1.33	304	-0.84	3.2
312.5	0.75	1.55	317.5	0.21	1.67	307.5	-0.8	3.07
317.5	0.82	1.35	322.5	0.17	1.32	312.5	-0.88	3.19
322.5	0.82	1.43	327.5	0.04	1.65	317.5	-0.91	3.2
327.5	0.69	1.28	332.5	0.3	1.77	322.5	-1	3.13
332.5	0.77	1.52	337.5	0.36	1.54	327.5	-0.97	3.1
337.5	0.75	1.51	342.5	0.38	1.74	332.5	-0.85	3.18
342.5	0.79	1.34	347.5	0.58	1.61	337.5	-0.95	3.16
347.5	0.68	1.47	352.5	0.23	1.61	342.5	-0.9	3.16
352.5	0.72	1.54	356	0.58	1.94	347.5	-1.07	3.1
356	0.69	1.84	362.5	0.26	1.56	352.5	-0.97	3.14
362.5	0.83	1.71	367.5	0.27	1.6	356	-0.9	3.29
367.5	0.86	1.62	372.5	0.17	1.81	362.5	-0.89	3.17
372.5	0.75	1.77	382.5	0.48	1.63	367.5	-0.89	3.19
377.5	0.84	1.34	387.5	0.39	1.59	372.5	-1.03	3.15
382.5	0.91	1.52	392.5	0.49	1.77	382.5	-0.94	3.22
387.5	0.84	1.67	397.5	0.08	1.48	387.5	-0.96	3.17
392.5	0.86	1.66	404	0.23	1.7	392.5	-0.97	3.17
397.5	0.81	1.56	407.5	0.23	1.73	397.5	-0.95	3.22
404	0.84	1.75	412.5	0.1	1.96	404	-0.84	3.23
407.5	0.79	1.61	417.5	0.45	1.85	407.5	-1.03	3.14
412.5	0.75	1.58	422.5	0.11	1.76	412.5	-0.94	3.12
417.5	0.78	1.54	427.5	0.14	1.9	417.5	-1	3.18
422.5	0.81	1.67	432.5	0.29	1.65	422.5	-1.15	3.12
427.5	0.84	1.73	437.5	0.49	1.88	427.5	-0.98	3.24
432.5	0.81	1.71	442.5	0.34	1.8	432.5	-1.02	3.13
437.5	0.79	1.64	447.5	0.33	1.64	437.5	-1.05	3.15

Appendix 1 (Cont): Stable isotope data from EW0408-85JC

PACL Depth (cmbsf)	PACL δ13C (‰)	PACL δ18O (‰)
442.5	0.83	1.67
447.5	0.75	1.64
454	0.62	1.85
457.5	0.74	1.69
462.5	0.77	1.65
467.5	0.74	1.55
472.5	0.82	1.71
477.5	0.73	1.64
482.5	0.8	1.74
487.5	0.85	1.73
492.5	0.85	1.6
497.5	0.89	1.76
504	0.65	1.75
507.5	0.8	1.85
512.5	0.78	1.82
517.5	0.72	1.62
522.5	0.73	1.91
527.5	0.59	1.77
532.5	0.6	1.59
537.5	0.64	1.69
543.5	0.6	1.83
548.5	0.62	1.88
555	0.33	2
559.5	0.36	1.69
564.5	0.46	1.61
569.5	0.45	1.76
574.5	0.57	1.7
579.5	0.56	1.8

BULL Depth (cmbsf)	Bull δ13C (‰)	Bull δ18O (‰)
454	0.22	1.8
457.5	0.14	1.7
462.5	0.06	1.88
467.5	0.14	1.7
472.5	-0.16	1.74
477.5	0.23	1.69
482.5	0.38	1.84
487.5	0.31	1.78
492.5	0.34	1.82
497.5	0.07	1.75
504	0.34	1.94
507.5	0.34	1.81
512.5	0.25	1.82
517.5	0.47	1.9
522.5	0.08	1.91
527.5	0.06	1.77
532.5	0.17	1.9
537.5	-0.09	1.73
543.5	0.19	2.03
548.5	-0.02	1.84
555	0.2	1.95
559.5	-0.12	1.64
564.5	-0.16	1.96
569.5	0.1	2.05
574.5	-0.21	1.56
579.5	-0.09	1.81
584.5	-0.02	1.93
589.5	-0.13	1.87

UVI Depth (cmbsf)	UVI δ13C (‰)	UVI δ18O (‰)
442.5	-1.12	3.22
447.5	-1.06	3.22
454	-1.03	3.28
457.5	-0.97	3.24
462.5		
462.5	-1.1	3.21
467.5	-1.01	3.28
472.5		
477.5	-1.08	3.27
482.5	-1.13	3.15
487.5	-0.94	3.26
492.5	-1.08	3.16
497.5	-1.07	3.26
504	-0.89	3.31
507.5	-1.02	3.23
512.5	-0.82	3.31
517.5	-1	3.21
522.5	-1.03	3.31
527.5	-1.01	3.31
532.5	-0.95	3.37
537.5	-1.3	3.29
543.5	-1.26	3.33
548.5	-1.25	3.4
555	-0.97	3.44
559.5	-1.13	3.41
564.5	-0.99	3.38
569.5	-1.05	3.42
574.5	-0.95	3.43

Appendix 1 (Cont): Stable isotope data from EW0408-85JC

PACL Depth (cmbsf)	PACL δ13C (‰)	PACL δ18O (‰)
584.5	0.51	1.75
589.5	0.52	1.73
594.5	0.44	1.76
599.5	0.43	1.67
605	0.25	1.95
609.5	0.37	1.85
614.5	0.42	1.58
619.5	0.23	1.72
624.5	0.23	1.87
629.5	0.24	1.76
634.5	0.21	1.74
639.5	0.29	1.69
644.5	0.37	1.78
649.5	0.38	1.61
655	0.13	1.71
659.5	-0.02	1.56
664.5	0.14	1.73
669.5	0.08	1.71
674.5	0.02	1.85
679.5	0.15	1.77
684.5	0.12	1.65
689.5	0.04	1.55
695.5	0.12	1.49
700.5	0.16	1.54
705	0.04	1.82
710.5	0.12	1.62
715.5	0.06	1.73
720.5	0.06	1.41

BULL Depth (cmbsf)	Bull δ13C (‰)	Bull d18O (‰)
594.5	-0.13	1.67
599.5	-0.09	1.57
605	-0.21	1.69
609.5	-0.18	1.78
614.5	-0.32	1.65
619.5	-0.13	1.63
624.5	-0.24	1.81
629.5	-0.28	1.83
634.5	-0.25	1.7
639.5	-0.34	1.73
644.5	-0.16	1.84
649.5	-0.5	1.68
655	-0.33	1.74
659.5	-0.43	1.98
664.5	-0.51	1.76
669.5	-0.42	1.95
674.5	-0.37	1.84
679.5	-0.52	1.82
689.5	-0.49	1.68
695.5	-0.61	1.53
700.5	-0.54	1.82
705	-0.55	1.61
710.5	-0.52	1.83
715.5	-0.63	1.6
720.5	-0.43	1.64
725	-0.34	1.75
728	-0.54	1.71
730.5	-0.28	1.82

UVI Depth (cmbsf)	UVI δ13C (‰)	UVI δ18O (‰)
579.5	-1.06	3.43
584.5	-1.03	3.35
589.5	-1.14	3.38
594.5	-1.28	3.4
599.5	-1.27	3.37
605	-0.91	3.33
609.5	-1.07	3.37
614.5	-1.23	3.4
619.5	-1.18	3.39
624.5	-1.18	3.48
629.5	-1.17	3.45
634.5	-1.11	3.41
639.5	-0.89	3.39
644.5	-1.21	3.46
649.5	-0.98	3.3
655	-1.02	3.52
659.5	-1.12	3.47
664.5	-1.16	3.52
669.5	-1.01	3.4
674.5	-1.15	3.45
679.5	-1.17	3.46
684.5	-1.06	3.44
689.5	-1.11	3.52
695.5	-1.12	3.42
700.5	-1.2	3.34
705	-0.93	3.41
710.5	-1.18	3.42
715.5	-1.13	3.45

Appendix 1 (Cont): Stable isotope data from EW0408-85JC

PACL Depth (cmbsf)	PACL δ13C (‰)	PACL δ18O (‰)
725	0.24	1.55
728	0.2	1.6
730.5	0.23	1.65
733	0.46	1.86
735.5	0.27	1.75
738	0.42	1.81
739.5	0.48	1.88
743	0.31	1.8
745.5	0.25	1.84
749	0.39	1.79
751	0.42	1.88
754	0.51	2.09
756.5	0.53	2.09
759	0.5	2.21
762.5	0.58	2.33
764.5	0.49	2.29
767	0.57	2.41
770	0.45	2.57
772	0.4	2.45
774.5	0.47	2.71
777	0.42	2.75
780	0.24	2.65
782.5	0.14	2.61
784.5	0.05	2.61
786.5	0.07	2.59
790	0.17	2.61
792	0.37	2.64
794.5	0.31	2.66

BULL Depth (cmbsf)	Bull δ13C (‰)	Bull δ18O (‰)
733	-0.41	1.58
735.5	-0.26	1.79
738	-0.1	2.01
739.5	-0.26	1.95
743	-0.34	1.96
745.5	-0.13	2.08
749	-0.1	2.02
751	-0.05	1.87
754	0.07	1.89
756.5	-0.06	2.1
762.5	0.02	1.86
764.5	-0.02	1.9
767	-0.07	1.81
770	-0.09	2.17
772	-0.18	1.98
774.5	-0.08	2.18
777	-0.06	2.09
780	-0.42	2.12
782.5	-0.59	2.1
784.5	-0.23	2.21
786.5	-0.31	2.14
790	-0.29	2.46
792	-0.24	2.33
794.5	-0.13	2.36
796.5	-0.14	2.6
799.5	-0.13	2.59
802	-0.06	2.37
804	-0.23	2.42

UVI Depth (cmbsf)	UVI δ13C (‰)	UVI δ18O (‰)
720.5	-0.7	3.57
725	-0.79	3.46
728	-0.92	3.51
730.5	-1.11	3.47
733	-1.1	3.6
735.5	-1.08	3.59
738	-1.07	3.71
739.5	-0.9	3.6
743	-1.08	3.6
745.5	-0.97	3.56
749	-0.93	3.64
751	-0.98	3.69
754	-0.91	3.72
756.5	-1.16	3.6
759	-1.12	3.64
762.5	-1.12	3.88
764.5	-1.18	3.64
767		
770	-1.23	3.91
772	-1.17	3.85
777	-1.51	3.62
780	-1.18	3.85
782.5		
784.5	-1.34	3.86
786.5	-1.13	3.93
790	-0.99	3.97
792	-1.42	3.97
794.5	-1.21	3.91

Appendix 1 (Cont): Stable isotope data from EW0408-85JC

PACL Depth (cmbsf)	PACL δ13C (‰)	PACL δ18O (‰)
796.5	0.25	2.7
799.5	0.11	2.44
802	0.16	2.46
804	0.2	2.68
806.5	0.07	2.19
810	0.21	2.39
812	0.11	2.32
814.5	0.1	1.84
817	0.26	2.05
819.5	0.19	2.03
820.5	0.42	2.41
821.5	0.28	2.24
822.5	0.26	1.78
823.5	0.15	1.93
824.5	0.23	2.33
825.5	0.17	2.36
826.5	0.14	2.29
828.5	0.22	2.65
830	0.31	2.95
832.5	0.14	3.05
834.5	0.16	2.82
837.5	-0.08	3.34
840	-0.09	3.11
844.5	-0.11	3.3
849.5	-0.11	3.52
854	-0.18	3.62
860.5	-0.11	3.46
865.5	-0.04	3.58

BULL Depth (cmbsf)	Bull δ13C (‰)	Bull δ18O (‰)
806.5	-0.03	2.17
810	-0.21	2.49
812	-0.42	1.74
814.5	-0.07	2.18
817	-0.15	2.41
819.5	-0.08	1.99
820.5	-0.36	2.12
823.5	-0.3	2.13
824.5	-0.11	2.27
825	0.06	2.68
830	-0.04	2.97
832.5	-0.34	2.68
834.5	-0.29	3.1
837.5	-0.45	2.86
840	-0.49	3.12
844.5	-0.58	3.23
849.5	-0.8	3.4
854	-0.51	3.17
860.5	-0.39	3.61
865.5	-0.73	3.5
876	-0.46	3.57
904	-0.43	3.5
954	-0.73	3.63
1004	-0.7	3.32
1054	-0.71	3.47
1103	-0.66	3.48
1153	-0.63	3.68

UVI Depth (cmbsf)	UVI δ13C (‰)	UVI δ18O (‰)
796.5	-1.2	4
799.5	-1.48	3.79
802	-1.5	3.91
804	-1.26	4.03
806.5	-1.2	3.91
810	-1.11	3.97
812	-1.48	3.81
814.5	-1.16	3.89
819.5	-0.97	3.12
823.5	-1.15	3.7
825	-1.08	3.59
830	-1.05	4.2
830	-0.91	4.18
832.5	-1.19	4.16
834.5	-0.94	4.19
837.5	-1.13	4.41
840	-1.2	4.38
844.5	-1.27	4.31
849.5	-1.22	4.36
854	-1.15	4.48
860.5	-1.27	4.35
865.5	-0.96	4.48
876	-1.13	4.48
904	-1.12	4.46
954	-0.88	4.54
1004	-0.81	4.66
1054	-1.48	4.54
1103	-1.12	4.69

Appendix 1 (Cont): Stable isotope data from EW0408-85JC

PACL Depth (cmbsf)	**PACL δ13C (‰)**	**PACL δ18O (‰)**
876	0.05	3.69
904	0.03	3.59
954	-0.08	3.61
1004	-0.06	3.71
1054	-0.23	3.58
1103	-0.07	3.59
1153	0	3.69
1203	0.03	3.56
1253	-0.11	3.54

UVI Depth (cmbsf)	**UVI δ13C (‰)**	**UVI δ18O (‰)**
1153	-0.8	4.53
1203	-0.7	4.88
1253	-0.76	4.67